Australian Government

Ansto

Research Selections

2013

ENVIRONMENT AND CLIMATE

NOVEL MATERIALS

LIFE SCIENCES

IMAGING

CHARACTERISATION AND PROCESSING

As the home to Australia's nuclear expertise, the Australian Nuclear Science and Technology Organisation (ANSTO) is one of Australia's largest research organisations.

Nuclear science and technology is a dynamic area of research that focuses on the building blocks of matter. Many of the most important questions society faces in areas such as health, climate change and industry are being investigated by ANSTO researchers.

At the heart of ANSTO's research capabilities is the OPAL reactor which is one of the world's newest and best multi-purpose research reactors. OPAL is used for scientific research, the production of medical radioisotopes, the activation of targets and the irradiation of silicon used for electronics.

ANSTO manages a collection of Australia's newest and most advanced particle accelerators in its Centre for Accelerator Science. These are used to analyze materials to determine their elemental composition and age, providing critical information for studies into human history and the environment.

ANSTO also operates the Melbourne-based Australian Synchrotron. Using a light source a million times brighter than the sun, the Synchrotron enables researchers to support industries in a wide range of subject areas including minerals, health, materials, manufacturing, food security, climate science, and energy.

As a Federal Government agency, ANSTO's provides policy advice to Government on all matters relating to nuclear science, technology and engineering, supporting its international roles and obligations. ANSTO is connected with all Australian and New Zealand universities through the Australian Institute of Nuclear Science and Engineering (AINSE), providing researchers access to Australia's nuclear science, technology and engineering expertise.

ENVIRONMENT AND CLIMATE

NOVEL MATERIALS

LIFE SCIENCES

IMAGING

CHARACTERISATION AND RESOURCE PROCESSING

Table of contents

Foreword

ANSTO is home to the Bragg Institute, one of the world's leading facilities for using neutron scattering and X-ray techniques to see the unseeable and solve complex research and industrial problems.

The Institute was named after the father and son team of Sir William Bragg and Sir William Lawrence Bragg whose work helped pave the way for X-ray crystallography and earned them a Nobel Prize in 1915.

We are likely to be reminded of their important pioneering work throughout 2014, which has been dubbed the International Year of Crystallography by UNESCO.

ANSTO's Bragg Institute has a worldwide community of scientists and engineers who are starting to flex the muscles of a dynamic suite of neutron beam instruments based here in Australia.

By examining the smallest particles of matter, researchers from Bragg are able to tackle some of the biggest questions facing us today, ranging from understanding the behaviour of cells in our bodies to the big picture of astro-physics and adding to the sum of our knowledge about the origins of the universe.

Another important development for research in Australia has been ANSTO taking over the operation of the Australian Synchrotron. This has strengthened our position as a truly national research organisation, and enabled many of Australia's best and brightest to work even more closely with us.

The Australian Synchrotron is a high performance facility that needs capital investment to further leverage its excellent work and serve new communities of users. ANSTO will continue to work with the science community and its supporters to secure its future.

While every researcher needs the right instruments to do their work, science is ultimately a conversation – and all of the projects in *Research Selections 2013* reflect this, involving collaborations with talented researchers from Australia and around the world.

There are many great contributions in *Research Selections 2013*: our studies of ice and stalagmites to give us a window into climate history; understanding the mechanisms behind magnets and ferro-magnetic fields; new ways to diagnose stroke and degenerative neurological diseases; detectors to aid hadron therapy for cancer patients; better understandings of haemoglobin; and the development of potential new environmental solutions for the minerals industry.

I think you will agree, future generations will benefit from this exciting work which adds to the bank of knowledge in key areas of health, environment, materials and solutions for our industries.

Once again, I congratulate the researchers who have contributed to *Research Selections* for starting and continuing these scientific conversations that will ultimately benefit us all.

Dr Adi Paterson
Chief Executive Officer
ANSTO

ENVIRONMENT AND CLIMATE

Understanding how earth systems work and being able to monitor changes helps us to better manage the environment. It allows researchers, industry and policymakers to make informed decisions about the ecosystems we depend upon, and ultimately improves our world.

ANSTO uses its accelerators and the OPAL research reactor to better understand a number of important areas of environmental science. This includes atmospheric studies such as tracking air pollution from coal-fired power stations in New South Wales and understanding the differences in carbon–dioxide circulation between the Northern and Southern hemispheres and its impact on climate.

Water and its sustainability is another area of focus for ANSTO. Our studies are probing cave formations to help understand the implications of Western Australia's reduction in rainfall and its longer-term socio-economic impact.

Furthermore, water's solid form – ice – is being studied to determine how it behaves under stress, an important feature in the movement of glaciers.

David Cohen and his team have collected fine particles in western Sydney for more than a decade.

Revealing the sources of Sydney's air pollution

01

Fine particles in our atmosphere can travel hundreds of kilometres every day. Their monitoring is crucial as they have significant impact on both human health and the environment.

Over the last decade, nuclear techniques for studying fine particles in the atmosphere have improved significantly, moving from simply analysing their chemical composition to combining meteorological data, such as wind patterns and trajectory with statistical modelling, to define where the pollution actually came from.

Consequently, it is now possible to not only determine the source of pollution via a chemical composition 'fingerprint,' but to also quantify that source's total contribution of fine particles in a specific location. In short, we can identify individual polluters and measure how many fine particles originated from those polluters.

Over more than a decade, David Cohen and his team have collected samples in the Richmond area of western Sydney. By using these combinatory techniques of analysing the particles' chemical composition and taking account of meteorological data with statistical modelling, they are able to quantify the effects of air pollution.

This demonstration project has found that up to half of the total sulfate air pollution in the greater Sydney region can be attributed to emissions from NSW's eight coal-fired power stations. Despite being located many kilometres outside of the greater Sydney metropolitan area, these coal-fired power stations have a significant impact on air quality in the CBD areas of Sydney. This information is used by air quality managers to inform pollution control measures and decision making.

David D. Cohen, Jagoda Crawford, Eduard Stelcer, Armand J. Atanacio

ANSTO

Introduction

As atmospheric fine particle pollution has significant impacts on our lives, there has been significant progress over the last decade to better identify its sources and hold polluters accountable. Increased computing power with new algorithms that handle big data sets has played an important role in advancing these studies. In order to handle multiple observations in environmental monitoring mathematical models are used to analyse the different types of data sets. For the study of air pollution we investigate fine particles and analyse the data using positive matrix factorisation (PMF) and multi-linear engine (ME) methods [1,2] for determining the number and composition of sources of pollution.

Coal-fired power stations are known emitters of fine particles PM2.5 (PM2.5 stands for particles of a size of 2.5 microns or less, i.e. 0.025 mm) and pollutant gases such as SO_x and NO_x. ANSTO researchers have developed techniques to determine the contributions of eight coal-fired power stations, which burn over 25 MT/year (yr) of low grade sulfur coal,

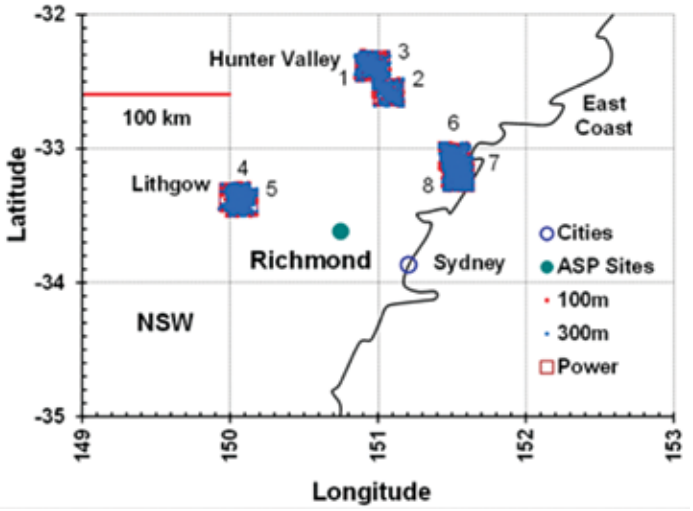

< Figure 1 (a)
Locations of eight coal powered power stations supplying Sydney. Boxes labelled 1 to 8 show the locations of the eight NSW coal-fired power stations. The 100m and 300m dots within each of these boxes show the number of wind back trajectories from Richmond site that intersected with each power station. The large symbol (●) shows the location of the Richmond sampling site.

< Figure 1(b)
The ANSTO cyclone sampler (foreground) at the Richmond site of the University of Western Sydney.

to the PM2.5 mass loading in the greater Sydney metropolitan area. We have applied and compared PMF and ME techniques for identifying the source by its elemental fingerprint and quantifying the contribution of a source to total pollution levels. Using the ME methods we included data of wind observations and profiles the trajectory positions. By combining these various parameters, sources external to the Sydney metropolitan region can uniquely be tied to fine particle measurements made within this region.

Study Site and Local Conditions

The locations of the eight coal-fired power stations supplying Sydney's electricity are shown in Fig. 1a. The average sulfur content of coal burnt for power generation in NSW at these stations is around 0.5% by weight. The power station emissions represent 243 kT/year of sulfur dioxide emissions across NSW. In the State of NSW, of the total 290 kT/yr of sulfur dioxide emissions produced each year, over 80% are from the coal-fired power stations.

The sampling site (Fig.1b) was located at Richmond (-33.618°S, 150.748°E) in an open grassed area in the grounds of the University of Western Sydney, 53 km northwest of the Sydney CBD. Samples were taken every Sunday and Wednesday for 24 hours from midnight to midnight. The site was influenced by sources from within the Sydney CBD region and sources external to the greater metropolitan area, such as the power stations.

Measuring chemical composition

Accelerator-based Ion Beam Analysis (IBA) techniques have been used at ANSTO for many decades to determine chemical composition of fine particulate matter. They are ideally suited to this task as they have the sensitivity to non-destructively measure elements from hydrogen to lead with concentration down to nanograms per cubic metre of air sampled. The measurements of the elemental contributions use the following techniques: Particle-Induced X-ray Emission (PIXE), Proton-Induced Gamma Emission (PIGE), Rutherford Backscattering (RBS) and Particle-Elastic Scattering (PESA) [3]. These four techniques together with laser absorption methods for black carbon analysis [4] were employed

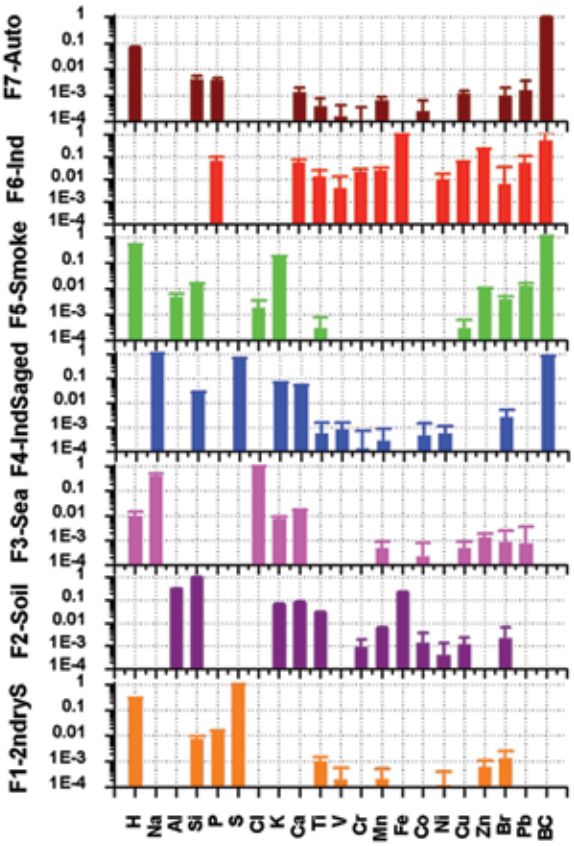

^ **Figure 2**
The seven factors or source fingerprints obtained from the standard positive matrix factorisation (PMF) analysis.

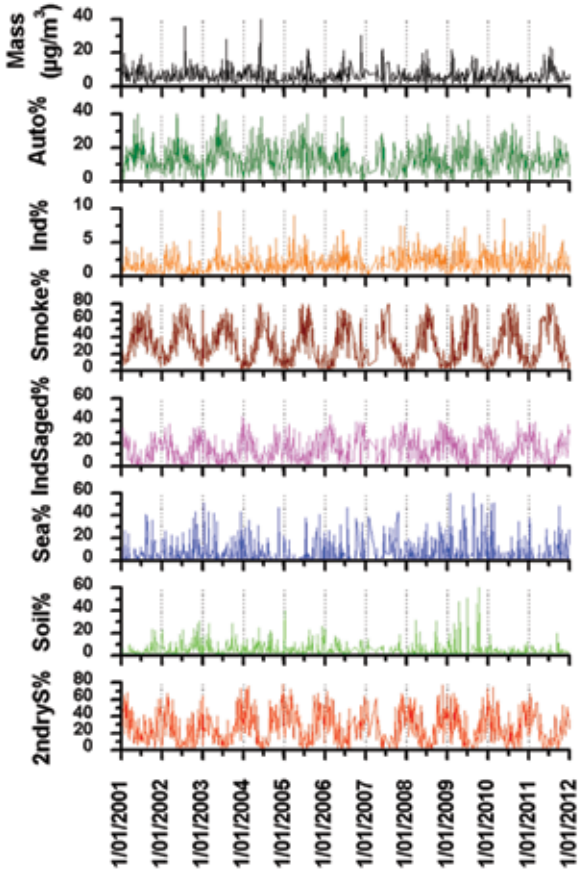

^ **Figure 3**
Time series plots for the total PM2.5 mass and the percentage mass contributions of the 7 standard PMF factors or fingerprints.

to determine 21 different element species between hydrogen (H) and lead (Pb). During this study, samples were taken every Sunday and Wednesday, providing 912 samples for analysis covering the period 2001-2011.

Positive matrix factorisation fingerprints and source contributions

For a data set of this size, the statistical approach of positive matrix factorisation (PMF) was applied to identify the pollution source by its elemental fingerprints, as well as to quantify the contributions of these sources to the total PM2.5 concentration. Figs. 2 and 3 show the results for analysing the measurements using PMF and Table 1 lists the sulphur contribution for the fingerprints.
We found that seven factors fit the data and we can thus determine the fingerprint of the source, see Fig. 2 and plot their daily contributions in Fig. 3. The total PM2.5 gravimetric mass could be explained to within 2% by these seven fingerprints and each elemental fingerprint was significantly determined at the 99% confidence interval in this PMF model.

The average percentage contributions to the total PM2.5 mass for each of these standard PMF sources during the study period, see Table 1a, shows that the two major sulfur sources, i.e. secondary sulfur (*2ndryS*) and industrial-aged sulfur (*IndSaged*), accounted for 40% of the mass followed closely by Smoke from biomass burning with 37%.
Table 1b shows that for the standard PMF analysis 73% of the measured total sulfur was associated with the *2ndryS* fingerprint and 27% with the *IndSaged* fingerprint. The remaining four fingerprints account for 23% of the fine mass, but were not really the focus of the current study as they were generally associated with diffuse or distributed sources and not associated with the eight coal-fired power stations point sources which we want to quantify here.

Fig. 3 shows the daily variations of these seven sources over the 11 year study period. Seasonal (summer-

%Fingerprint masses for different scenarios		
Fingerprint	**Standard PMF 7 Factors**	**ME 9 Factors**
Secondary sulfur - 2ndryS (total)	27.3±0.6	25.3±0.8
2ndrySPower		12.7±0.4
2ndrySnoPower		12.6±0.4
Industrial aged sulfur - IndSaged (total)	12.4±0.8	14.3±0.7
IndSagedPower		5.60±0.3
IndSagednoPower		8.70±0.4
Soil	4.76±0.4	4.90
Sea	5.54±0.4	5.40
Smoke	37.1±0.7	33.8
Industry	1.75±0.7	1.50
Auto	11.2±0.8	14.8
Total%	100±5	100±5

< Table 1 (a)
Percentage contributions to the total PM2.5 mass for each of the fingerprints in the standard PMF analyses and for the ME analyses described below.

	Sulfur contributions (%)	
	Standard PMF	**ME**
Fingerprint	7 Factors	9 Factors
2ndryS (total)	72.9±4	74.8±4
2ndrySPower		36.5±2
2ndrySnoPower		38.3±2
IndSaged (total)	27.1±2	25.2±2
IndSagedPower		10.6±0.8
IndSagednoPower		14.6±1

< Table 1 (b)
Percentage contributions to the total measured sulfur content in the fine PM2.5 fraction for each of the fingerprints in the standard PMF analyses and for the ME analyses described below.

winter) variations are clearly obvious. For example, the winter smoke is 60%-80% of the fine mass while the summer smoke is generally less than 10%. This is due mainly to domestic wood fires used for heating in the winter in many Sydney homes.

This seven factor standard PMF analysis produced two sulfur containing fingerprints, 2ndryS and IndSaged both of which were a mixture of several possible sources. However, it does not provide a power station fingerprint or a breakdown of how much of 2ndryS or IndSaged sources were power-station related. To achieve this we need to apply the more sophisticated ME analysis to our dataset.

Combining wind back trajectories and statistical analysis

Here, we use the multi-linear engine (ME) approach to split the two sulfur fingerprints *2ndryS* and *IndSaged* obtained in the standard PMF analysis into two components each. The first component are contributions of wind back trajectories from Richmond [4,5] which passed over at least one of the eight identified power stations (*Power*) and the second component are contributions that did not pass over any power stations (*noPower*). Consequently, the seven standard PMF fingerprints of Fig. 2 are turned into nine fingerprints which were then analysed by ME techniques. These new methods have been fully discussed in reference [7].

This ME analysis produced not only nine source fingerprints and their contributions, but also a range of power and non-power sulfur source fingerprint masses contributing to the total PM2.5 mass loadings at the Richmond site. This is a unique aspect of this approach as this enabled us to

define Power fingerprints and to put limits on the possible contributions these fingerprints – and consequently the power stations – made to the measured fine (PM2.5) mass at the Richmond receptor site. These contributions are summarised by the ME data in the right-hand columns of Table1.

Associating the fine particle samples to their origins

Using PMF techniques we could identify and quantify seven different fingerprints of sources of fine particles collected at the outskirts of Sydney. Two of these fingerprints, secondary sulfate and aged-industrial sulfur were each split in two and, through wind back trajectories, sorted into two groups those passing over coal-fired power stations and those not. ME techniques together with wind back trajectory data from [6] were then applied to define fingerprints associated with coal-fired power stations as well as quantifying their contributions to total PM2.5 mass loadings.

There are eight coal-fired power stations in NSW burning 25 MT/yr of coal and emitting 243 kT/yr of SO_2 which is converted by water and sunlight to sulfate particles. These power stations were many kilometres outside the greater Sydney metropolitan area, but still had a significant impact on the fine particle mass loadings measured at the sampling site within the metropolitan area. The PM2.5 eleven year average mass at the Richmond sampling site was 6.48 µg/m^3. The corresponding ammonium sulfate estimate was 1.65 µg/m^3 or 26% of the PM2.5 mass. The two PMF fingerprints, secondary sulfate (*2ndryS*) and aged industrial sulfur (*IndSaged*) accounted for 27% and 12% respectively, making a total of 39% of the PM2.5 mass. Using wind back trajectories we could distinguish these two fingerprints into power and non-power contributions. By subsequently running an ME analysis over them, we were able to produce coal-fired power station fingerprints. These power related fingerprints were responsible for approximately 18% of the total PM2.5 mass and 47% of the total sulfate measured at the sampling site. On average, up to a half of the total sulfate measured in the greater Sydney region can be attributed to coal-fired power station emissions.

REFERENCES

[1] Paatero, P., Tapper, U., 1994. Positive Matrix Factorisation: A non-negative factor model with optimal utilisation of error estimates of data values, Environmetrics, Vol 5, 111-126.

[2] Cohen, D.D., Crawford, J., Stelcer, E., Bac, V.T., 2010. Characterisation and source apportionment of fine particulate sources at Hanoi from 2001 to 2008. *Atmospheric Environment* 44, 320-328.

[3] Cohen, D.D., 1998. Characterisation of atmospheric fine particles using IBA techniques. *Nuclear Instruments and Methods in Physics Research Section B: Beam Interactions with Materials and Atoms* 136, 14-22.

[4] Taha, G., Box, G.P., Cohen, D.D., Stelcer, E., 2007. Black carbon measurement using laser integrating plate method. *Aerosol Science and Technology* 41, 266-276.

[5] Draxler R.R., 1991. The accuracy of trajectories during ANATEX calculated using dynamic model analysis versus rawinsonde observations. Journal of Applied Meteorology 30, 1466-1467.

[6] Draxler R.R., Rolph G.D., 2003. Hybrid Single-Particle Lagrangian Integrated Trajectory (HYSPLIT), model. http://www.arl.noaa.gov/ready/hysplit4.html.

[7] Cohen, D. D., Crawford J., Stelcer E., Atanacio A., 2012. A new approach to the combination of IBA techniques and wind back trajectory data to determine source contributions to long range transport of fine particle air pollution. Nucl. Instru. Methods in Physics Research B273, 186-188.

Cross section of a 2000 year old Western Australian cave stalagmite.

Studying Western Australian caves to help us understand climate change

02

On average, there is now 17 per cent less rainfall across Western Australia's south-western region than was recorded prior to 1970. This rainfall reduction has economic, social and environmental implications for the region, in particular for the growing capital of Perth, as well as water-dependent industries in the state.

Only short term rainfall records (110 years or so) are available to work with, so scientists researching the cause of this rainfall decrease need to apply different climate research methods to get a longer-term understanding of rainfall patterns to assist with predicting the rainfall patterns. Interestingly, it is cave stalagmites that are helping to provide the answers.

Cave stalagmites are a rock formation that rises from the floor of a cave due to the accumulation of material deposited on the floor from minerals dissolved in dripping water. These structures form slowly over thousands of years and with nuclear techniques, scientists are able to use the stalagmites to help unlock thousands of years of rainfall-sensitive data, preserved in the crystallised calcium carbonate.

The first step in this process is to assess whether one of potentially hundreds of individual stalagmites in a cave is suitable for generating past climate records and that's where ANSTO comes in. Working in Western Australia, Pauline Treble and her colleagues monitored drip water and studied how sensitive and accurate individual stalagmites are as indicators of rainfall and climate change.

In fact, using nuclear techniques and their expertise, ANSTO researchers have recently produced one of the longest cave monitoring datasets in Australia, from Golgotha Cave in south-west Western Australia. The data has confirmed the cave's suitability for gathering stalagmite-based rainfall records.

Pauline C. Treble[1], Chris Bradley[2], Anne Wood[3], Andy Baker[4]

[1] ANSTO, [2]University of Birmingham, United Kingdom, [3]Department of Environment and Conservation, Western Australia, [4]University of New South Wales, New South Wales

South-west Western Australia climate change

Rainfall is now on average 17 per cent less across the south-west Western Australia region compared with earlier data prior to 1970 [1]. Due to the consequent reduction in surface water availability has had large economic, social and environmental impacts in this region, which includes Western Australia's capital Perth, due to economically important water-dependent industries and population growth pressure. Much effort has been directed to understand the cause of this decline. But it remains difficult to assess the role of natural variability from the current short-duration meteorological record (110 years or so) because of the multi-decadal nature of the dry period. Hence, there is an urgent need to extend baseline information on natural climate variability for this region. Reconstructing past-climates using climate-sensitive 'proxies' in cave stalagmites has emerged as an effective way to achieve this [2].

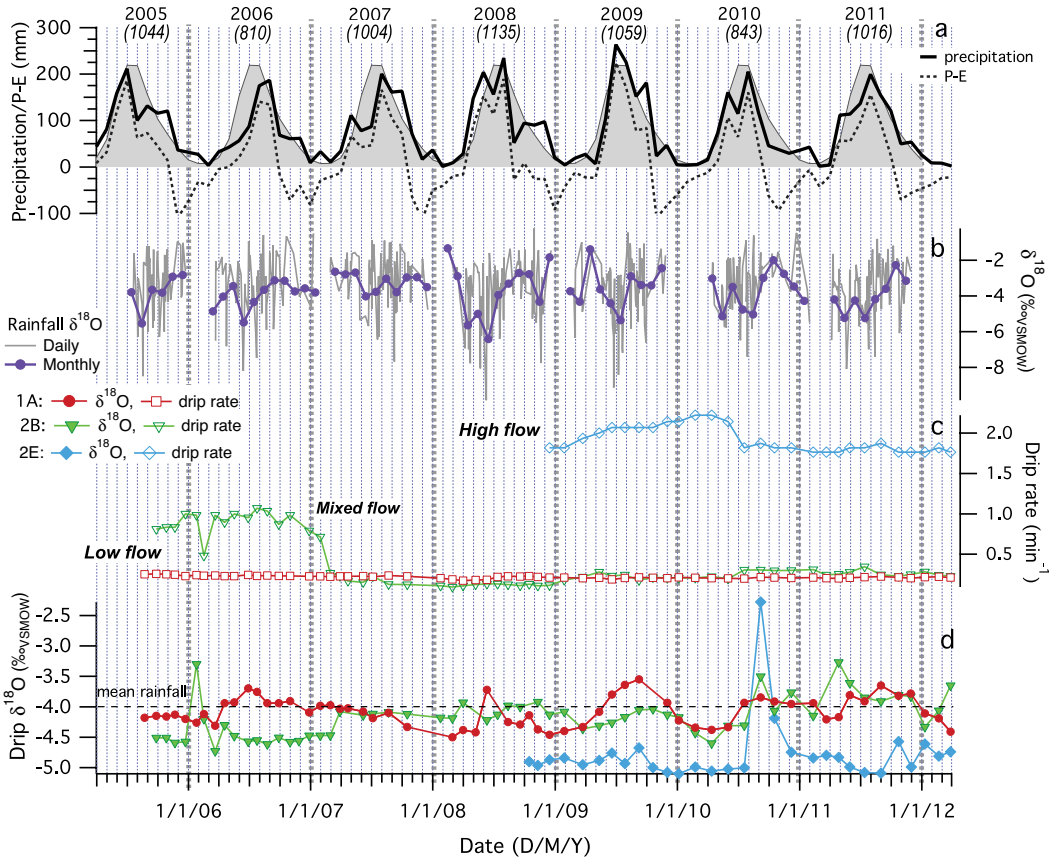

^ Figure 1

Precipitation and precipitation minus evapotranspiration (P-E) (a); rainfall oxygen isotopic composition or $\delta^{18}O$ (b); and cave observations of drip rate (c) and drip $\delta^{18}O$ (d) at three sites in the cave high-flow drips (blue diamonds) display distinctly lower drip $\delta^{18}O$ owing to selective recharge of a secondary reservoir by high-magnitude rainfall events. Not all data from all sites are shown. See [3] for full report.

'Climate' records from caves

We have demonstrated previously that climate-sensitive 'proxies' of rainfall which become preserved in growing stalagmites may be used to track climate change in south-western WA stalagmites [2]. This was achieved by measuring the geochemical record in a modern stalagmite from this region which had grown on a tourist boardwalk between 1911 and 1992 [2]. We cut open the stalagmite and measured trends in the oxygen isotopic ratio ($^{18}O/^{16}O$ or $\delta^{18}O$) along the stalagmite growth axis using mass spectrometry. We were able to verify that the speleothem recorded the post-1970 dry period because of the change in the $^{18}O/^{16}O$ ratio due to fewer intense storm events, which typically carry more ^{18}O-depleted moisture, during the dry period [2].

The extension of the south-west WA paleoclimate record is currently underway, however, a critical part of this study required a long-term monitoring program to attempt to capture the drying signal in the caves via measurements of the dripwater. Drip points were carefully studied for over six years. The cave was fitted out with data loggers and water collection devices, and Department of Environment and/or ANSTO staff visited the caves each month to collect the data.

Our findings

In summary, our six-year-long cave study (see Fig. 1), has led to a number of findings that have important implications for our ultimate goal of reconstructing paleoclimate records from south-west WA stalagmites.

We found that our monitored cave is particularly suitable as: 1) the dripwater preserved the oxygen isotope ($\delta^{18}O$) from the rainfall; 2) the cave had a high infiltration rate (typically <1 year from recharge); and 3) negligible isotopic impact of evapotranspiration [3], i.e. the sum of evaporation and plant transpiration from the land surface to atmosphere. Our study also captured some of the driest years on record in the region and this 'dry' signal was detectable in the dripwater. Consequently, we can reconstruct the long-term rainfall records from the stalagmites in this cave.

Implications for paleoclimate records

Our study also reinforced the importance of investing in long-term cave monitoring projects when

Pauline Treble making measurements in Golgotha Cave, south-west Western Australia. Photo: Andy Baker.

Cross-section of a 2,000 year old stalagmite from Golgotha Cave. (Height of stalagmite is approximately 10 cm.) Photo: Pauline Treble.

constructing stalagmite paleoclimate records as we found that not all of our sites captured the rainfall signal in the same way. A key uncertainty in this research is how the hydrological pathways in the cave ceiling may interfere with the transfer of the rainfall signal, e.g. by way of mixing, storage, attenuation and bypass flow [4,5]. This process is poorly understood. Our findings showed that low-flow drip sites, typical of much of the cave, are recharged by an even distribution of rainfall events evidenced by the agreement between mean dripwater and rainfall $\delta^{18}O$; and by the (attenuated) seasonal $\delta^{18}O$ cycles similar to that observed in rainfall (Fig. 1). In contrast, our high-flow sites are sustained by a secondary reservoir recharged by isotopically distinct high-magnitude rainfall events.

Stalagmite records from our low-flow sites are thus most likely to reflect mean conditions and be the most straightforward to interpret. However, records from high-flow sites with their bias to high-magnitude events will provide a useful comparison to detect multi-decadal (or longer) shifts in the intensity of storms, such as that observed in the meteorological record since the 1970s.

Next steps

Our long intensive study of the cave environment has paved the way to a better understanding of the climate records preserved in Golgotha Cave stalagmites. The stalagmites from the studied drips have now been removed and the construction of the records, extending as far back as 8,000 years, is now in progress. These records will provide long datasets of natural variability in south-west WA climate that are critically needed for testing climate models and leading to improved water resource and land management planning.

Acknowledgements

The authors would like to thank the Department of Environment and Conservation, WA for allowing access to cave sites and supporting the fieldwork. Thank you to Ian Fairchild, Warren Bond, Paul Rustomji, Andy Spate for assistance with fieldwork and to Cath Jex, Michael Gagan, Monika Markowska, Carol Tadros and Joan Cowley for assistance with lab analyses.

REFERENCES

[1] Hope, P., Timbal, B., & Fawcett, R. Associations between rainfall variability in the south-west and south-east of Australia and their evolution through time. (2010). *International Journal of Climatology*, 30(9), 1360-1371.

[2] Treble, P. C., Chappell, J., Gagan, M. K., McKeegan, K. D., & Harrison, T. M. (2005). *In situ* measurement of seasonal delta O-18 variations and analysis of isotopic trends in a modem speleothem from south-west Australia. *Earth And Planetary Science Letters*, 233(1-2), 17-32.

[3] Treble, P. C., Bradley, C., Wood, A., Baker, A., Jex, C. N., Fairchild, I. J., et al. (2013). An isotopic and modelling study of flow paths and storage in Quaternary aeolinite, SW Australia: implications for speleothem paleoclimate records. *Quaternary Science Reviews*, 64, 90-103.

[4] Bradley, C., Baker, A., Jex, C. N., & Leng, M. J. (2010). Hydrological uncertainties in the modelling of cave drip-water $\delta^{18}O$ and the implications for stalagmite palaeoclimate recontructions. *Quaternary Science Reviews*, 29(17-18), 2201-2214.

[5] Fairchild, I. J., & Baker, A. (2012). Speleothem Science: *From process to past environments*. Oxford: Wiley-Blackwell.

ANSTO's Quan Hua, Vlad Levchenko and Andrew Smith (R-L) with a cross section of a Tasmanian Huon Pine.

Study helps make carbon dating a more accurate chronological tool

03

The use of bomb-pulse radiocarbon has become widespread as a precise dating tool for the last 60 years, leading to new applications in forensic science, biology, physiology, plant and animal growth, and climate studies.

Carbon-14 (^{14}C) was generated by nuclear explosions in the atmosphere due to weapons testing, mostly in the 1950s and 1960s, and the resultant $^{14}CO_2$ gradually being distributed throughout Earth's atmosphere and essentially put a mark in time and can be used as an accurate dating technique. The atmospheric $^{14}CO_2$ level is now approaching its natural pre-bomb value.

In the troposphere – the region of Earth's atmosphere below about 10,000 metres – the level of bomb-derived $^{14}CO_2$ was extremely variable in space and time. For this reason, if we want to radiocarbon-date materials formed during the last 60 years, we need to know what those atmospheric levels were – both when and where. Fortunately tree rings, studied in this research, have recorded this information as the trees have photosynthesised the $^{14}CO_2$ into cellulose in their annual rings.

In this study, researchers from ANSTO and Naresuan University measured the level of radiocarbon in tree rings from Thailand, Indonesia and Australia, using ANSTO's particle accelerators. The results, together with published radiocarbon data from tree rings and atmospheric carbon dioxide samples from around the world, revealed that the level of atmospheric $^{14}CO_2$ during the early bomb period from the mid-1950s to the late 1960s was strongly influenced by world-wide atmospheric circulation patterns.

Using this compilation, we have been able to reconstruct regional and temporal records of atmospheric $^{14}CO_2$ levels to make carbon dating a more accurate chronological tool.

Quan Hua[1], Mike Barbetti[2], Vlad Levchenko[1], Andrew Smith[1]

[1] ANSTO, [2]Naresuan University, Thailand

Natural and bomb-derived ^{14}C

Radiocarbon or ^{14}C is continuously formed in the atmosphere by interactions of the cosmic-ray secondary neutron flux with atmospheric ^{14}N. This is a purely natural process. Following its production, ^{14}C is oxidised to form atmospheric $^{14}CO_2$, (or atmospheric ^{14}C in short), which is then transferred to the oceans through air-sea gas exchange and enters living organisms (e.g., plants and animals) via photosynthesis, food-chain and metabolic processes. Consequently, the ^{14}C content of living organisms is in equilibrium with that of the atmosphere. Once the ^{14}C uptake ceases (e.g., at the death of an animal or when wood cellulose is formed), the ^{14}C content of the organism starts to decrease at a rate determined by its half-life of 5730 years. This is the basis for traditional radiocarbon dating for samples older than 1950, which in favourable cases can be as precise as ±20 calendar years.

A large amount of ^{14}C was artificially produced between 1945 and 1980 when hundreds of nuclear weapons were detonated in the atmosphere (Fig. 1a). Nuclear bomb blasts produced intense fluxes of thermal neutrons, which in turn reacted with atmospheric

a)

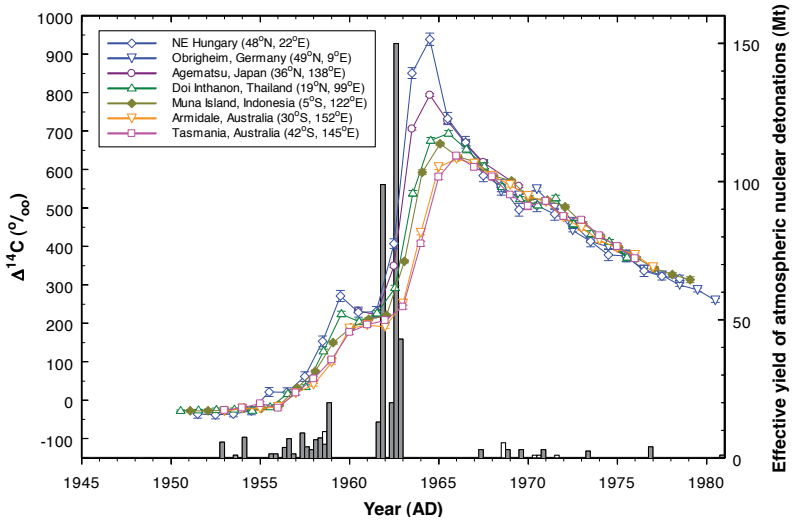

< Figure 1 (a)

Tree-ring ^{14}C at different latitudes and the magnitude of atmospheric nuclear detonation. Grey and white bars represent total effective yield of atmospheric nuclear detonations for 3-month periods for the Northern and Southern Hemisphere, respectively.

b)

< Figure 1 (b)

Cross-section of Thai three-leaf pine tree DIK 235/1 with rings from 1916 to 1994, from which a sub-section was used for AMS ^{14}C analysis.

^{14}N to form ^{14}C. As a result, the concentration of ^{14}C in the atmosphere increased dramatically in the late 1950s and early 1960s, and peaked in the mid-1960s at nearly double the pre-bomb level. Significantly different atmospheric ^{14}C levels between consecutive years during the period from 1955 onwards offer the possibility of dating recent terrestrial materials by ^{14}C with a resolution that can be as good as a single year. Such applications require a detailed knowledge of the radiocarbon bomb-pulse.

New tree-ring ^{14}C data

We have measured ^{14}C in tree rings from the tropics and southern mid-latitudes where atmospheric ^{14}C data are scarce. It is worth noting that tree-ring ^{14}C is a direct representation of atmospheric ^{14}C values during the growing season of tree rings [1]. The tree rings used in our study included three-leaf pine (*Pinus kesiya*) from Doi Inthanon, Thailand (Fig. 1b), teak (*Tectona grandis*) from Muna Island, Indonesia, *Pinus radiata* from Armidale, Australia, and Huon pine (*Lagarostrobos franklinii*) from Tasmania, Australia. Four sets of single tree rings from the early 1950s to the mid-1970s were pre-treated to alpha-cellulose then converted to graphite for Accelerator Mass Spectrometry (AMS) ^{14}C analysis using ANTARES and STAR accelerators at ANSTO [2].

Our results together with published data for the northern hemisphere (NH) are shown in Fig. 1a. The levels of the tree-ring ^{14}C bomb peaks decrease from north to south indicating a fast transport of bomb ^{14}C within 0.5-1 year

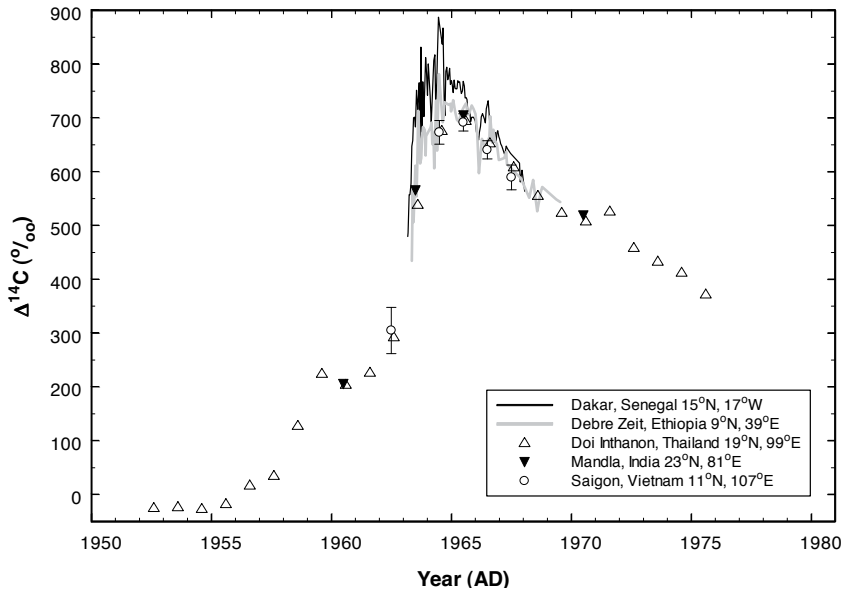

< Figure 2
Radiocarbon in tree rings versus atmospheric ^{14}C at similar latitudes for the northern tropics. Lines represent atmospheric ^{14}C data. Symbols depict tree-ring ^{14}C values.

from the northern temperate regions to the tropics and a further 0.5-1 year to the southern temperate regions.

Influence of atmospheric circulation on regional ^{14}C

As most of the atmospheric nuclear tests were conducted in the northern hemisphere (Fig. 1a), there were large, transient ^{14}C disequilibria in the troposphere (north versus south and high-latitudes versus low-latitudes) during the early bomb period from the mid-1950s to the late 1960s. This significantly increased the ^{14}C-contrast between regional air masses.

Figure 2 shows our Thailand data in comparison with published ^{14}C data at similar, northern-tropical latitudes in tree rings at Mandla (India) and Saigon (Vietnam), and in atmospheric CO_2 samples from Debre Zeit (Ethiopia) and Dakar (Senegal). The tree-ring data match each other very well. They also match very well with ^{14}C data for Debre Zeit, but all of them exhibit much lower ^{14}C values than the atmospheric data for Dakar.

The significant difference between Dakar ^{14}C values, and those from Debre Zeit, Mandla, Saigon and Doi Inthanon can be attributed to the summer African/Asian monsoon, and the position of the Inter-Tropical Convergence Zone (ITCZ) during the summer time relative to the locations of these sites [3]. During the growing season of northern hemisphere tree rings (May-August), Dakar and the latter sites are on different sides of the ITCZ (Fig. 3). Dakar is located north of the summer ITCZ and receives air masses from northern mid-latitudes. Meanwhile, the latter sites are located south of the summer ITCZ and influenced by southern hemisphere (SH) air (carried by the summer African/Asian monsoon) with a ^{14}C level significantly lower than that for the northern mid-latitudes during the early bomb period.

The ^{14}C levels of Muna Island in the southern tropics are significantly higher than those derived from mid-latitude southern hemisphere ^{14}C records (e.g., Armidale and Tasmania) for the periods of rapidly rising atmospheric ^{14}C (Fig. 1a). During the growing season of southern hemisphere tree rings (November–February), Muna is located well north of the winter ITCZ (Fig. 3) and strongly influenced by northern hemisphere air masses carried by the winter Asian monsoon [4]. Meanwhile Armidale and Tasmania remain covered by southern hemisphere air masses containing much less ^{14}C than those from the northern hemisphere during the early bomb period.

Zonal atmospheric ^{14}C data for dating

The spatial distribution of bomb radiocarbon during the early bomb period did not have a simple latitudinal gradient but consisted of various, more-or-less uniform zones separated by atmospheric

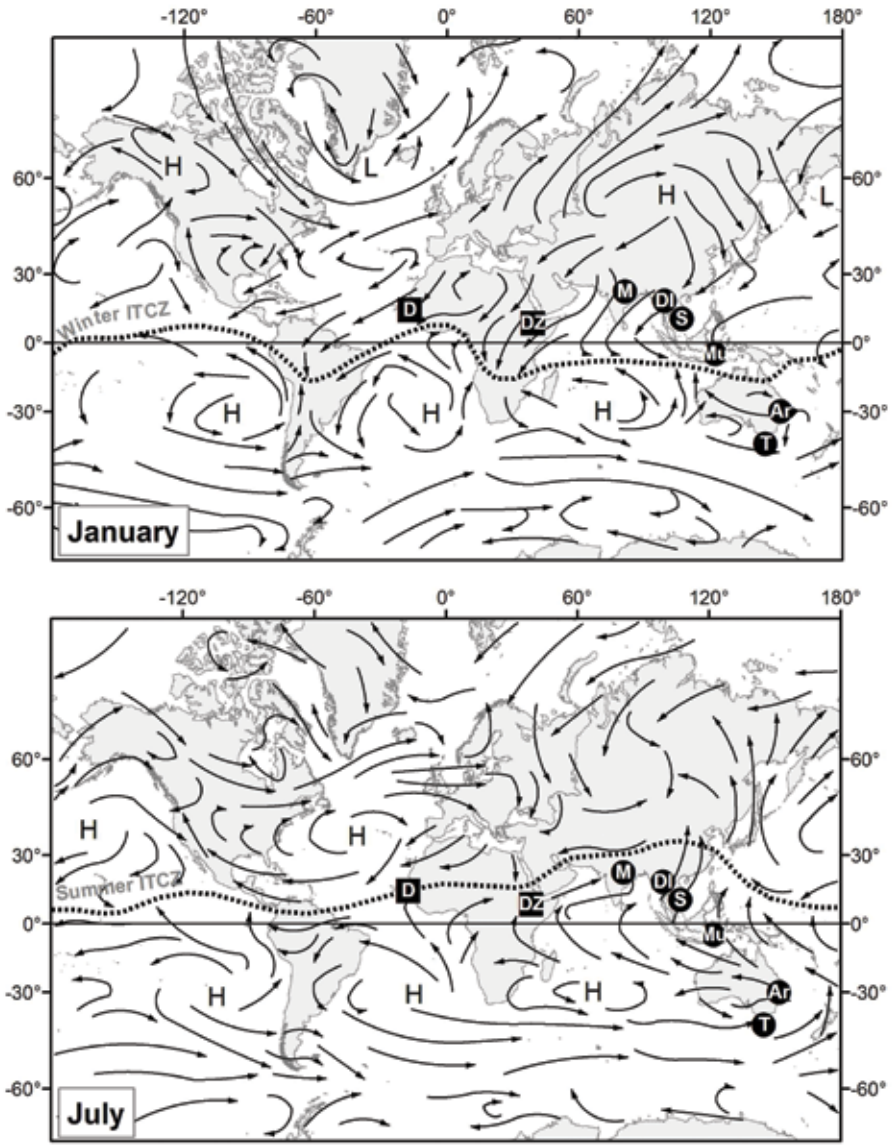

< Figure 3

Mean positions of the Inter-Tropical Convergence Zone (ITCZ) for January and July and global atmospheric circulation together with locations of atmospheric stations (squares) and tree ring sites (circles). H is a typical centre of high atmospheric pressure, and L is a centre of low atmospheric pressure. Atmospheric stations indicated are D, Dakar and DZ, Debre Zeit. Tree ring sites indicated are Ar, Armidale; DI, Doi Inthanon; M, Mandla; Mu, Muna Island; S, Saigon and T, Tasmania.

circulation cell boundaries and the ITCZ positions [3-5]. Based on this, we have reconstructed five zonal ^{14}C levels namely NH zones 1, 2 and 3, and SH zones 3 and 1-2 [5] (see Fig. 4 a and b).

The highest atmospheric ^{14}C level during this period was in NH zone 1, where most of the excess ^{14}C was injected into the troposphere. The level of atmospheric ^{14}C decreased from north to south as the excess ^{14}C was transferred southwards by atmospheric circulation. The spatial distribution of bomb ^{14}C in the southern hemisphere would probably consist of three zones similar to those for the northern hemisphere. However, the excess ^{14}C became diffused after it was transported over the broad and seasonally moving ITCZ resulting in an almost uniform ^{14}C level for the region south of the winter ITCZ (SH zone 1-2).

In summary, our results have significantly improved our knowledge of the influence of atmospheric circulation on regional ^{14}C differences, which is very important for accurate radiocarbon dating. In addition, five zonal ^{14}C data sets have been reconstructed to be used as "radiocarbon calibration curves" for improved bomb-pulse ^{14}C dating in order to facilitate a fast growing demand in the application of bomb radiocarbon in various research disciplines including forensic studies, biomedical research and soil carbon dynamics.

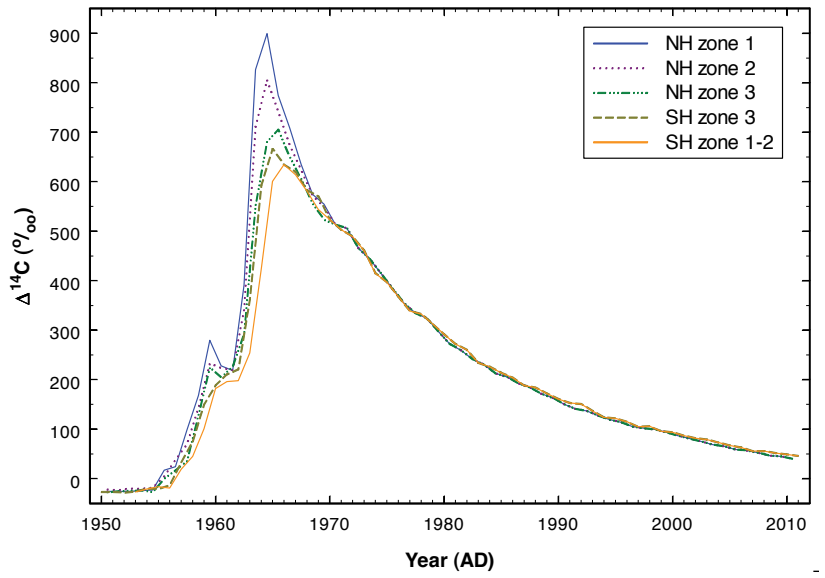

< Figure 4 (a)
Regional tropospheric ^{14}C curves for the period 1950-2010 for five different zones.

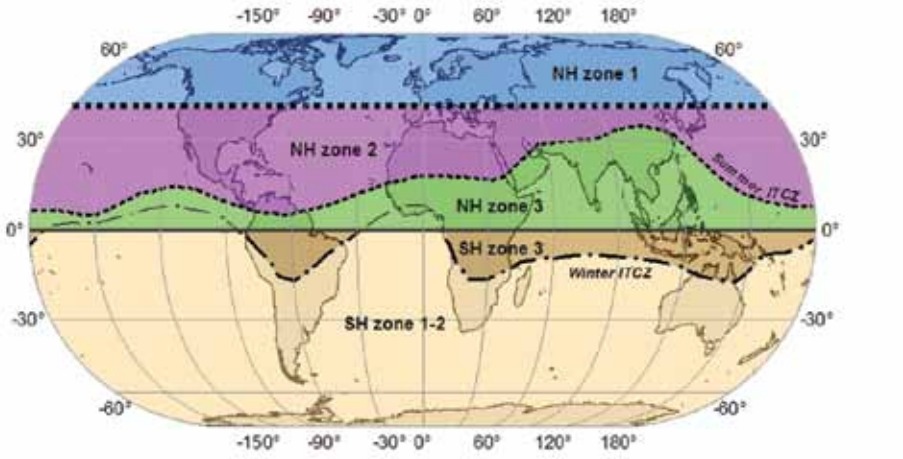

< Figure 4 (b)
The five zones into which the tropospheric ^{14}C levels have been reconstructed.

Acknowledgements

We would like to thank Stuart Hankin for the preparation of Figures 3 & 4.

REFERENCES

[1] Cain, W.F., & Suess, H.E. (1976). Carbon-14 in tree rings. *Journal of Geophysical Research*, 81(21), 3688-3694.

[2] Fink, D., Hotchkis, M., Hua, Q. et al. (2004). The ANTARES AMS Facility at ANSTO. *Nuclear Instruments and Methods in Physics Research* B, 223-224, 109-115.

[3] Hua, Q., & Barbetti, M. (2007). Influence of atmospheric circulation on regional $^{14}CO_2$ differences. *Journal of Geophysical Research*, 112, D19102.

[4] Hua, Q, Barbetti, M., Levchenko, V.A., D'Arrigo, R.D., Buckley, B.M., & Smith, A.M. (2012). Monsoonal influence on Southern Hemisphere $^{14}CO_2$. *Geophysical Research Letters*, 39, L19806.

[5] Hua, Q., Barbetti, M., & Rakowski, A.Z. (2013). Atmospheric radiocarbon for the period 1950-2010. *Radiocarbon*, 55, 2059-2072.

ANSTO's neutron diffraction studies on large ice samples are helping to predict sea level rises and better understand climate.

Neutron scattering helps predict the future of polar ice sheets

04

Predicting the behaviour of large masses of ice such as glaciers and polar ice sheets is challenging. Ironically, to better understand what is happening to these massive structures requires in-depth analysis at the atomic scale.

The results of ANSTO's study on large ice samples is helping explain the behaviour of ice, and more accurately model glacier movement, predict sea level rises and ultimately, better understand our climate.

A neutron diffraction study conducted by ANSTO's Vladimir Luzin and his colleagues aimed to determine principle mechanisms of ice deformation and provide quantitative characterisation of the processes and their evolution during ice plastic flow.

Vladimir Luzin[1], Sandra Piazolo[2], Christopher J. L. Wilson[3], Christophe Brouzet[4], Mark Peternell[5]

[1] ANSTO, [2]Macquarie University, New South Wales, [3]Monash University, Victoria,
[4]École Normale Supérieure de Lyon, Université Claude Bernard, France, [5]University of Mainz, Germany

Ice deformation

Ice is a very special material in two respects: it is a crystalline material with very weak hydrogen bonds and, in natural conditions, its homologous temperature (the temperature measured in the units of melting point) is very high. Both these facts make deformation of ice very dynamic and very sensitive to temperature, strain rates, microstructure and defect structure.

Ice has been studied for a long time (for example, Robert Boyle studied the properties of ice in the 1660s). Experimental studies are usually based either on mechanical measurement of ice masses or studies of individual grains, by means of optical methods or electron backscatter diffraction analysis for microanalysis; both are limited with respect to the practical number of individual grains that can be examined. The fact that samples can usually only be analysed before and after deformation does not necessarily provide information on dynamic behaviour. Thus, our understanding of the dynamics of ice rheology, its flow under pressure, and microstructure evolution remains incomplete. To close this gap, we combine ice deformation experiments with *in situ* neutron diffraction which allows continuous monitoring of the evolution of rheology, texture and microstructural characteristics over time.

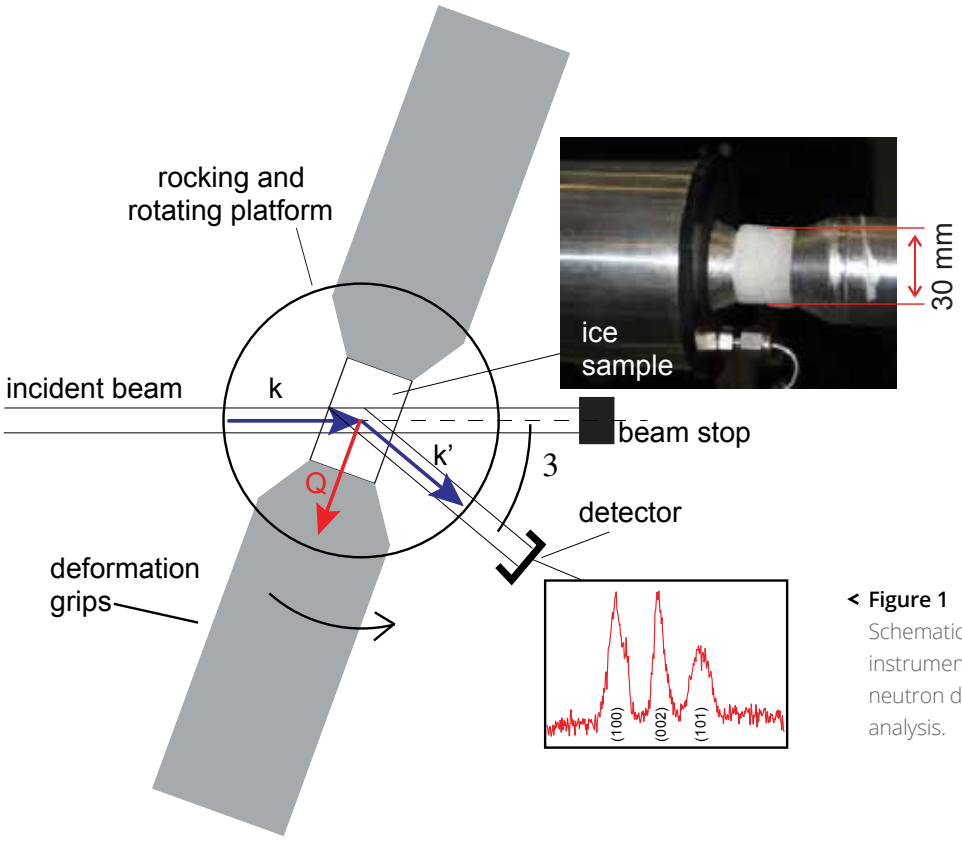

< Figure 1
Schematic illustration of the Kowari instrument configuration for *in-situ* neutron diffraction and texture analysis.

Sample preparation

Deuterated ice (D_2O) was studied rather than normal ice (H_2O), as is normal in neutron research involving hydrogen: substituting deuterium increases the useful neutron signal, while reducing background and attenuation. As a consequence, relatively large samples were studied, providing statistically reliable results on ice behaviour relatively quickly - with high time resolution and all in accurately controlled temperature and strain rate conditions.

Cylindrical samples (diameter ~2.5 cm, length ~3.2 - 4.0 cm) were prepared from polycrystalline heavy water ice with no crystallographic preferred orientation and the equilibrium microstructures characterised by a mean grain size of ~500 µm (measured optically) and a normal grain size distribution. This was achieved by freezing blocks of ice, crushing them and sieving and sorting size ranges before compacting the resulting powders into cylindrical shapes using special moulds. The substitution of H_2O to D_2O does not fundamentally affect any other properties of the resulting ice other than a shift in the melting point to 3.7°C.

Neutron diffraction in-situ experiment

The neutron diffractometer Kowari [1] was used to measure the deuterated ice samples. Experiments where performed at a temperature of -7°C (T_h = 0.96), a temperature more or less typical for naturally deforming ice sheets and glaciers. During the neutron measurements, samples were mounted in a load frame equipped with custom-built grips and an environmental chamber, both of which were specifically designed to maintain the required temperature.

A neutron wavelength of 2.4 Å and detector position of 38° were chosen, so that three separate diffraction peaks, (100), (002), and (101), could be simultaneously viewed within the Kowari detector coverage of 15°.

Each neutron diffraction experiment consisted of two major steps. Firstly, diffraction patterns were collected over a range of different directions with respect to the sample by rotating the load frame and sample away from the compression axis, see ω in Fig. 1. The range over which ω was varied was

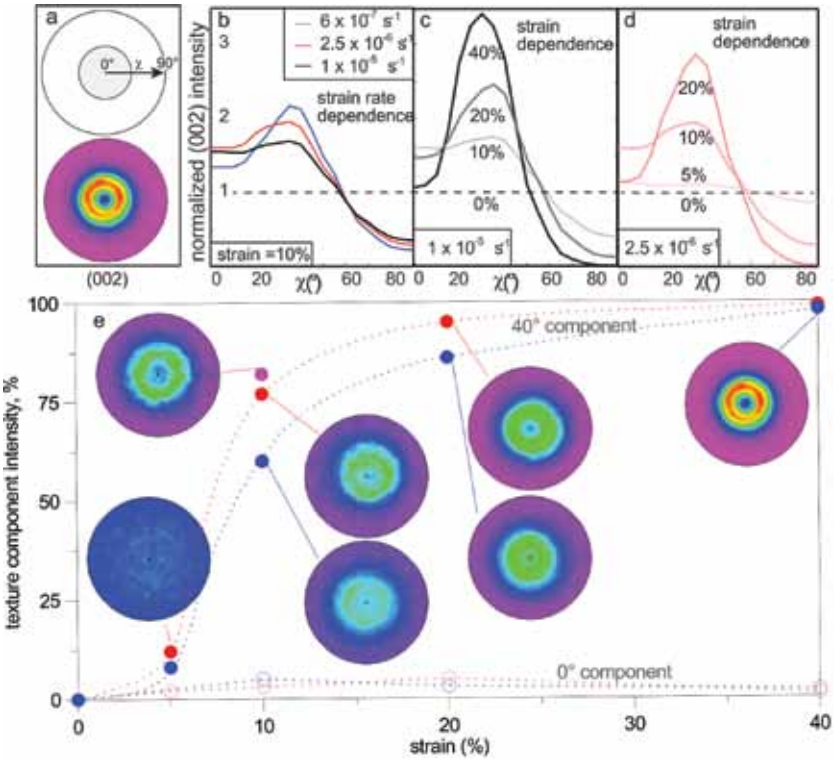

< Figure 2

(a) Partial pole figure data (top) and full pole figure data (bottom) are cylindrically symmetric due to the symmetry of the loading conditions. This allows all full pole figures (e) to be presented in one dimensional sections (b-d) showing the strain-rate dependence (b) or strain dependence for fast (c) and medium strain-rates. In the figure only the (002) pole figure data are presented. Textures from all samples were analysed in terms of fibre texture components (standard distributions over the surface of a sphere similar to a Gaussian distribution) and presented quantitatively in (e).

±35°. In this way, the most preferred orientation of crystals could be traced by comparing the neutron pattern in the axial direction and with those away from it. In technical terms, partial pole figures were measured and this was achieved as deformation was applied to the sample (the principle of *in situ* experiment) and its strain-stress curve recorded. Each individual partial pole figure measurement took 20-30 min. while the whole deformation experiment, depending on strain and strain rate, occurred over 12-24 hours (depending on strain and strain rate) and provided good time/strain resolution.

The same neutron diffraction patterns (using a special statistical analysis of the diffraction peak intensities) also provided information about the mean grain size. Consequently, grain size evolution was continuously recorded *in situ*. This *in situ* measurement was compared with traditional optical grain size analysis on thin sections prepared from the deformed samples after completion of the experiment, providing additional verification of neutron data.

In the second step, each sample was removed from the load frame and mounted in a device for orienting the sample (a two-circle Eulerian cradle equipped with a heating-cooling device, a cryo-furnace). In each case the samples were kept below -80°C while stereographic projection of the crystallographic directions present in the grain, so-called pole figures, were measured for the three diffraction peaks corresponding to the indices (100), (002) and (101) to fully characterise the texture of the samples. Several series of deformation experiments with constant strain rates of 6 x 10^{-7} s^{-1} (slow), 2.5 x 10^{-6} s^{-1} (medium) and 1 x 10^{-5} s^{-1} (fast) of between 5% and 40% were carried out to a bulk strains.

Results of deformation measurements

The neutron texture measurements unambiguously demonstrate evidence of the activation of the major slip systems[1], innate to the hexagonal crystal structure of ice. This is a combination of basal, prismatic and pyramidal slip systems. Through

[1] certain crystallographic planes and directions in which dislocation motions occur and that produce plastic deformation

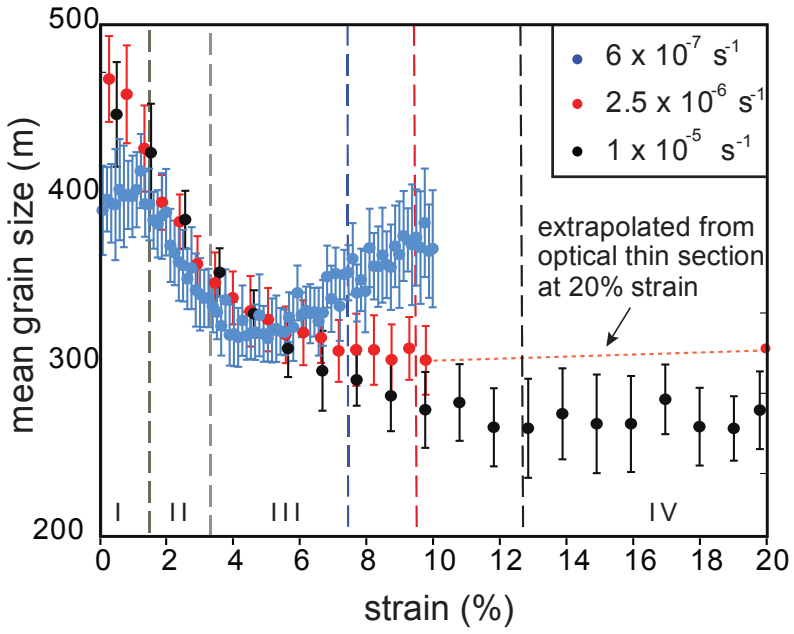

< Figure 3

Mean grain sizes derived by statistical analysis of the neutron diffraction data for three different strain rates: fast, medium, and slow.

slip along specific planes and directions, initially randomly oriented polycrystalline ice polycrystals develop a preferred orientation during deformation. As deformation progresses, we observe a weak single central *c*-axis maximum in the direction of compression that transforms into a strong girdle distribution at 35-40° to the compression axis as shown in Fig. 2. We attribute this behaviour to a switch from a mainly basal slip to pyramidal slip.

Figure 3 shows *in situ* data of the mean grain-size. By combing the data from the pole figures (Fig. 2) and the grain size (Fig. 3) we can follow the dynamic behaviour that is a fine balance between several processes:

(i) dislocation movement forming small-angle grain boundaries;

(ii) recrystallisation by grain boundary migration resulting in an overall reduction of the mean dislocation density and grain growth; and

(iii) recrystallisation by heterogeneous nucleation when new small grains grow rapidly in areas of high dislocation density (this recrystallisation tends to reduce the dislocation density and grain size).

These processes are temperature and strain-rate dependent: with decreasing strain rate, the grain boundary migration becomes increasingly dominant.

Figure 4 shows the observed overall rheological behaviour that adds to the understanding of the underlying micro-mechanical mechanisms of deformation. We find that plastic deformation is accommodated by a combination of processes and by the dynamic competition between these processes. At different stages of deformation (marked as stages I, II, II and IV in Fig. 2-4), some of the mechanisms become more dominant. For example, the dislocation-related hardening at earlier stages is followed by weakening due to recrystallisation by heterogeneous nucleation and grain boundary migration. At later stages (larger strains), near-steady state rheology is reached - accompanied by equilibrium texture and grain size.

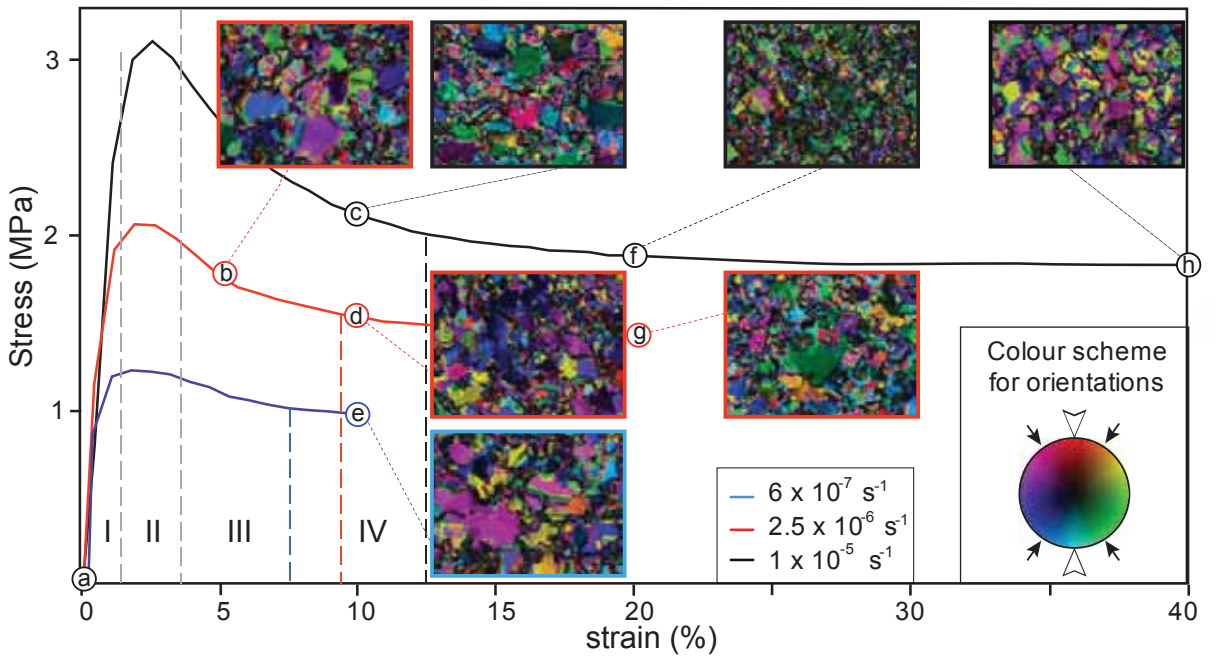

Figure 4
Rheological behaviour (strain-stress curves) and microstructures obtained through the analysis of thin (~250 µm) ice sections cut parallel to the compression axis. Images were obtained using a Fabric Analyser/ Microscope with a 5 µm resolution. The width of each image is 4.8 mm. Using optical Fabric Analyser only the ice *c*-axis direction at each pixel can be determined. The different colours indicate different c-axis directions in respect to the compression axis and arrows indicate the position of the girdle at 35-40°.

Conclusion

Studying these rheological features of ice deformation combined with neutron diffraction techniques we are able to provide results that can now be incorporated into modelling of ice mass rheological behaviour. Clearly, this will be important for problems such as modelling glacier movement, the prediction of sea level rise and ultimately understanding climate change.

REFERENCE

[1] Kirstein O., Luzin V., and Garbe U. (2009). The Strain-Scanning Diffractometer Kowari, *Neutron News*, 20(4), 34-36

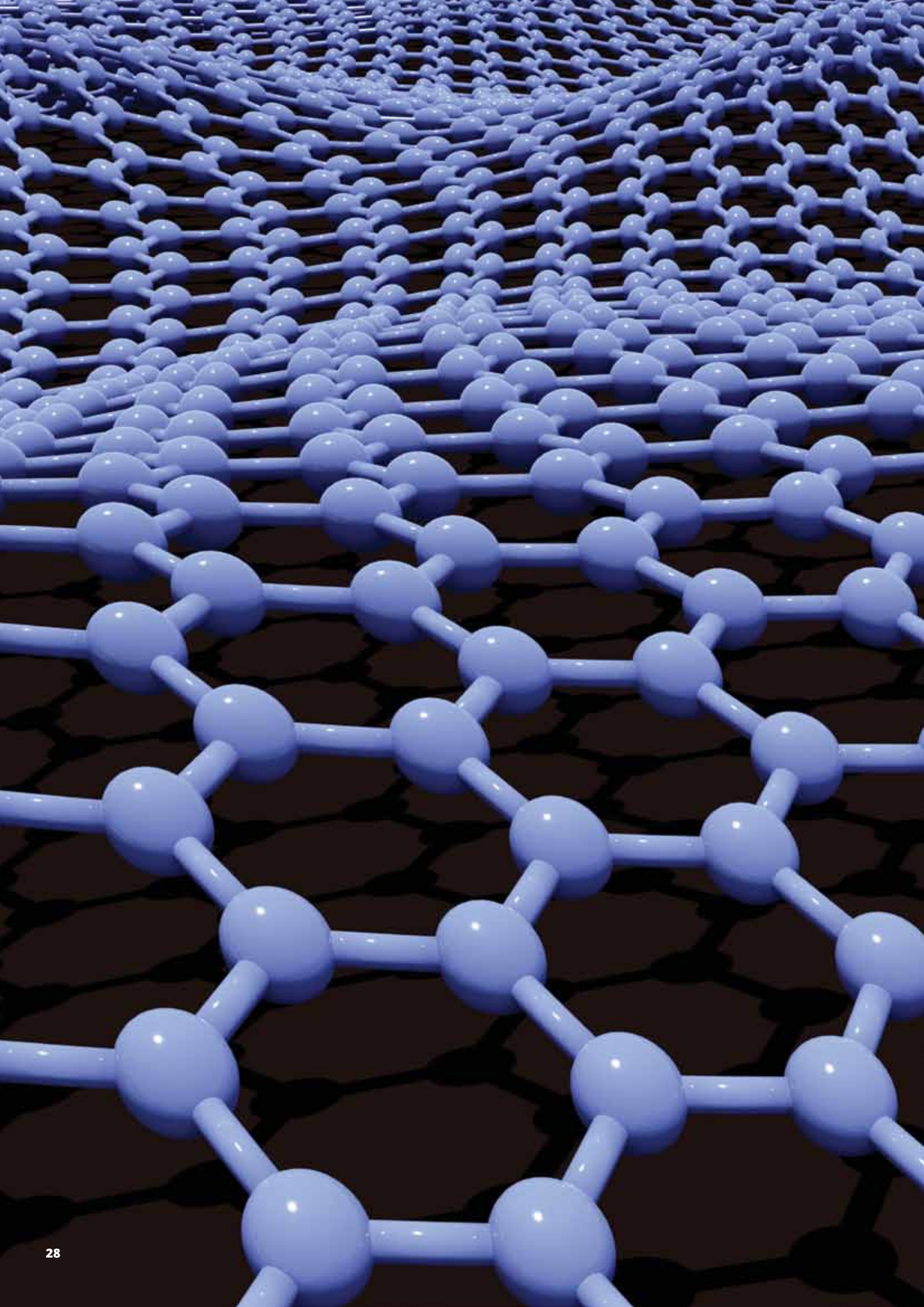

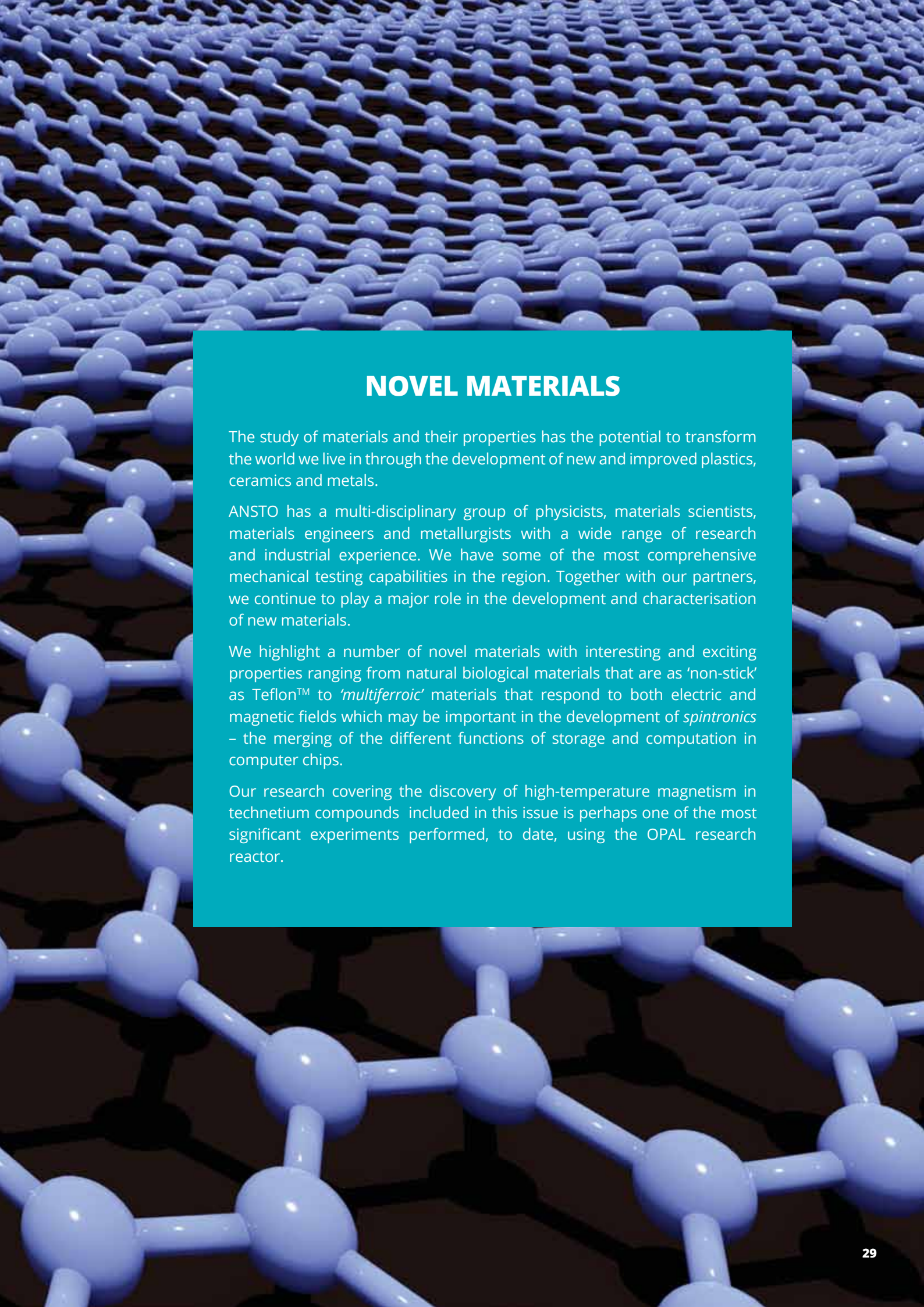

NOVEL MATERIALS

The study of materials and their properties has the potential to transform the world we live in through the development of new and improved plastics, ceramics and metals.

ANSTO has a multi-disciplinary group of physicists, materials scientists, materials engineers and metallurgists with a wide range of research and industrial experience. We have some of the most comprehensive mechanical testing capabilities in the region. Together with our partners, we continue to play a major role in the development and characterisation of new materials.

We highlight a number of novel materials with interesting and exciting properties ranging from natural biological materials that are as 'non-stick' as Teflon™ to *'multiferroic'* materials that respond to both electric and magnetic fields which may be important in the development of *spintronics* – the merging of the different functions of storage and computation in computer chips.

Our research covering the discovery of high-temperature magnetism in technetium compounds included in this issue is perhaps one of the most significant experiments performed, to date, using the OPAL research reactor.

ANSTO's (L-R) Anthony Duff, Karyn Wilde and Peter Holden in the National Deuteration Facility laboratory.

Study aids development of antifungal agents

01

Fungal spore amyloid protein, hydrophobin, is interesting because of its strong water-resistance and highly robust properties. This study investigated hydrophobin's protein coat as there is an interest in these materials in respect to their ability to self-assemble into a robust surface layer.

Understanding the structure of this fungal spore will be useful for the design of antifungal agents such as antifungal creams or other medications.

This collaborative study between ANSTO, the Universities of Sydney and New South Wales and the Harvard Medical School is the first study of its type and has pointed the way for further exploration of this material and its potential uses.

Vanessa K. Morris[1], Rasmus Linser[2], Karyn L. Wilde[3], Anthony P. Duff[3], Margaret Sunde[1], Ann H. Kwan[1]

[1]School of Medical Sciences and School of Molecular Bioscience, University of Sydney
[2]School of Chemistry, University of New South Wales, and Harvard Medical School, USA, [3]ANSTO

The water-repellent protein – hydrophin EAS

In view of supporting the design of antifungal agents the authors studied the properties of the protein coat on a fungal spore. This coat is formed by a protein, named EAS, from *Neurospora crassa*, which is water-repellent, i.e. hydrophobic, and classified as a class I hydrophobin. EAS forms a layer with defined morphology that covers the spore surface, with a hydrophobic surface towards the air, and a hydrophilic surface towards the spore contents, and it serves many functional purposes. At microscopic resolution, the protein forms a structure of rodlets packed into a single-molecule thick layer as shown in Fig. 1. This layer is extremely robust, resistant to all, but the most acidic conditions, and is as hydrophobic as Teflon™ (see Fig. 2). The rodlets are insoluble and cannot be crystallised, and this severely limits the applicability of many methods to characterise them at a molecular level.

Sample preparation

The structures of the soluble form of EAS and a functional truncated variant, $EAS_{\Delta 15}$, were previously determined by solution Nuclear Magnetic Resonance (NMR) spectroscopy. The structures display a β-sheet topology characteristic to hydrophobins as can be seen in Fig. 2 [1]. The surface exhibits a clear separation of charged and hydrophobic amino acid residues that makes the proteins highly amphipathic and surface-active, illustrated in Fig.3.

The samples studied were produced by standard recombinant methods using laboratory strain E. coli. These recombinant proteins were verified as having the same functional characteristics as the native proteins, including the ability to spontaneously assemble into rodlet monolayers at hydrophobic–hydrophilic interfaces with the same regular, well-packed morphology as is observed on fungal spores and the same ability to reverse the wettability of surfaces.

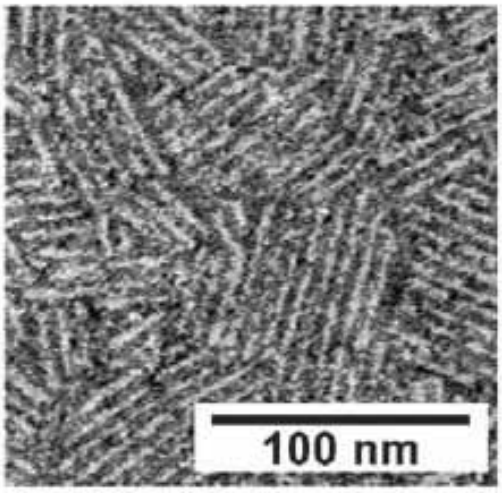

< Figure 1
Negatively stained transmission electronmicrograph of EASD15 rodlets.

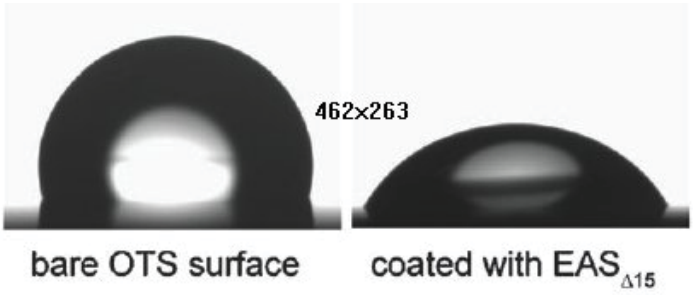

< Figure 2
Water droplets on bare octadecyltrichlorosilane (OTS)-treated silicon wafer and on $EAS_{\Delta 15\text{-coated}}$ OTS-treated silicon wafer layer.

Due to the insoluble and non-crystalline nature of the rodlets, solid-state NMR spectroscopy is the method of choice for studying the underlying molecular structure at atomic resolution. The method observes local atomic order within a sample without long-range order.

To increase the informative signal and resolution in the NMR spectra, the samples were prepared using either double isotopic labelling with the stable isotopes carbon-13 and nitrogen-15, or triple isotopic labelling with the additional stable isotope hydrogen-2. Hydrogen-2 (also called deuterium) labelling serves to reduce signal loss arising from the otherwise very high natural abundance of hydrogen-1. Labelling with nitrogen-15 and carbon-13 enables the sample to be probed through these atom types and increases spectral resolution. Selective introduction of hydrogen-1 in the sample over a heavily hydrogen-2 labelled background allows detection of the sparse hydrogen-1 signals which are otherwise impossible to be observed. High yield and efficient labelling of the samples was obtained through the National Deuteration Facility at ANSTO, which has developed methods specifically for isotopic substitution in proteins.

The measurements

A number of solid-state NMR spectra were recorded on the double- and triple-labelled samples. Specifically, the nitrogen-15/hydrogen-1 correlation spectrum recorded on $EAS_{\Delta 15}$ rodlets shows that a subset of signals stands out against a broad and poorly defined bulk. These observations suggest that the $EAS_{\Delta 15}$ rodlets have a twofold molecular composition, with a structurally conserved and tightly packed core giving rise to the well-defined signals, among a heterogeneous ensemble of disordered regions giving rise to the broad signals. Significantly, a comparison of this nitrogen-15/hydrogen-1 spectrum and a comparable solution spectrum recorded on EAS monomers reveals the protein fold has substantially altered upon rodlet formation. In particular, the solid-state $EAS_{\Delta 15}$ rodlet spectrum includes new signals from the amino acids glutamine or asparagine. These amino acid types are commonly found to be well-ordered in amyloid structures and have been implicated in strengthening the structure [2].

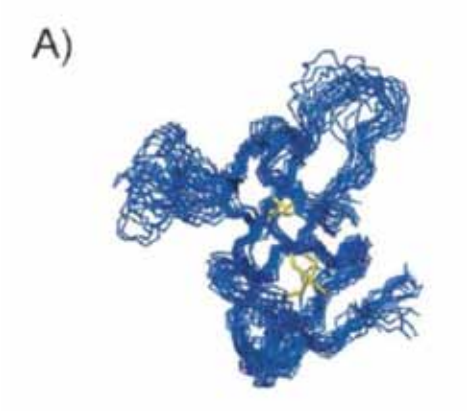

< Figure 3
Overlay of the 20 lowest energy structures of monomeric $EAS_{\Delta 15}$ (protein database code 2k6a).

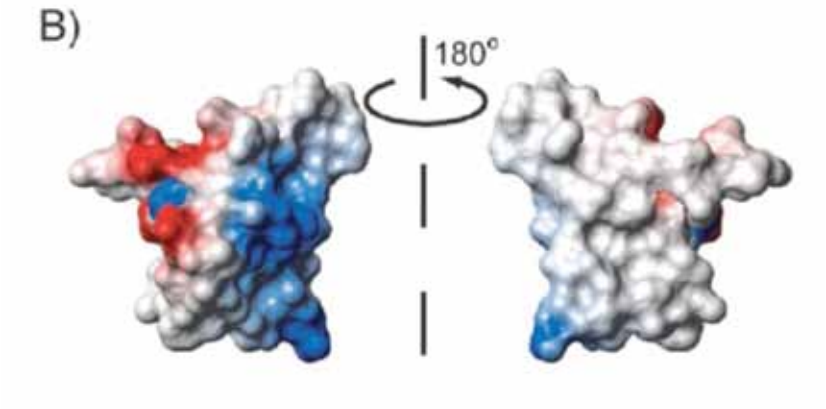

< Figure 4
Electrostatic surface of monomeric $EAS_{\Delta 15}$ showing positive charge in blue, and negative charge in red, and uncharged areas are white/uncoloured. The image shows strong charge variation on one side, and nearly no charge on the other side. This causes the first side to be highly hydrophilic, and is consistent with the second side being hydrophobic.

Identifying the structure

Despite significant disorder in the samples, signals from 18 amino acid residues could be identified in the carbon-13/carbon-13 correlation spectrum recorded on the double-labelled rodlets. The positions of these signals were indicative of ordered β-sheet structure. This ordered core β-sheet structure is known to be typical of amyloid structures, but the solid-state NMR data obtained here gives direct experimental evidence that this ordered β-sheet structure is new and is formed after substantial structural changes in the monomer, consistent with the hypothetical model [3,4].

In the final model, it is concluded that the rodlets are built upon a defined β-sheet core, with the remainder of the protein accommodated in many possible ways that does not affect the larger-scale rodlet-rodlet lateral packing or the overall amphipathicity of the monolayer. The structural heterogeneity of the non-β-sheet core may offer additional functionalities and exploration of these possibilities remains part of ongoing research.

REFERENCES

[1] A. H. Kwan, I. Macindoe, P. V. Vukasin, V. K. Morris, I. Kass, R. Gupte, A. E. Mark, M. D. Templeton, J. P. Mackay, M. Sunde, J. Mol. Biol. (2008), 382, 708 – 720.

[2] M. S. Dueholm, S. V. Petersen, M. Sonderkaer, P. Larsen, G. Christiansen, K. L. Hein, J. J. Enghild, J. L. Nielsen, K. L. Nielsen, P. H. Nielsen, D. E. Otzen, Mol. Microbiol. (2010), 77, 1009 – 1020.

[3] J. P. Mackay, J. M. Matthews, R. D. Winefield, L. G. Mackay, R. G. Haverkamp, M. D. Templeton, Structure (2001), 9, 83 – 91;

[4] A. H. Y. Kwan, R. D. Winefield, M. Sunde, J. M. Matthews, R. G. Haverkamp, M. D. Templeton, J. P. Mackay, Proc. Natl. Acad. Sci. USA (2006), 103, 3621 – 3626.

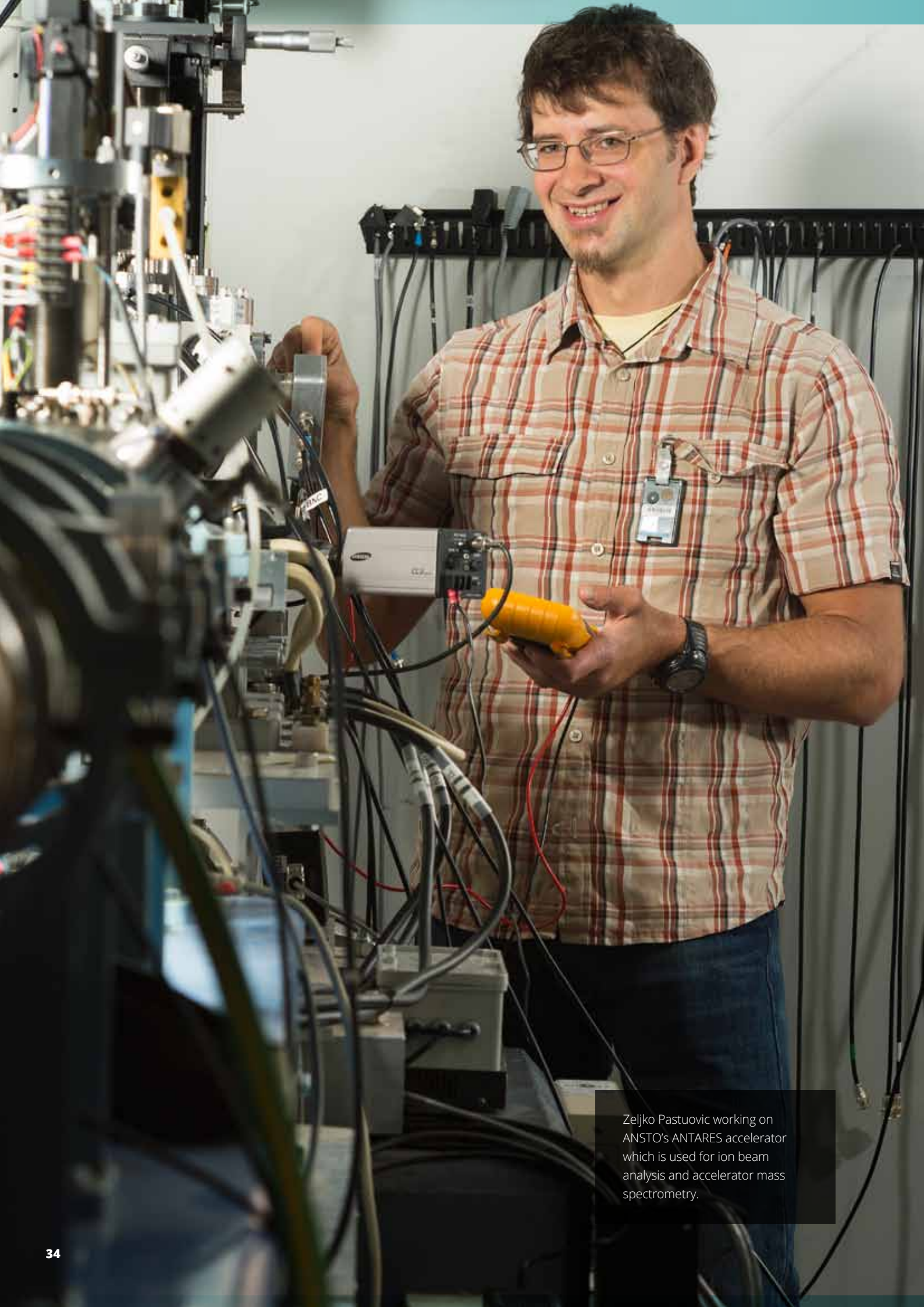

Zeljko Pastuovic working on ANSTO's ANTARES accelerator which is used for ion beam analysis and accelerator mass spectrometry.

Developing electronic devices capable of withstanding harsh radiation

02

Studies performed by Zeljko Pastuovic at ANSTO's microprobe facility, in collaboration with a team of international researchers, are helping to understand, model and predict the detrimental influence of ionising radiation on semiconducting materials required in millions of electronic devices. The research aims to develop materials and devices that are able to better withstand the damaging effects of high energy particles present in harsh radiation environments, such as solar cells, and power satellites in space, as well as materials used in high-energy physics and accelerators. These studies will help semiconductor, aerospace and other industries to better understand and extend the life of electronic devices.

Zeljko Pastuovic[1], Ettore Vittone[2], Rainer Siegele[1], Ivana Capan[3], Gyorgy Vizkelethy[4], David Cohen[1], Milko Jaksic[3]

[1]ANSTO, [2]University of Torino, Italy, [3]Ruđer Bošković Institute, Zagreb, Croatia, [4]SANDIA, Albuquerque, USA

Low-level radiation damage in semiconductor devices

It is known that the electronic and spectroscopic performances of semiconductor devices and detectors progressively degrade during the exposure to ionising radiation. Understanding of the mechanisms underlying the material damage induced by ionising radiation is fundamental to evaluate the lifetime of electronic devices in high radiation environments (e.g. solar cells in space radiation environments or radioisotope-power voltaic cells).

The new model for interpretation of radiation damage data offers criteria for the identification of radiation resistant semiconductor materials. These criteria or set of parameters are the property of material, independent of the experimental conditions (i.e. the type of ionising radiation used for both damage production and testing).

Emphasis is given to the "single ion" implantation at ANSTO, studies of defects produced in the single heavy ion cascade, and the ion-beam induced charge (IBIC) detection technique [1] for electronic microstructures and radiation damage characterisation. The presented experimental protocol and robust theoretical model (valid in a low-level damage approximation–well below the amorphisation threshold value) provide a tool for the radiation hardness testing and comparison of materials used for semiconducting device fabrication.

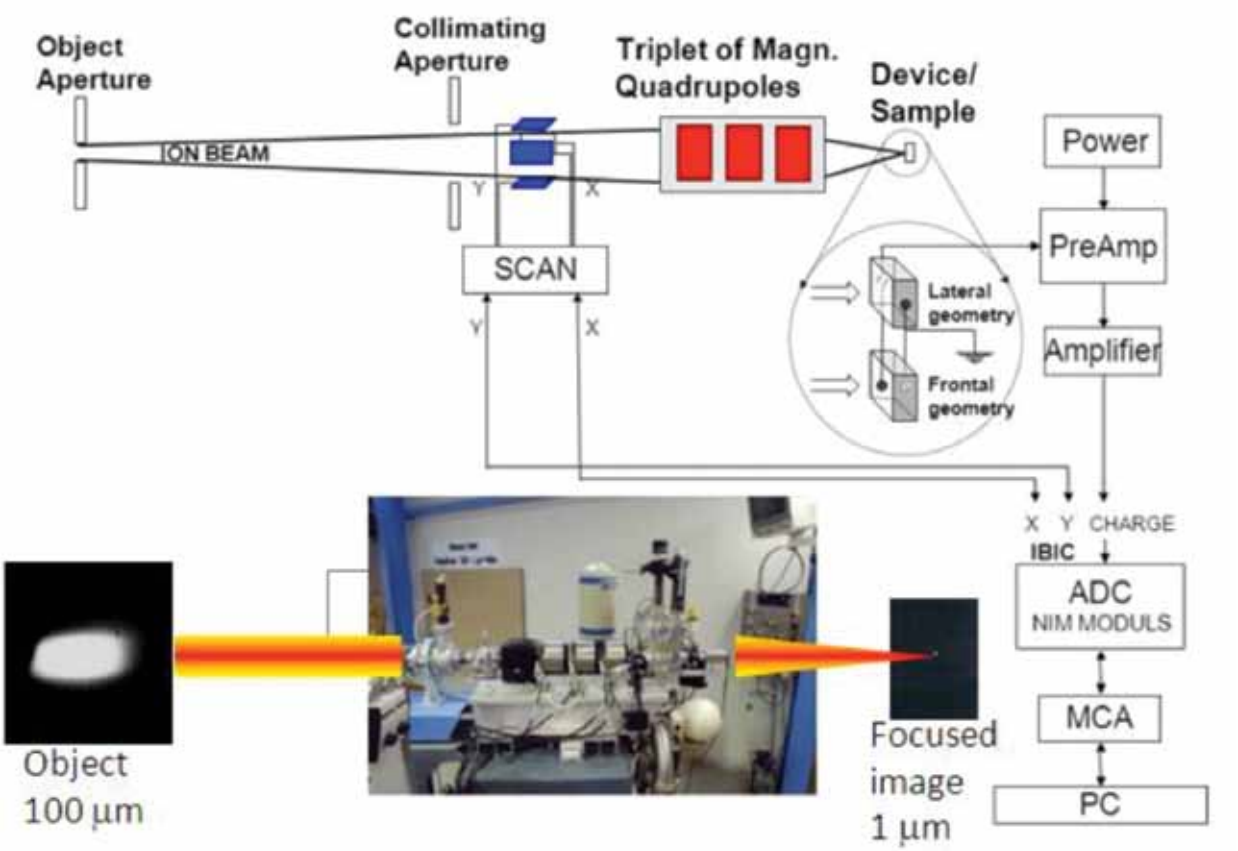

Figure 1

The schematics of the ANTARES microprobe setup including the ion-beam focusing system, microbeam raster scanning control system and data-acquisition system as used for ion implantation and materials characterisation.

Single heavy ion implantation tool at ANSTO

The ANTARES microprobe shown in Fig. 1, is a unique experimental tool which is capable of delivering a beam of fast ions, with energies per unit mass in the 0.1-1.0 MeV/u range, of majority elements from the periodic table up to Pb with a magnetic rigidity $ME/q2<150$ MeV/e^2 (M = ion mass, E = ion energy and q = ion charge) focused down to a micrometre size. Because of such high rigidity value, a great variety of ion species can be implanted through surface layers into the bulk of materials, i.e. the implantation at a required 3D position in testing devices, well below surface layers, up to tens or even hundred of microns deep. The microbeam scanning pattern is computer controlled via a data-acquisition system. The total implanted fluence (ion dose) depends on: i) microbeam current (particle rate), ii) scanning frequency (microbeam "dwell time" per pixel), iii) pixel size, and iv) number of scans. The particle rate can be varied from single ions to 1011 ions per second according to experimental requirements.

Simulating the induced defects

Considering heavy-charged particles only (hadrons and ions), the main cause of device degradation is the formation of electrically active defects following the displacement of atoms from their sites in the lattice, due both to the collisions of the primary irradiating particle with lattice atoms and to the recoil cascade. Vacancies are subsequently formed if the kinetic energy imparted by these collisions overcomes the threshold energy value (named displacement energy E_d) required to displace a target atom to more than one atomic spacing away from its original site. A simulation of the spatial distribution of generated vacancies along cascades of five individual Si ions implanted in silicon during one single "dwell time" interval irradiation of a single pixel area calculated by the Monte Carlo SRIM2013 code [2], shown in Fig. 2. The spatial distribution of stable defect species in the semiconductor material created by ionising radiation can be assumed to be proportional to the initial vacancy distribution generated by ionising radiation in the first approximation, i.e. when the total induced defect concentration is well below the material amorphisation threshold value and subsequent processes of the vacancy recombination, defect clustering, and

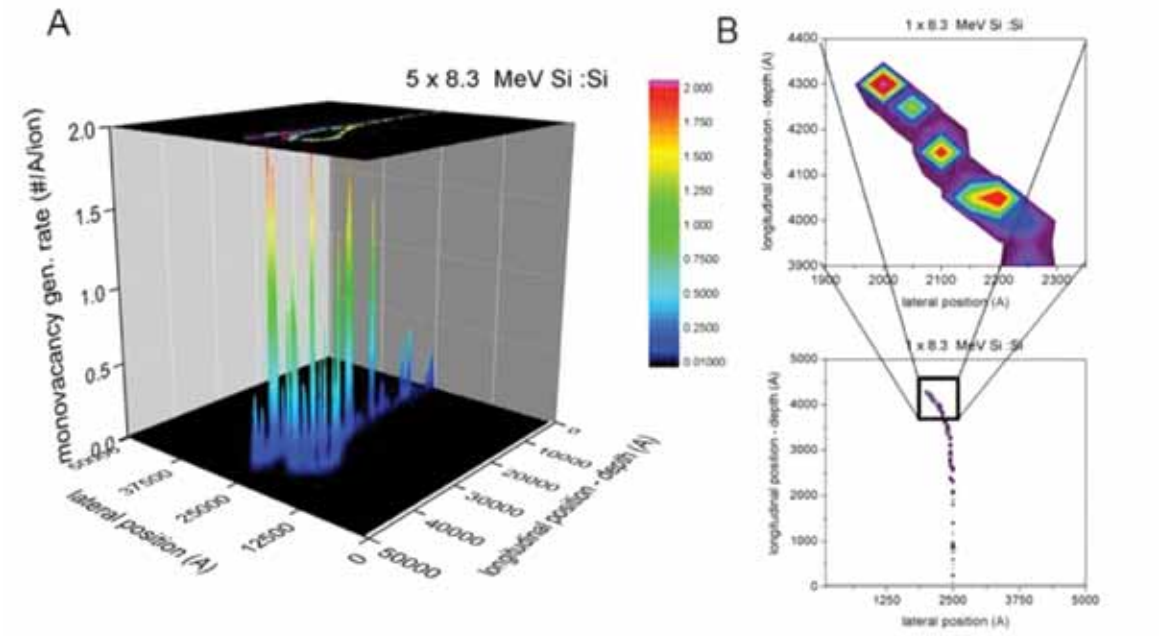

Figure 2

Monte-Carlo SRIM simulation for the high energy heavy Si ions implantation in a silicon crystal matrix: A) the cumulative vacancy concentration distribution originating from five different negligible overlapping ion-projectile cascades corresponding to irradiation during each interval known as "dwell time" a microbeam spends at a position of every pixel before moving to another adjacent pixel; B) the surface projection of one typical cascade showing extent of the disordered region of approximately 100 nm across is shown in more detail identifying positions of increased vacancy concentration as regions of increased probability for subsequent vacancy-related defect formation.

lattice relaxation are neglected. In that particular case, the most important effect induced by displacement damage in a semiconductor material is an increase of the non-equilibrium carrier trapping / recombination / generation rate. In a depleted region, such as the active region of a semiconductor detector is, the defects capture free charge carriers of either sign as they pass through, resulting in incomplete charge collection.

Characterisation of defects

Deep-level transient spectroscopy (DLTS) has been used to study vacancy-related defects formed in bulk silicon after implantation of silicon ions at room temperature. For this study, Schottky diodes (diodes with low forward voltage drop and a very fast switching action) prepared from specially grown, i.e. n-type Czohralski-grown, silicon wafers have been irradiated by the focused ion beam with a 0.1 μA/cm^2 particle current density and up to a fluence value of 10^{10} cm^{-2}. Depth profiling of implanted silicon layer was performed by means of DLTS at two different voltage settings. Differential DLTS analysis of the vacancy-rich region in self-implanted silicon reveals the formation of broad vacancy-related defect state(s) at E_c –0.4 eV, E_1 is shown in Fig. 3. Direct measurement of the electron capture cross-section associated with these states at E_c –0.4 eV, prior to any annealing, does not show the exponential behaviour typical for simple point defects. The logarithmic capture kinetics is in accordance with the theory of majority carrier capture at extended or cluster-related defects. Our DLTS results suggest that small clusters of V_2 (–/0) defects with activation energy close to E_c –0.4 eV are created in the highly disordered regions of silicon before any annealing. Complete suppression of the VO and V_2(=/–) states in DLTS results is explained according to the model of local compensation of the carrier concentration in highly disordered regions located within the ion cascade region [3]. We have also detected formation of two deep electron traps at E_c –0.56 eV (E_2) and E_c –0.61 eV (E_3) in the interstitial-rich region, before any annealing.

Charge collection efficiency analysis and modelling

The degradation of the charge-collection efficiency (CCE) of a semiconductor detector due to the damage induced by ions of different mass and energy can be interpreted on the basis of a simplified theory of the IBIC technique [1] and the Shockley-Read-Hall theory [4]. The new model,

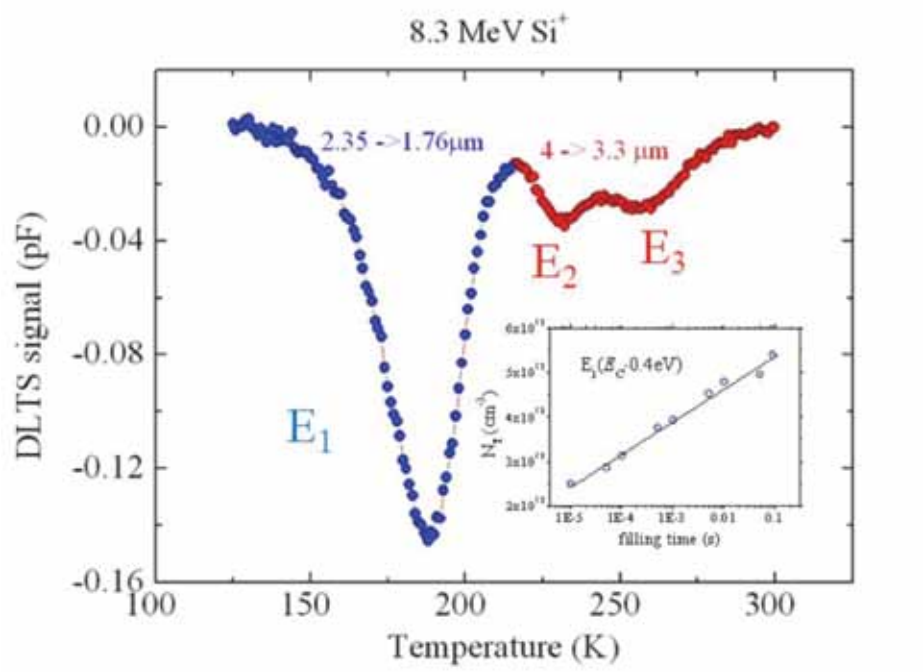

Figure 3

Three deep defect states created following individual Si ion implantation of the low *n*-type doped Czochralski grown silicon are identified by differential deep-level transient spectroscopy, DLTS, analysis of vacancy-rich (blue circles) and interstitial-rich (red circles). The inset figure shows the results of carrier capture cross-section analysis determining the majority of created stable di-vacancy V_2 point defects are actually not separated individual point defects but small clusters of gathered point defects.

based on the previous model we developed [5], leads to the definition of "*effective fluence*" Φ*. The parameter *effective fluence* involves vacancy and ionisation profiles extracted from the SRIM or similar codes, as well as the transport properties of charge carriers generated in active region of semiconducting device. The most notable advantage of the proposed approach to modelling the CCE degradation (i.e. particle induced radiation damage) as a function of the new parameter *effective fluence* is independent of the ion type and energy. It can be numerically calculated in the low damage regime. Fig. 4 illustrates that the slope of the CCE degradation as function of Φ*, i.e. the effective damage factor *k**, is proportional to the fraction of the electrically active trap per vacancy generated. This parameter can be considered an index that would reliably rank the relative radiation hardness of semiconductors in order to optimise the selection procedure for devices working in high radiation environment. Our approach has proved to be more efficient to condense the CCE degradation data into a single curve than the phenomenological displacement damage dose analysis [6], whose NIEL (Non Ionizing Energy Loss) scaling (i.e. the comparison of the total deposited energy for displacement of target atoms by different ions or any other particle creating damage, e.g. pions, neutrons, electrons etc.), was proven to be valid only in the case of constant vacancy profile across the whole region of interest of the semiconducting device [7].

Implications for the development of future devices

The most important outcomes of our radiation hardness studies on simple silicon diodes are:

1. The experimental protocol which requires focused ion beams with different masses and energies is, in principle, suitable to be applied to any semiconductor device.

2. The interpretative model requires the output of SRIM, charge carrier capture cross-sections for traps which are identified by DLTS analysis and the knowledge of the electrical features of the devices (mainly weighting potentials and drift velocities).

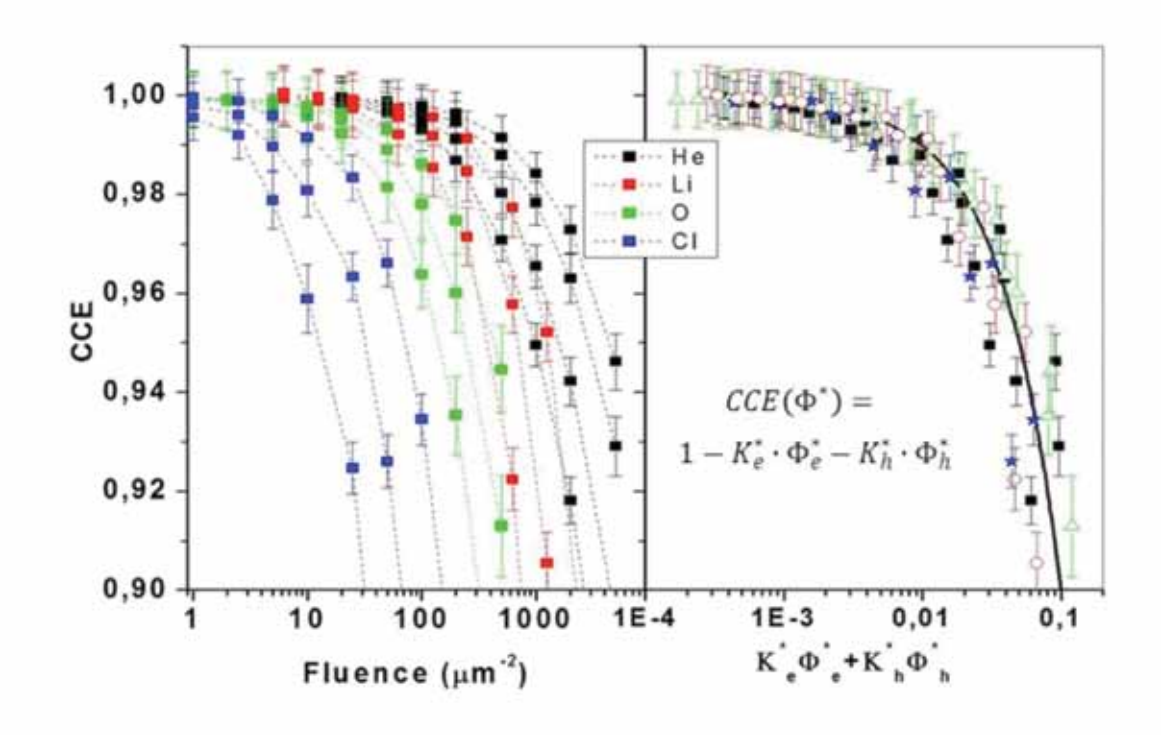

Figure 4

Measured charge-collection efficiency, CCE, values (symbols) and parabolic interpolation (lines) for 1.4 MeV He ion detection in selected areas of biased silicon diodes irradiated with different fluences of several damaging particles (1.4 MeV He, 2.15 MeV Li , 4.0 MeV O and 11 MeV Cl). The left panel shows the commonly used presentation of CCE values as a function of fluence, whereas in the right panel, the same measured CCE values are presented as a function of the *effective* fluence value, which is the output of our theoretical modelling – condensation of the ion-beam induced charge, IBIC, data presented in the framework of the new IBIC model is clearly obvious.

3. The output of these analyses is the evaluation of the k_e and k_h factors, i.e. the number of active electrical traps formed per single vacancy initially created. These factors can be considered as fingerprints of the semiconductor material radiation hardness.

All presented results might have significant implications for development of future radiation-hard materials and devices, particle detection and microdosimetry.

Acknowledgments

We would like to acknowledge the support of the ANSTO Accelerator Science Project, the EU FP7 projects: Particle Detectors, SPIRIT and ENSAR, and the IAEA CRP#11016.

REFERENCES

[1] M.B.H. Breese, E. Vittone, G. Vizkelethy, P.J. Sellin, Nucl. Instrum. Methods Phys. Res. B 264, 345 (2007).

[2] http://www.srim.org

[3] E.V. Monakhov, J. Wong-Leung, A. Yu. Kuznetsov, C. Jagadish, B.G. Svensson, Phys. Rev. B 65, 245201 (2002).

[4] S.M. Sze, Physics of Semiconductor Devices, 2nd Edition, Wiley, New York 1981.

[5] Z. Pastuovic, E. Vittone, I. Capan, M. Jaksic, Appl. Phys. Lett. 98 091201 (2011).

[6] S.R. Messenger, E.A. Burke, G.P. Summers, M.A. Xapsos, R.J. Walters, E.M. Jackson, B.D. Weaver, IEEE Trans. Nucl. Sci. 46, No.6, 1595 (1999).

[7] Z. Pastuovic, M. Jaksic, G. Kalinka, M. Novak, A. Simon, IEEE Trans. Nucl. Sci. 56, No.4, 2467 (2009).

James Hester and Annemieke Mulders setting up an experiment at ANSTO's high-intensity powder diffractometer, Wombat.

Deeper understanding paves the way for high performing information technologies

03

Magnetic and ferroelectric materials are essential components in dozens of electronic devices and machines we use every day – but some of the mechanisms underlying their behaviour are not well understood. This study by ANSTO's James Hester and his colleagues is aimed at better understanding these mechanisms, and subsequently developing higher-performing and more capable information technologies.

Magnets are used in components ranging from speakers, electric motors and some power plugs through to computer hard drives and automatic teller machine cards. Ferroelectric materials are not only used in some types of Random Access Memory (RAM) devices and in Radio Frequency Identification (RFID) equipment, but also for electronic toll collections on toll roads, security and access management systems and for tracking goods and animals.

Magnetic materials respond to changes in an applied magnetic field. These changes are usually 'remembered' after the field has been turned off. Similarly, ferroelectric materials have a spontaneous electric polarisation that can be reversed by applying an external electric field, and the new polarisation remains when the electric field is removed.

Magnetism and ferroelectricity are usually mutually exclusive, but there is a handful of materials that are known to possess both magnetic and ferroelectric properties – they are called 'multiferroic'. Multiferroic materials have the potential to be extremely useful, for example, in the control of the magnetic components in memory-storage devices through electric manipulation, which provides faster storage and retrieval of information.

Annemieke Mulders[1], Maciej Bartkowiak[1], James Hester[2], Ekaterina Pomjakushina[3], Kazimierz Conder[3]

[1] University of New South Wales, Canberra, [2] ANSTO, [3] Paul Scherrer Institute, Switzerland

Frustrated charges

Rather than arising from covalent bonding between ions, ferroelectric polarisation may instead arise from frustrated charge order, as reported for $LuFe_2O_4$. This compound is of particular interest as the magnetism originates from the same Fe ions as the ferroelectricity, suggesting that there will be strong magneto electric coupling. In addition, both ferroelectric and magnetic ordering take place at or near ambient temperature, opening the way to room-temperature applications.

$LuFe_2O_4$ forms a series of stacked Fe-containing bilayers (Fig. 1). Charge ordering occurs when the valence of each Fe ion forms a regular pattern, as indicated by the red Fe^{3+} and blue Fe^{2+} atoms in the figure. This charge order results in a net polarisation of the bilayer along both the [110] (diagonal within the layer) and [001] directions (perpendicular to the layers). The purple arrows indicate the magnetic moments of the iron ions. These bilayers are stacked parallel or antiparallel along the c-axis to form a ferroelectric or antiferroelectric alignment.

Long-range magnetic order is signalled by the appearance of peaks in neutron diffraction patterns, and intensity changes in these peaks give insight

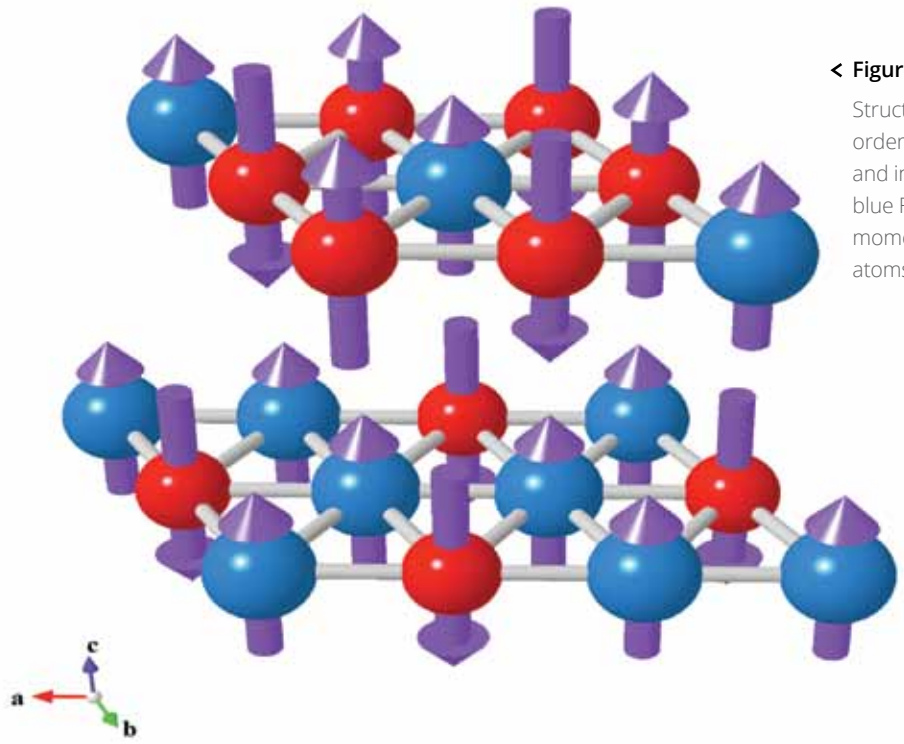

< Figure 1

Structure of $LuFe_2O_4$ [3] in the charge-ordered state showing the FeO_5 bilayer and indicating small red Fe^{3+} and large blue Fe^{2+} ions, with purple magnetic moments of 5 μB and 4 μB. The oxygen atoms are omitted for the sake of clarity.

into the nature of the ordering. The magnetic order in a single crystal of $LuFe_2O_4$ was therefore investigated using the Wombat high-intensity neutron diffractometer [1] at ANSTO in single-crystal mode. A change in the magnetic long-range order was observed when an applied electric field was present while cooling through the magnetic-ordering temperature [2]. Fig.2 shows that the long-range charge order that is promoted by the electric field is stabilised by the magnetic order, as demonstrated by the increased intensity of all magnetic domains.

A possible mechanism for stabilisation of the magnetic order

It is proposed that antiferromagnetic order in the Fe bilayers facilitates the formation of long-range charge order because electron hopping between the sheets of the bilayer is assisted by the alignment of the Fe^{2+} and Fe^{3+} spins. According to Hund's rules for determining the distribution of electron spins between available orbitals, all the available orbitals should be populated by single electrons with the same spin before any opposite spin electrons are added. Therefore, Fe^{3+} has five 3*d* electrons with spin up, and Fe^{2+} has five 3*d* electrons with spin up and one with spin down. This latter spin down electron can jump from Fe^{2+} to the Fe^{3+} much more easily if the spin-down states of the latter are empty. This is the case for parallel alignment of the Fe^{2+} and Fe^{3+} moments. Thus, electron hopping in the majority Fe^{2+} layer is arrested, because the Fe^{2+} and Fe^{3+} ions have opposite moments, while 3*d* electron hopping is promoted in the minority Fe^{2+} layer because some neighbouring Fe^{2+} and Fe^{3+} ions have parallel moments (double-exchange mechanism). This creates a convenient mechanism to switch between ferroelectric and antiferroelectric arrangements of the bilayers. As such, the magnetism assists the ferroelectric order to align with the electric field and enhance the electric polarisation.

Future perspectives

This work has led to a constructive hypothesis regarding stabilisation of ferroelectric ordering in multiferroic materials. The essential ingredients in such a scheme are a mixed-valence ion with partially filled orbitals; a structure in which these ions are distributed in hexagonal bilayers; and sufficient

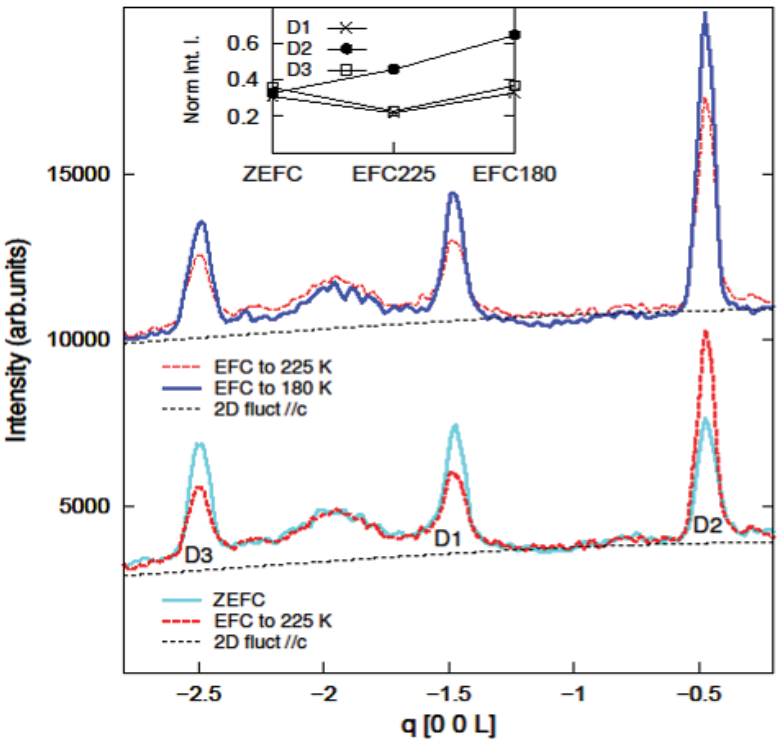

< Figure 2

Neutron intensity recorded along the (1/3 1/3 L) direction at T = 180 K, as a function of the electric-field-cooling (EFC) procedure. The magnetic state obtained after electric-field-cooling to 225 K is compared to the magnetic state obtained after zero-electric-field-cooling (ZEFC) (bottom) and to the magnetic state obtained after electric-field-cooling to 180 K (top, shifted for clarity). The black dotted line indicates 2-dimensional magnetic order in the a-b plane, with moments along the c-axis. The inset shows the integrated intensity, normalised to the total intensity at zero-electric-field-cooling, as a function of the electric-field-cooling sequence.

interaction between the ions to allow electron hopping. Materials synthesis informed by this scheme will potentially lead to multiferroics with desirable properties, including devices that are switchable at ambient temperatures.

REFERENCES:

[1] http://www.ansto.gov.au/research/bragg_institute/facilities/instruments/wombat

[2] A. M. Mulders, M. Bartkowiak, J. R. Hester, E. Pomjakushina, and K. Conder, *Phys. Rev.* B 84, 140403(R) (2011).

[3] K. Momma and F. Izumi, *J. Appl. Crystallogr*. 41, 653 (2008).

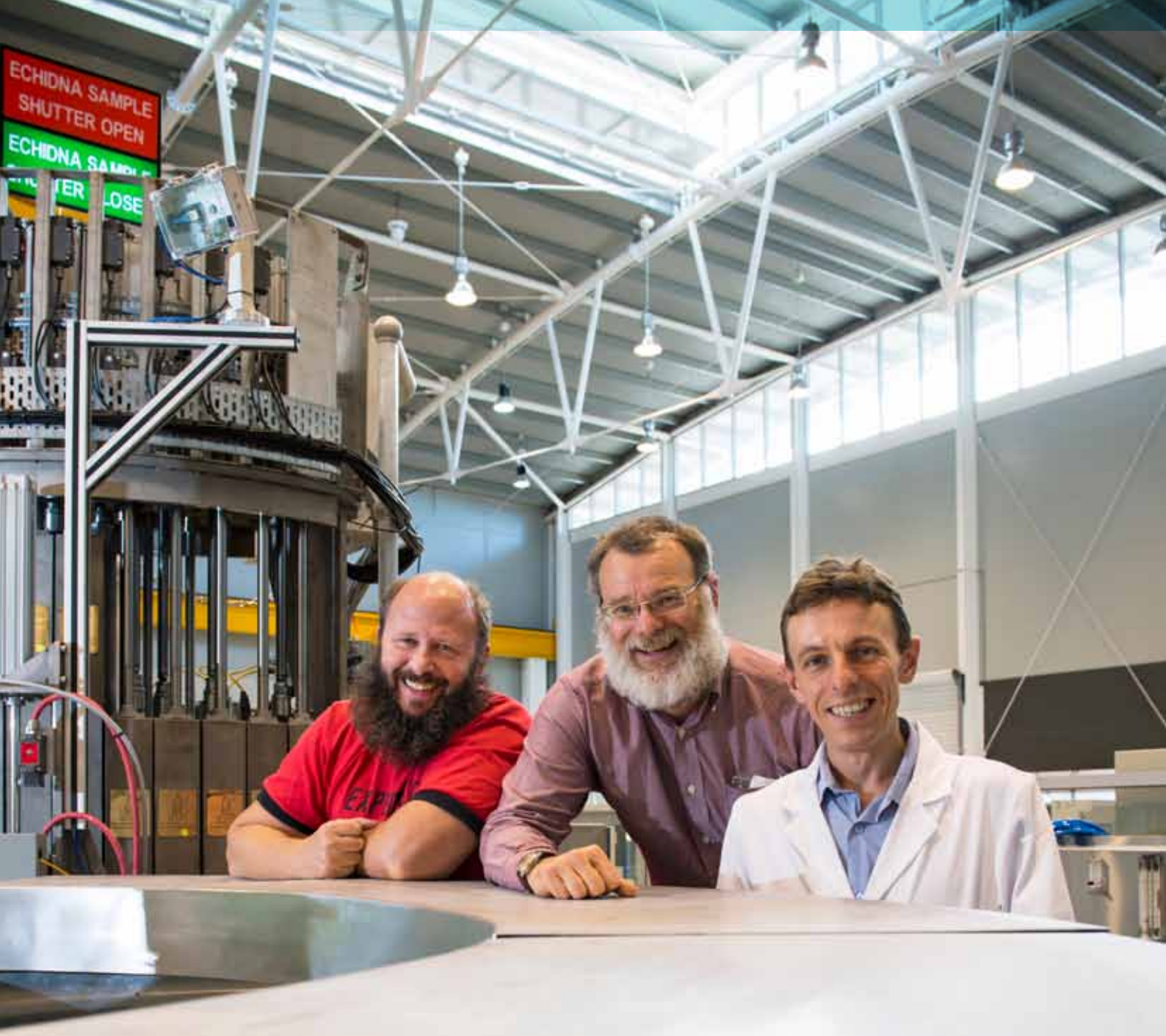

(L-R) Gordon Thorogood, Brendan J. Kennedy, and Max Avdeev next to ANSTO's high-resolution powder diffractometer, Echidna.

Studies to improve storage and immobilisation of nuclear waste

04

Technetium is a rare element that was discovered more than 80 years ago and is found on Earth in very few locations and at extremely low concentrations. It is the lightest element that does not have a stable (i.e. non-radioactive) isotope and for this reason the chemistry and physics of technetium-containing materials can be a challenging subject to study.

Technetium is the base material in one of the most widely used radiopharmaceuticals (nuclear medicines) used to diagnose heart disease, cancer and skeletal injuries but it also forms a critical part of the nuclear fuel cycle. Its presence in used fuel elements poses significant challenges in nuclear waste management.

ANSTO researchers and their colleagues discovered that ternary technetium oxides possess very unusual physical properties. Neutron diffraction studies at ANSTO's OPAL research reactor were used to shed light on the magnetic structure of technetium containing materials and provide essential information for further studies of magnetism in these technetium compounds.

The knowledge gained from this and subsequent studies will help researchers better understand the chemical and physical properties of technetium compounds, and thus open new ways to improving methods for storing and immobilising nuclear waste containing technetium.

G.J. Thorogood[1], B.J. Kennedy[2], M. Avdeev[1]

[1]ANSTO, [2]University of Sydney

Characteristics of technetium

Technetium is the lightest element, see Table 1, that does not have a stable isotope and can be found on Earth in extremely low concentrations only at the locations of natural nuclear reactors, such as Oklo in Africa [1]. Nevertheless, it occupies a central position in contemporary nuclear medicine, being one of the most commonly used radiopharmaceuticals. Technetium is also a critical part of the nuclear fuel cycle, and its presence in used fuel elements poses significant challenges in storage and immobilisation of nuclear waste.

Despite the obvious technological and economic importance of technetium, the progress in experimental research of its compounds has been slow in contrast to the neighbours in the Periodic Table. In particular, the oxides $SrMoO_3$ and $SrRuO_3$ have been extensively studied and both show unique electronic and magnetic properties. The conductivity of the former is amongst the highest of all metal oxides, and the latter is a rare example of a ferromagnetic 4d metal oxide. It might be expected, therefore, that $SrTcO_3$ shows unusual electronic and magnetic properties, but prior to this work just how unusual these were was unclear. These compounds are called 'perovskite' as they have a similar structure as the mineral $CaTiO_3$ (named after the Russian mineralogist Lev Perovski). The physical properties of perovskites are of interest in materials science due to their superconductivity, magnetoresistance, ionic conductivity, and a multitude of dielectric properties of importance in microelectronics and telecommunication.

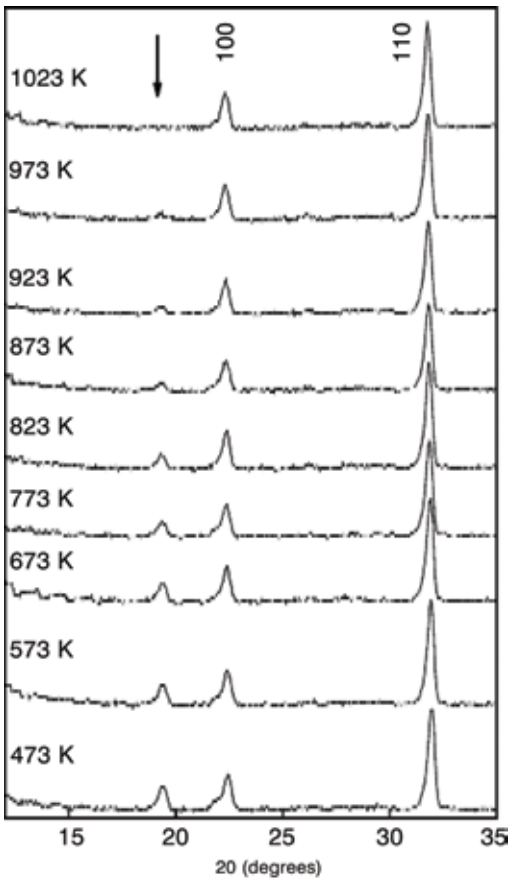

Chromium	Manganese	Iron
24	25	26
Cr	Mn	Fe
51.996	54.938	55.845(2)
Molybdenum	**Technetium**	**Ruthenium**
42	43	44
Mo	Tc	Ru
95.96(2)	[97.91]	101.07(2)
Tungsten	**Rhenium**	**Osmium**
74	75	76
W	Re	Os
183.84	186.21	190.23(3)

< Table 1

Technetium in the Periodic Table.

< Figure 1

Portions of the observed neutron patterns from $SrTcO_3$ (wavelength $\lambda = 1.538$Å) illustrating the evolution of the magnetic reflections. The variable-temperature neutron diffraction measurements established the temperature at which magnetic ordering is destroyed by thermal fluctuations (Néel temperature). The Néel temperature in excess of 1000 K is the highest for any metal oxide not containing a 3d transition metal.

Sample preparation

We prepared polycrystalline samples of the two perovskites $SrTcO_3$ and $CaTcO_3$ using the facilities at ANSTO's Institute for Materials Engineering. Subsequently, we performed neutron diffraction on the two oxides using the Echidna diffractometer [2] at the OPAL facility. Neutron diffraction has two advantages for this work, firstly it provides great sensitivity to the positions of the oxygen atoms, something that is essential to determine accurate and precise structures of these types of oxides; and secondly neutrons have their own magnetic moments and thus can be used to probe magnetic structures.

Structure determination

Neutron diffraction measurements (Fig. 1) of both samples showed magnetic ordering at room temperature. Analysis of the high-resolution neutron diffraction data revealed that $SrTcO_3$ adopts a distorted perovskite structure with G-type antiferromagnetic ordering, see Fig. 2 left structure.

Variable-temperature neutron-diffraction measurements where then performed to investigate the evolution of crystal structure on heating and establish the Néel temperature, i.e. the temperature at which magnetic ordering is destroyed by thermal fluctuations. These measurements demonstrated that $SrTcO_3$ is isostructural with $SrRuO_3$ and displays the same sequence of structures upon heating [3]. More remarkable was its Néel temperature, above 1000 K. This is the highest Neel temperature (T_N) for any metal oxide that does not contain a 3d transition metal.

Electronic structure calculations confirmed that the ground state corresponded to G-type antiferromagnetic and that the d-orbitals of Tc^{+4} are strongly hybridized with the p-orbitals of oxygen driving T_N up [4]. These calculations suggest that replacing Sr with Ca should result in a reduction in the Néel temperature. This was experimentally verified, using a combination of neutron and synchrotron X-ray diffraction data [5]. A significant difference between $CaTcO_3$ and $SrTcO_3$ was that the former displayed no crystallographic phase transitions upon heating, although evidence for magnetostriction was found (Fig. 3) at the Néel temperature of 800 K. Magnetostriction is a property of magnetic materials causing them to alter shape or dimensions during the magnetisation process, due to internal stresses. In this case, as the temperature rises and magnetisation is lost, the lattice parameters, and hence volume, return to the linear extrapolation.

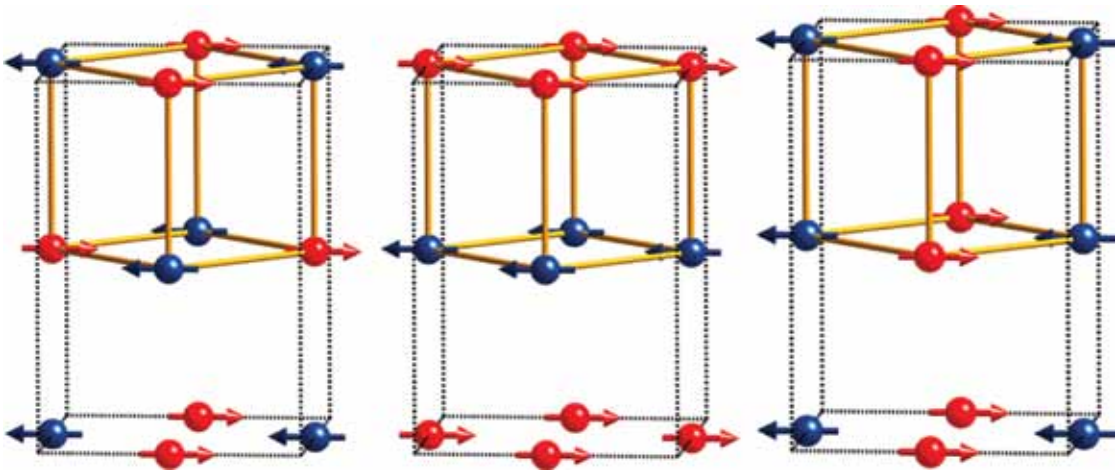

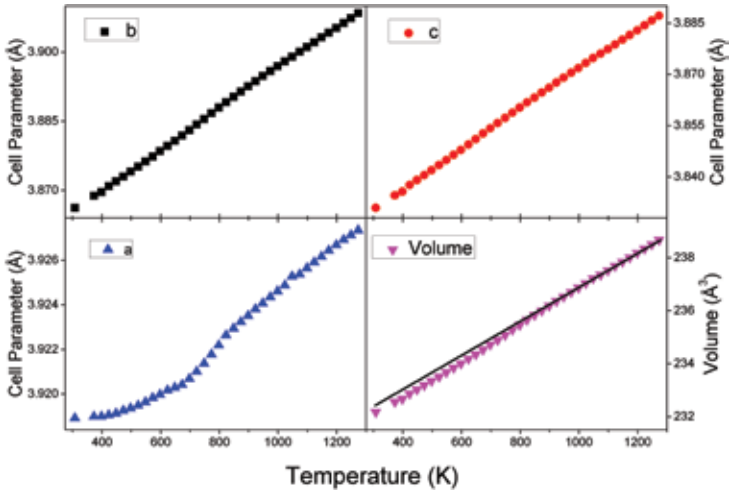

^ Figure 2

The magnetic structures tested against the neutron powder diffraction data collected for $SrTcO_3$. The leftmost model, G-type antiferromagnetic ordering, was found in the material.

< Figure 3

Temperature dependence of lattice parameters (a, b, c and the unit-cell volume) for $CaTcO_3$ from analysis of synchrotron X-ray diffraction data [5]. The solid line is a linear extrapolation of the high-temperature volume.

Our results

Using both neutron powder and synchrotron X-ray diffraction methods we have demonstrated that $SrTcO_3$ has a G-type antiferromagnetic structure with a Néel temperature above 1000 K, the highest for any metal oxide not containing a 3*d* transition metal. We have also shown that, by substituting Ca for Sr, the Néel temperature is lowered to 800 K with evidence for magnetostriction without a phase change as seen in the $SrTcO_3$. We now plan to study other Tc perovskites to see if they also have interesting magnetic properties, as well as other mechanisms for inducing magnetic properties in Tc materials.

REFERENCES

[1] Schwochau, K., *Technetium: chemistry and radiopharmaceutical applications*. John Wiley & Sons: (2000).

[2] K. D. Liss, B. Hunter, M. Hagen, T. Noakes, S. Kennedy, *Physica B-Condensed Matter* (2006), 385-86, 1010.

[3] Thorogood, G. J.; Avdeev, M.; Carter, M. L.; Kennedy, B. J.; Ting, J.; Wallwork, K. S., Structural phase transitions and magnetic order in $SrTcO_3$. *Dalton Transactions* (2011), 40 (27), 7228-7233.

[4] Rodriguez, E. E.; Poineau, F.; Llobet, A.; Kennedy, B. J.; Avdeev, M.; Thorogood, G. J.; Carter, M. L.; Seshadri, R.; Singh, D. J.; Cheetham, A. K., High Temperature Magnetic Ordering in the 4d Perovskite $SrTcO_3$. *Physical Review Letters* (2011), 106 (6), 067201.

[5] Avdeev, M.; Thorogood, G. J.; Carter, M. L.; Kennedy, B. J.; Ting, J.; Singh, D. J.; Wallwork, K. S., Antiferromagnetism in a technetium oxide. Structure of $CaTcO_3$. *J. Am. Chem. Soc.* (2011), 133 (6), 1654-1657.

LIFE SCIENCES

Using nuclear tools and techniques, ANSTO undertakes a range of research into common diseases including coronary heart disease, stroke and neurodegenerative diseases, like Alzheimer's and Parkinson's, to improve the health of all Australians.

The studies presented in this section use the wide-ranging techniques available at ANSTO: from radioisotopes produced for labelling particular compounds to accelerator science and neutron scattering.

Using some of these techniques, we gain further knowledge of how cells behave in the event of a stroke and study the role of calcium in neurons to better understand the onset of dementia.

Another study investigates organisms that live and operate at different temperatures - chickens, humans, platypus and the salt-water crocodile - and how their thermal stability is influenced by the oxygen-carrying haemoglobin.

(L-R) Benjamin Fraser, Anwen Krause-Heuer, Lidia Matesk and Tien Pham in the radiochemistry laboratory.

New imaging agents to diagnose stroke

01

Stroke is Australia's second largest killer after coronary heart disease, and affected 60,000 Australians in 2011. Stroke costs the Australian health system more than $2 billion annually and is expected to increase with Australia's ageing population, unless incidence rates can be lowered [1].

Diagnosing a stroke as quickly as possible is the key to achieving positive outcomes for patients. By applying their knowledge of how cells behave in the event of a stroke, ANSTO's Anwen Krause-Heuer and her colleagues at the French Atomic Energy Agency (CEA) have developed molecules that will help do just that and result in early diagnosis.

The processes of cell division and programmed cell death - called apoptosis – keeps living organisms in a stable state. Between 50 and 70 billion cells die in an adult human every day. This happens by cells communicating with one another and activating a series of enzymes that initiate apoptosis. In some instances, programmed cell death can stop occurring normally, leading to disease. During a stroke, cells are starved of oxygen. This activates particular enzymes, called caspases, which then begin the process of cell death causing irreparable damage.

ANSTO and CEA researchers worked together on a joint project to develop small molecules which can be radiolabelled with fluorine-18 and bound to the enzymes involved in apoptosis. The intention is that the compound can then, potentially, be injected into a patient so that a PET scan reveals pictures of the affected brain area, allowing the stroke to be diagnosed more quickly.

It is intended that this Australian-French research will contribute to the development of an innovative new radiopharmaceutical that enables earlier diagnosis and greater treatment options for stroke patients.

Anwen Krause-Heuer[1], Nicholas Howell[1], Lidia Matesic[1], Geetanjali Dhand[1], Tien Pham[1], Franck Sobrio[2]

Ivan Greguric[1], Benjamin Fraser[1]

[1]ANSTO, [2]Commissariat à l'énergie atomique (CEA)/LDM-TEP, Caen, France

Enzymes initiating cell death

During cell death, i.e. apoptosis, a cascade of signals from extracellular molecules activate a cell receptor. Subsequently this receptor creates a response by altering intracellular molecules. This signal transduction cascade activates particular enzymes: the **cy**steine-dependant **asp**artyl prote**ase** (caspase) family of enzymes that ultimately results in cell death. There are 11 known human caspases which are divided into three groups. The Group 1 caspases (caspase-1, -4, -5, -11 and -12) are involved in inflammation. Group 2 caspases (caspase-2, -8, -9 and -10) are involved in apoptosis by initiating the Group 3 caspases (caspase-3, -6 and -7), which are known as executioner caspases [2]. Group 3 caspases destroy key cellular substrates and activate the processes that degrade cellular DNA [3]. It is the executioner caspases, specifically caspase-3 and caspase-7 that are of most interest in the imaging of apoptotic disease. Small molecules that can bind to caspases will travel to areas of the body with high apoptotic activity, providing the ability to diagnose the diseases that are causing this event. Potentially, inhibiting these caspases from participating in apoptosis may also have therapeutic applications in treating diseases such as stroke.

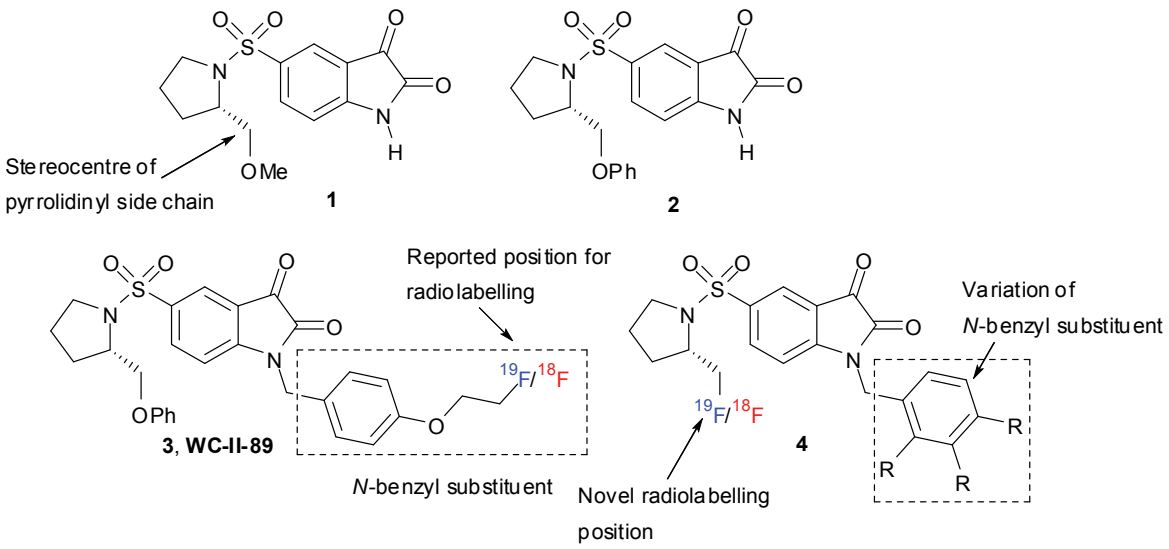

^ Figure 1
Structures of isatin-based caspase inhibitors, showing positions for [^{18}F]-radiolabelling and variation of *N*-benzyl substituent.

Substances to inhibit cell death

There are certain synthetic chemical substances that are known to be inhibitors of caspases. Isatin derivatives, illustrated in Fig. 1, are some of the first non-peptide based inhibitors, and they have previously been shown to be potent and selective inhibitors of caspase-3 and -7. Early examples from this class of inhibitors include **1** and **2** (Fig. 1), which demonstrated the importance of the stereochemistry of the pyrrolidine ring. Numerous *N*-substituted variants of **1** and **2** (Fig. 1) have been synthesised, with the variants containing benzyl groups (such as **3**, in Fig. 1) some of the most potent caspase inhibitors. This position has also served as a method for introducing a fluorine-18 atom, for non-invasive positron emission tomography (PET) imaging studies for diagnosis of apoptotic diseases. The compound WC-II-89 (**3** in Fig. 1) is a potential [^{18}F]-radiotracer for imaging caspase-3 activation in rats [4]; however, it has some drawbacks, such as low tracer clearance from the body and high tracer levels in the blood [5]. Our work has followed on from this in attempts to further optimise this class of compounds, by investigating the pyrrolidinyl side chain (**4** in Fig. 1) as an alternate and novel position for [^{18}F]-radiolabelling.

Rationale

Fluorine-18 is the major radioisotope used in PET scans for disease diagnosis. [^{18}F]-Radiolabelled caspase inhibitors have previously demonstrated potential as PET imaging agents, however, further optimisation of radiotracers is required. We have designed and synthesised a series of twelve new *N*-alkylated 2-(fluoromethyl)pyrrolidinylsulfonyl isatins (Fig. 1: general structure **4** & Fig. 2). [^{18}F]-Radiolabelling at the novel position of the pyrrolidinyl side-chain produced compounds with increased water-solubility/decreased fat-solubility (more hydrophilic), which may improve characteristics such as metabolic stability, clearance from the body, and brain uptake. Modifications of the *N*-alkyl substituent allowed for further fine tuning to the fat-solubility of the molecule (more lipophilic). Tailoring the fat-solubility may improve the ability of the compound to pass through the cell membrane and get inside the cell, whilst importantly retaining the caspase selectivity and potency.

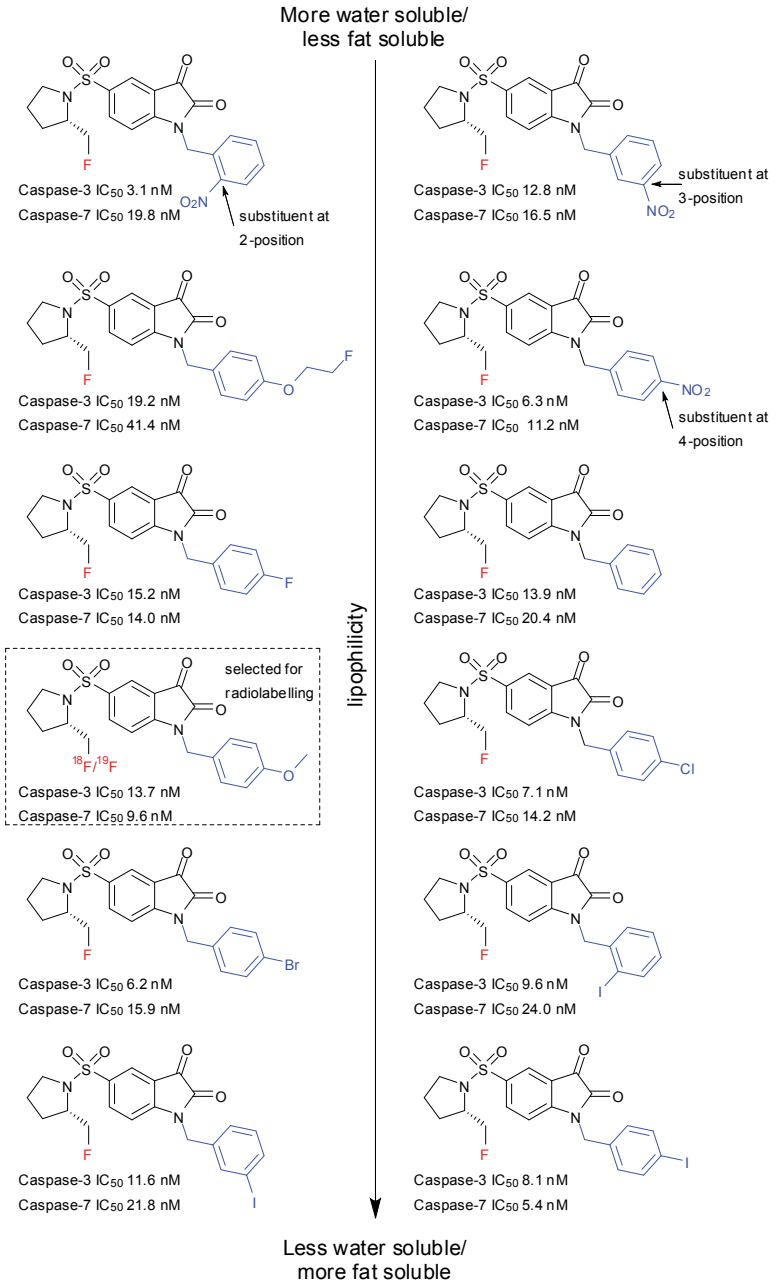

< Figure 2

Structures of the twelve new compounds synthesised, highlighting the changes to the N-benzyl substituent (shown in blue). *In vitro* caspase inhibition of each molecule against caspase-3 and -7 is also shown.

In vitro caspase inhibition

In vitro enzyme screening was conducted for each new compound synthesised to assess inhibition of caspase-3 and -7, and selectivity for these caspases over others (caspase-1, -6 and -8). This assay measured the concentration of the compound at which the caspase activity was reduced to 50%, or IC_{50} value: the lower the value, the more potent the inhibitor.

All compounds were inactive against caspase-1, -6 and -8 , whilst highly potent against caspases-3 and -7, indicating good selectivity. We found that replacing the methyl (Fig. 1: **1**) or phenyl (Fig. 1: **2, 3**) group on the pyrrolidinyl side chain with a fluorine atom (Fig. 1: **4**) gave molecules with similar caspase inhibition, validating our rationale of providing an alternate position for radiolabelling. The *N*-benzyl derivatives synthesised (see Fig. 2) all displayed very low IC_{50} values (less than 50 nM) against caspase-3 and -7 inhibition; with 4-benzyl substituted compounds the most potent.

Although changing the position of the substituent from the 4-position to either the 2- or 3- position retained activity for caspase-3 and -7, the compounds displayed decreased selectivity, with some inhibitory activity towards caspase-1 and -6 observed.

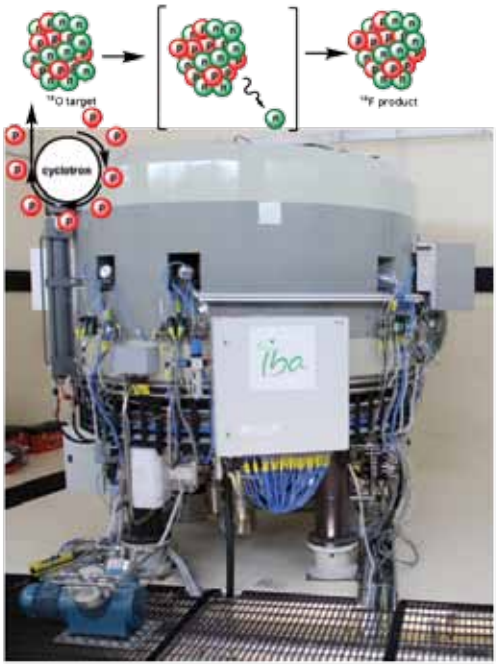

< Figure 3
Cyclotron production of $^{18}F^-$.

v Figure 4
Chemical structures of compounds involved in [^{18}F]-radiolabelling reactions.

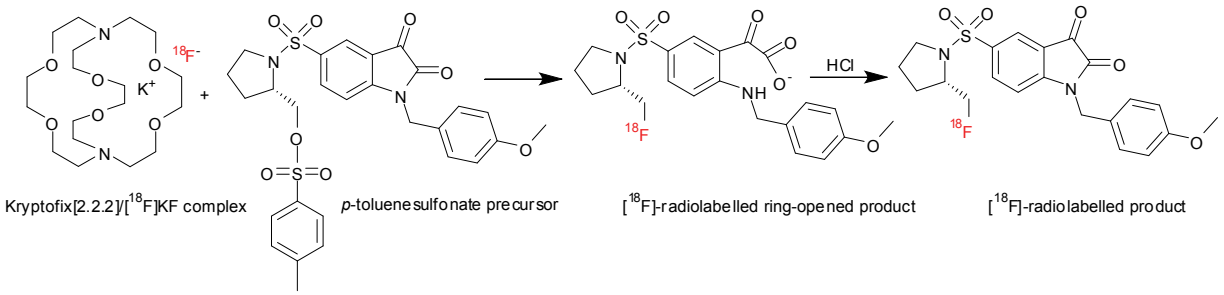

This suggests that the substituent position on the benzyl group may be important for interaction with the active site on the enzyme.

Radiochemistry

[^{18}F]-HF was produced at ANSTO's Camperdown facilities, using the ^{18}O(p, n)^{18}F nuclear reaction. In this reaction, protons are accelerated in a cyclotron and bombarded onto an ^{18}O-water target, causing the knockout of one neutron from the nucleus, resulting in a [^{18}F]-nucleus. Fig. 3 shows a schematic view of the nuclear reaction process and the cyclotron at the Camperdown facility.

Initial proof-of-principle [^{18}F]-radiolabelling was conducted on the *p*-methoxy compound due to its intermediary lipophilicity (Fig. 2).

Initially, the [^{18}F]-HF aqueous solution is treated with Kryptofix[2.2.2] and potassium carbonate and dried to remove water. The Kryptofix acts to complex the potassium ion, leaving a highly nucleophilic "naked" [^{18}F]-fluoride ion, shown in Fig. 4. The *p*-methoxy labelling precursor was then reacted with the [^{18}F]-fluoride, followed by treatment with HCl to close the isatin ring (Fig. 4). After treatment with HCl, the crude reaction mixture was then purified using high-pressure liquid chromatography (HPLC) to yield the [^{18}F]-labelled product in 15% radiochemical yield and high radiochemical purity.

The identity of the product was confirmed by co-injection of the [^{18}F]-radiolabelled compound with the non-radioactive standard compound. The chromatogram obtained is shown in Fig. 5 [6] demonstrating that the radiolabelled product and the non-radioactive standard co-eluted at the same retention time.

What is next?

A second inhibitor will be selected for radiolabelling to investigate potential differences in the biological behaviour of the compounds. The two successfully [^{18}F]-radiolabelled caspase inhibitors will undergo *in vivo* evaluation in an animal model for stroke, including PET imaging, biodistribution and radiometabolite studies. This evaluation will be carried out with our partners in France. Our collaborative project will contribute towards developing a novel radiopharmaceutical for apoptosis imaging, particularly in stroke patients to allow an earlier diagnosis and greater treatment options.

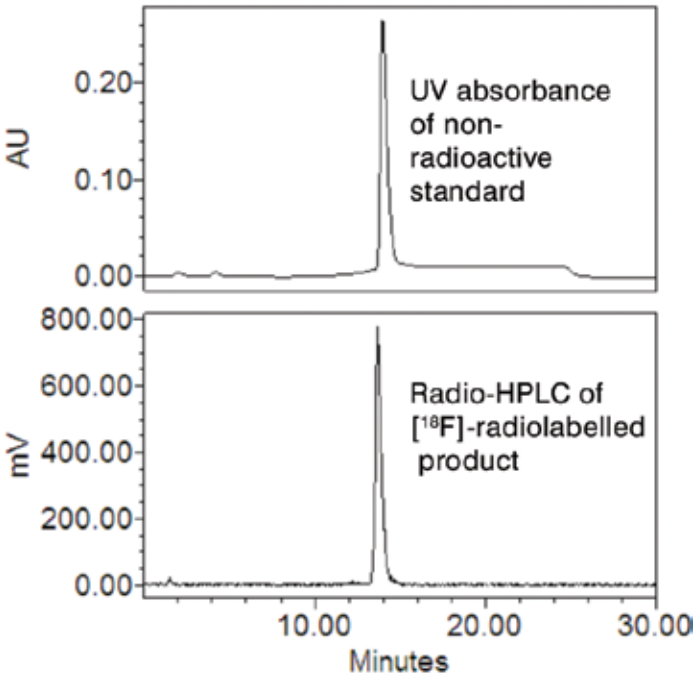

< Figure 5
Absorbance at 254 nm (top) and corresponding radio-HPLC (bottom) of collected [^{18}F]-radiolabelled product co-injected with non-radioactive [^{19}F]-standard.

Acknowledgements

Further radiochemical optimisation experiments were performed in conjunction with our collaborators at CEA/LDM-TEP in Caen, France, through the support of a France-Australia Science Innovation Collaboration Early Career Fellowship awarded to Dr Lidia Matesic in 2012. Anwen Krause-Heuer was supported by the 2011 ANSTO Graduate Development Program.

REFERENCES

[1] National Stroke Foundation Australia, 2012; Available from: www.strokefoundation.com.au.

[2] Hacker, H.-G., M.T. Sisay, and M. Gütschow, Allosteric modulation of caspases. Pharmacology & therapeutics (Oxford), 2011. 132(2): p. 180.

[3] Liu, X., et al., DFF, a Heterodimeric Protein That Functions Downstream of Caspase-3 to Trigger DNA Fragmentation during Apoptosis. Cell, 1997. 89(2): p. 175-184.

[4] Zhou, D., et al., Synthesis, radiolabeling, and in vivo evaluation of an F-18-labeled isatin analog for imaging caspase-3 activation in apoptosis. Bioorganic & Medicinal Chemistry Letters, 2006. 16(19): p. 5041-5046.

[5] Chen, D.L., et al., Radiolabeled isatin binding to caspase-3 activation induced by anti-Fas antibody. Nuclear Medicine and Biology, 2012. 39(1): p. 137-144.

[6] Krause-Heuer, A.M., et al., A new cla ss of fluorinated 5-pyrrolidinylsulfonyl isatin caspase inhibitors for PET imaging of apoptosis. MedChemComm, 2013. 4(2): p. 347-352.

ANSTO biologist, Nick Howell's research is contributing to better treatments for diseases such as Alzheimer's and Parkinson's.

Research to aid the detection and treatment of dementia

02

As a result of many successful health strategies, technologies and initiatives, life expectancy in Australia is higher now than ever before. Although this is a good result, an increasingly ageing population comes with a number of challenges including a growing number of people with age-related disabilities.

Dementia is the most common cause of disability in Australians over the age of 65. The term 'dementia' actually encompasses more than 100 degenerative disorders, including Alzheimer's, Parkinson's and Huntington's diseases, that affect the central nervous system, and in particular the brain. In order to develop better treatments, we first need to better understand the basic underlying disease processes.

We know that calcium plays an important role in neurons, which are cells that are essential for a healthy functioning human nervous system. An alteration in calcium homeostasis is one of the events known to initiate irreversible deterioration of the nervous system, which ultimately leads to degeneration of brain tissue.

By measuring particle induced X-ray emissions in sections of inflamed rat brain tissue, ANSTO's Nick Howell and his colleagues have been able to capture images of changes in calcium distribution. These images give potential insight into the early stages of dementia and help scientists better understand how these diseases start and progress.

It is hoped that the results of this research will enable scientists to not only detect these diseases before symptoms are visible, but also contribute to the development of better treatments.

Nicholas Howell[1], Paul Callaghan[1], Rainer Siegele[1], Richard Banati[1,2]

[1] ANSTO, [2]University of Sydney, New South Wales.

Neurodegenerative disorders

As in many other developed countries, increasing life expectancy through successful health strategies is giving Australia a significant and growing aging population. The impact of the aging population on the health system is significant, with dementia in particular being the greatest cause of disability in Australians over 65 years, and the fourth largest cause of disability overall The societal burden of dementia currently costs the health and aged care sector $4.9 billion per annum.

Neurodegenerative disease encompasses a spectrum of over 100 disorders, of which Alzheimer's disease, Parkinson's disease and Huntington's disease are the most common. Younger and older populations are also impacted by neurological disorders such as stroke and epilepsy, with approximately 400,000 people impacted by each disease.

In order to develop treatments, we need to increase our understanding of underlying disease processes that are common to these conditions. Excitotoxicity is the pathological process by which nerve cells in the brain are damaged or killed by

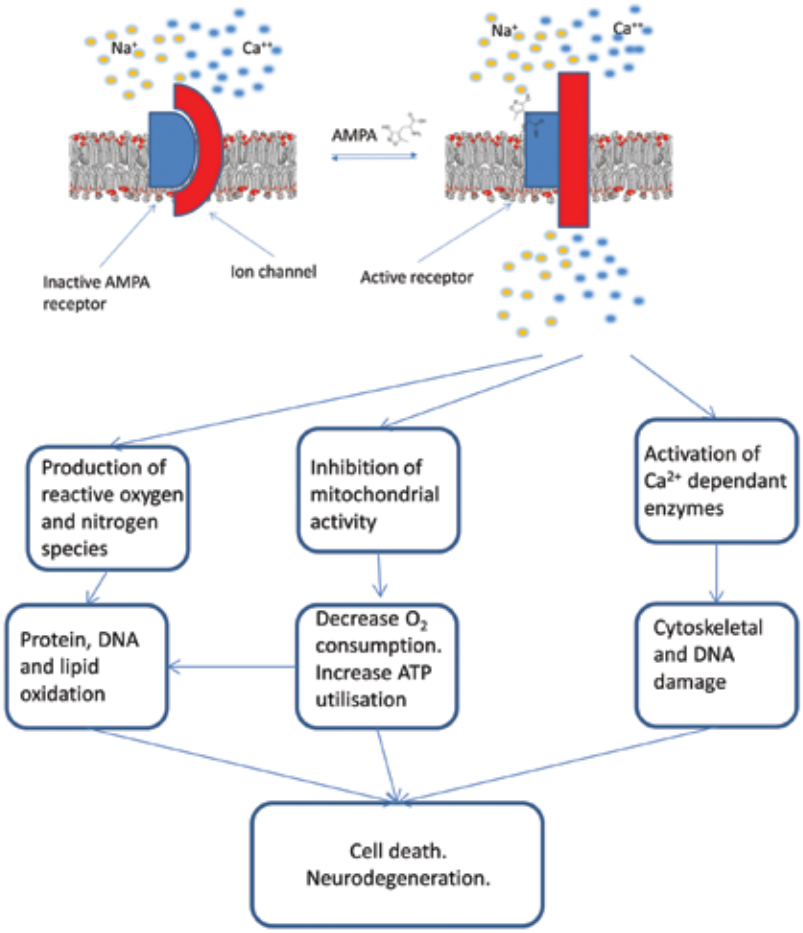

< Figure 1
AMPA- an excitatory amino acid analogue for the endogenous neurotransmitter glutamate.

a disease process initiated by an excessive release of a compound in the brain that is used to communicate between specific neurons, called glutamate [1]. The resulting excessive stimulation of the receptor target for glutamate, allows the influx of calcium ions (Ca^{+2}) through the outer membrane, which in turn stimulates a number of catabolic processes and results in an increase in the levels of free radicals and hence oxidative damage to proteins lipids and DNA. This results in an immune response within the affected area of brain, and eventually neurodegeneration [2].

Ca^{+2}: Friend or Foe?

Ca^{+2} ions are fundamentally important to cell survival. Intracellular calcium plays a great diversity of roles such as signal transduction, muscle contraction, neurotransmitter release and is a cofactor required for many enzymatic reactions [3]. Extracellular Ca^{2+} is an important cation for maintenance of electrical potential across cellular membranes, the driving force for many cellular functions.

Additionally Ca is fundamentally important in neurotransmission the process of chemical communication between neurons, which occurs at the synapse. Electrical communication from one neuron (presynaptic) to the next (postsynaptic) requires the release of a chemical (neurotransmitter) from the presynaptic neuron to bind to and activate the receptors of the adjacent neuron (postsynaptic). This cascading event results in the propagation of signal and the creation of nerve pulses. The energy required for neurotransmission is stored as an electronic membrane potential across the external membrane of the neuron [2]. When the electrical signal arrives, influx of Ca^{+2} through voltage or ligand gated ion channels allows the efflux of neurotransmitters.

In excitotoxic brain injury, aspects of this process go wrong. Large fluxes of concentrations of Ca^{+2} within cells are a key feature of the initiation of the excitotoxic process. Excitotoxicity occurs when receptors for the neurotransmitter glutamate are overstimulated, leading to an excessive influx of extra cellular Ca^{2+}. This increase in intracellular Ca^{2+} leads to the over-activation of a number of enzyme families of proteases, nucleases and lipases which then alter or damage vital components of the cell including membranes, proteins and DNA [4]. Increased intracellular Ca^{2+}

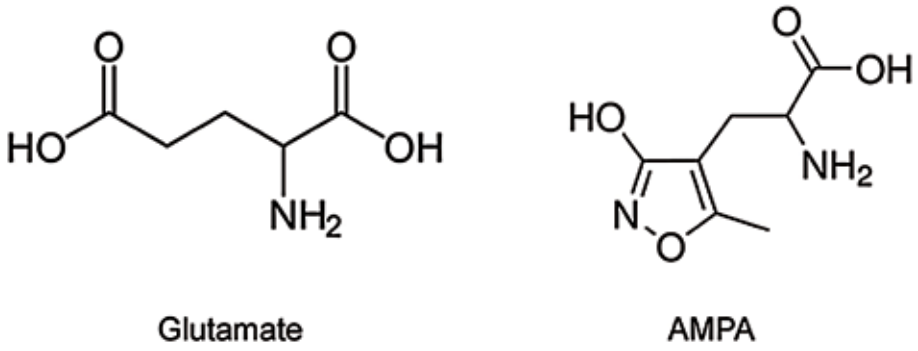

^ **Figure 2**
AMPA- an excitatory amino acid analogue for the endogenous neurotransmitter glutamate.

also removes the membrane potential across the inner mitochondrial membrane causing the mitochondria to swell and release various reactive oxygen species; see scheme in Fig. 1 [5].

The reaction of the immune response within the brain can be visualised via microglia, brain macrophage cells, which migrate to the site of injury and engulf the dead and dying neurons [5].

Inducing excitotoxic injury

We have employed a well-characterised model of excitotoxicity in these studies, in which the stimulus, the excitatory amino acid, α-amino-3-hydroxy-5-methyl-4-isoxazolepropionic acid (AMPA), (see Fig. 2) was injected stereotaxically into the striatal brain region (responsible for cognitive processes) of male Wistar rats (but only on one side) under anaesthesia. After recovery, the excitotoxic process and resulting neuroinflammation proceeds for seven days after which the samples are collected [6].

Imaging: altered calcium homeostasis using μPIXE

The ANSTO high-energy heavy-ion microprobe and particle induced X-ray emission device (PIXE) offers a unique capability of generating quantitative 'maps' of the distribution of elements in post-mortem tissue. Using other histopathological methods, such as immunohistochemistry which shows neuroimmune activation, we can correlate the images with other processes coincide with the time the sample is taken.

We used micro-PIXIE (μPIXE) to image the distribution of calcium concentration in cryo-sectioned brain tissue. Using a 3 MeV proton beam with a spot size of about 7–10 μm and a beam current of 0.5–0.8 nA, various atoms within the tissue section are excited and the resulting X-ray fluorescence spectra recorded. As shown in Fig. 3, the characteristic X-ray lines in the spectra clearly show fluorescence of P, S, Cl, K and Ca, which are critical electrolytes in all cells. We also observed characteristic lines for Fe, Zn, Mn and Br, some of which are present as trace elements. By fitting the known spectral profiles for these elements, quantitative maps of the distributions of them within the brain section can be reconstructed, as shown in Fig. 4) [7].

The reconstructed image illustrates significant increases in calcium concentration within the right striatum, where excitotoxicity was elicited.

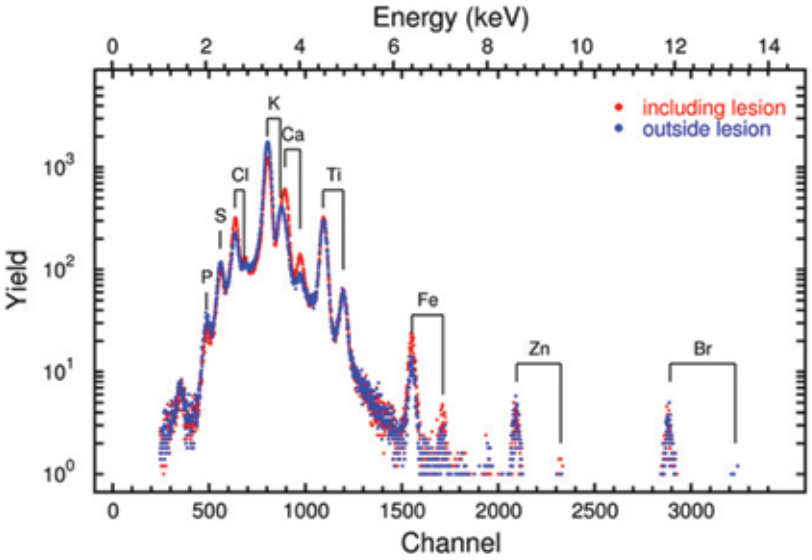

< Figure 3

µPIXE spectra taken over a 2 x 2 mm² area in the region of the neuroinflammation and for comparison a spectrum over the same area on the right brain hemisphere.

Reductions in K and S are seen within the site of excitotoxic injury, indicating reduced cellular density as a result of neurodegeneration. Adjacent brain sections displayed significant up-regulation, demonstrated with immunohistochemistry, of integrin αM (Fig. 5), a cell surface protein involved in the adhesion and migration of immune cells. This indicates that the endogenous immune cells of the brain, the microglia, are 'activated' in response to neurodegeneration within the area.

What can we learn from calcium?

Imaging elemental distributions in the brain using µPIXE has demonstrated large fluxes of calcium concentration, in response to excitotoxic injury.

Currently, excitotoxic injury is visualised by analysing the level of neuroinflammation. As calcium influx is the major initiating factor of excitotoxic injury, this method—developed at ANSTO—has the potential to visualise the excitotoxic process before the resulting neuroinflammation. This provides another unique approach for assessing disease, in particular the correlation of *in-vivo* pathology with post-mortem alterations. In-vitro methods on biopsy material are the mainstay of histopathological assessment of disease clinically. Validating the use of *in-vivo* imaging, such as positron emission tomography (PET), from biopsy histopathology data allows greater power in assessing disease progression in patients compared to invasive procedures or situations where biopsies are not possible. It is hoped that imaging calcium elemental distribution will give the ability to visualise the early time points and origin of the injury. This approach can be used as an indicator of 'prodromal' or disease initiation before symptoms appear in diseases (initially in animal models) such as:

- Neurodegenerative disease
- Epilepsy
- Amphetamine related cognitive dysfunction

This will allow a greater understanding of the initiating factors and brain regions in response to various stimuli thereby increasing our understanding of the role of this fundamental process in many related pathologies.

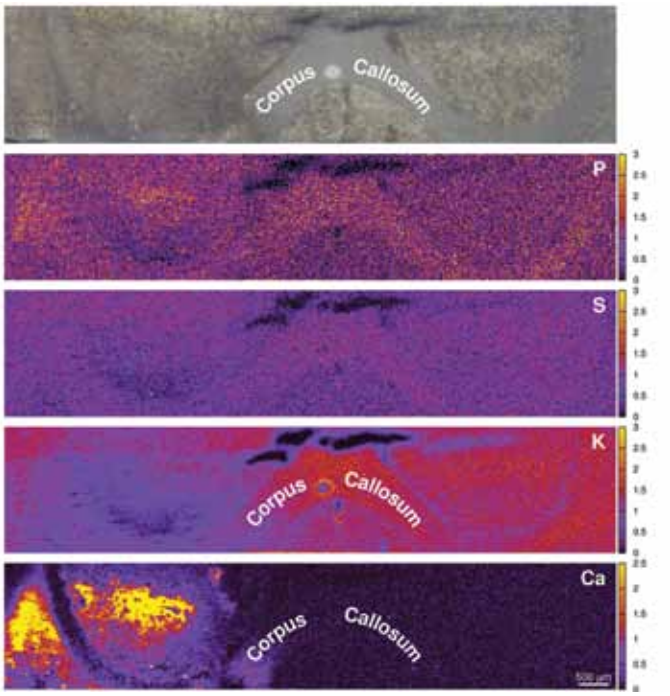

< Figure 4
Elemental maps of Ca, K, S and P, together with an optical image of the analysed area.

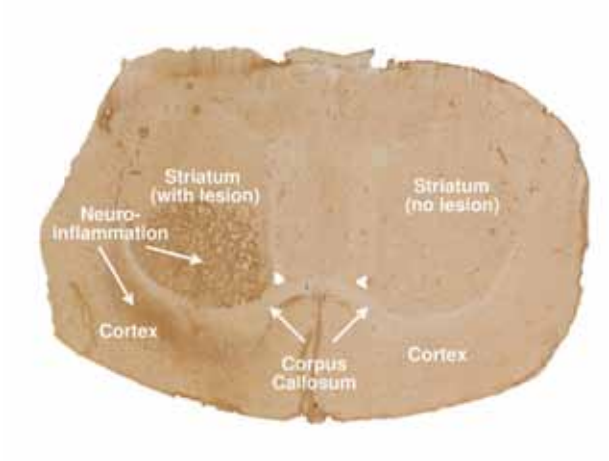

< Figure 5
Optical image of a rat brain section. The image clearly shows the region of the neuroinflammation in the AMPA lesioned rat. The sample was stained by OX-42 immunohistochemistry, a biomarker for microglial activation resulting from localised excitotoxic damage of neurons.

REFERENCES

[1] Bondy, S.C. and C.P. LeBel, *The relationship between excitotoxicity and oxidative stress in the central nervous system*. Free Radical Biology and Medicine, 1993. 14(6): p. 633-642.

[2] Patel, D.R. and C. Feucht, *Basic Concepts of Neurotransmission*. Pediatric Clinics of North America, 2011. 58(1): p. 21-31.

[3] Williams, R.J.P., *The evolution of the biochemistry of calcium, in New Comprehensive Biochemistry*, K. Joachim and M. Marek, Editors. 2007, Elsevier. p. 23-48.

[4] Gümrü, S. and F. Arýcýoðlu, *Ampakines: Selective AMPA receptor modulators with potential benefits*. MÜSBED, 2012. 2(4): p. 143-148.

[5] Nam, M.-K., et al., *Essential roles of mitochondrial depolarization in neuron loss through microglial activation and attraction toward neurons*. Brain Research, (0).

[6] P.D. Callaghan, et al. in *World Molecular Imaging Congress*. 2009. Montreal, Canada.

[7] Hackett, M.J., et al., *Investigation of the mouse cerebellum using STIM and μ-PIXE spectrometric and FTIR spectroscopic mapping and imaging*. Nuclear Instruments and Methods in Physics Research Section B: Beam Interactions with Materials and Atoms, 2011. 269(20): p. 2260-2263.

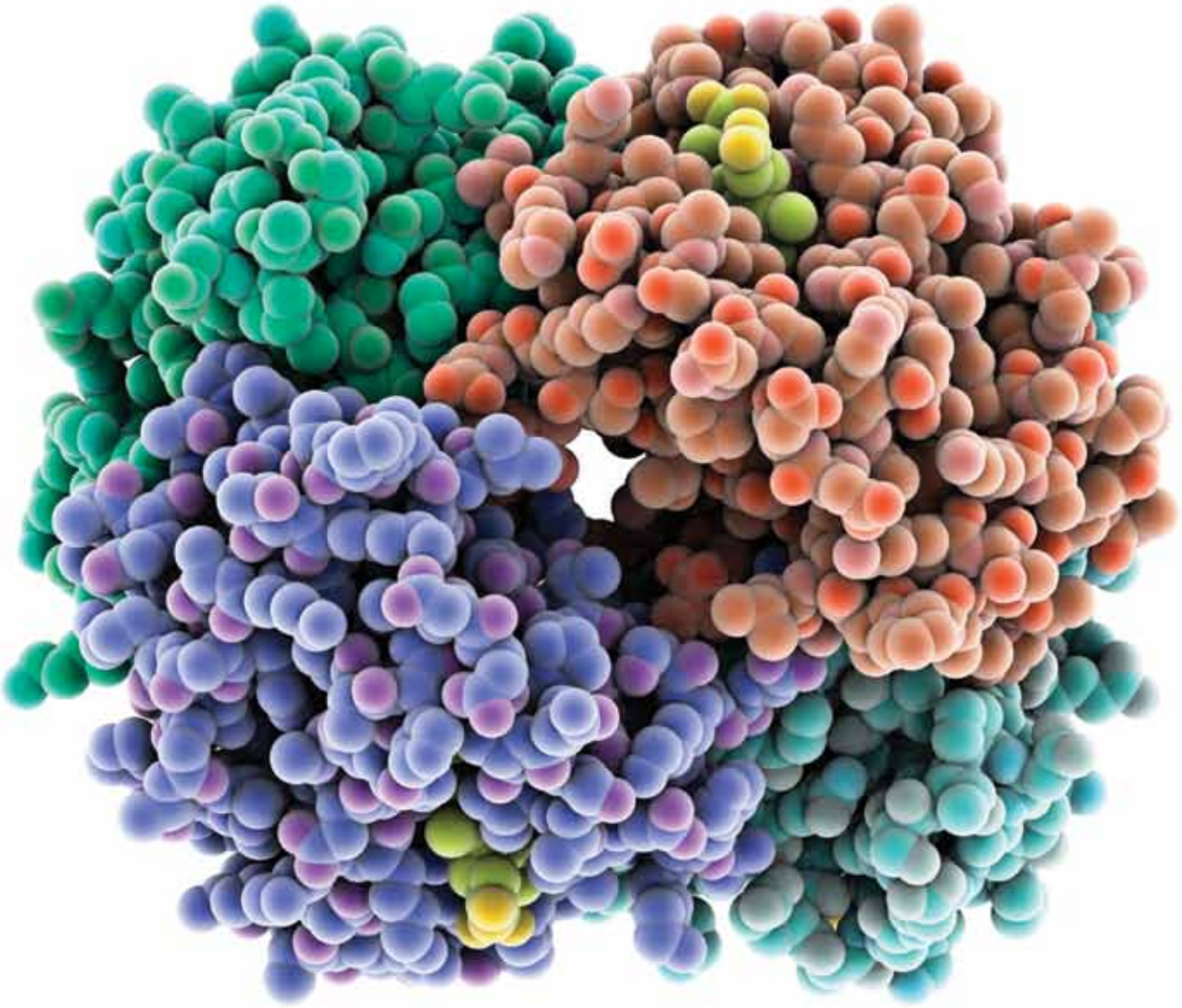

Haemoglobin is essential for the effective functioning of human bodies, with haemoglobin deficiencies causing diseases such as anemia.

Haemoglobin study sheds light on one of our bodies most important molecules

03

Haemoglobin molecules store oxygen in the body, and red blood cells transport this vital storage unit around the body. Haemoglobin is essential for the effective functioning of our bodies, with haemoglobin deficiencies causing diseases such as anemia. It is therefore important that we understand how haemoglobin works and what factors affect its functioning. In this study researchers look at how haemoglobin molecular operations are optimised based on body temperature by comparing haemoglobin function in different animals.

Chris Garvey and researchers from France and Germany have been working to gain a better understanding of the molecular basis for this optimisation which involves a complex interplay between structure and the internal flexibility of the structure.

To undertake this study, the researchers selected haemoglobins from species which regulate their body temperature over a range of external conditions, including platypus, domestic chicken and humans, and species which do not have a regulated body temperature, including the salt water crocodile.

The researchers discovered that there is a positive correlation between the thermal stability of the environment around these oxygen storage cells (i.e. the protein) and its resilience - shedding light on how haemoglobin may have evolved to carry oxygen best at different body temperatures in different species.

Computer simulations were used to examine which part of the haemoglobin molecule from different species was responsible for the change in the overall softness of the protein.

Having gained a better understanding of haemoglobin function, the next steps are to examine observations in the context of oxygen affinity, or how well haemoglobin molecules hold on to oxygen. This will be possible with further development of instruments at ANSTO's OPAL research reactor facilities.

Christopher J. Garvey[1], Sophie Sacquin-Mora[2], Andreas Stadtler[3]

[1] ANSTO, [2]Institut de Biologie Physico-Chimique, France
[3]Jülich Center for Neutron Science and Institute for Complex Systems, Germany

Introduction

Molecular biology tools have made it possible to test hypotheses about the functioning of biomolecules by directly manipulating the structure. However, this research followed an older experimental tradition, comparative physiology, where aspects of biological functioning are compared in the context of animals with differing physiology [1]. This traditional method was coupled with the tools of modern soft condensed matter science; computer simulations together with neutron and optical spectroscopy, which measure the momentum and energy changes to neutrons when they interact with a sample, to reveal information about the softness of protein [2].

Haemoglobins were selected from species which regulate their body temperature over a range of external conditions (platypus, domestic chicken and humans) and a species which does not have a regulated body temperature (salt water crocodile).

Experimental techniques revealed not only changes in arrangements and internal motions of the molecule within the basic globular shape but also in the thermal stability of each haemoglobin molecule. Researchers found a positive correlation between the thermal stability of the environment around these oxygen storage cells (i.e. the protein) and its resilience.

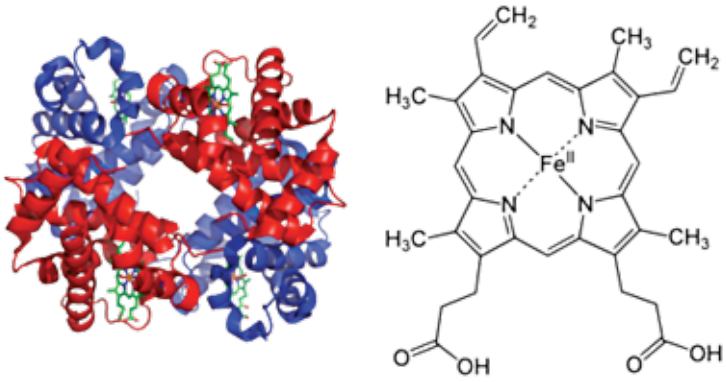

< Figure 1
The folding of four haemoglobin molecules into the overall globular tetrameric structure (Hb_4 - RHS). Each heme group (LHS) which is the site of oxygen storage is shown in green in the Hb_4 unit.

< Table 1

Species	Body temperature (°C)	Melting temperature (°C)	Force Constant (N m^{-1})
Platypus	33	60.5	0.11±0.01
Human	36.6	63.8	0.15±0.02
Chicken	41	68.7	0.23±0.03
Salt water crocodile	25-34	68.3	0.18±0.02

Haemoglobin

Although there is a high degree of similarity between haemoglobin molecules from different species, computer simulations were used to examine which part of the haemoglobin molecule from different species was responsible for the change in the overall softness of the protein.

Having gained a better understanding of haemoglobin function, researchers are now looking to examine these observations in the context oxygen affinity, i.e. how well haemoglobin molecules hold on to oxygen, which will be possible with further development of instruments at ANSTO's OPAL reactor facilities.

Haemoglobin is a polymer of various amino acids (protein) which in its native state is folded into a compact globular shape which includes four separate haemoglobin molecules (Fig. 1). In vertebrates the haemoglobin molecule has been enclosed in a highly specialised cell known as the erythrocyte, or red blood cell. The haemoglobin tetramer, Hb_4, is predominantly found inside red blood cells. The red blood cell is a recent evolution; it is present in the circulation of most vertebrates where it carries an extremely concentrated solution of the oxygen storage protein haemoglobin (about 30%) around the body where it is essential for metabolic processes. In its normal functioning in endotherms (animals that metabolically regulate their body temperature, e.g. platypus, domestic chicken and human) it is regulated at a relatively narrow range of temperatures, the body temperature. Ectotherms (e.g. the saltwater crocodile) do not metabolically regulate their body temperature but instead use behavioural strategies. The physiological problem that must be solved by the haemoglobin molecule is that it must store oxygen from the atmosphere in the lungs, and in the peripheral circulation in the small blood vessels found in many sorts of tissue; but it must also release the oxygen so that it may be used for metabolic activity.

Oxygen is held in one of four heme groups (Fig. 1). Various factors are already known to influence the binding of O_2 to these sites including the binding of other O_2's to the other sites within the tetramer, the presence of different phosphate molecules which are related to cell metabolism [3] and pH. In this study we have examined the haemoglobin from endotherms with a range of body temperatures and an ectotherm in the context of the operating body temperature (Table 1 [4]).

The Measurements

The backscattering spectrometers IN13 [5] and SPHERES [6] were used to study the scattering of neutrons, or the change in path of neutrons as a function of angle as well as the energy change in these neutrons. The information obtained was the average fluctuation of hydrogen around its average position within the Hb4 molecule. For hydrogen atoms on a ridged molecule this value is small. For softer molecules the fluctuation is greater and made as a function of temperature the measurement allows us to measure a mean force elastic constant. Our measurements suggest that that a certain amount of water is necessary to obtain and maintain the internal motions necessary for biological function of haemoglobin, but also at this level for the endotherm the force constant parallels the order of

< Figure 2
The neutron spectometers, IN13 (left) at the Instiute Laue Langevin (Grenoble, France) [5], and SPHERES at Jülich Centre for Neutron Science (Garching, Germany) [6].

the body temperature, that is to say the platypus has the softest haemoglobin and that the chicken has the stiffest (table 1). The crocodile's haemoglobin is quite stiff compared to the other haemoglobins but it must function over a range of temperatures.

Circular dichroism spectroscopy measures the differences in absorption of two different polarisations of light in the ultra-violet/visible regime. This method was used to determine the different folding of the four haemoglobin molecules within the overall globular shape as a function of temperature. Specifically we focussed on the loss of a particular aspect of the structure, the α-helix, using the spectra at the 222 nm (ultraviolet) region, and a temperature at which there is a partial unfolding of the structure. We found that for the endotherms studied the order of the unfolding temperature is the same as the body temperature. These measurements are used to indicate the overall stability of the haemoglobin molecules in its functional structure.

Combining results with the computer simulations

While the haemoglobins molecules for each species are quite similar, they all fold into the same basic tetrameric globular structure, but they differ subtly by the chemistry along the chain of the haemoglobin. We have used computer simulations to understand which regions of the folded protein are responsible for the changes in the thermal stability and overall softness of the proteins. The initial step was to build a credible three dimensional model of the arrangements of the molecule within the overall globular shape—the precise three dimensional structure is not known for platypus and crocodile haemoglobin. The simulations allowed us to determine which residues are responsible for changes in the force constant for the overall molecules determined by neutron spectroscopy.

In terms of the biological function of the haemoglobin molecule in different species we have investigated the rigidity of the environment (protein) around the oxygen storage site. Each Hb4 molecule must function to allow the oxygen to bind and be released according to physiological need. Our further investigations aim to understand these observations in the context of oxygen affinity, but we also speculate that some of the mediators of oxygen affinity may be associated with changes in the internal dynamics of the haemoglobin molecule. Further developments of the instrumentation at the OPAL reactor will allow us to pursue our research at Australian facilities.

REFERENCES

[1] Prosser, C. L. (1975). Prospects for comparative physiology and biochemistry. Journal of Experimental Zoology, 194(1), 345-347. doi: 10.1002/jez.1401940122

[2] Zaccai, G. (2000). Biochemistry - How soft is a protein? A protein dynamics force constant measured by neutron scattering. [Review]. Science, 288(5471), 1604-1607. doi: 10.1126/science.288.5471.1604

[3] Benesch, R., & Benesch, R. E. (1969). Intracellular Organic Phosphates as Regulators of Oxygen Release By Haemoglobin. [Article]. Nature, 221(5181), 618-&. doi: 10.1038/221618a0

[4] Stadler, A. M., Garvey, C. J., Bocahut, A., Sacquin-Mora, S., Digel, I., Schneider, G. J., . . . Zaccai, G. (2012). Thermal fluctuations of haemoglobin from different species: adaptation to temperature via conformational dynamics. Journal of the Royal Society Interface, 9, 2845-2855. doi: 10.1098/rsif.2012.0364

[5] http://www.ill.eu/instruments-support/instruments-groups/instruments/in13/

[6] http://www.fz-juelich.de/jcns/EN/Leistungen/Instruments2/Dynamics/SPHERES/_node.html

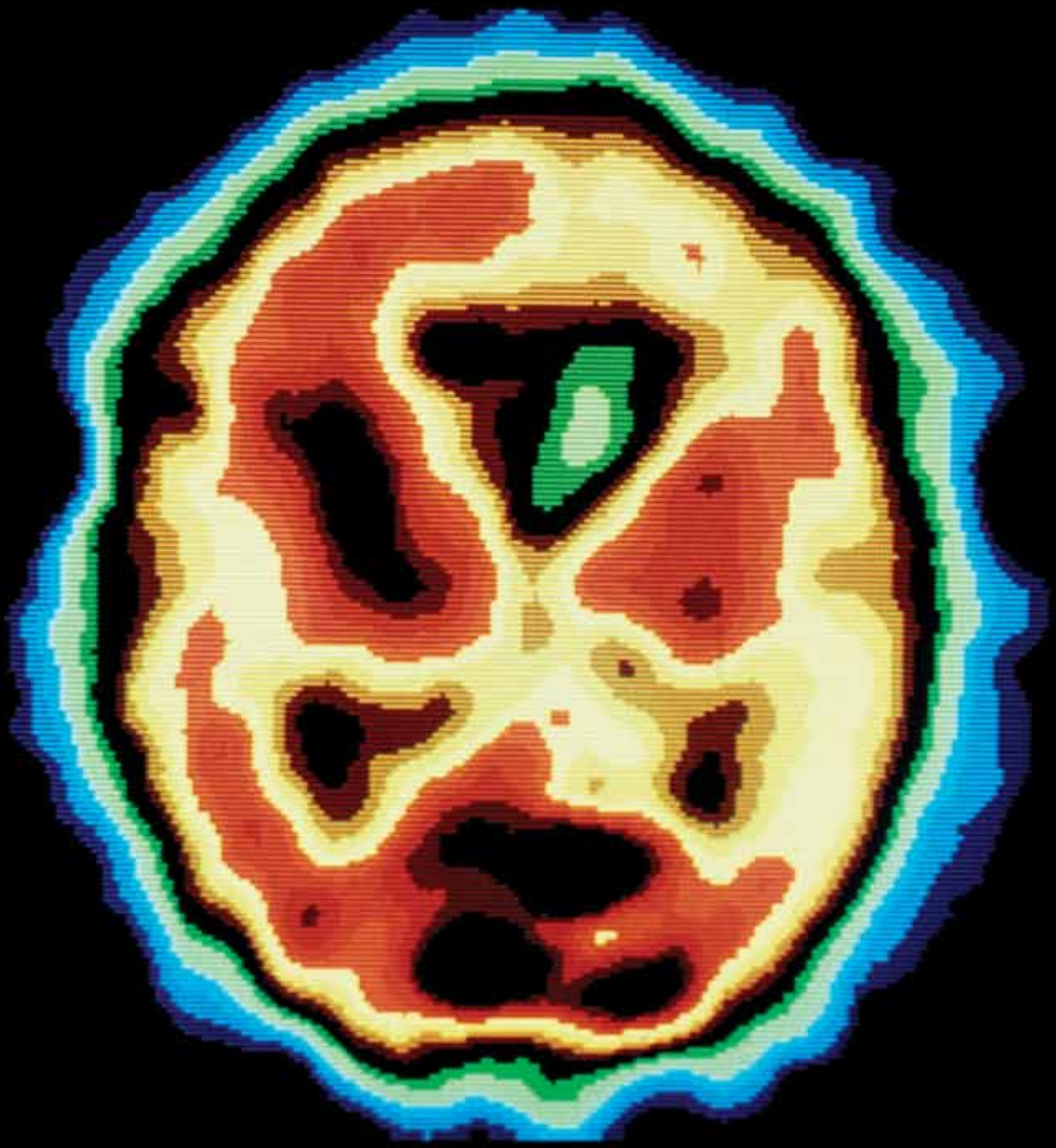

IMAGING

Accurate diagnosis is fundamental to good quality health care. ANSTO produces nuclear medicines for diagnosis, with around 10,000 doses of nuclear medicine distributed to Australians each week, and undertakes research using medical imaging to understand biological processes to develop new treatments.

Advancing medical imaging continues to be a priority for ANSTO. This section highlights developments in dosimetry (measuring radiation) and improvements in imaging tools by using parameterisation, modelling and simulation.

ANSTO and the University of Wollongong developed tiny microdosimeters that can assess the dose levels of individual cells. The researchers then tested them in facilities in Germany and Japan using accelerated protons or carbon ions, widely known as hadron therapy, exploring future prospects of cancer treatment.

Tools for improving Positron Emission Tomography (PET) imaging are presented that use simulation tools and sophisticated data processing, as well as work on improving data analysis tools for the measurement of physiological parameter (related to cognition, memory, pleasure and others).

Another study using various imaging techniques (PET/SPECT/CT) at pre-clinical stage investigates the way in which the body clears itself of chemotherapy agents to make medication doses safer.

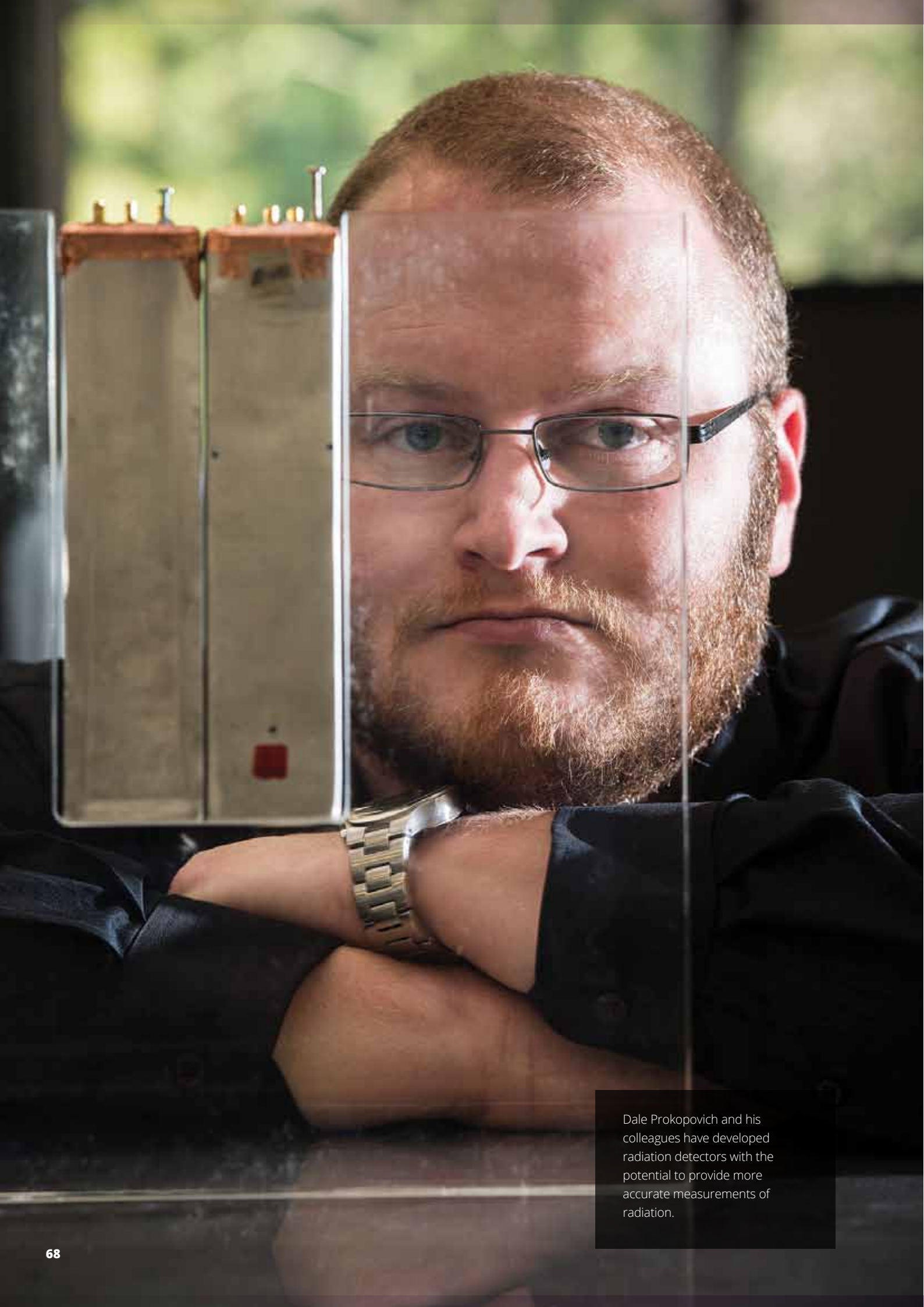

Dale Prokopovich and his colleagues have developed radiation detectors with the potential to provide more accurate measurements of radiation.

Miniature radiation dose detectors to aid hadron therapy cancer treatment

01

Nuclear medicine, specifically charged particles produced in research reactors and accelerators, is effectively used overseas for treating a variety of cancers. Recent developments in particle accelerator technology have led to dedicated facilities, which use mainly proton and carbon ions, and are collectively known as hadron therapy facilities.

Hadron therapy is an alternative radiotherapy cancer treatment which is being increasingly used when other treatment options, such as conventional radiotherapy, cannot be employed because of risk to vital organs close to the tumour.

In order to improve hadron therapy treatment, it is vital to have an accurate measurement of the dose the patient is receiving, not only in the treatment area, but also in any surrounding critical organs such as the brain and nervous tissue, eyes, and reproductive organs.

A collaborative effort by scientists from ANSTO and the University of Wollongong has resulted in the development of a new, miniature radiation dose detector that uses silicon, similar to that used in the manufacture of computer processors and USB flash memory devices. Scientists have fabricated these detectors, called microdosimeters, to be equivalent in size to human cells, and they have been successfully tested at hadron therapy facilities in Japan and Germany.

Testing demonstrated that these microdosimeters have the potential to provide a more accurate measurement of the radiation dose received by the area being treated and the surrounding sensitive organs. Further testing is now planned to continue developing and improving this cutting-edge technology.

Dale A. Prokopovich[1,2], Jayde Livingstone[2], Maria Martisikova[3], Hiroshi Yasuda[4], Michael L. F. Lerch[2] Marco Petasecca[2], Mark I. Reinhard[1,2], Anatoly B. Rosenfeld[2]

[1] ANSTO, [2]Centre for Medical Radiation Physics, University of Wollongong, [3]Heidelberg Ion Therapy facility, Germany, [4]National Institute of Radiological Sciences, Japan

In 1946, Robert Wilson at Harvard University first proposed the use of charged particles such as protons for treating cancer [1]. Charged particles were perceived as being advantageous over conventional X-rays on account of the ability to deposit energy deep in the body with limited dose to the entry tissue. It took over fifty years until particle accelerator technology was ready to take advantage of the physical properties of charged particle energy loss before patient treatment with protons, helium and carbon ions commenced within dedicated hospital settings.

'Hadron therapy' using carbon ions is now a significant modality for the treatment of cancers that are untreatable using other methods (unresponsive to conventional radiotherapy and/or chemotherapy) or located close to a critical organs or structures (e.g. eye, brainstem, spinal

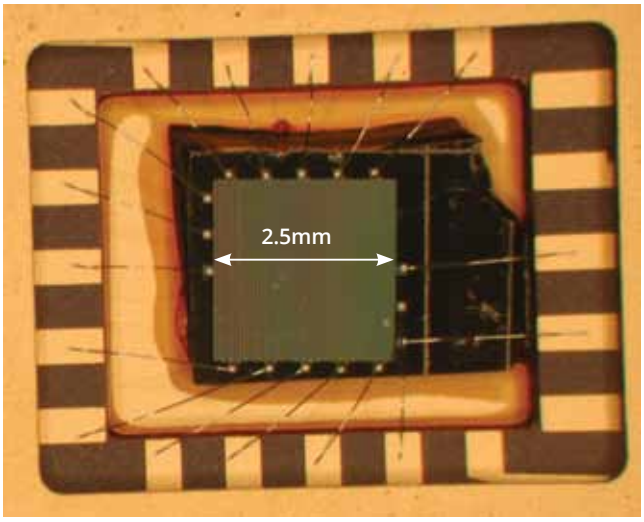

< Figure 1
Microscope image of a second-generation SOI Microdosimeter showing the small individual cells.

column, etc.) where healthy tissue damage is unacceptably high with conventional radiotherapy. The major advantages of hadron therapy stem from the accuracy in dose delivery to the cancerous tissue while sparing radiation exposure of the surrounding healthy tissue. Additionally, in the case of hadrons, the majority of the dose is deposited at the end of the range of the particle within the 'Bragg peak' allowing treatment of deep seated cancers. Dedicated hadron therapy facilities are in clinical operation in Japan, Germany and, more recently, Italy, with hundreds of patients being successfully treated at each facility every year.

To further improve the efficacy of hadron therapy new methods of measuring the dose to the patients, both in the treatment volume and to surrounding critical structures are needed. Existing dosimetry methods rely on relatively large thimble sized gas chambers to estimate the dose effects to a human cell. With treatment beams having spatial profiles as small as 1 mm and the dimensions of gas chambers in the order of 1 cm, this approach is grossly inadequate, leading to the incorrect assessment of the dose throughout the target volume.

An alternative approach uses detectors fabricated from silicon using the same technology as in the manufacture of computer processors and memory devices. Known as 'Silicon on Insulator (SOI) Microdosimetry' the use of semiconductor nanofabrication allows for the fabrication of detectors with equivalent sizes to human cells. We present here results from testing these SOI Microdosimeters in carbon ion therapy fields at the Heavy Ion Medical Accelerator Chiba (HIMAC) in Chiba City, Japan and the Heidelberg Ion Therapy (HIT) facility in Germany.

Silicon on Insulator (SOI) Microdosimetry

SOI Microdosimetry has been used to investigate the dosimetric properties of a variety of hadron therapy treatment fields at both in-field and out-of-field regions. The energy loss of the ionising radiation through matter is described by the 'Bragg curve' which results in a pronounced 'Bragg peak' depositing the energy ultimately in the cancer cells, but in our study in the dosimeter. The small physical volume of the packaged SOI Microdosimeter device (illustrated in Fig. 1) allows for measurement of spatially resolved microdosimetric spectra at a variety of positions along the Bragg peak and at positions distal and perpendicular to the Bragg peak where dose attributable to neutrons, fragmentation and gamma rays can be present. Monoenergetic He and C ion beams were studied at the HIMAC facility in Japan while a scanning beam spread out (SOBP) Bragg peak was studied at the Heidelberg facility. The measurements displayed excellent reproduction of the Bragg peak as well as measurements of the out-of-field dose contribution.

SOI microdosimetry provides a means to measure the dosimetric properties at the cellular level of an unknown mixed radiation field. Understanding the energy deposition by radiation at the cellular level allows for better prediction of biological response. SOI Microdosimetry uses the principles of microdosimetry [2,3] applied to small cellular-sized sensitive silicon volumes. The SOI Microdosimeter consists of a parallel array of 10x10x10 μm^3 sized silicon sensitive volumes or 'cells". These cells measure the small amount of energy deposited within the small volume which can then be used to determine a Radiobiological Effectiveness (RBE) of the radiation field regardless of its composition. This allows for the measurement of a dose equivalent to tissue from any arbitrary radiation field regardless of energy or composition unlike other methods of dosimetric measurement.

The SOI microdosimeter has previously been successfully tested in a variety of mixed radiation protection fields including those associated with proton therapy, fast neutron therapy, boron neutron capture therapy (BNCT) [4], high energy quasimonoenergetic neutrons at the TSL facility in Uppsala, Sweden [5], the CERF facility at CERN [6]

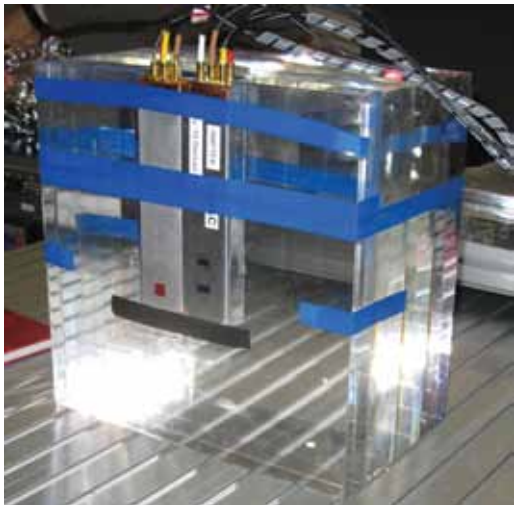

< Figure 2
The SOI Microdosimeters (first and second-generation) mounted side by side (grey aluminium boxes with cables) in a PMMA (Polymethyl Methacrylate) phantom. The phantom simulates surrounding tissue for the dosimetry measurements.

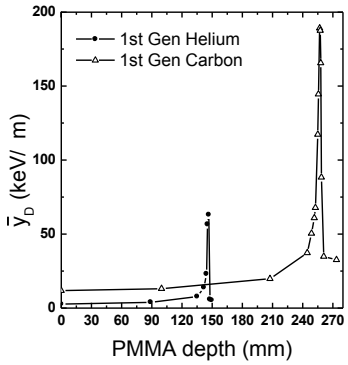

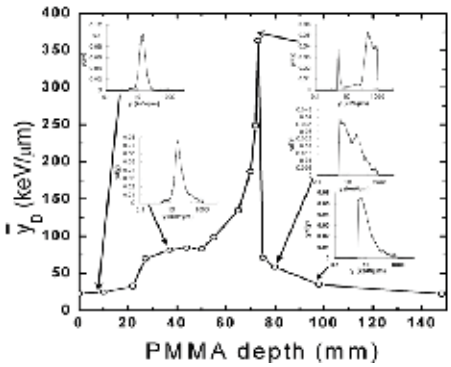

< Figure 3
The measured dose-mean lineal energy deposition at the HIMAC facility for both 150 MeV/u helium and 400 MeV/u carbon ions taken with a 1st Generation SOI Microdosimeter.

< Figure 4
The measurement of the dose-mean lineal energy deposition along the central axis of a 5 x 5 x 5 cm^3 cubic spread out Bragg peak at the Heidelberg Ion Therapy facility. Selected positions along the SOBP are shown as lineal energy deposition spectra.

and the Space Heavy Ion Radiation field at the NASA Radiation Facility [7]. This is the first time that SOI Microdosimeters have been used in a carbon ion therapy field which is much more complex due to fragmentation and production of secondary particles within the treatment volume.

In the context of hadron therapy, SOI microdosimetry offers the potential to measure, with a single detector, the dose and microdosimetric properties of both the primary hadron field and surrounding regions where neutrons and particle induced fragmentation reaction products are present. It is very important to improve the understanding of dose to surrounding regions as this would represent the healthy and sensitive tissue of organs that the hadron therapy treatment aims to spare from damage.

A treatment field delivered by a broad beam of 150 MeV/u (energy of the particle per nucleon) helium ions and 400 MeV/u carbon ions were studied at the HIMAC facility at NIRS, Japan. A scanning beam 5x5x5 cm^3 cubic spread out Bragg peak (SOBP), centred at a depth in water of 61.8 mm as well as a brain tumour treatment plan were also studied at the Heidelberg Ion Therapy (HIT) facility in Germany. These beams were chosen to investigate both the Bragg peak doses using SOI Microdosimetry as well as the out-of-field dose components.

Setting up the experiments

The measurements were acquired using the SOI Microdosimeters connected to a spectroscopic readout system which allows measurement of each individual dose event from each particle within the cells of the microdosimeter.

The SOI Microdosimeters were placed in various positions along the central axis of the different heavy ion therapy radiation fields. For the depth measurements at HIMAC polystyrene (density 1.04 g/cm^3) solid water sheets of variable thicknesses were used to change the effective tissue depth of the therapy beam in relation to the position of the SOI Microdosimeter. At HIT, a modular Polymethyl Methacrylate (PMMA) phantom was used to adjust the position of the Bragg peak relative to the SOI Microdosimeter, see Fig. 2. The PMMA density (1.18 g/cm^3) was adjusted for the calculations to determine the depth in water of the SOBP measurements.

Out-of-field measurements were performed at positions distal to the Bragg peak position in order to investigate the contribution from the nuclear fragments, neutrons and other

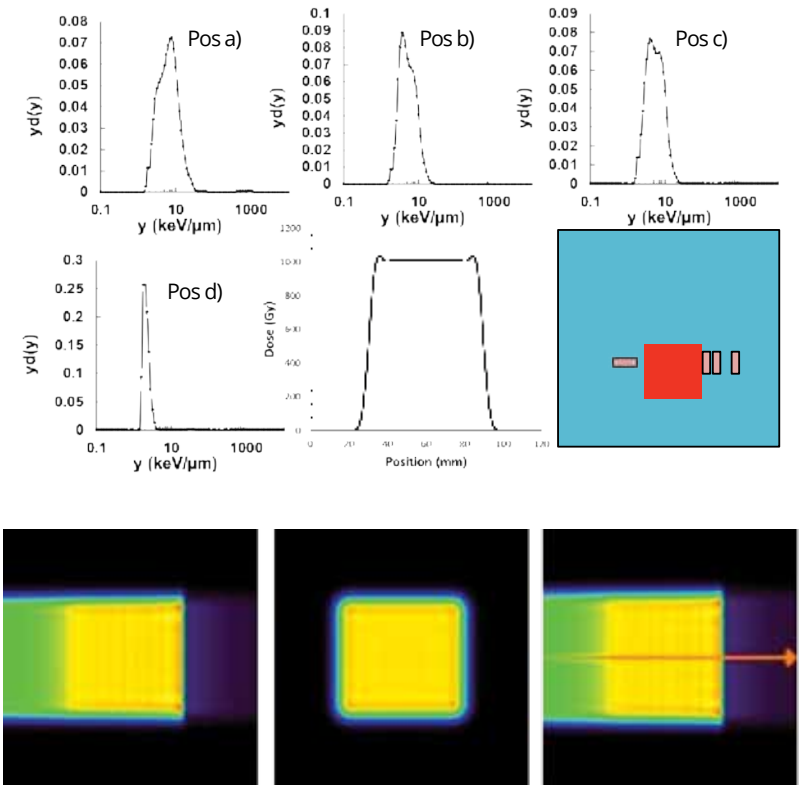

< Figure 5

Lateral measurements of the microdosimetric spectra for the cubic irradiation. The measurements show that the particles emitted from the irradiation area are directed laterally. All of the measurements were taken at a depth of 42 mm inside the phantom.

Pos a) 25 mm from beam isocentre, Pos b) 28 mm from beam isocentre, Pos c) 48 mm from beam isocentre, Pos d) Same position as Pos a) but rotated 90° towards upstream direction (Shown on opposite side for figure clarity).

The three images at the bottom show the dose profiles (coronal, sagittal and transverse) from the treatment planning software.

secondary radiation types. At HIT, lateral out-of-field measurements were also taken for the scanning SOBP from right on the edge of the cubic SOBP to 23 mm from the edge of the SOBP. Rotation of the SOI Microdosimeter by 90° will give an indication of the direction and therefore the origin of the secondary radiation dose components.

Results

The results of the dose-mean lineal energy depositions acquired along the axis of the monoenergetic broad beam irradiations at HIMAC can be seen in Fig. 3. These measurements were performed with a 150 MeV/u (600 MeV total) helium-ion beam and a 400 MeV/u (4.8 GeV total) carbon-ion beam. The lineal energy deposition results for positions distal to the Bragg peak show some contribution from fragmentation and neutrons, particularly evident in the results for the carbon ion beam. These components contribute to the increased dose contribution past the end of the Bragg peak. Neutrons deposit energy past the Bragg peak due to the creation of recoil protons from the surrounding material (PMMA, solid water or tissue in a patient). It is critical to understand the dose from these components as in a patient it may be next to a critical or an organ which could be sensitive to DNA damage from radiation which may contribute to secondary cellular mutations.

The SOBP measurements at HIT for a 5x5x5 cm^3 cubic dose volume are shown in Fig. 4. The lineal energy deposition spectra for various positions are indicated along the SOBP measurements. The high spatial resolution SOI microdosimeter allowed accurate investigation of the microdosimetric energy deposition features. These radiobiological ^{12}C SOBP features could not previously be measured with a TEPC (Tissue Equivalent Proportional Counter) or cell experiments. At the very distal part of the SOBP, a contribution from the nuclear fragments which originated within SOBP produces a very high lineal energy peak. These high energy lineal energy deposition events are mostly associated with low energy ^{12}C ions and fragments with the low lineal energy peak related to fast neutron contribution. These contributions are well separated from each other. At the most downstream measurement of the SOBP the continuum from the neutron only component can be clearly seen with a small peak from fragments at around 10 keV/µm with a maximum lineal energy deposition at around 1 MeV/µm. The neutron component is still a major contributor to the lineal energy deposition spectrum - a depth of 25 mm past the distal edge of the SOBP and continues well into the depth of the phantom and could still be slightly measured at over 75 mm past the end of the Bragg peak.

The measurements lateral to the SOBP show that the majority of the lateral low energy neutron components come from within the treatment volume. By rotating the SOI Microdosimeter, the side profile of the sensitive volumes becomes almost negligible and the SOI Microdosimeter becomes more sensitive to interactions from particles originating upstream of the beam. The lineal energy deposition spectra at

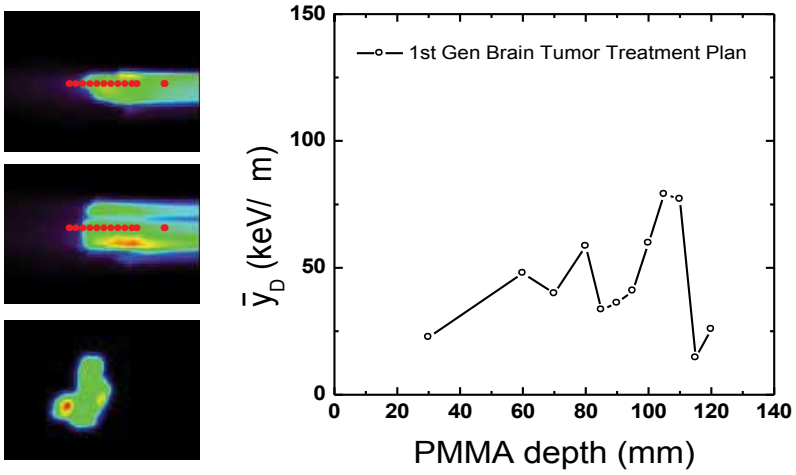

< Figure 6

Left, top to bottom: The Transverse, Coronal and Sagittal slices of the dose treatment plan for a patient brain tumor treatment along the beam isocentre. The red marks indicate measurement positions.

Right: The response along the isocentre of the SOI Microdosimeter.

different positions and orientations are shown in Fig. 5. These measurements indicate that the majority of secondary particles are produced within the SOBP volume.

The SOI Microdosimeter was also used to measure the dose from positions along the isocentre of a brain tumour treatment plan. The measurements are shown in Fig. 6. The SOI microdosimeter is able to accurately reproduce the intricate dose plan and can be used to verify the complicated dose profile.

Next steps

SOI Microdosimetry not only successfully measures the lineal energy depositions around treatment regions of various hadron therapy beams, but it also effectively measures the lineal energy deposition from a broad beam Bragg peak as well as a scanning beam SOBP. The out-of-field measurements revealed the contribution from the short range fragments close to the distal edge of the carbon ion Bragg peaks as well as a significant neutron component.

The SOBP measurement showed an increase in the dose-mean lineal energy deposition at the distal edge of the SOBP. This illustrates the advantage of using the small physical volume of a SOI microdosimeter compared to a much larger conventional TEPC.

For the next steps we will be testing the SOI Microdosimeters in a passive SOBP at HIMAC for comparison with the active scanning SOBP measurements taken at HIT. These measurements will indicate the source of the overestimation of dose at the end of the SOBP.

REFERENCES

[1] Wilson, R. R., "Radiological Use of Fast Protons", Radiology, 47, (1946), pp. 487-491

[2] Rossi, H. H. and Zaider, M. (1996). Microdosimetry and Its Applications, Springer. ISBN 3-54058541-9

[3] ICRP, (1983). Protection against Ionizing Radiation in the Teaching of Science. ICRP Publication 36. Ann. ICRP 10 (1).

[4] Bradley, P.D., Rosenfeld, A.B. and Zaider, M., "Solid state microdosimetry", NIM-B, vol. 184, issue 1-2, 2001, pp. 135-157

[5] Prokopovich, D. A., Reinhard, M.I., Cornelius, I.M. and Rosenfeld, A.B., "Response of a PIN Diode and SOI Microdosimeter to the TSL Quasi-Monoenergetic Neutron Field", IEEE Trans. Nucl. Sci., Vol. 58(6), (2011), pp. 3321 - 3327

[6] Prokopovich, D. A., Reinhard, M. I., Taylor, G. C., Hands, A., and Rosenfeld A. B., "Comparison of SOI Microdosimeter and Tissue Equivalent Proportional Counter Measurements at the CERF Facility", IEEE Trans. Nucl. Sci., 59(5)3, pp 2501-2505, (2012), DOI 10.1109/TNS.2012.2210733

[7] Wroe, A., Rosenfeld, A., Reinhard, M., Pisacane, V., Ziegler, J., Nelson, M., Cucinotta, F., Zaider, M., Dicello, J., "Solid State Dosimetry with Heavy Ions for Space Applications", IEEE Trans. Nucl. Sci., Vol. 54(6), (2007), pp. 2264-2271

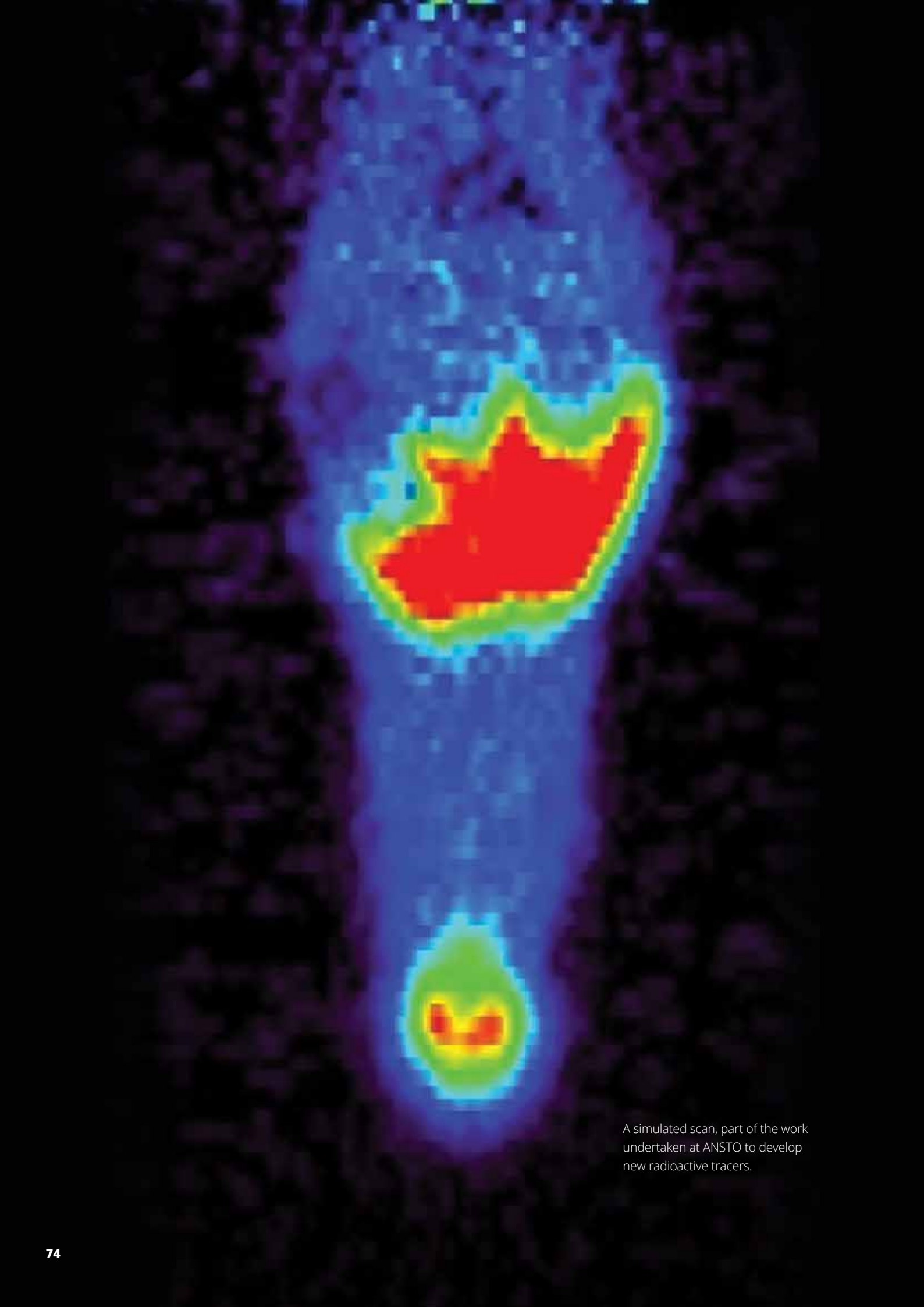

A simulated scan, part of the work undertaken at ANSTO to develop new radioactive tracers.

Generating realistic three-dimensional biological imaging

02

Positron Emission Tomography (PET) scanning is a relatively common medical imaging technique that uses radioactive tracers - chemical compounds in which one or more atoms have been replaced by a radioisotope that can be seen on a scan - to observe processes occurring inside the body. Such processes may include blood flow, oxygen use or sugar metabolism. This complex three-dimensional imaging technique requires sophisticated data processing methods to correct, reconstruct and analyse the PET information produced, and simulation tools are often used to design, optimise and validate these data processing methods.

Anthonin Reilhac-Laborde and his ANSTO colleagues are researching and developing new radioactive tracers, using pre-clinical imaging, for which there are little or no reliable PET data simulation programs available. The team have successfully adapted and validated the simulation tool PET-SORTEO. The study involved simulating raw PET data acquisition, as well as its correction and reconstruction. The validation showed that the simulation-produced results accurately reflecting those that would be generated from actual experiments.

The new, validated simulation tool will be used to benefit the scientific research community in many ways including the production of publicly available simulated PET databases for commonly used radioactive tracers. This will be an invaluable resource for other researchers optimising their PET data processing methods for their pre-clinical studies.

Anthonin Reilhac-Laborde, Frederic Boisson, Catriona Wimberley, David Zahra, Hamze Hasar, Marie-Claude Gregoire

ANSTO

Positron Emission Tomography

Positron Emission Tomography (PET) is an important nuclear medical imaging technique allowing the observation of the distribution in space and time of an injected molecule in the body. It is mainly used to investigate functional processes occurring in the body. PET scanners detect pairs of gamma rays emitted indirectly by a positron-emitting radionuclide or tracer, which is introduced into the body on a biologically active molecule. Three-dimensional (3D) image time sequences of the tracer concentration within the body are then reconstructed from the detected events. However, physical phenomena like photon scattering, attenuation and scanner limitation, such as spatial and time resolution, bias the detected signal and adequate corrections take place before, during and after the reconstruction step. Finally, mathematical models are used to translate the 3D image time series into biological parameters or body functions, such as blood flow, oxygen use, sugar metabolism, enzyme activity, neuroreceptor binding site density and occupancy, to name a few.

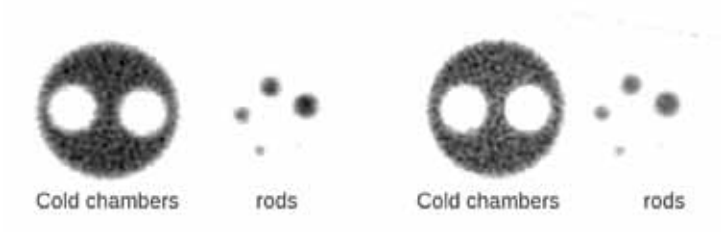

Experiment

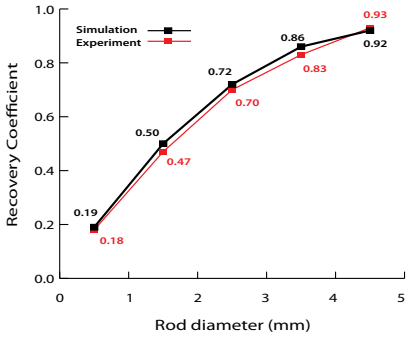

Simulation

Recovery Coefficient

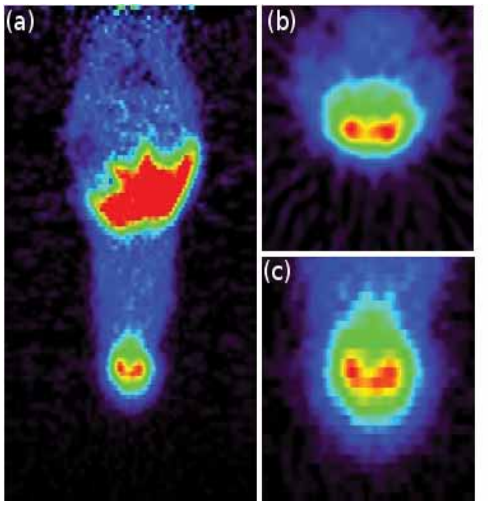

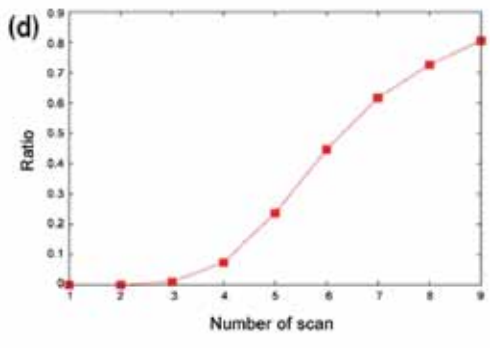

^ Figure 1
Experimental and simulated results obtained using the NU-4 2008 Image Quality Phantom and the associated Recovery coefficient measurements.

< Figure 2
(a) Coronal slice of a simulated Raclopride scan, (b) and (c) zooms of the brain extracted from a transverse and coronal slice, respectively. (d) Graph showing the detectability of receptor density variation in a Raclopride simulated experiment as a function of the number scans included in each group.

PET imaging is both sophisticated and complex, and the accuracy and exploitability of the final parameters rely on the adequate choice of methods and parameters for the acquisition, correction, reconstruction and data processing. Our research focuses on improving the quality of the PET data, not only by optimising the current processing methods, but also by designing and proposing to the community novel data-processing techniques. Monte-Carlo-based simulation of PET data plays a key role as it provides the underlying information, offering us the possibility to compare directly the outcome of the targeted method with a reference.

Validation of the PET-SORTEO simulation tool for pre-clinical scanners

PET-SORTEO is a Monte-Carlo-based simulator which enables fast generation of realistic PET data. This simulation model has been thoroughly validated and used for the geometries of clinical scanners [1]. As data processing techniques are specific to each scanner (clinical or pre-clinical), they must be optimised and revalidated (and often redesigned) as the images are different in quality (e.g. noise, spatial resolution). ANSTO's research develops and investigates new tracers in medical research and therefore we mainly focus on pre-clinical imaging using mice and rats, a domain in which no reliable fast PET data simulation program was available. Consequently, we put in place the tools and resources for the simulation of realistic pre-clinical images.

In this work, we first adapted and validated the PET-SORTEO simulation tool for the geometry of the Siemens Inveonsmall animal PET scanner, the most widely distributed scanner (ANSTO owns and operates three of them). A thorough validation of the processing line has been carried out involving the simulation of the raw PET data acquisition along with correction and reconstruction. Each time the validation compared simulated data with measurements (e.g. spatial resolution, count rate performance, scatter fraction) made in the same conditions using the actual scanner.

Fig. 1 shows an experimental and simulated PET image obtained using the NU-4 2008 Image Quality Phantom and the associated Recovery coefficient measurements as a function of the rod diameter. The recovery coefficient for a given rod is the ratio of the rod activity measured from the reconstructed image and the (unbiased) activity measured in a large region. The recovery coefficients measured for different rod diameters help to characterise the final spatial resolution. An ideal PET scanner would offer infinite spatial resolution, yielding a recovery coefficient of 1 for any source diameter.

Simulating realistic pre-clinical images with PET-SORTEO

PET-SORTEO is currently used intensively by ANSTO and its collaborators as a tool in various projects such as the optimisation of dual mice PET acquisition, image reconstruction, image registration, partial-volume-effects correction, statistical noise removal, kinetic modelling method and statistical analysis. We present here a study regarding the detectability of small biological variations using standard acquisition protocol and processing methods. In this study, two groups of 9 [^{11}C]Raclopride dynamic PET scans each were simulated using PET-SORTEO and a digital model of a mouse. The molecular distribution in the body and its evolution across time used in the simulation of the first group was representative of the distribution observed in healthy mice. We simulated the second group using exactly the same mouse model and activity distribution except for a very small brain structure, called the striata, in which the activity set corresponded to a 10% decrease in receptor density. Each simulated experiment was corrected, reconstructed and the receptor density maps were derived using standard methods and parameters. The detectability of the 10% receptor density variation between the two groups was computed as the ratio of the voxels found to be statistically different (paired t test, $p < 0.05$) in the striata with the total number of voxels (a voxel is a volumetric pixel or volumetric picture element) in the same region.

Fig. 2 (a,b,c) shows an example of simulated images of raclopride distribution in mouse and (c) the obtained detectability, as a function of the number of scans per group included in the study. Results indicate that with nine scans per group, the 10% variation is detected in 80% of the volume of the structure.

This simple study provided us with a state of play of the sensibility obtained with this imaging technique, when using standard processing methods in Raclopride experiments and sets the framework for optimisation strategies that are currently under investigation.

Future

The development of PET-SORTEO continues as we are planning to adapt and validate the simulation tool for other scanner geometries. In addition, we are planning to generate publicly open databases of simulated PET volumes for commonly used radiotracers. Such databases are highly desirable for the assessment and validation of PET data processing methods.

REFERENCES

[1] Reilhac A., Batan G., Michel C., Grova C., Tohka J., Collins D.L., Costes N., and Evans A.C.: PET-SORTEO: validation and development of database of simulated PET volumes, *Nuclear Science*, IEEE Transactions on 52(5), 1321–1328, October 2005

[2] Reilhac A., Lartizien C., Costes N., Sans S., Comtat C., Gunn R.N., and Evans A.C.: PET-SORTEO: a Monte Carlo-based Simulator with high count rate capabilities, *Nuclear Science*, IEEE Transactions on 51(1), 46–52, February 2004

[3] Lartizien C., Kuntner C., Goertzen A. L., Evans A. C., and Reilhac A.: *Validation of PET- SORTEO Monte Carlo simulations for the geometries of the MicroPET R4 and Focus 220 PET scanners*., Phys. Med. Biol. 52(16), 4845–62, August 2007

[4] Boisson F., Wimberley C., Zahra D., Pham T., Perkins G., Hamze H., Gregoire M.-C. and Reilhac A.: A NEMA NU 2008 *Validated simulation platform for optimizing biological studies with the Inveon pre-clinical PET scanner*., In Preparation.

Research by Arvind Parmar (left) and Frederic Boisson is helping improve cancer patient treatments.

Research helps make cancer medication doses safer and more effective

03

Treating cancer patients with drugs requires a fine balance between killing tumour cells without damaging normal cells, and managing the body's clearance of anti-cancer drugs so as to be effective without being toxic to the patient. If the body clears chemotherapy drugs too quickly, the tumour attacking action is lost, while slower metabolism of anti-cancer drugs results in higher concentrations of these drugs in the body which in turn causes toxicity and forces treatment to be delayed or stopped. A better understanding of how to achieve this fine balance will help in the treatment of cancer patients.

ANSTO's Arvind Parmer and his colleagues have used the radiopharmaceutical technetium (^{99m}Tc) sestamibi, which acts as a marker, to investigate drug clearance and toxicity. Cancer-free and cancer-bearing mice were studied using various medical imaging techniques to follow the distribution of the markers and better understand the underlying mechanisms in cancer treatment.

The new understanding of how to use medical imaging to monitor clearance of chemotherapy medication, gained through this study, can now be applied in future studies aimed at identifying patients at risk of toxicity. This will ultimately lead to better tailoring of medication doses for individual patients, which will make cancer treatment safer and more effective.

Arvind Parmar[1], Frederic Boisson[1], Marie-Claude Gregoire[1], Andrew Katsifis[1], John Allen[2], Graham R. Robertson[2], Stephen Clarke[3]

[1]ANSTO, [2]ANZAC Research Institute, University of Sydney, New South Wales
[3]University of Sydney, Royal North Shore Hospital, New South Wales.

The challenges of chemotherapy

When treating cancer patients with drugs, it is crucial to maintain a fine balance between killing tumour cells without damaging normal cells and managing the body's clearance of anti-cancer drugs. Anti-tumour action is lost if the drug is cleared too rapidly, while slower metabolism of chemotherapy drugs results in higher concentrations in the body which, in turn, causes toxicity resulting in the delay or termination of treatment. One factor known to contribute to altered drug clearance in cancer patients is inflammation associated with the growth of tumours.

We have previously found that the presence of a tumour causes a reduction in the enzymes and drug transporters in the liver that take up drugs from the bloodstream into organs such as liver, brain and bone marrow as well as pumping toxins out of the body. This reduction results in slower clearance of drugs. Because of this some patients develop adverse side effects from chemotherapy [1].

How can molecular imaging help?

To assess the impact of tumour-derived inflammation on the activity of one family of drug transporters throughout the body, the bio-distribution of the radiopharmaceutical markers ^{99m}Tc-sestamibi in cancer bearing and non-cancer bearing mice was investigated. The radioisotope Technetium, ^{99m}Tc, is combined with a pharmaceutical agent to create a marker for nuclear imaging. For the imaging we used the new Inveon Tri-modality small-animal imaging system located at the Brain and Mind Research Institute (BMRI), an imaging facility run jointly with ANSTO. The imaging system is versatile as it can combine three techniques Single-Photon Emission Computed Tomography (SPECT), Positron Emission

Imaging scanner	Protocol	Animal model	Radiotracer
Inveon Tri-modality PET/ SPECT/CT	SPECT: 99mTc-60 projection, ROR 30mm, 1 revolution, 15s projection, 20mm travel, 9 x 20mins scan (3hr total scan time) CT: 220° rotation 220 Projection, 4x4 bin, 113.22µm effective pixelsize, 600ms exposure 50kVp, 500µA, 3072x2048, DS1.	Balb/c xDBA mice(n=3) engrafted with Colon 26 (C26) tumour cells Balb/c xDBA healthy normal mice (n=3) as a control group	30 Mbq/100µl of ^{99m}Tc-sestamibi intravenously, which is exported from cells via drug transporters

Table 1
Imaging system.

Tomography (PET) and Computed Tomography (CT) in a single integrated scanner (see Table 1 for details). This provides three-dimensional imaging of multiple dynamic volumes and that are required for our measurements of bio-distributions.

In our studies, we tested the ability of ^{99m}Tc-sestamibi to act as a predictive marker for drug clearance and toxicity in normal tissues. Our results will clarify the mechanism linking cancer-induced inflammation to reduced drug clearance and provide options for future clinical trials in cancer patients.

Imaging the biodistribution

Analysis of the imaging data shows that Colon 26 (C26) tumour-bearing mice have slower rates of clearance of ^{99m}Tc-sestamibi in kidneys, intestines, gall bladder and liver compared to the control mice (Figs.1&2)

This finding was supported by *ex-vivo* tissue biodistribution data using a gamma counter which reduced accumulation was evident in intestines, liver, urine and bile fluid in the tumour groups compared to the controls (Fig.3).

The significant differences in ^{99m}Tc-sestamibi biodistribution and clearance indicate changes in the activity of transport proteins. As these drug transporters make a major contribution to clearance of many anti-cancer agents this study demonstrates the potential to use SPECT imaging with ^{99m}Tc-sestamibi for predicting drug clearance and toxicity in humans.

The Future

We are in the initial stages of understanding how to monitor the clearance of chemotherapeutic

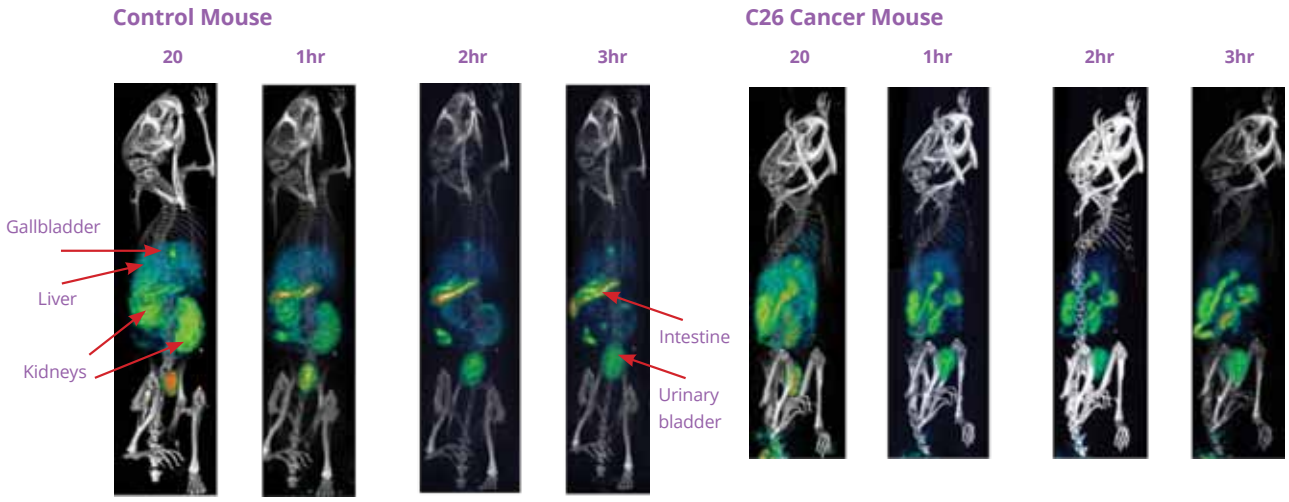

Figure 1
The SPECT/CT images of ^{99m}Tc sestamibi confirm predominant uptake in liver, kidneys and bladder at initial time points. At later time points, remarkable activity can be seen in intestine and urinary bladder. The increased retention of sestamibi in various organs in tumoured mice compared to normal mice is apparent over 3hrs.

drugs based on these results. The differences in drug biodistribution and pharmacokinetics for tumour-bearing versus control mice are significant and lay the foundations for subsequent experiments aimed at reversing inflammatory signalling associated with cancer in mice.

We now plan to perform imaging with first line anti-cancer drugs as a prelude to clinical studies in human cancer patients to identify those at risk of excessive toxicity. We aim to characterise the functional impact of tumour-induced inflammation on anti-cancer drug pharmacokinetics and identify strategies to normalise drug handling, leading to improved individualisation of anti-cancer drug dosing, and hence safer and more effective chemotherapy for patients.

Progressively, we hope to establish diagnostic biomarkers to identify patients at greater risk of toxicity from chemotherapy prior to its use, enabling better surveillance and more appropriate use of prophylactic antibiotics and growth factors. The new knowledge generated from these studies has the potential to fundamentally change cancer chemotherapy dosing strategies to improve the safety and efficacy of cancer treatment.

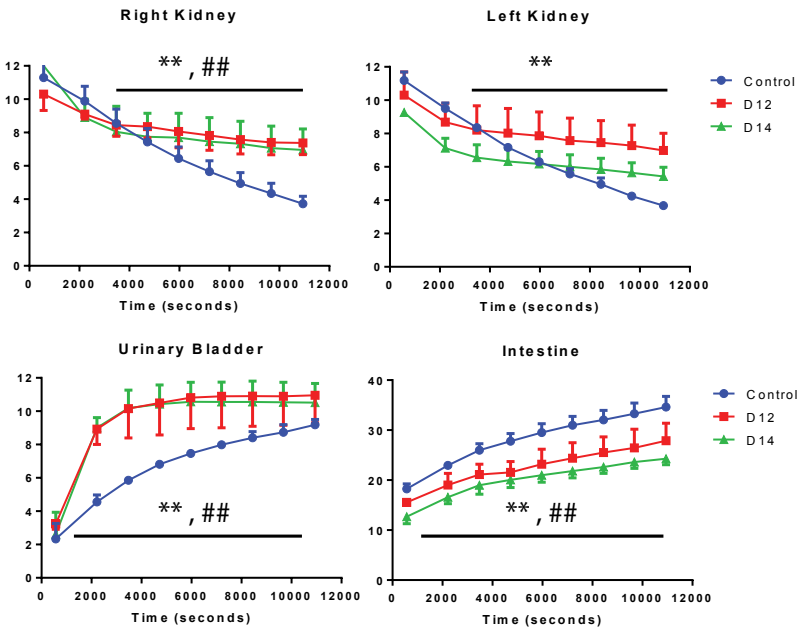

Figure 2

0-3 hrs time activity curve of Tc-99m sestamibi for various organs in normal mice, day 12 (D12 in red) and day 14 (D14 in green) tumour mice. (n=3). Data expressed as mean counts in tissue + Standard Error from Mean).. ** $p < 0.05$ D12 group compared to control, ## $p < 0.05$ D14 group compared to control.

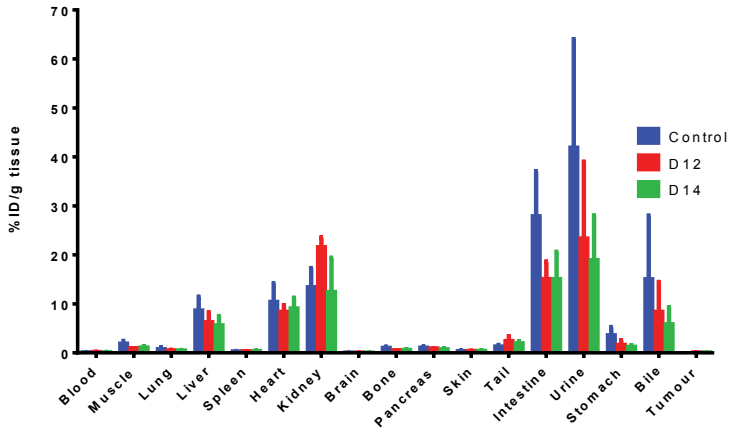

Figure 3

Biodistribution data of Tc-99m sestamibi at the 3hour time point for various organs in normal mice, day 12 (D12 in red), and day14, (D14 in green), Tumour mice. (n=3), data expressed as Mean ID/g+ SEM (Mean injected dose/gram of tissue+ Standard Error from Mean).

Acknowledgement

This study is a component of NHMRC project grant ID#632848 –"Improving the use of chemotherapy" 2010-2012.

REFERENCES

[1] Sharma R, Kacevska M, London R, Clarke SJ, Liddle C, Robertson G. Down regulation of drug transport and metabolism in mice bearing extra-hepatic malignancies. British Journal of Cancer. (2008);98:91–7.

[2] Boisson F, Zahra D, Parmar A, Gregoire M.C, Meikle S, Hamse H, Reilhac A. Imaging capabilities of the Inveon SPECT system using single and multi-pinhole collimators. Journal of Nuclear Medicine (Accepted)

Catriona Wimberley's research is improving our understanding of neurological diseases.

04

Improved understanding of progression rates in Parkinson's and Alzheimer's disease, and schizophrenia

Degenerative neurological diseases, such as Parkinson's and Alzheimer's disease or schizophrenia have devastating impacts on sufferers and their loved ones. ANSTO researchers have conducted research into an improved data analysis method for estimating changes in physiological parameters over time.

This work has made it possible for certain parameters to be applied to a broader range of experimental conditions and disease states than previously possible, and is enabling researchers to better understand the extent to which changes in these parameters are due to a disease's progression or are a response to treatments.

Positron Emission Tomography (PET) is a key medical imaging technique used to obtain dynamic images of functional processes in the body and monitor receptors in the central nervous systems associated with cognition, memory, learning, motivation, motor control and pleasure.

Abnormal function of these receptors is a factor in degenerative neurological and neuropsychiatric diseases. Physiological parameters related to the receptors can be estimated from the PET and can be monitored over time. Being able to pick up small changes in these parameters, can lead to a better understanding of these diseases, their triggers and treatments.

Catriona Wimberley[1], Anthonin Reilhac[2], Frederic Boisson[2], Kristina Fischer[3], Marie-Claude Gregoire[2]

[1]Brain and Mind Research Institute, University of Sydney, [2]ANSTO,
[3]Department of Preclinical Imaging and Radiopharmacy, Eberhard Karls University of Tübingen, Germany

Set up of the study

By injecting a radiotracer into an organ we can monitor how that tracer advances in an organ of interest over a certain time period, called a spatio-temporal distribution. Traditionally, a dynamic series is acquired after radiotracer injection, and the information about the distribution of the radiotracer is collected using Positron Emission Tomography (PET). In parallel, the radiotracer concentration delivered to the organ is measured, generally via blood sampling, and an input function to the system is derived.

The dopamine D2 receptor system is involved in many neurodegenerative and neuropsychiatric disorders such as Parkinson's Disease, Alzheimers and Schizophrenia. [^{11}C]raclopride is a PET radioligand that is used extensively to study dopamine D2 receptor availability in the striatum (a region in the brain rich in these receptors) in normal conditions as well as for studying pathologies, changes in response to treatment or pharmacological

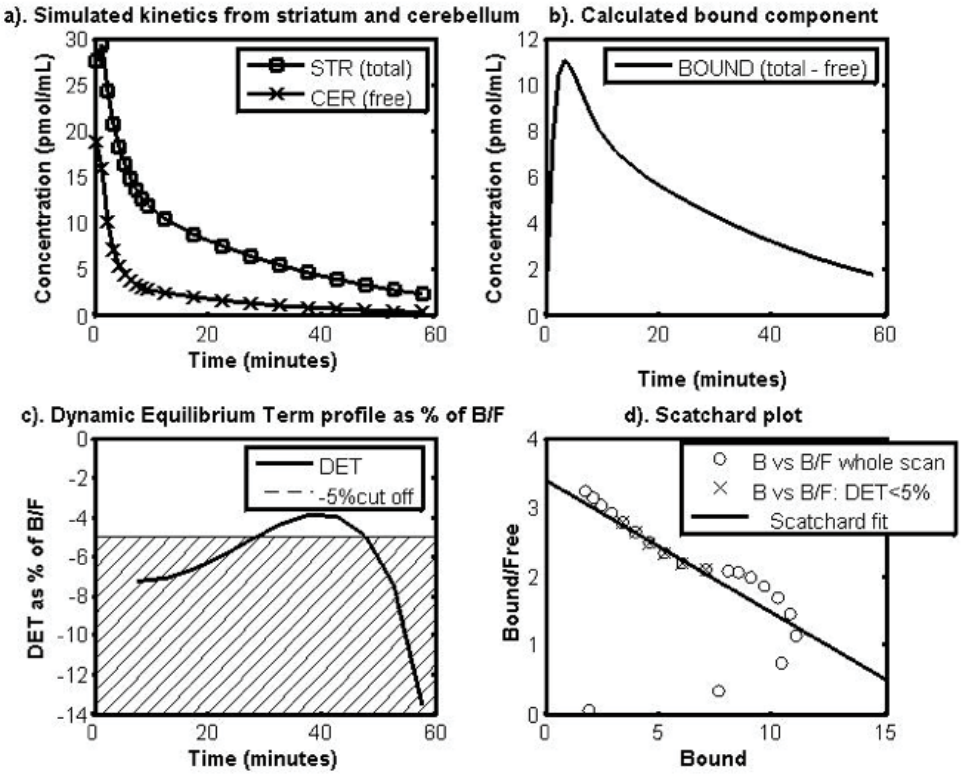

^ Figure 1

Data-driven method for choosing the optimal time window. Determination of the portion of the curve to use as guide by the residual term: a) Simulated time activity curves (TACs) of the target brain region, the striatum (total) and the reference region, the cerebellum (free), b) the TACs for the bound component, c) the dynamic equilibrium term (DET) profile from time t* as % of the ratio of B/F and cross hatching to indicate the cut-off point at 5 % and d) the Scatchard plot using the B and F from the TACs. The crosses show where the section taken when using the data driven method based on the DET profile.

intervention. The parameters that describe the receptor system are the receptor density (B'max), which describes the number of receptors in the area of the brain and receptor system being studied and the apparent affinity (1/appKd) which describes the affinity that the particular ligand has for the receptor. By monitoring these parameters (receptor density, B'max, and affinity, 1/appKd) over time we obtain a longitudinal study of neurodegenerative diseases, from PET data.

To calculate the parameters of the receptor system

Several methods have been derived to estimate biological parameters such as metabolism/incorporation rate or receptor density/affinity from the PET data. Most of them rely on the concept of compartmental analysis [1] which requires an arterial blood sample. Multiple injection protocols coupled with non-linear compartmental analysis, in the rodent have been used [2,3] to fully identify all the model parameters and thus biological values, such as receptor density, B'max, and apparent affinity, appKd, for the radioligand. These complex procedures

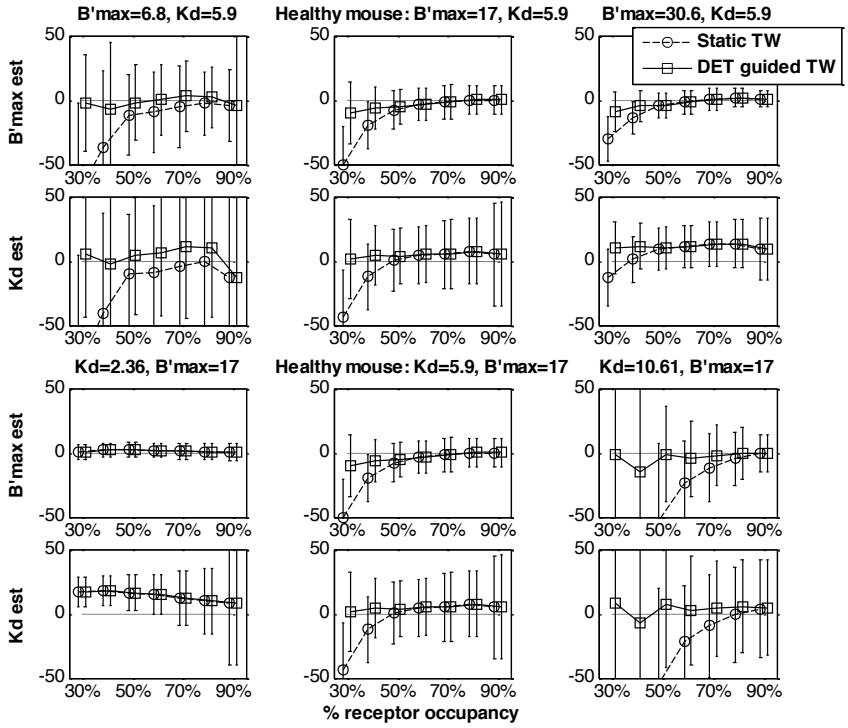

Figure 2

Percent relative error of parameter estimates (receptor density B'max, and apparent affinity appKd) for the two time windows, a static time window (circles) as has been used in the past and the data driven time window (squares) which uses the dynamic equilibrium term, or DET- with equivalent noise added for a range of receptor occupancy (injected dose) levels and a range of simulation parameters: B'max simulated at three different levels, i.e. a) 6.8, b) 17 and c) 30 and appKd simualted at d) 2.36, e) 5.9 and f) 10.6. Note that the lowest occupancy points for the static time window curves in the plots a) and f) are out of range. The values of the error in these cases are: B'max = 6.8, error = 75% and appKd = 10.61, error = 380% respectively.

cannot be used in longitudinal studies because they require blood sampling for an arterially sampled input function and long-time anaesthesia (up to three hours).

There are simplified methods that have been developed, such as the Simple Reference Tissue Model. These methods are used because they simplify the experimental protocol and do not require arterial blood sampling. However, these methods are used to determine the binding potential, or BP [4], which is defined as the ratio of receptor density, B'max, and affinity, appKd. A change in BP can therefore result from a change in B'max and/or appKd and this can lead to misinterpretation, especially when both individual parameters vary.

A simple, single injection protocol that could produce stable and robust estimates of both B'max and appKd for a range of experimental conditions and disease states would be most ideal for use in longitudinal neuro-receptor studies.

Determining the parameters for the D2 dopamine receptor system using the partial saturation approach

The partial saturation approach (PSA) was originally proposed by Delforge et al. [5,6] to estimate B'max and appKd independently in a single-injection/ single-scan experiment without blood sampling. The method is based on setting up an 'in-vivo equilibrium state' after a single injection of ligand to partially saturate the target receptors. The method exploits the natural decrease in bound ligand concentration to give a range of values for free ligand in the brain (F) and ligand bound to receptors (B) needed for a Scatchard analysis. Scatchard analysis is a graphical method used to determine B'max and appKd, usually used for *in vitro* binding experiments, but adapted for *in vivo* methods. It requires a dose of the ligand that is sufficiently large to occupy a significant percentage of receptor sites, but not so large so that a significant decrease can be observed during the limited time of the scan (1 hour at most).

The aim of this work was to increase the range and applicability of the Partial Saturation Approach (PSA) by developing a data-driven strategy for determining B'max and appKd, and validating the strategy using a simulation model based on experimental mouse PSA data by Fischer et al[7] with the ultimate goal of generalising the method for use with [^{11}C]raclopride PET experiments in the mouse brain.

Validating the method

To be able to apply the PSA confidently, the following assumptions needed to be validated for a range of receptor occupancy levels and over a range of experimental conditions. Firstly, the method requires the use of an independent measurement of the free ligand concentration, which is estimated using a reference region, the cerebellum (CER). Secondly, an apparent equilibrium state needs to be achieved, and a time window of data chosen to reflect that. And thirdly, the occupancy of the receptors in the target region, the striatum (STR) must be sufficient to allow a good range of Bound and Free values, needed for the analysis, over the time of the PET scan.

The data driven method for analysing the PSA data is shown in Fig. 1. It involves isolating where in the kinetic curves from the PET scan a dynamic equilibrium is reached by using the dynamic equilibrium term (DET) as an indicator. The DET shows the rate of change of the B over time as a proportion of the B/F value, i.e. the ratio of the ligand bound to receptors (B) and the free ligand in the brain (F). Ideally, to be in equilibrium, the rate of change of B and therefore the DET would be zero, however, as it is a dynamic system, in vivo, the DET will never be zero. Instead, the data used in the estimation of B'max and appKd is taken from the point at which the DET component is <5% of B/F.

A range of simulated PET experiments was generated to test and validate the method described above for a wide range of experimental conditions, such as receptor occupancy levels (by varying the injected dose of ligand) and disease states (by varying the B'max and appKd levels) as well as adding realistic PET noise to the simulations to gauge the effect of noise on the accuracy and robustness of the estimates. The simulations were based on PET experimental data from Fischer et al [7] . The analysis method as above was applied to the simulated PET data and the parameter estimates compared against just using a static

time window of 10-50 minutes, the common method for analysing the PSA data. The plots in Fig. 2 show that for most of the experimental conditions simulated the estimates using the DET-guided time window gives much more accurate estimates, especially at low levels of receptor occupancy. Using the DET-guided time window the estimates are not correlated with the occupancy level, as is the case with the static time window, especially for occupancy levels lower than 50%. That means that in PET experiments variability in the occupancy levels will not translate into variability in parameter estimates.

Using the method under other conditions

This study extended and validated the PSA method with the DET guided time window as an appropriate tool for estimating B'max and appKd with [^{11}C]raclopride in the rodent. It is now possible to use the PSA for a broader range of experimental conditions than previously done. These conditions include pharmaceutical or disease-induced changes of B'max and appKd, and a range of receptor occupancy levels. Being able to explore the availability of dopamine receptors in the striatum using [^{11}C]raclopride with a simple and straightforward method will help to assess changes due to disease state or pharmacological intervention in longitudinal studies.

REFERENCES

[1] Watabe, H., Ikoma, Y., Kimura, Y., Naganawa, M. & Shidahara, M. PET kinetic analysis--compartmental model. Ann Nucl Med 20, 583-8 (2006).

[2] Mauger, G. et al. Multiinjection approach for D2 receptor binding quantification in living rats using [lsqb]11C[rsqb] raclopride and the [beta]-microprobe: crossvalidation with in vitro binding data. J Cereb Blood Flow Metab 25, 1517-1527 (2005).

[3] Gregoire, M.-C. BrainPet, 2007 PO5-3U(2007).

[4] Lammertsma, A.A. & Hume, S.P. Simplified Reference Tissue Model for PET Receptor Studies. NeuroImage 4, 153-158 (1996).

[5] Delforge, J. et al. Quantification of benzodiazepine receptors in human brain using PET, [11C]flumazenil, and a single-experiment protocol. J Cereb Blood Flow Metab 15, 284-300 (1995).

[6] Delforge, J. *et al*. Quantitation of benzodiazepine receptors in human brain using the partial saturation method. J Nucl Med 37, 5-11 (1996).

[7] Fischer, K. et al. Noninvasive nuclear imaging enables the *in vivo* quantification of striatal dopamine receptor expression and raclopride affinity in mice. Journal of nuclear medicine : official publication, Society of Nuclear Medicine 52, 1133-41 (2011).

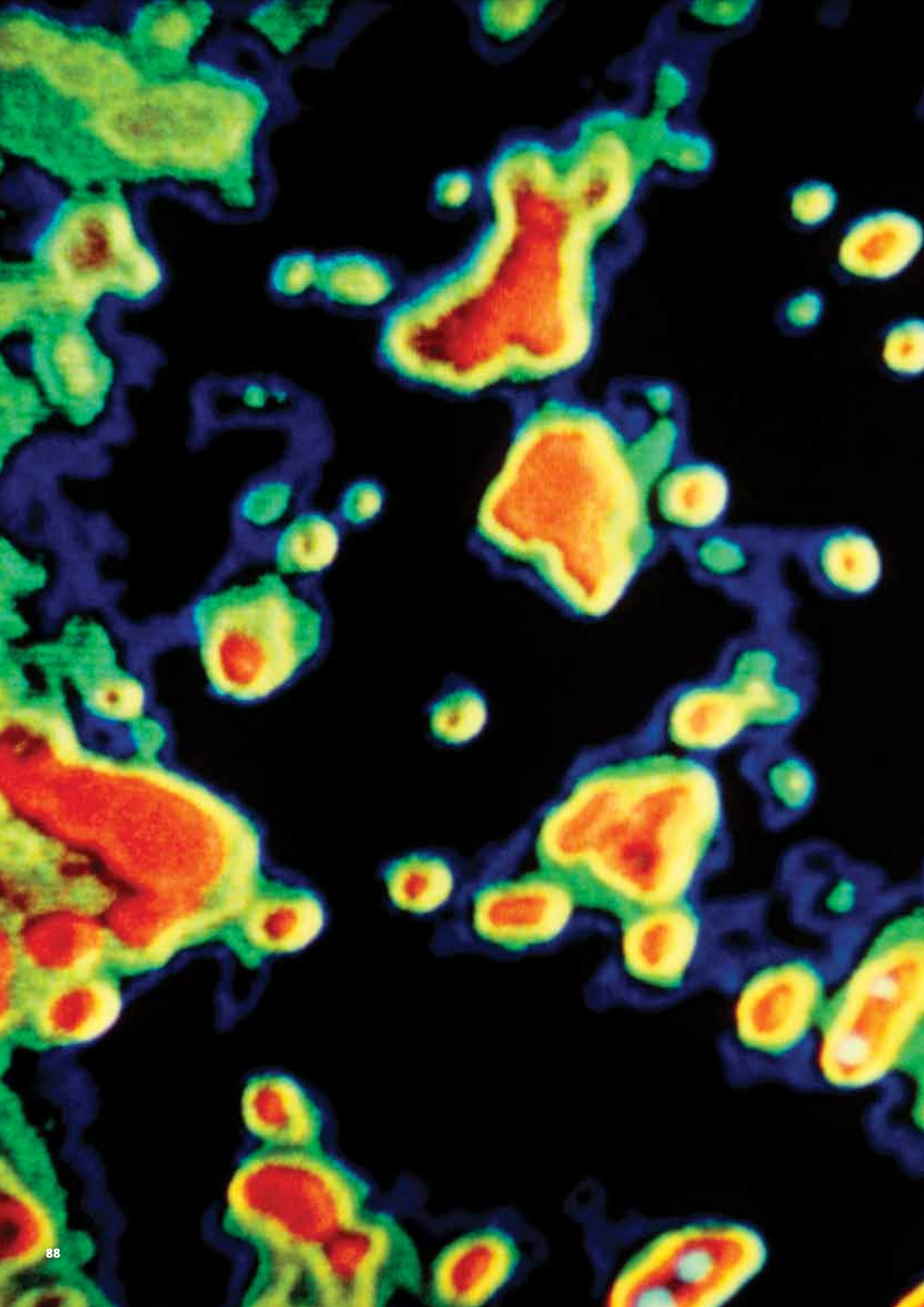

CHARACTERISATION AND RESOURCE PROCESSING

Characterisation is not only used for materials but also for analysing systems and processes. ANSTO's characterisation work is applied for national security and safety as well as in research for the resource industry.

Two studies from ANSTO Minerals in this section provide exciting outcomes for the resources industry for new processes in uranium recovery: one study looks at processes using sea water or saline bore water in uranium extraction avoiding the use of precious fresh water. Another study optimises uranium extraction during phosphoric acid processing providing better outcomes not only by recovering uranium for the energy sector, but also for the agricultural sector by removing uranium that exist as an impurity in commercial fertilisers.

The section concludes with a study that test 'apps' for radiation doses for smart phones as well as their functionality and usefulness and a nuclear forensic study demonstrates how thorough characterisation of legacy materials determines where and how these samples were produced.

Marina Fainerman-Melnikova, Karin Soldenhoff, James Quinn, Abigail Wilson and Deborah Wilkins (L-R) are studying alternative ways for extracting uranium from unranium ore.

Development of processes for the recovery of uranium from saline leach liquors

01

Uranium is extracted from uranium ore via a process called leaching, which uses sulphuric acid as the leaching agent. The presence of chloride in sulphuric acid leach liquors has a detrimental impact on conventional uranium recovery techniques, such as solvent extraction and ion exchange. One way to reduce chloride levels is to limit the recycling of process water, replacing it with clean, fresh water. This is of concern to many mines, particularly in Australia, where fresh water can be scarce.

ANSTO has recently conducted research into alternative solvent extraction and ion exchange processes that are impervious to chloride in the process water. The objective of the research is to provide processing options to use sea water or saline bore water in uranium hydrometallurgical circuits which would deliver reduced operating costs and positive environmental outcomes.

The early results of this research have been encouraging, revealing mixed reagents solvent systems and alternative ion exchange processes that have the potential to offer solutions and have pointed the way to further investigations.

Karin Soldenhoff, Marina Fainerman-Melnikova, Deborah Wilkins, James Quinn, Abigail Wilson

ANSTO

How yellow cake is produced from ore

One of the conventional methods of extracting uranium from ores is by leaching the ores with sulphuric acid, using an oxidant to promote leaching of the uranium minerals. The resultant leach solutions are treated by solvent extraction (SX) or ion exchange (IX) technologies to purify and concentrate the uranium to a product stream prior to its recovery by precipitation (Fig. 1).

These technologies are well established and for SX processes make use of long chain tertiary amines as the main constituents of commercial solvent formulations. In an SX process, the uranium is transferred to the solvent in the extraction circuit, rejecting to the raffinate elements arising from the dissolution of gangue-minerals. The solvent then proceeds to the strip circuit, where it is contacted with a strip solution that encourages the uranium to transfer back into the aqueous phase. In IX processes, strong base anion exchange resins containing quaternary amine functionality , are widely used to affect the transfer of uranium from the leach liquor to a product stream.

Why salinity is a problem for uranium producers

Common to the SX or IX processes is the extraction of uranium via an anion exchange mechanism, where uranium is extracted as negatively charged uranyl sulphate complexes. Chloride, when present as an anion in leach solutions, is also extracted and has a deleterious impact on the process by competing with uranyl sulphate and decreasing the loading capacity of the solvents and the resins.

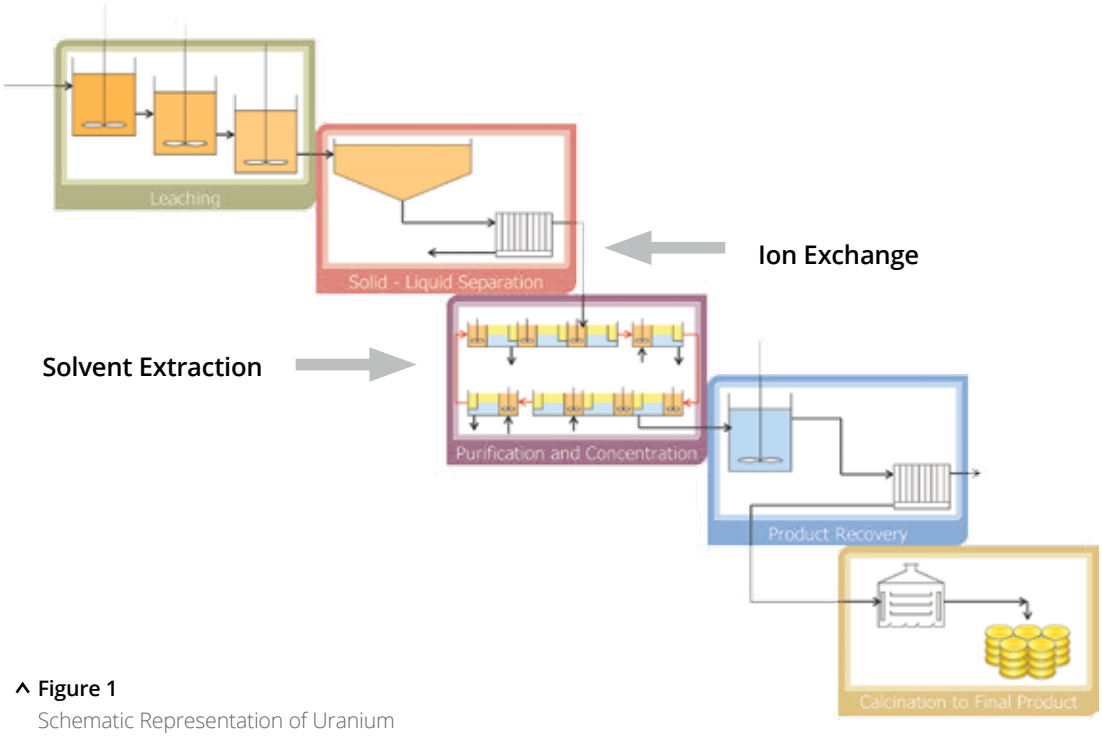

^ **Figure 1**
Schematic Representation of Uranium Processing.

< **Figure 2**
Arid region of Australia.

Industrial experience has shown that the chloride concentration in liquors must be limited to less than 3-5 g/L to avoid significant impact. Chloride can be introduced to the process in different ways including through the entrainment of chloride in the ore, the presence of chloride in aquifer waters, the use of chemicals such as chlorate added as an oxidant in leaching or the use of sodium chloride for solvent stripping. With recycling of process waters, the concentration of chloride can build up and it needs to be controlled via a bleed stream and replenished with low salinity process water.

In arid regions of Australia (Fig. 2), low salinity water is not always readily available and there are economic and environmental incentives to be able to use high salinity bore water or sea water as a process water source, thus preserving precious natural high quality water resources.

Processes that thrive in saline and hypersaline environments

ANSTO has been investigating alternative processes that tolerate high chloride and have developed a number of process options that can be adapted to suit a range of uranium and chloride concentrations in leach liquors arising from in-situ recovery, heap leach or tank leach operations.

Ion exchange with weak base resins

Following an extensive resin screening program, ANSTO identified a number of weak base anion exchange resins suitable for application in leach liquors containing chloride. These resins satisfy important process relevant criteria but are not effective at chloride concentrations higher than 10 g/L Cl. The proposed ANSTO weak base

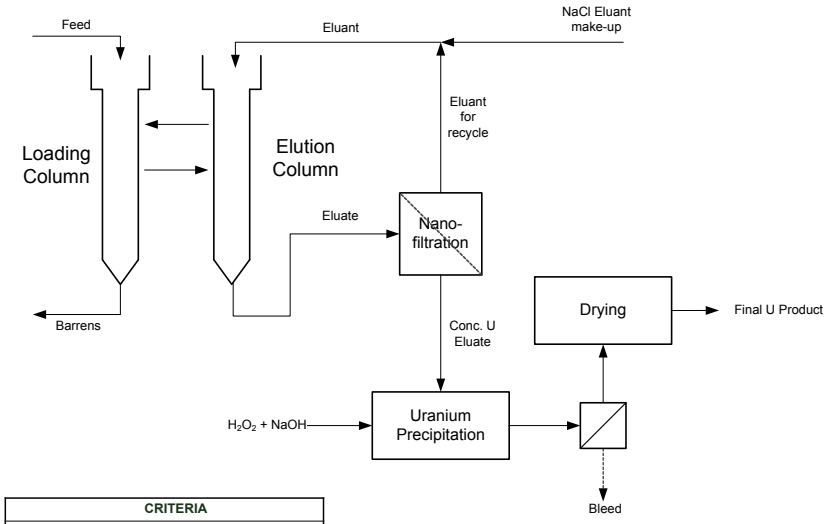

CRITERIA
• Suitably high resin loading capacity at 10 g/L Cl
• Resin selectivity for uranium over impurities
• Favourable elution
• Suitable uranium adsorption and elution rates
• Seamless integration with conventional uranium recovery steps
• Minimizing reagent consumption

< Figure 3
ANSTO weak base ion exchange process for saline liquors.

anion exchange process is outlined in Fig. 3. It consists of a uranium IX adsorption step, followed by sodium chloride elution. The eluate is treated by nanofiltration, allowing for recycle of permeate back to the elution circuit. This offers significant scope for minimising reagent consumption. The concentrate stream can be directly fed to a uranium precipitation circuit using hydrogen peroxide.

Ion exchange with chelating resins

As the chloride concentrations in the leach liquors approach those of sea water (~ 20 g/L Cl) and, anion exchangers are not able to function. To extract uranium, a cation exchanger is needed which by definition, does not respond to increases in chloride concentration. It is known that cation exchangers are not selective towards uranium, and therefore, any proposed uranium recovery process will have to address the co-adsorption of other metal impurities. Of particular relevance is the co-adsorption of ferric ion, which is commonly present.

There are several classes of commercial cationic chelating resins that have been investigated, including resins containing iminodiacetic, sulphonic/ phosphonic or aminophosphonic functional groups. Although exhibiting high resin uranium loadings, all suffer from drawbacks either with respect to the lack of selectivity, difficulty in elution or requiring regeneration so work in this area is ongoing.

Solvent extraction with mixed reagents

DEHPA, (di-2-ethylhexylphosphoric acid), is an acidic reagent that extracts via a cation exchange mechanism, and was one of the first solvents used industrially for uranium extraction. DEHPA extracts many cationic species, in addition to the uranyl cation (UO_2^{2+}). Chloride is not loaded and therefore does not limit extraction. However, it is the lack of selectivity, especially towards ferric ion that was a contributory factor in DEHPA being superseded by tertiary amines in industrial application.

Our work with mixed solvents containing both DEHPA and Alamine 336 (a tertiary amine) has shown that these systems do not extract iron (III) or chloride as strongly, and achieve relatively high uranium loadings (5-7 g/L U) at seawater chloride concentrations (20 g/L) and higher (Figs. 5 and 6). Small amounts of co-extracted iron (III) can be readily scrubbed from the solvent using dilute sulphuric acid. Uranium can be stripped with an alkali (1 M Na_2CO_3) or with sulphuric acid. However, the mixed solvent requires higher concentrations (5.6 M H_2SO_4) than conventional strong acid stripping circuits for tertiary amine which require only 4 M H_2SO_4. Such differences are important to overall plant economics and ANSTO continues to investigate mixed reagents systems that satisfy all the criteria for a successful process.

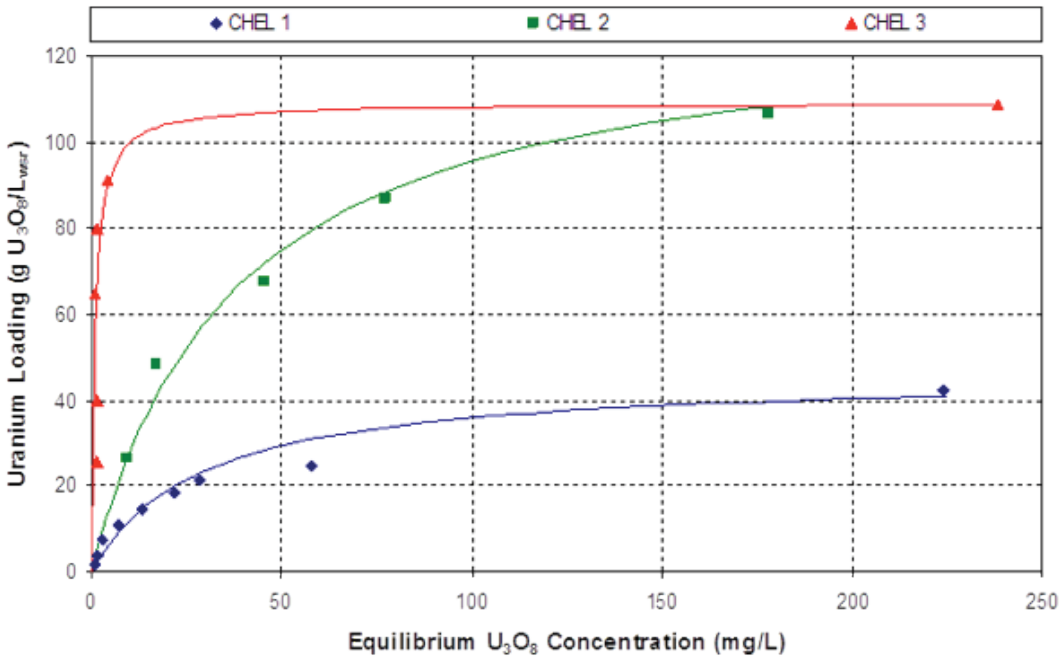

Figure 4
Loading isotherms for uranium with chelating resins at 22 g/L chloridechloride.

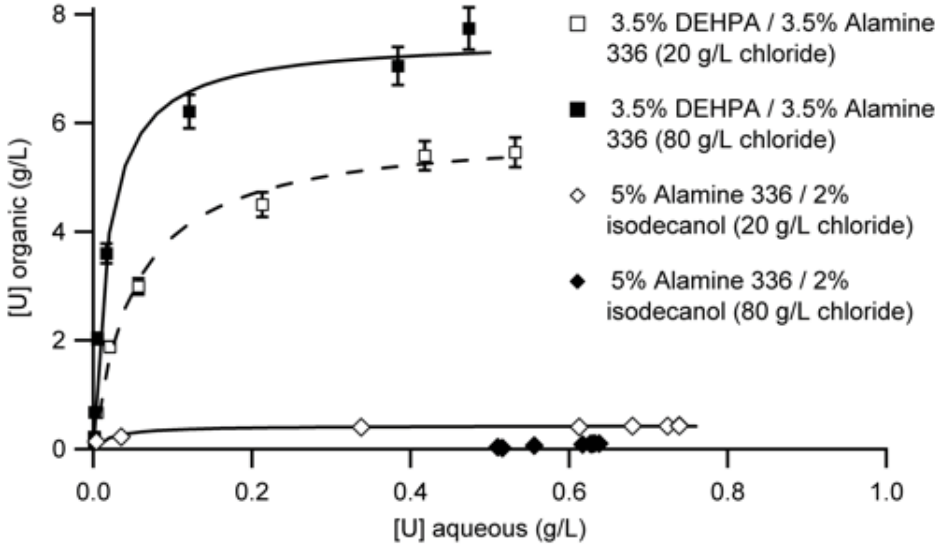

Figure 5
Solvent extraction of uranium by mixed solvent (3.5% DEHPA / 3.5% Alamine 336) and conventional solvent (5% Alamine 336).

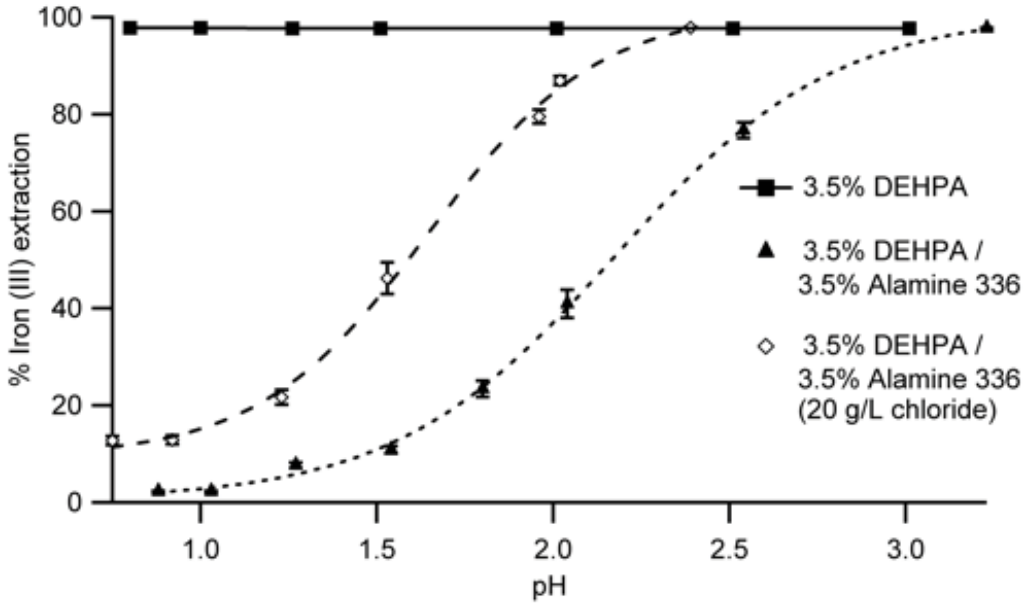

Figure 6
Suppression of iron (III) extraction with the addition of Alamine 336 to DEHPA.

REFERENCES

[1] Fainerman-Melnikova, M., & Soldenhoff, K. (2012). Uranium extraction from saline solutions using weak base anionic resins. *CIM Journal*, 3(2), 117-124.

[2] Manis, A., Soldenhoff, K., & Ovinis, M. (2011). *Membranes in Uranium Processing*. Paper presented at the AusIMM, Adelaide, South Australia.

[3] Wilson, A., Fainerman-Melnikova, M., & Soldenhoff, K. (2011). *What are the Options for an Intergrated IX Process to Recover Uranium from Saline and Hypersaline Liquors*. Paper presented at the ALTA 2011 Uranium, Perth, Western Australia.

[4] Quinn, J., Wilkins, D., & Soldenhoff, K. (2013). Solvent extraction of uranium from saline leach liquors using DEHPA/Alamine 336 mixed reagent. *Hydrometallurgy*.

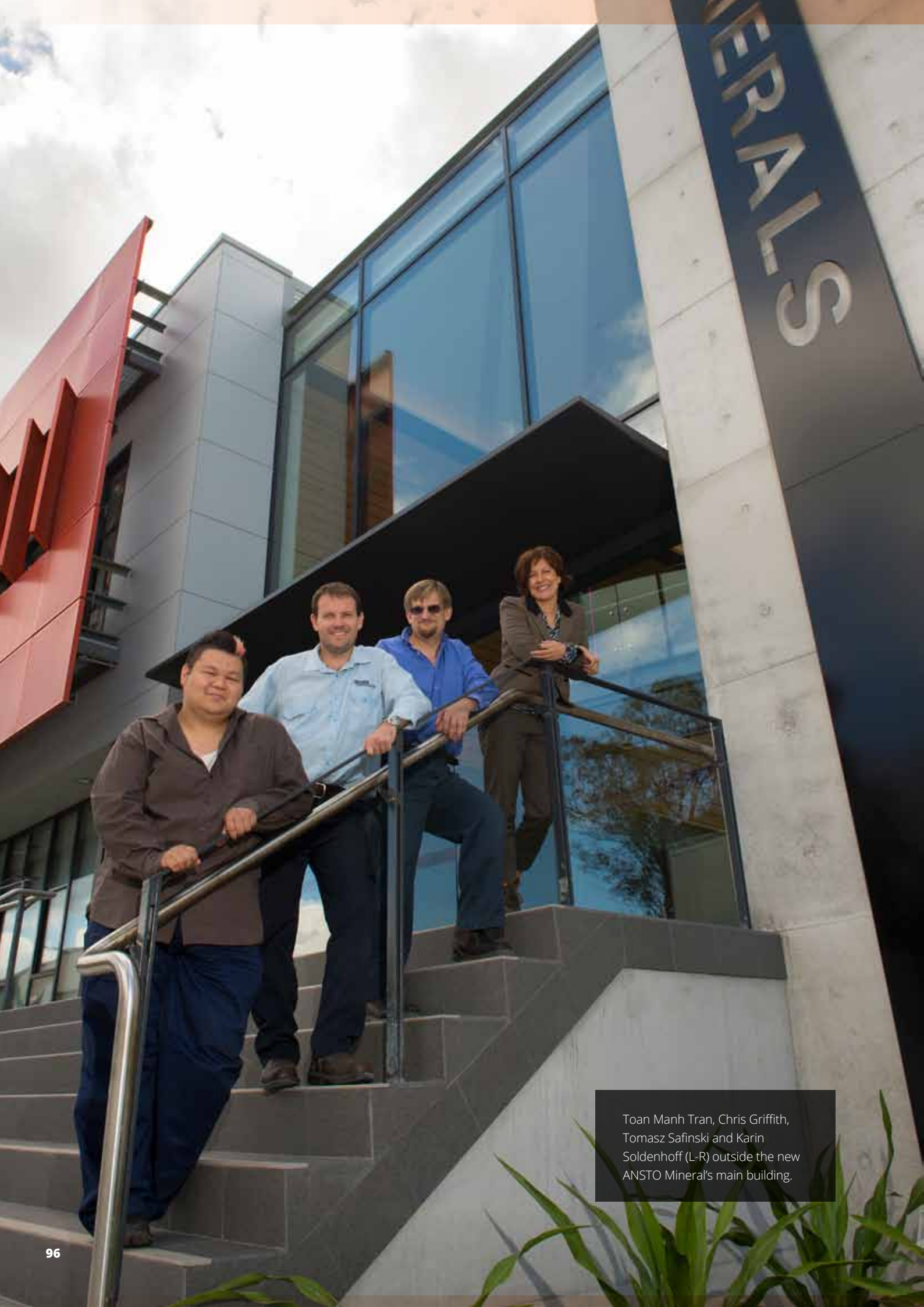

Toan Manh Tran, Chris Griffith, Tomasz Safinski and Karin Soldenhoff (L-R) outside the new ANSTO Mineral's main building.

Recovery of uranium as a by-product of phosphoric acid production

02

Uranium is a valuable resource used worldwide to generate power for millions of people. The uranium present in phosphate rocks and reporting to phosphoric acid during processing is currently not being recovered because the necessary technology is not economically viable.

There is estimated to be up to 25 megatonnes of uranium around the world stored in phosphate, representing an extensive untapped global resource.

ANSTO has partnered with the Uranium technology company Urtek LLC to develop the PhosEnergy® process to recover uranium from phosphoric acid. Uranium recovery in this context is important for the energy sector as well as the agricultural sector, as it provides a means of removing uranium present as an impurity in fertiliser production. The PhosEnergy® process is integrated into phosphoric acid production, resulting in a cleaner phosphoric acid product whilst recovering uranium as a by-product.

The process uses ion exchange resin technology to concentrate and separate the uranium from the phosphoric acid. The ANSTO team, led by Karin Soldenhoff, has had to overcome the technical challenge of significantly improving the effectiveness of the resin used to extract the uranium. Once this was achieved in the laboratory, the process was tested continuously at ANSTO using feed liquors sourced from operating plants worldwide. The process is now well on its way to commercialisation. Based on the results obtained, Urtek built and successfully operated a PhosEnergy® demonstration plant in the United States.

Toan Manh Tran, Tomasz Safinski, Chris Griffith, Karin Soldenhoff

ANSTO

The PhosEnergy® process

The PhosEnergy® process targets the recovery of uranium from phosphoric acid. This patented process [1] is new technology being commercialised by Urtek LLC, which is jointly owned by Cameco Corporation and Uranium Equities Limited. ANSTO has been a partner in the development of this technology since 2008. The PhosEnergy® process provides a dual benefit in the all-important areas of energy and food security:

i) Recovery of uranium as a by-product, extracting additional value from a well established conventional process, and

ii) Removes uranium as an impurity from the phosphoric acid, which is a precursor to fertilizer production

This process is based on ion exchange technology and specialized pre-treatment of the phosphoric acid. The process, outlined in Fig. 1, removes uranium from the wet process phosphoric acid (WPA) process, with no impact), without impacting on the downstream process for phosphoric acid production.

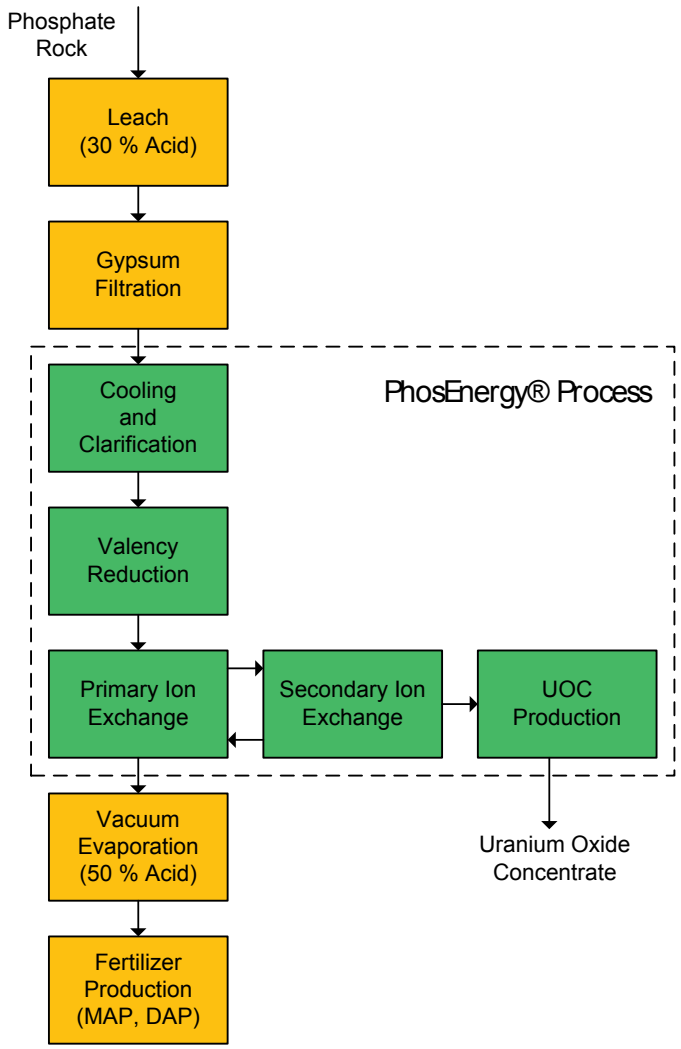

< Figure 1
Schematic of the PhosEnergy® process integrated in the wet phosphoric acid process.

Conventional phosphoric acid production

Uranium occurs in sedimentary marine phosphate deposits, at concentrations ranging between 30 and 300 parts per million U_3O_8. Currently the uranium is not recovered, but it has been estimated that globally there is up to 25 megatonne (Mt) of contained uranium present in phosphate resources [2].

Phosphoric acid is recovered from the phosphate rock, containing the mineral apatite ($Ca_5(PO_4)_3(F,Cl,OH)$). The phosphate rocks host uranium in isomorphous substitution for calcium (same structural position) . The typical chemical composition of phosphate rock is presented in the Table 1. Apatite is acid soluble. The conventional process route for recovery of phosphoric acid is to digest the rock with sulphuric acid, producing phosphogypsum (calcium sulphate dihydrate) as a by-product of the reaction. This process is known as the Wet Phosphoric Acid (WPA) process. Two main process routes are employed, the dihydrate and hemihydrate routes. These refer to the hydration of the gypsum which is affected by the processing conditions used. In the dihydrate route, which is more commonly used, the uranium stays in solution, while its nuclear

Typical chemical composition of phosphate rock			
P_2O_5	29-38 %	U_3O_8	120-240 ppm
Fe_2O_3	0.2-1 %	Rare Earth Oxide	0.1-1 %
Al_2O_3	0.1-1 %	Cl	0.01-0.7 %
CaO	48-52 %	K_2O	0.1-0.4 %
MgO	0.2-0.8 %	F	3.3-4.3 %
SiO_2	0.2-5 %	Organic Carbon	0-0.4 %

< Table 1
Typical chemical composition of phosphate rock.

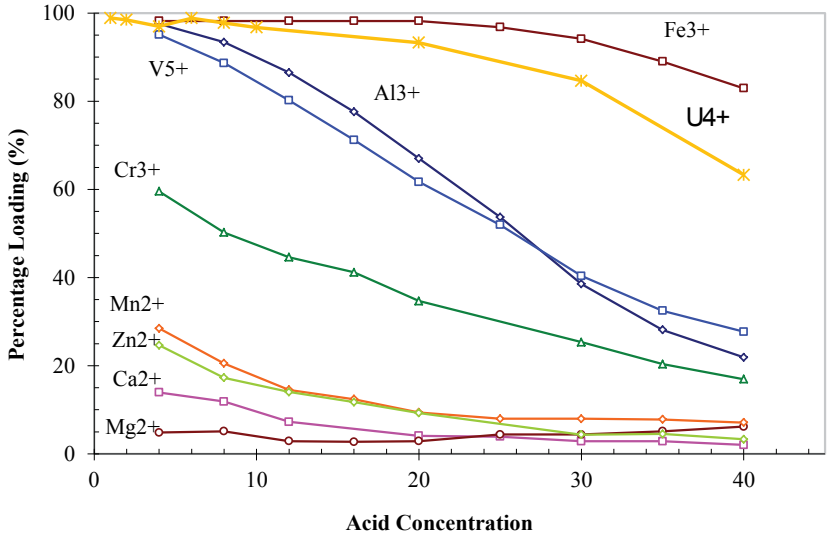

< Figure 2
Loading of key metals on aminophosphonic resin. Synthetic feed solutions for these tests containing 100 mg/L of each metal.

decay progeny such as radium are precipitated with the gypsum. The PhosEnergy® process targets the recovery of uranium from the WPA Process dihydrate route.

Uranium has historically been recovered from phosphoric acid at an industrial scale using solvent extraction (SX) technology. The last plants operating were shut down in 1998, mainly due to the decrease in the uranium price, which rendered the process uneconomic. In addition, there were operational issues associated with crud formation and phase disengagement, which required extensive pre-treatment of the acid, including cooling, filtration and clarification; adsorption onto activated carbon, desaturation, and clay treatment. Post-treatment of the SX raffinate to remove entrained organic was also required.

In the early stages of process development, ion exchange (IX) was identified as a technology better suited for feed liquors containing the relatively low concentration of uranium present in WPA solutions (<300 mg/L U_3O_8). IX processes tend to have lower capital and operating costs compared to SX. Additional advantages include greater tolerance for organic acids present in the feed, a wider range of operating temperature and no requirement for post-treatment of phosphoric acid.

The technical challenge

The resins employed for uranium loading from WPA are classed as 'chelating resins' and possess aminophosphonic acid functional

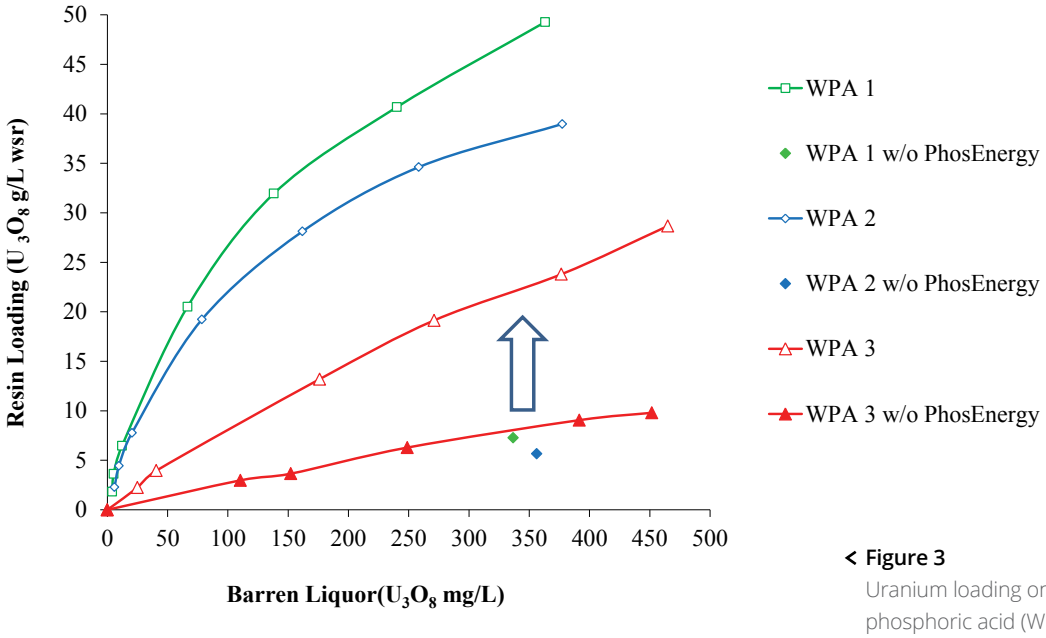

< Figure 3

Uranium loading on the resin from phosphoric acid (WPA) liquors.

WPA Liquors Sourced from Operating Plants.

groups. These resins are used in industrial applications such as brine softening. As highlighted by the data presented in Fig. 2, this type of resin is not very selective for uranium, but it is capable of extracting uranium at 30% P_2O_5 concentration typical of WPA. Ferric ion adsorbs strongly on the resin, and needs to be reduced to the divalent oxidation state. Aluminium and vanadium are also well extracted.

In synthetic solutions, made up of uranium, iron and P_2O_5, at concentrations similar to those found in WPA liquors, and with the iron suitably reduced, uranium loading on the resin is acceptable. However, with similar treatment of WPA liquors obtained from operating sites, the uranium loading on the resin was found to be very low. The PhosEnergy® technology has overcome this challenge as highlighted in the data presented in Fig. 3, which shows a significant improvement in uranium loading after PhosEnergy® solution pre-treatment. Plant solutions from different plant sites have been tested at ANSTO (Fig. 4) and they all responded to the PhosEnergy® technology.

Process development phases and research outcomes

Staged process development has been undertaken over a period of five years. The first stage was batch laboratory test work carried out at bench scale, where resins were screened, and the crucial development was carried out in terms of proof of concept to achieve the required loading of uranium on the resin. Both synthetic and plant liquors were used for this work [3].

The second stage was to test the ion exchange process continuously and several mini-pilot plant campaigns were carried out at ANSTO to integrate the pre-treatment, primary IX adsorption and elution as well as secondary IX. The objective of this work was to reproduce the success of the batch test work in a continuous process and quantify reagent consumptions for liquors sourced from different parts of the word [4].

Based on the results obtained, Urtek built a PhosEnergy® demonstration plant, which was shipped to the United States of America. This plant was commissioned in May and operated from June to August 2012 (Fig. 5). The results of the Pre-Feasibility Engineering Study have been released and estimate operating costs at US$18/lb of U_3O_8, which are relatively low compared to worldwide uranium production costs [5]. Urtek is now seeking to enter into the next phase of development of on-site demonstration to provide information for a definitive feasibility study, which is a significant step towards the commercialisation of this technology.

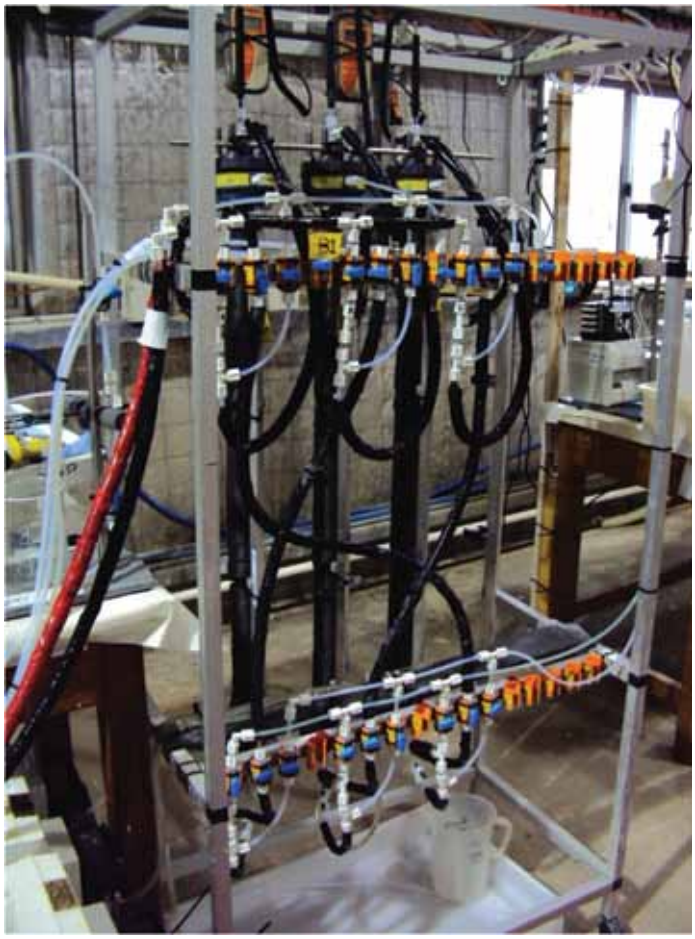

< Figure 4
Early configuration of mini-plant test work at ANSTO.

< Figure 5
Inside the PhosEnergy containerised demonstration plant.
(Photo courtesy Urtek).

REFERENCES

[1] Bristow et al, Extraction of Uranium from Wet-Process Phosphoric Acid, US 2010/0028226 A1, Feb. 4, 2010.

[2] Jasinski, S. M. (2013). Phosphate Rock Statistics and Information. Retrieved 8 March, 2013, from http://minerals.usgs.gov/minerals/pubs/commodity/phosphate_rock/.

[3] Soldenhoff, K., Tran, M.T., Griffith, C. (2009). Recovery of Uranium from Phosphoric Acid by Ion Exchange. Technical Meeting on "Uranium from Unconventional Resources" organised by the International Atomic Energy Agency (IAEA), Vienna, Austria, 4-6th Nov 2009.

[4] Davidson, D., Jones, B. (2011).Urtek's PhosEnergy Process, Workshop on "Uranium Recovery from Phosphates and Phosphoric Acid" organised by the International Atomic Energy Agency (IAEA) , Marrakech, Marocco, 31st Oct-4th Nov 2011.

[5] Uranium Equities Limited (CAN 009799553), PFS Results for PhosEnergy Process, ASX Announcement , 5 March 2013, Retrieved 15 March, 2013, from http://urtekllc.com/.

Andrew Wotherspoon and Alison Flynn testing the Radioactivity Counter app in ANSTO's Instrument Calibration Facility.

Smart phone radiation detector 'app' tests positive

03

The popularity of smart phones continues to grow, with the availability of an ever-growing range of applications, or 'apps', increasing their functionality and usefulness.

One such app is 'Radioactivity Counter', which claims to enable the phone to work as a dosimeter, which measures a person's exposure to radiation. The app claims to accurately detect the dose in the radiation unit microGray per hour (μGy/h) using the phones in-built camera, which is not only sensitive to visible light, but to higher energy gamma photons. Alison Flynn and her ANSTO colleagues tested the performance of this "app" against its claims.

The application was assessed on two different phones: the Apple iPhone 4S and the Samsung Galaxy S2. The phones were tested using ANSTO's Instrument Calibration Facility and the results showed the application is indeed able to measure exposure to radiation. It delivers a linear response to changes in dose, meaning the device can be accurately calibrated to reliably determine the potential dose rate to which a person is exposed.

Alison Flynn, Andrew Wotherspoon, Stewart Gill, Anthony Overton, Mark Reinhard

ANSTO

How to detect radiation in a metal-oxide-semiconductor chip

The increasing popularity of smart phones and portable devices, and the availability of a wide range of downloadable applications (or 'apps') for such technology, continues to introduce new functionality and utility. Radiation detector apps are now available commercially for both Apple and Android devices. These apps utilise the ionising radiation sensitivity of on board silicon-based complementary metal-oxide-semiconductor (CMOS) cameras to monitor radiation levels in the surroundings. The CMOS devices are small silicon chips used in cameras to detect visible light, but can also detect the higher wavelengths of gamma-ray and x-rays.

The device's response to ionising radiation is not normally evident to the user as the signal is very small when compared to that of visible light and is undetectable in the short image acquisition times in the order of 100 milliseconds. The application of black electrical tape over the camera lens eliminates the visible light response allowing the penetrating gamma-rays and/or x-rays to be observed.

The radiation detector app uses the phone to record the number of times it detects an interaction and that number is converted into the dose received by the phone. This study aims to determine how well the application works as a dosimeter.

With the application of the black tape, the device will be sensitive to gamma-rays and x-rays but will be unable to detect beta or alpha particles or neutrons.

Testing procedure

In order to accurately work as a dosimeter the phone must have a linear response to the dose rates which it is exposed to. This means that the device can be accurately calibrated and that its dose determinations will be reproducible. Also the device should give the same result regardless of the orientation in which it is being held i.e. its angular dependence.

< Figure 1
This shows the display the iPhone with the app running and a ^{137}Cs source placed behind the phone. The top right panel shows the response of the camera, with dots representing where gamma-ray photons have interacted in the CMOS chip.

Two smartphone devices were evaluated using the Instrument Calibration Facility (ICF) at ANSTO. The ICF consists of a range of ^{137}Cs sources and a movable platform. Each source can achieve a range of different dose rates, once the operator has entered the desired dose rate the position of that dose rate is calculated and the platform moves to the desired distance from the source.

The two smart phones tested were the iPhone 4S and the Samsung Galaxy S2. For each phone the camera was covered with black tape and care was taken to ensure that no light was entering the camera. For a range of dose rates from 1 to 349,796 microsieverts per hour (µSv/h) (for x-ray and gamma rays Gy and Sv are equivalent) each phone was used to acquire five one minute counts for each dose rate. For a constant dose rate the phones were rotated to determine the angular dependence.

Results

For both phones the counts per minute recorded were directly proportional to the dose rate for dose rates above 20 µGy/h for the Samsung and 30 µGy/h for the iPhone with results shown in Fig. 2. The average dose rate on a long haul flight is around 7 µGy/h. The poorer performance of the iPhone is attributed to the fact that only the front camera could be used; there is a possibility that light from the display of the screen could be detected in the camera through the top layer of glass.

The dose rate at which the phones can accurately calculate the dose rate is equivalent to 0.2 Sv if exposed for an entire year, this is 200 times higher than the Australian Radiation Protection and Nuclear Safety Agency (ARPANSA) dose limit for the general public of 1 mSv [1]. In a situation where this level of exposure is only for a short period of time this dose should be avoided if possible, but has no long term consequences. To reach their yearly limit a person would have to be exposed to 20 µGy/h for approximately 50 hours. The app would allow a person to vacate to a location where they would receive a lower dose.

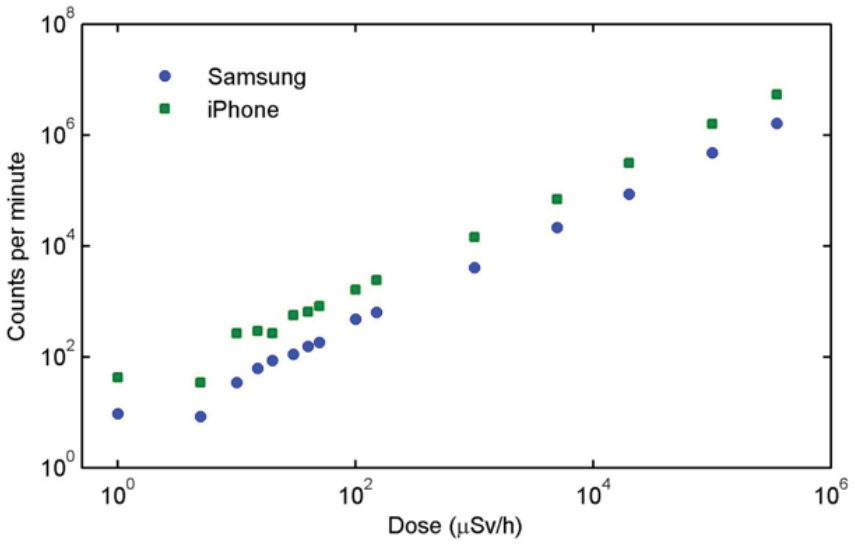

< Figure 2
The counts per minute recorded with both phones. A linear relationship shows that by observing the number of counts recorded the dose can determined.

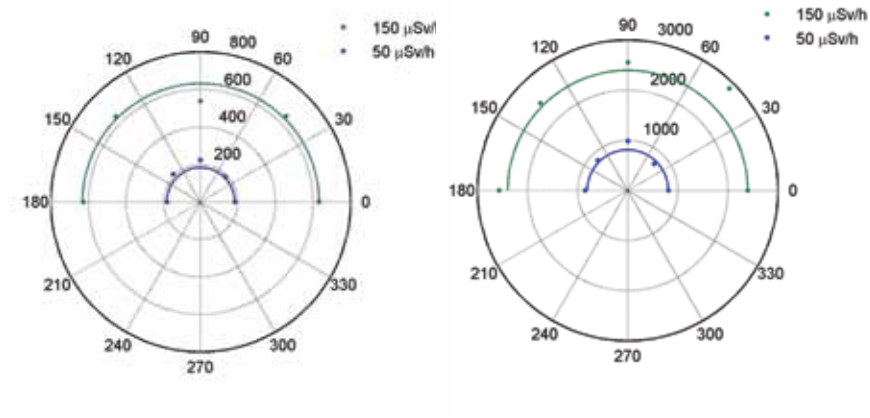

< Figure 3
The angular response of the Samsung Galaxy S2 smartphone to two different dose rates, 50 µSv/h and 150 µSv/h. The dots represent the number of counts recorded by the phone at different orientation angles.

< Figure 4
The angular response of the iPhone 4S smartphone to two different dose rates, 50 µSv/h and 150 µSv/h. The dots represent the number of counts recorded by the phone at different orientation angles.

These results show that the devices can accurately determine the dose rate which a person is exposed to and that the phone is sensitive enough to detect radiation at levels which are significant in a radiological event.

The angular response of the phone from 0° to 180° for a dose rate of 50 µSv/h and 150 µSv/h is shown in Fig. 3 and Fig. 4. These results show that both phones have a response which is independent of the orientation of the phone. As the phones show no significant angular response the app is very useful in determining the dose rate to a person, with no anomalous results.

REFERENCES

[1] ICRP. (1990). 1990 Recommendations of the International Commission on Radiological Protection. *ICRP Publication, 60*(ICRP 21), 1-3.

Information from ANSTO's nuclear forensics studies will be used for developing national nuclear forensics libraries.

Nuclear forensics unlocks history of radioactive samples

04

ANSTO's Nuclear Forensics Research Facility (NFRF) investigates unique signatures of nuclear and radioactive materials to identify the origin and/or processing history of 'unknown' samples. The information from such studies will be used for developing national nuclear forensics libraries. These libraries will strengthen nuclear safeguards and help combat nuclear terrorism by providing a valuable resource for nuclear forensic scientists conducting investigations on illicit samples.

In this study, ANSTO researchers investigated a sample of nuclear material in order to identify its unique chemical, isotopic and microstructural signatures. The sample was a uranium fuel pellet - a legacy sample which had not previously been well characterised. The pellet was typical of those manufactured at ANSTO (then called the Australian Atomic Energy Commission) as part of a fuel development research program in the late 1970s to early 1980s.

To test the integrity of the analytical and administrative procedures developed within the NFRF, the pellet sample underwent nuclear forensic analysis as a completely unknown sample. The physical, chemical and microstructural characteristics of the pellet were sufficiently distinct to enable its identification, its age and its processing history.

With the success of this testwork, further investigations are planned in collaboration with other international nuclear forensic laboratories.

Elizabeth Keegan, Tim Palmer, Dale Prokopovich, Martin Stewart, Joel Davis, Elaine Loi, Tegan Evans

Gordon Thorogood, Sam Moricca, Mark Reinhard

ANSTO

ANSTO is involved in international studies in nuclear forensics which include analytical method development, contributions to international guidance on nuclear forensics in support of the IAEA and participation in nuclear forensic laboratory inter-comparison exercises. In addition, at the time of this study ANSTO chaired the nuclear forensic working group of the Global Initiative to Combat Nuclear Terrorism.

Drawing together expertise from across the entire organisation in diverse disciplines such as radiochemistry, nuclear physics and materials science, combined with its knowledge of the nuclear fuel cycle, ANSTO's Nuclear Forensics Research Facility (NFRF) researches unique signatures of nuclear and radioactive materials suitable for developing national nuclear forensics libraries, which will provide a valuable resource for nuclear forensic scientists conducting investigations.

Recently, ANSTO researchers investigated a legacy sample of nuclear material that had not previously been

< Figure 1
The received package contained a glass jar, sealed with packaging tape containing a solid, dark coloured material in pellet form and some fragmented solid material.

well characterised in order to ascertain its unique signatures. The pellet was typical of those manufactured at ANSTO (then called the Australian Atomic Energy Commission) as part of a fuel development research program in the late 1970s to early 1980s. To test the integrity of the procedures developed within the NFRF, the pellet sample underwent nuclear forensic analysis as a completely unknown sample. Findings in regard to physical, chemical and microstructural characteristics of the pellet allowed a determination that the signatures analysed in this work were sufficiently distinct to allow its identification.

Non-destructive testing

The packaged pellet sample was receipted into the NFRF in February, 2012. Dose rate measurements indicated that the package contained a small amount of low-level radioactive material.

Typically, the first step in a nuclear forensic analysis process is 'categorisation', an initial examination to assess the radiological or other hazards associated with the sample prior to further investigation [1]. This step was carried out in a restricted access laboratory able to handle radioactive material. The package was carefully opened in a laminar flow cabinet (so as not to contaminate the sample) and the contents photographed and documented. Sample tracking records were initiated to record the movement of the sample, and any subsequent subsamples, across the ANSTO site (which forms part of the NFRF chain of custody requirements).

The package was found to contain a glass jar which contained a dense, solid pellet and some particulate material (see Fig. 1). Notable visual features of the pellet were its black colour, chipping along each edge of the pellet, striations along the length of the pellet with one end face flattened whilst the other end was concave (see Fig. 2). An orange 'rusty' appearance was evident along the length of pellet. The pellet was examined using optical microscopy and its physical parameters were measured; it was found to have a mass of 31.8 g, length 19.3 mm and a diameter of 14.4 mm. The density was 10.2 g/cm^3, very close to the theoretical density (10.96g/cm^3) of ceramic uranium dioxide (UO_2) material. High

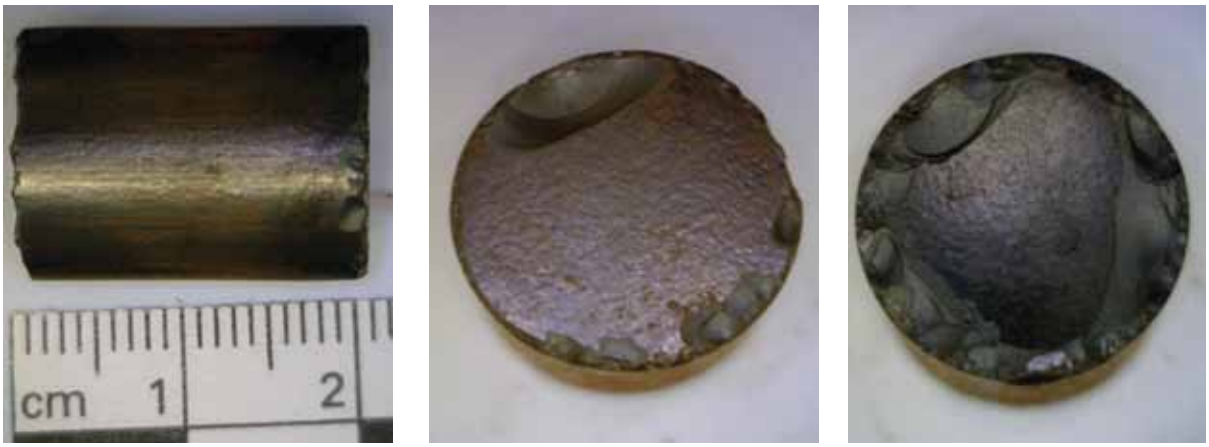

Figure 2
Optical microscopy images of the pellet showing striations along its length (left), flat face (14.4 mm diameter) with chipping (middle) and concave end of pellet with chipping (right).

resolution gamma-ray spectroscopy was used to measure uranium isotopic content and the presence of any fission or activation products. The measurements indicated that the pellet was composed of natural uranium (i.e. natural isotopic abundance of ^{238}U, ^{235}U and ^{234}U) and that the pellet had not been irradiated in a nuclear reactor (i.e. it did not contain plutonium or other activation or fission products). The 'as-received' pellet was analysed using a portable X-ray fluorescence (XRF) spectrometer to give a semi-quantitative measurement of the elemental content. The resulting XRF spectrum indicated that the pellet was mainly uranium with trace amounts of iron. Further testing using inductively coupled plasma mass spectrometry (see below) indicated that the iron was present on the surface of the pellet only.

Destructive testing

Following non-destructive testing, small sub-samples (~ 0.5 g) of the pellet were subjected to destructive analysis. Metallographic sample preparation procedures were performed in ANSTO's Institute of Materials Engineering (IME) Active Metallography Laboratory. Cut sections were mounted in Epoxy resin and polished for examination by scanning electron microscopy (SEM) and X-ray diffraction (XRD).

SEM was performed to examine the pellet microstructure and sample homogeneity. The microstructure of the material reflects processing history and thereby gives an indication of how the pellet was manufactured. An approximate elemental composition was determined using energy dispersive X-ray spectroscopy (EDS).

Results of SEM EDS found the material to consist of uranium and oxygen, in a ratio of 1:2. X-ray diffraction (XRD) confirmed that the material was uranium dioxide, UO_2. The SEM backscattered electron image showed the level of porosity and also that the sample was homogeneous. Angular selective backscatter (ASB, see Fig. 3) images showed uniformity in the microstructure. The grain size was approximately 10 µm and sub-grain striations were evident.

Further testing of the pellet was carried out using inductively coupled plasma mass spectrometry (ICP-MS). Prior to this analysis, sub-samples (~0.1 g each) were dissolved in acid. Uranium isotopic analysis using ICP-MS confirmed that the uranium was of natural abundance. Elemental analysis indicated that the

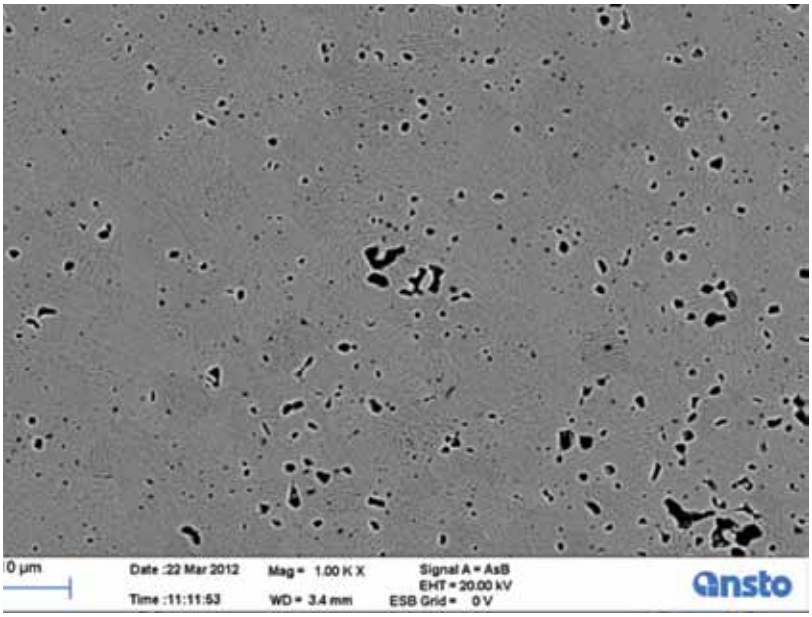

< Figure 3
Scanning electron microscopy angular selective backscatter image showing grain size and morphology and some high-resolution sub-grain information.

material used to produce the pellet was very pure i.e. it contained low concentrations of elemental impurities. The age of the material (i.e. time elapsed since the uranium material used to produce the pellet was last chemically processed) is one of the key parameters when deciphering its history. By radiochemically separating Th from U and measuring ^{230}Th and ^{234}U by isotope dilution mass spectrometry (IDMS), the ^{230}Th/^{234}U isotope chronometer was used to measure the 'age' of the uranium used to manufacture the pellet. The resulting age was approximately 40 years. It should be noted that this is a 'model' age; it assumes Th was completely separated from U during uranium processing and that the material experienced 'closed system' behaviour since it was purified.

Data Interpretation

The physical dimensions of this fuel pellet were fairly distinctive and consistent with pellets fabricated at ANSTO (AAEC) as part of a fuel development research program in the mid-late 1970s to early 1980s although Harwell (UK Atomic Energy Research Establishment) was doing similar work at the time. Chemical characteristics of the pellet (isotopic, elemental and phase composition) were also consistent with pellets that were manufactured at ANSTO under this research program. The age of the pellet also fits this time-frame. Microstructural parameters, such as grain size, porosity and sub-grain structure, examined using scanning electron microscopy, were typical of the pellets produced at ANSTO as part of this fuel pellet production program.

During the purported time-frame over which the pellet was fabricated various processing parameters were investigated and many pellets were produced. For fuel pellet manufacture, UO_2 powder needed to be compacted into a dense solid. The powder was placed into a die cavity between two punches; the upper punch had a convex face in order to produce a concave face on the final fuel pellet. The purpose of this concave face was to create a space between adjacent pellets in a fuel rod for fission gases produced during irradiation of the pellet in a reactor to escape. The upper punch was pressed at high pressure and high temperature (hot pressing) to compact the UO_2 powder. On completion of pressing, the punches were raised and the compacted solid was ejected from the die. UO_2 powder exhibits elastic behaviour and on emergence from the die it expands. Most likely this expansion was responsible for the chips that were observed at the ends of the pellet. Fig. 2 shows rust coloured striations on the sides of the pellet (see image on left) that may have been produced during the ejection process.

Microstructural results revealed uniformity in the microstructure which was consistent with the granulation, sieving and blending that occurred during processing. The measured grain

< Tim Palmer prepares the optical microscope for examination of the pellet sample.

size (10 µm, see Fig. 3) matched that expected for this production route. The sub-gain striations were consistent with the grains having been pre-compacted from fine UO_2 powder. The source of the UO_2 powder used to produce the pellets varied over the period of fabrication research. The most likely source of this natural uranium was Australia. At the time the pellet was manufactured, research was conducted using depleted, natural and enriched uranium. Natural uranium was used for experimental work into fuel for CANDU (CANada Deuterium Uranium) reactors, which use natural uranium fuel.

Future work

Further investigations into identification of high confidence nuclear forensic signatures on other nuclear or radiological material for the development of national nuclear forensic libraries are planned in collaboration with other international nuclear forensic research facilities.

REFERENCES

[1] International Atomic Energy Agency, Nuclear Forensics in Support of Investigations (Nuclear Forensics Support/Revision 1), in IAEA Nuclear Security Series No. 2 Implementing Guide, 2012, IAEA: Vienna

ANSTO

Facts and Figures 2012

Financial Statement ($AUD'000)

	2012 Research		2012 Total ANSTO	
Expenditure				
Operations	67,758	57%	228,325	65%
Investments	51,567	43%	122,191	35%
Total	119,325	100%	350,516	100%
Exp according to source of income				
Federal Govt. funding	112,298	94%	276,170	79%
Third Party	7,027	6%	74,346	21%
Third Party revenue				
Private Industry	5,981	85%	73,212	98%
Grants #1	1,046	15%	1,134	2%
Total	7,027	100%	74,346	100%

#1 Includes grants from Government, Universities and CRCs

The total expenditure by ANSTO for 2012 was AUD $350.5 million. This represents a ~11% increase from the previous year. Of this total amount, AUD $119 million or 34% was utilised in scientific research. Federal Government (block) funding represented 94% of this revenue and 6% came from third parties. These third parties include significant private investment (85%) while the rest came through grants and Government, Universities and Co-Operative Research Centres (CRCs).

ANSTO Employees

At the end of 2012, ANSTO had 1,154 full time equivalent employees. The chart below shows ANSTO's continued reliance on Technical and Engineering Staff (54.2%) for a successful user-based research facility.

ANSTO employment categories

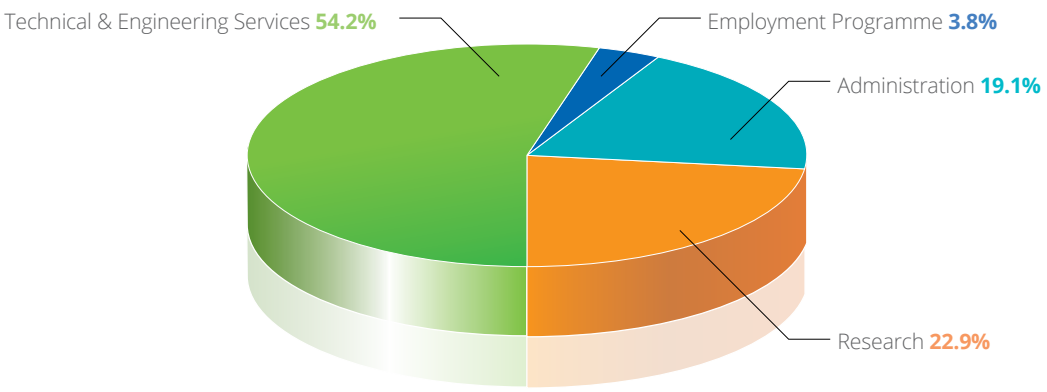

User Facilities

In 2012 the neutron beam lines at the OPAL reactor and the two accelerators (ANTARES and STAR) attracted ~350 users, coming from more than 75 institutions in over 20 countries.

Schools, Workshops and Reviews

Schools

- "Texture Analysis with MTEX" school at ANSTO 30 July – 3 August 2012;
- ANSTO Science 'Facts and Fiction' 2 August, University of Western Sydney, Parramatta, 1250 students 14 August, Monash University, Melbourne, 960 students;
- 3rd Accelerator School, 26 November – 3 December at the Australian Synchrotron;
- School "Powder Diffraction at OPAL and at the Australian Synchrotron: Experiment Planning to Data Analysis" 12-14 November 2012 at ANSTO.

Workshops, symposia, conferences

- Workshop "Current State and Future of Neutron Stress Diffractometers" 10-12 January 2012 at ANSTO;
- Workshop "Second Guide Hall for OPAL" 16-18 April 2012 at ANSTO
- Workshop "A Hadron Therapy Strategy for Australia" 20 April 2012 in Sydney;
- Workshop "3rd Australian Cyclotron Users' Workshop" on 27 April 2012 in Melbourne;
- GICNT Tabletop exercise "Iron Koala: Information Sharing During Nuclear Smuggling Events" 28-30 May 2012 in Sydney;
- Workshop "7th International Workshop on Sample Environment at Neutron Scattering Facilities" 16-20 September 2012 in Sydney;
- Workshop "20th International Workshop on Electron Cyclotron Resonance Ion Sources (ECRIS-2012)" 25-28 September 2012 in Sydney;
- Conference "12th South Pacific Environmental Radioactivity Association Conference (SPERA 2012)" 16-19 October 2012 at AINSE;
- Workshop "Bilateral Workshop on Nanostructured Materials for Magnetic and Spintronic Devices" 31 October – 1 November 2012 at the Italian Embassy in Canberra;
- Conference "SAS2012 International Small-Angle Scattering Conference" 18-23 November 2012 in Sydney;
- Symposium "Structure and Dynamics of Condensed Matter by Scattering Methods – Professor John W White Symposium" 25-28 November 2012 in the Hunter Valley;
- Workshop ANSTO and SINAP (Shanghai Institute of Applied Physics), 10-11 December 2012 at ANSTO (including signing of ANSTO/SINAP Memorandum of Understanding).

Reviews

- Institute of Materials Engineering (IME) Review. The review of this Institute considered its performance and facility, quality and impact of its research, project structure, its overall strategic direction, governance and safety. It took place 21-24 February 2012; the review panel was chaired by Professor Robin Grimes (Imperial College London, UK), and included Professor John Norrish (University of Wollongong), Dr Greg Storr (Nuclear Operations, ANSTO), Professor John White (Australian National University), Professor Brian Wirth (University of Tennessee, USA).
- Bragg Institute - Beam Instrument Advisory Group met on 23 February 2012 to review the major capital projects. The committee was chaired by Dr Dan Neumann (NIST Center for Neutron Research, USA).
- Bragg Institute – Advisory Committee Meeting. This committee provides strategic advice to the Institute under its chair, Professor Peter Colman (Walter and Eliza Hall Institute) 19-20 April 2012.

School “Powder Diffraction at OPAL and at the Australian Synchrotron: Experiment Planning to Data Analysis

Workshop “Current State and Future of Neutron Stress Diffractometers

Workshop “Second Guide Hall for OPAL”

GICNT Table top exercise"Iron Koala: InformationSharing During Nuclear Smuggling Events"

Workshop "7th International Workshop on Sample Environmentat Neutron Scattering Facilities"

Symposium "Structure and Dynamics of Condensed Matter by Scattering Methods– Professor John W White Symposium"

Australian Institute of Nuclear Science and Engineering (AINSE)

Background

The Australian Institute of Nuclear Science and Engineering (AINSE) provides a platform for training and cooperation in the nuclear science and engineering fields. Its membership comprises 46 Australian and New Zealand universities and science organisations, including ANSTO, making it one of few scientific institutions in Australia with such a wide membership. AINSE facilitates access to ANSTO's and other associated nuclear capabilities through research grants, fellowships and support for conferences and workshops.

Research Awards

Access to ANSTO's nuclear science and technology is the primary purpose of these awards. They enable close cooperation between ANSTO research scientists and university-based researchers and their students and involve a substantial use of ANSTO's scientific infrastructure. In 2012, more than 200 of these research projects were supported with a total value of $1,806,352.

Honours Scholarships

In 2012, AINSE supported ten Honours Scholarships to provide extra financial support to a number of excellent students that have a project utilising the research facilities at ANSTO. The scholarship provides a stipend of $5000 to each student. The students' supervisors must hold a current AINSE Research Award to support the facility access as well as travel and accommodation requirements.

Post Graduate Research Awards

A Post Graduate Research Award (PGRA) offers students a top-up stipend of $7,500 per annum and provides financial support for access to ANSTO's scientific infrastructure and expertise. An allowance for travel expenses to and accommodation at Lucas Heights is also awarded.

Twenty new AINSE PGRAs were awarded in 2012. Sixteen scholarships were finalised bringing the total number of scholars to 71. Through its PGRA program, AINSE has now helped train 329 students in aspects of nuclear science and associated techniques of analysis. Many more students have been assisted with their research by gaining access to ANSTO facilities through AINSE Awards made to their supervisors.

Research Fellowships

In 2012, AINSE has supported a total of eight Research Fellows. These are three-year fellowships which can be extended to a total of five years where appropriate. In 2012, Dr Neeraj Sharma was awarded a Fellowship based at The University of New South Wales and working at ANSTO on his project 'Developing improved materials for energy generation and storage'.

Dr David Turner concluded his fellowship in December 2012 and is now employed as ARC Future Fellow at Monash University.

Schools, Workshops and Reviews

AINSE conferences play a major part in the exchange process for scientific and technological information, providing a forum for debate and an opportunity for young researchers to present their work. In 2012, AINSE hosted Radiation 2012, 12th South Pacific Environmental Radioactivity Association Conference and the 10th AINSE-ANBUG Neutron Scattering Symposium.

In addition to these events, participants from member organisations were assisted with travel and accommodation to attend 16 other AINSE -supported conferences in 2012.

Publications

During 2012, notification was received of more than 250 publications reporting the results from AINSE supported research projects. ANSTO staff were co-authors on more than half of these publications.

Looking ahead into the future

AINSE is currently undergoing a rigorous strategic planning process, to review how AINSE has delivered on its goals over the past and set the course for AINSE moving into the future by re-defining its vision and mission. This will determine what difference AINSE will make in a changing environment and how these activities will contribute to outcomes of importance to Australia. In planning for its future, AINSE is drawing on the expertise and experience of a wide range of stakeholders in universities, business and government.

ANSTO Publications 2012

Ahmed, R., Faisal, N. H., Paradowska, A. M., & Fitzpatrick, M. E. (2012). Residual strain and fracture response of Al_2O_3 coatings deposited via APS and HVOF techniques. Journal of Thermal Spray Technology, 21(1), 23-40.

Ahsan, M., Tesfamichael, T., Ionescu, M., Bell, J., & Motta, N. (2012). Low temperature CO sensitive nanostructured WO_3 thin films doped with Fe. Sensors and Actuators B-Chemical, 162(1), 14-21.

Alam, E., Dominey-Howes, D., Chague-Goff, C., & Goff, J. (2012). Tsunamis of the northeast Indian Ocean with a particular focus on the Bay of Bengal region-A synthesis and review. Earth-Science Reviews, 114(1-2), 175-193.

Aly, Z., Vance, E. R., & Perera, D. S. (2012). Aqueous dissolution of sodium aluminosilicate geopolymers derived from metakaolin. Journal of Nuclear Materials, 424(1-3), 164-170.

Aravind, N., Sissons, M. J., Fellows, C.M., Blazek, J., & Gilbert, E. P. (2012). Effect of inulin soluble dietary fibre addition on technological, sensory, and structural properties of durum wheat spaghetti. Food Chemistry, 132(2), 993-1002.

Aravind, N., Sissons, M., Egan, N., Fellows, C. M., Blazek, J., & Gilbert, E.P. (2012). Effect of beta-Glucan on technological, sensory, and structural properties of durum wheat pasta. Cereal Chemistry, 89(2), 84-93.

Atanacio, A. J., Nowotny, J., & Prince, K. E. (2012). Reactivity between In_2O_3 and TiO_2 (rutile) studied using secondary ion mass spectrometry (SIMS). Separation and Purification Technology, 91, 96-102.

Atanacio, A. J., Nowotny, J., & Prince, K.E. (2012). Effect of oxygen activity on surface composition of in-doped TiO_2 at elevated temperatures. Journal of Physical Chemistry C, 116(36), 19246-19251.

Atuchin, V. V., & Zhang, Z. (2012). Chemical bonding between uranium and oxygen in U^{6+}-containing compounds. Journal of Nuclear Materials, 420(1-3), 222-225.

Auckett, J. E., Studer, A. J., Sharma, N., & Ling, C. D. (2012). Floating-zone growth of brownmillerite $Sr_2Fe_2O_5$ and the observation of a chain-ordered superstructure by single-crystal neutron diffraction. Solid State Ionics, 225, 432-436.

Avdeev, M., Sale, M., Adams, S., & Rao, R. P. (2012). Screening of the alkali-metal ion containing materials from the Inorganic Crystal Structure Database (ICSD) for high ionic conductivity pathways using the bond valence method. Solid State Ionics, 225, 43-46.

Azman, N. Z. N., Siddiqui, S. A., Ionescu, M., & Low, I. M. (2012). Synthesis and characterisation of ion-implanted epoxy composites for X-ray shielding. Nuclear Instruments & Methods in Physics Research Section B-Beam Interactions with Materials and Atoms, 287, 120-123.

Baczmanski, A., Gaj, A., Le Joncour, L., Wronski, S., Francois, M., Panicaud, B., Braham, C., & Paradowska, A. M. (2012). Study of stress localisation in polycrystalline grains using self-consistent modelling and neutron diffraction. Philosophical Magazine, 92(24), 3015-3035.

Baikie, T., Schreyer, M. K., Wong, C. L., Pramana, S. S., Klooster, W. T., Ferraris, C., McIntyre, G. J. , & White, T. J. (2012). A multi-domain gem-grade Brazilian apatite. American Mineralogist, 97(10), 1574-1581.

Baker, A., Bradley, C., Phipps, S. J., Fischer, M., Fairchild, I. J., Fuller, L., Spoetl, C., & Azcurra, C. (2012). Millennial-length forward models and pseudoproxies of stalagmite delta O-18: an example from NW Scotland. Climate of the Past, 8(4), 1153-1167.

Balogh, A. G., Baba, K., Cohen, D. D., Elliman, R. G., Ensinger, W., & Gyulai, J. (2012). Modification, synthesis, and analysis of advanced materials using ion beam techniques. Advances in Materials Science and Engineering. Art. No. 431297.

Barraud, N., Kardak, B. G., Yepuri, N. R., Howlin, R. P., Webb, J. S., Faust, S. N., Kjelleberg, S., Rice, S. A., & Kelso, M. J. (2012). Cephalosporin-3'-diazeniumdiolates: Targeted NO-donor prodrugs for dispersing bacterial biofilms. Angewandte Chemie-International Edition, 51(36), 9057-9060.

Bartkowiak, M., Mulders, A. M., Scagnoli, V., Staub, U., Pomjakushina, E., & Conder, K. (2012). Evolution of charge order through the magnetic phase transition of $LuFe_2O_4$. Physical Review B, 86(3), Art. No. 035121.

Baszczuk, A., Dabrowski, B., Kolesnik, S., Chmaissem, O., & Avdeev, M. (2012). Structural and physical properties of Re substituted B-site ordered and disordered $SrCo_{1-x}Re_xO_{3-delta}$ (x=0.1, 0.25, 0.5). Journal of Solid State Chemistry, 186, 240-246.

Beale, T. A. W., Beutier, G., Bland, S. R., Bombardi, A., Bouchenoire, L., Bunau, O., Di Matteo, S., Fernandez-Rodriguez, J., Hamann-Borrero, J. E., Herrero-Martin, J., Jacques, V. L. R., Johnson, R. D., Juhin, A., Matsumura, T., Mazzoli, C., Mulders, A. M., Nakao, H., Okamoto, J., Partzsch, S., Princep, A. J., Scagnoli, V., Strempfer, J., Vecchini, C., Wakabayashi, Y., Walker, H. C., Wermeille, D., & Yamasaki, Y. (2012). REXS contribution to electronic ordering investigation in solids. European Physical Journal-Special Topics, 208(1), 89-98.

Ben Yahia, H., Shikano, M., Koike, S., Tatsumi, K., Kobayashi, H., Kawaji, H., Avdeev, M., Miiller, W., Ling, C. D., Liu, J., & Whangbo, M-H. (2012). Synthesis and characterization of the crystal structure and magnetic properties of the new fluorophosphate $LiNaCo[PO_4]F$. Inorganic Chemistry, 51(16), 8729-8738.

Ben Yahia, H., Shikano, M., Sakaebe, H., Koike, S., Tabuchi, M., Kobayashi, H., Kawaji, H., Avdeev, M., Miiller, W., & Ling, C. D. (2012). Synthesis and characterization of the crystal structure, the magnetic and the electrochemical properties of the new fluorophosphate $LiNaCo[PO_4]F$. Dalton Transactions, 41(38), 11692-11699.

Bendeich, P. J., Muransky, O., Hamelin, C. J., Smith, M. C., & Edwards, L. (2012). Validated numerical analysis of residual stresses in safety relief valve (SRV) nozzle mock-ups: Influence of axial restraint on distortion and residual stress predictions. Computational Materials Science, 62, 285-288.

Bentley, P. M., Kennedy, S. J., Andersen, K. H., Rodriguez, D. M., & Mildner, D. F. R. (2012). Correction of optical aberrations in elliptic neutron guides. Nuclear Instruments & Methods in Physics Research Section A-Accelerators Spectrometers Detectors and Associated Equipment, 693, 268-275.

Bernardini, F., Tuniz, C., Coppa, A., Mancini, L., Dreossi, D., Eichert, D., Turco, G., Biasotto, M., Terrasi, F., De Cesare, N., Hua, Q., & Levchenko, V. (2012). Beeswax as dental filling on a neolithic human tooth. Plos One, 7(9, Art. No. e44904.

Bhati, M., Lee, C., Gadd, M. S., Jeffries, C. M., Kwan, A., Whitten, A. E., Trewhella, J., Mackay, J. P., & Matthews, J. M. (2012). Solution structure of the LIM-homeodomain transcription factor complex Lhx3/Ldb1 and the effects of a pituitary mutation on key Lhx3 interactions. Plos One, 7(7), Art. No. e40719.

Bhattacharyya, D., Demkowicz, M. J., Wang, Y. Q., Baumer, R. E., Nastasi, M., & Misra, A. (2012). A transmission electron microscopy study of the effect of interfaces on bubble formation in He-implanted Cu-Nb multilayers. Microscopy and Microanalysis, 18(1), 152-161.

Bhattacharyya, D., Dickerson, P., Odette, G. R., Maloy, S. A., Misra, A., & Nastasi, M. A. (2012). On the structure and chemistry of complex oxide nanofeatures in nanostructured ferritic alloy $U_{14}YWT$. Philosophical Magazine, 92(16), 2089-2107.

Blackburn, J. L., Engtrakul, C., Bult, J. B., Hurst, K., Zhao, Y. F., Xu, Q., Parilla, P. A., Simpson, L. J., Rocha, J. D. R., Hudson, M. R., Brown, C. M., & Gennett, T. (2012). Spectroscopic Identification of Hydrogen Spillover Species in Ruthenium-Modified High Surface Area Carbons by Diffuse Reflectance Infrared Fourier Transform Spectroscopy. Journal of Physical Chemistry C, 116(51), 26744-26755.

Blanchard, P. E. R., Clements, R., Kennedy, B. J., Ling, C. D., Reynolds, E., Avdeev, M., Stampfl, A. P. J., Zhang, Z., & Jang, L-Y. (2012). Does local disorder occur in the pyrochlore zirconates? Inorganic Chemistry, 51(24), 13237-13244.

Bloch, E. D., Queen, W. L., Krishna, R., Zadrozny, J. M., Brown, C. M., & Long, J. R. (2012). Hydrocarbon separations in a metal-organic framework with open iron(II) coordination sites. Science, 335(6076), 1606-1610.

Boardman, D., Reinhard, M. I., & Flynn, A. (2012). Principal component analysis of gamma-ray spectra for radiation portal monitors. IEEE Transactions on Nuclear Science, 59(1), 154-160.

Boekelheide, Z., Saerbeck, T., Stampfl, Anton P. J., Robinson, R. A., Stewart, D. A., & Hellman, F. (2012). Antiferromagnetism in Cr Al and relation to semiconducting behavior. Physical Review B, 85(9), Art. No. 094413.

Bongiovanni, R., Nelson, A., Vitale, A., & Bernardi, E. (2012). Ultra-thin films based on random copolymers containing perfluoropolyether side chains. Thin Solid Films, 520(17), 5627-5632.

Bot, A., Gilbert, E. P., Bouwman, W. G., Sawalha, H., den Adel, R., Garamus, V. M., Venema, P., van der Linden, E., & Floeter, E. (2012). Elucidation of density profile of self-assembled sitosterol plus oryzanol tubules with small-angle neutron scattering. Faraday Discussions, 158, 223-238.

Bourdier, T., Pham, T. Q., Henderson, D., Jackson, T., Lam, P., Izard, M., & Katsifis, A. (2012). Automated radiosynthesis of F-18 PBR111 and F-18 PBR102 using the Tracerlab FXFN and Tracerlab MXFDG module for imaging the peripheral benzodiazepine receptor with PET. Applied Radiation and Isotopes, 70(1), 176-183.

Bowen, M. T., Keats, K., Kendig, M. D., Cakic, V., Callaghan, P. D., & McGregor, I. S. (2012). Aggregation in quads but not pairs of rats exposed to cat odor or bright light. Behavioural Processes, 90(3), 331-336.

Brand, H. E. A., Scarlett, N. V. Y., & Grey, I. E. (2012). In situ studies into the formation kinetics of potassium jarosite. Journal of Applied Crystallography, 45, 535-545.

Brant, W. R., Schmid, S., Kuhn, A., Hester, J., Avdeev, M., Sale, M., & Gu, Q. (2012). Rapid lithium insertion and location of mobile lithium in the defect perovskite $Li_{0.18}Sr_{0.66}Ti_{0.5}Nb_{0.5}O_3$. Chemphyschem, 13(9), 2293-2296.

Button, D., Hotchkis, M. A. C., & Milford, G. N. (2012). Design of a compact electron cyclotron resonance ion source for medium charge state light ions. Review of Scientific Instruments, 83(2), Art. No. 02A322.

Cadogan, J.M., Lemoine, P., Slater, B. R., Mar, A. & Avdeev, M. (2012). Neutron Diffraction Study of the Hexagonal Perovskite-Type Compound $LaCrGe_3$. Solid State Phenomena, 194, 71-74.

Carilli, J., & Walsh, S. (2012). Benthic foraminiferal assemblages from Kiritimati (Christmas) Island indicate human-mediated nutrification has occurred over the scale of decades. Marine Ecology Progress Series, 456, 87-99.

Carilli, J., Donner, S. D., & Hartmann, A. C. (2012). Historical temperature variability affects coral response to heat stress. Plos One, 7(3), Art. No. e34418.

Carolan, J. V., Mazumder, D., Dimovski, C., Diocares, R., & Twining, J. (2012). Biokinetics and discrimination factors for delta C-13 and delta N-15 in the omnivorous freshwater crustacean, Cherax destructor. Marine and Freshwater Research, 63(10), 878-886.

Carrilli, J. G., Gamboa, R. A., Flores-Johnson, E. A., & Gonzalez-Chi, P. I. (2012). Ballistic performance of thermoplastic composite laminates made from aramid woven fabric and polypropylene matrix. Polymer Testing, 31(4), 512-519.

Cartwright, I., Weaver, T. R., Cendon, D. I., Fifield, L. K., Tweed, S. O., Petrides, B., & Swane, I. (2012). Constraining groundwater flow, residence times, inter-aquifer mixing, and aquifer properties using environmental isotopes in the Southeast Murray Basin, Australia. Applied Geochemistry, 27(9), 1698-1709.

Chague-Goff, C., Andrew, A., Szczucinski, W., Goff, J., & Nishimura, Y. (2012). Geochemical signatures up to the maximum inundation of the 2011 Tohoku-oki tsunami - Implications for the 869 AD Jogan and other palaeotsunamis. Sedimentary Geology, 282, 65-77.

Chague-Goff, C., Goff, J., Nichol, S. L., Dudley, W., Zawadzki, A., Bennett, J. W., Mooney, S. D., Fierro, D., Heijnis, H., Dominey-Howes, D., & Courtney, C. (2012). Multi-proxy evidence for trans-Pacific tsunamis in the Hawai'ian Islands. Marine Geology, 299, 77-89.

Chague-Goff, C., Niedzielski, P., Wong, H. K. Y., Szczucinski, W., Sugawara, D., & Goff, J. (2012). Environmental impact assessment of the 2011 Tohoku-oki tsunami on the Sendai Plain. Sedimentary Geology, 282, 175-187.

Chantler, C.T., Rae, N. A., Islam, M.T., Best, S.P., Yeo, J., Smale, L.F., Hester, J., Mohammadi, N., & Wang. F. (2012). Stereochemical analysis of ferrocene and the uncertainty of fluorescence XAFS data. Journal of Synchrotron Radiation, 19, 145–158.

Cheetham, M. D., Wong, V. N. L., Bush, R. T., Sullivan, L. A., Ward, N. J., & Zawadzki, A. (2012). Mobilisation, alteration, and redistribution of monosulfidic sediments in inland river systems. Journal of Environmental Management, 112, 330-339.

Chen, D., Cao, L., Hanley, T. L., & Caruso, R. A. (2012). Facile synthesis of monodisperse mesoporous zirconium titanium oxide microspheres with varying compositions and high surface areas for heavy metal ion sequestration. Advanced Functional Materials, 22(9), 1966-1971.

Chen, X., Wilde, K. L., Wang, H., Lake, V., Holden, P. J., Middelberg, A. P. J., He, L., & Duff, A. P. (2012). High yield expression and efficient purification of deuterated human protein galectin-2. Food and Bioproducts Processing, 90(C3), 563-572.

Chiang, C-Y., Su, H-C., Wu, P-J., Liu, H-J., Hu, C-W., Sharma, N., Peterson, V. K., Hsieh, H-W., Lin, Y-F., Chou, W-C., Lee, C-H., Lee, J-F., & Shew, B-Y. (2012). Vanadium substitution of $LiFePO_4$ cathode materials to enhance the capacity of $LiFePO_4$ based lithium-ion batteries. Journal of Physical Chemistry C, 116(46), 24424-24429.

Chou, S-L., Ionescu, M., Wang, J-Z., Winton, B., & Liu, H-K. (2012). Irradiation Si on carbon nanotube paper as a flexible anode material for lithium-ion batteries. Nanoscience and Nanotechnology Letters, 4(2), 169-172.

Choucair, M., & Stride, J. A. (2012). The gram-scale synthesis of carbon onions. Carbon, 50(3), 1109-1115

Choucair, M., Gong, B., & Stride, J. A. (2012). Engineering solvothermal reactions to produce multi-walled carbon nanotubes. Journal of Nanoparticle Research, 14(6), Art. No. 901.

Choucair, M., Tse, N. M. K., Hill, M. R., & Stride, J. A. (2012). Adsorption and desorption characteristics of 3-dimensional networks of fused graphene. Surface Science, 606(1-2), 34-39.

Christie, M. P., Whitten, A. E., King, G. J., Hu, S.-H., Jarrott, R. J., Chen, K.-E., Duff, A. P., Callow, P., Collins, B. M., James, D. E., & Martin, J. L. (2012). Low-resolution solution structures of Munc18:Syntaxin protein complexes indicate an open binding mode driven by the Syntaxin N-peptide. Proceedings of the National Academy of Sciences of the United States of America, 109(25), 9816-9821.

Ciampi, S., James, M., Le Saux, G., Gaus, K., & Gooding, J. J. (2012). Electrochemical "Switching" of Si(100) modular assemblies. Journal of the American Chemical Society, 134(2), 844-847.

Clarke, L. J., Robinson, S. A., Hua, Q., Ayre, D. J., & Fink, D. (2012). Radiocarbon bomb spike reveals biological effects of Antarctic climate change. Global Change Biology, 18(1), 301-310.

Clifton, L. A., Johnson, C. L., Solovyova, A. S., Callow, P., Weiss, K. L., Ridley, H., Le Brun, A. P., Kinane, C. J., Webster, J. R. P., Holt, S. A., & Lakey, J. H. (2012). Low resolution structure and dynamics of a colicin-receptor complex determined by neutron scattering. Journal of Biological Chemistry, 287(1), 337-346.

Cohen, D. D., Crawford, J., Stelcer, E., & Atanacio, A. J. (2012). A new approach to the combination of IBA techniques and wind back trajectory data to determine source contributions to long range transport of fine particle air pollution. Nuclear Instruments & Methods in Physics Research Section B-Beam Interactions with Materials and Atoms, 273, 186-188.

Cohen, D. D., Crawford, J., Stelcer, E., & Atanacio, A. J. (2012). Application of positive matrix factorization, multi-linear engine and back trajectory techniques to the quantification of coal-fired power station pollution in metropolitan Sydney. Atmospheric Environment, 61, 204-211.

Cohen, T. J., Nanson, G. C., Jansen, J. D., Jones, B. G., Jacobs, Z., Larsen, J. R., May, J. H., Treble, P., Price, D. M., & Smith, A. M. (2012). Late Quaternary mega-lakes fed by the northern and southern river systems of central Australia: Varying moisture sources and increased continental aridity. Palaeogeography Palaeoclimatology Palaeoecology, 356, 89-108.

Comarmond, M. J., Payne, T. E., Collins, R. N., Palmer, G., Lumpkin, G. R., & Angove, M.J. (2012). Inhibition of uranium(VI) sorption on titanium dioxide by surface iron(III) species in ferric oxide/titanium dioxide systems. Environmental Science & Technology, 46(20), 11128-11134.

Cortie, D. L., & Lewis, R. A. (2012). The importance of scattering, surface potential, and vanguard counter-potential in terahertz emission from gallium arsenide. Applied Physics Letters, 100(26), Art. No. 261601.

Cortie, D. L., Lin, K. W., Shueh, C., Hsu, H. F., Wang, X. L., James, M., Fritzsche, H., Brueck, S., & Klose, F. (2012). Exchange bias in a nanocrystalline hematite/permalloy thin film investigated with polarized neutron reflectometry. Physical Review B, 86(5), Art. No. 054408.

Cortie, D. L., Shueh, C., Chen, P-S., Gao, J-F., Klose, F., van Lierop, J., & Lin, K-W. (2012). Probing exchange bias effects in CoO/Co bilayers with pillar-like CoO structures. Japanese Journal of Applied Physics, 51(11), Art. No. 11PG01.

Cortie, D. L., Stampfl, A. P. J., Klose, F., Du, Y., Wang, X. L., Zhao, H. Y., Kimura, H., & Cheng, Z. X. (2012). The magnetic structure of an epitaxial $BiMn_{0.5}Fe_{0.5}O_3$ thin film on $SrTiO_3$ (001) studied with neutron diffraction. Applied Physics Letters, 101(17), Art. No. 172404.

Courtney, C., Dominey-Howes, D., Goff, J., Chague-Goff, C., Switzer, A. D., & McFadgen, B. G. (2012). A synthesis and review of the geological evidence for palaeotsunamis along the coast of southeast Australia: The evidence, issues and potential ways forward. Quaternary Science Reviews, 54, 99-125.

Curnoe, D., Xueping, J., Herries, A. I. R., Kanning, B., Tacon, P. S. C., Zhende, B., Fink, D., Yunsheng, Z., Hellstrom, J., Yun, L., Cassis, G.,Bing, S., Wroe, S., Shi, H., Parr, W. C. H., Shengmin, H. & Rogers, N. (2012). Human Remains from the Pleistocene-Holocene transition of Southwest China suggest a complex evolutionary history for East Asians. Plos One, 7(3), Art. No. e31918.

Dalton, V.S., Verdurand, M., Walker, A., Hodgson, D.M. & Zavitsanou, K. (2012) Synergistic effect between maternal infection and adolescent cannabinoid exposure on serotonin 5HT1A receptor binding in the hippocampus: testing the two hit hypothesis for the development of schizophrenia. ISRN Psychiatry, 2012, 451865.

Danilkin, S. A., Avdeev, M., Sale, M., & Sakuma, T. (2012). Neutron scattering study of ionic diffusion in Cu-Se superionic compounds. Solid State Ionics, 225, 190-193.

Danilkin, S.A., Yethiraj, M., Saerbeck, T., Klose, F., Ulrich, C., Fujioka, J., Miyasaka, S., Tokura, Y., & Keimer, B. (2012). TAIPAN: First results from the thermal triple-axis sspectrometer at OPAL Research Reactor. JPCS 340(1), 012003.

Darwish, T. A., Evans, R. A., & Hanley, T. L. (2012). Spiropyran chromene and spirooxazine, melange a trois: Molecular logic systems through selective and reversible deactivation of photochromism mediated by CO_2 gas. Dyes and Pigments, 92(2), 817-824.

Darwish, T. A., Smith, A. R. G., Gentle, I. R., Burn, P. L., Luks, E., Moraes, G., Gillon, M., Holden, P. J., & James, M. (2012). Deuteration of molecules for neutron reflectometry on organic light-emitting diode thin films. Tetrahedron Letters, 53(8), 931-935.

Darwish, T. A., Tong, Y., James, M., Hanley, T. L., Peng, Q., & Ye, S. (2012). Characterizing the photoinduced switching process of a nitrospiropyran self-assembled monolayer using In situ sum frequency generation spectroscopy. Langmuir, 28(39), 13852-13860.

Davies, J. B., Bosi, S. G., & Baldock, C. (2012). A genipin-gelatin gel dosimeter for radiation processing. Radiation Physics and Chemistry, 81(8), 1263-1265.

Davis, J. A., Ganesan, K., Alves, A. D. C., Guatelli, S., Petasecca, M., Livingstone, J., Lerch, M. L. F., Prokopovich, D. A., Reinhard, M. I., Siegele, R. N., Prawer, S., Jamieson, D., Kuncic, Z., Pisacane, V. L., Dicello, J. F., Ziegler, J., Zaider, M., & Rosenfeld, A. B. (2012). Characterization of a novel diamond-based microdosimeter prototype for radioprotection applications in space environments. IEEE Transactions on Nuclear Science, 59(6), 3110-3116.

Dedeurwaerdere, S., Callaghan, P.D., Pham, T., Rahardjo, G., Amhaoul, H., Berghofer, P., Quinlivan, M., Mattner, F., Loc'h, C., Katsifis, A., & Grégoire, M.C. (2012). PET imaging of brain inflammation during early epileptogenesis in a rat model of temporal lobe epilepsy. EJNMMI Research, 2(1), 1-13.

Deng, G., Thiyagarajan, R., Radheep, D. M., Pomjakushina, E., Medarde, M., Krzton-Maziopa, A., Wang, S., Arumugam, S., & Conder, K. (2012). Floating zone crystal growth and magnetic properties of bilayer manganites $Pr(Sr_{1-x}Ca_x)(2)Mn_2O_7$. Journal of Crystal Growth, 353(1), 25-30.

Denoyer, D., Kirby, L., Waldeck, K., Roselt, P., Neels, O. C., Bourdier, T., Shepherd, R., Katsifis, A., & Hicks, R. J. (2012). Preclinical characterization of F-18-D-FPHCys, a new amino acid-based PET tracer. European Journal of Nuclear Medicine and Molecular Imaging, 39(4), 703-712.

Diao, H., Yan, C., Bell, J. M., Lu, L., Zhang, G. P., Kabra, S., Liss, K. D., & Chen, M. W. (2012). Compressive behaviour of nanocrystalline Mg-5Al alloys. Materials Technology, 27(1), 85-87.

Dimitrijev-Dwyer, M., He, L., James, M., Nelson, A., Wang, L., & Middelberg, A. P. J. (2012). The effects of acid hydrolysis on protein biosurfactant molecular, interfacial, and foam properties: pH responsive protein hydrolysates. Soft Matter, 8(19), 5131-5139.

Dissanayake, S. E., Chan, C., Ji, S., Lee, J., Qiu, Y., Rule, K. C., Lake, B., Green, M., Hagihala, M., Zheng, X. G., Ng, T. K., & Lee, S. H. (2012). Magnetic-field-induced instability of the cooperative paramagnetic state in $Zn_xCo_{4-x}(OD)_6Cl_2$. Physical Review B, 85(17), Art. No. 174435.

Doutch, J. J., Quantock, A. J., Joyce, N. C., & Meek, K. M. (2012). Ultraviolet Light Transmission through the Human Corneal Stroma is reduced in the periphery. Biophysical Journal, 102(6), 1258-1264.

Doutch, J., Hough, M. A., Hasnain, S. S., & Strange, R. W. (2012). Challenges of sulfur SAD phasing as a routine method in macromolecular crystallography. Journal of Synchrotron Radiation, 19, 19-29.

Driza, N., Blanco-Canosa, S., Bakr, M., Soltan, S., Khalid, M., Mustafa, L., Kawashima, K., Christiani, G., Habermeier, H. U., Khaliullin, G., Ulrich, C., Le Tacon, M., & Keimer, B. (2012). Long-range transfer of electron-phonon coupling in oxide superlattices. Nature Materials, 11(8), 675-681.

Du, F., Ohgushi, K., Nambu, Y., Kawakami, T., Avdeev, M., Hirata, Y., Watanabe, Y., Sato, T. J., & Ueda, Y. (2012). Stripelike magnetism in a mixed-valence insulating state of the Fe-based ladder compound $CsFe_2Se_3$. Physical Review B, 85(21), Art. No. 214436.

Duffort, V., Caignaert, V., Pralong, V., Barrier, N., Raveau, B., Avdeev, M., Zheng, H., & Mitchell, J. F. (2012). Tetragonal $YBaFe_4O_{7.0}$: A stoichiometric polymorph of the "114" ferrite family. Journal of Solid State Chemistry, 191, 225-231.

Dung, N. H., Zhang, L., Ou, Z. Q., Zhao, L., van Eijck, L., Mulders, A. M., Mulders, A. M., Avdeev, M., Suard, E., van Dijk, N. H., & Brueck, E. (2012). High/low-moment phase transition in hexagonal Mn-Fe-P-Si compounds. Physical Review B, 86(4), Art. No. 045134.

Ehlers, G., Huq, A., Diallo, S. O., Adriano, C., Rule, K. C., Cornelius, A. L., Fouquet, P., Pagliuso, P. G., & Gardner, J. S. (2012). Low energy spin dynamics in the spin ice $Ho_2Sn_2O_7$. Journal of Physics-Condensed Matter, 24(7), Art. No. 076005.

Ener, S., Neuhaus, J, Petry, W., Mole, R., Hradil, K., Siewert, M., Gruner, M. E., Entel, P., Titov, I., & Acet, M. (2012). Effect of temperature and compositional changes on the phonon properties of Ni-Mn-Ga shape memory alloys. Physical Review B, 86(14), Art. No. 144305.

Fabian, C. P., Luca, V., Chamelot, P., Massot, L., Caravaca, C., & Lumpkin, G. R. (2012). Experimental and simulation study of the electrode reaction mechanism of La^{3+} in LiCl-KCl eutectic molten salt. Journal of the Electrochemical Society, 159(4), F63-F67.

Fainerman-Melnikova, M., & Soldenhoff, K. (2012). Uranium extraction from saline solutions using weak base anionic resins. CIM JOURNAL, 3(2), 117-124.

Falahat, S., Koeble, T., Schumann, O., Waring, C., & Watt, G. (2012). Development of a surface scanning soil analysis instrument. Applied Radiation and Isotopes, 70(7), 1107-1109.

Fernandez, D. I., Le Brun, A. P., Whitwell, T. C., Sani, M.A., James, M., & Separovic, F. (2012). The antimicrobial peptide aurein 1.2 disrupts model membranes via the carpet mechanism. Physical Chemistry Chemical Physics, 14(45), 15739-15751.

Fischer, M. J., & Mattey, D. (2012). Climate variability and precipitation isotope relationships in the Mediterranean region. Journal of Geophysical Research-Atmospheres, 117, Art. No. D20112.

Flores-Johnson, E. A., & Li, Q. M. (2012). Structural behaviour of composite sandwich panels with plain and fibre-reinforced foamed concrete cores and corrugated steel faces. Composite Structures, 94(5), 1555-1563.

Flores-Johnson, E. A., Muransky, O., Hamelin, C. J., Bendeich, P. J., & Edwards, L. (2012). Numerical analysis of the effect of weld-induced residual stress and plastic damage on the ballistic performance of welded steel plate. Computational Materials Science, 58, 131-139.

Fong, W-K., Malic, N., Evans, R. A., Hawley, A., Boyd, B. J., & Hanley, T. L. (2012). Alkylation of Spiropyran Moiety provides reversible photo-control over nanostructured soft materials. Biointerphases, 7(1-4), Art. No. 3.

Freire, T. S. S., Clark, M. W., Comarmond, M. J., Payne, T. E., Reichelt-Brushett, A.J., & Thorogood, G. J. (2012). Electroacoustic isoelectric point determinations of bauxite refinery residues: different neutralization techniques and minor mineral effects. Langmuir, 28(32), 11811-11820.

Fucke, K., McIntyre, G. J., Wilkinson, C., Henry, M., Howard, J. A. K., & Steed, J. W. (2012). New insights into an old molecule: interaction energies of theophylline crystal forms. Crystal Growth & Design, 12(3), 1395-1401.

Gallat, F. X., Laganowsky, A., Wood, K., Gabel, F., van Eijck, L., Wuttke, J., Moulin, M., Haertlein, M., Eisenberg, D., Colletier, J. P., Zaccai, G., & Weik, M. (2012). Dynamical coupling of intrinsically disordered proteins and their hydration water: comparison with folded soluble and membrane proteins. Biophysical Journal, 103(1), 129-136.

Gatta, G. D., McIntyre, G. J., Bromiley, G., Guastoni, A., & Nestola, F. (2012). A single-crystal neutron diffraction study of hambergite, $Be_2BO_3(OH,F)$. American Mineralogist, 97(11-12), 1891-1897.

Gatta, G. D., McIntyre, G. J., Swanson, J. G., & Jacobsen, S. D. (2012). Minerals in cement chemistry: A single-crystal neutron diffraction and Raman spectroscopic study of thaumasite, $Ca_3Si(OH)_6(CO_3)(SO_4)\cdot 12H_2O$. American Mineralogist, 97(7), 1060-1069.

Gault, B., Cui, X. Y., Moody, M. P., De Geuser, F., Sigli, C., Ringer, S. P., & Deschamps, A. (2012). Atom probe microscopy investigation of Mg site occupancy within delta ' precipitates in an Al-Mg-Li alloy. Scripta Materialia, 66(11), 903-906.

Geiger, C. A., Gatta, G. D., Xue, X., & McIntyre, G. J. (2012). A neutron/X-ray diffraction, IR, and H-1/Si-29 NMR spectroscopic investigation of armenite: Behavior of extra framework Ca cations and H_2O molecules in microporous silicates. Zeitschrift Fur Kristallographie, 227(7), 411-426.

Gerth, S., Klimczak, M., Nelson, A., & Magerl, A. (2012). Near Surface Crystallization of Pluronic P123. JPCS, 340(1), Art. No. 012088.

Gillespie, R., Camens, A. B., Worthy, T. H., Rawlence, N. J., Reid, C., Bertuch, F., Levchenko, V., & Cooper, A. (2012). Man and megafauna in Tasmania: closing the gap. Quaternary Science Reviews, 37, 38-47.

Goff, J., & Chagué-Goff, C. (2012). A review of palaeo-tsunamis for the Christchurch region, New Zealand. Quaternary Science Reviews, 57(0), 136-156.

Goff, J., Chague-Goff, C., Archer, M., Dominey-Howes, D., & Turney, C. (2012). The Eltanin asteroid impact: possible South Pacific palaeomegatsunami footprint and potential implications for the Pliocene-Pleistocene transition. Journal of Quaternary Science, 27(7), 660-670.

Goff, J., Chague-Goff, C., Nichol, S. L., Jaffe, B., & Dominey-Howes, D. (2012). Progress in palaeotsunami research. Sedimentary Geology, 243, 70-88.

Goff, J., McFadgen, B. G., Chague-Goff, C., & Nichol, S. L. (2012). Palaeotsunamis and their influence on Polynesian settlement. Holocene, 22(9), 1067-1069.

Goossens, D. J., Henderson, L. S. F., Trevena, S., Hudspeth, J. M., Avdeev, M., & Hester, J. R. (2012). The crystal and magnetic structures of $LaCa_2Fe_{3-x}M_xO_8$ (M=Al, Ga, In). Journal of Solid State Chemistry, 196, 238-242.

Goossens, D. J., Whitfield, R. E., & Studer, A. J. (2012). Optimising Sintering in Metal Injection Moulding Using In Situ Neutron Diffraction. Materials Science Forum, 706-709, 1737-1742.

Goto, K., Chague-Goff, C., Goff, J., & Jaffe, B. (2012). The future of tsunami research following the 2011 Tohoku-oki event. Sedimentary Geology, 282, 1-13.

Gouramanis, C., Dodson, J., Wilkins, D., De Deckker, P., & Chase, B. M. (2012). Holocene palaeoclimate and sea level fluctuation recorded from the coastal Barker Swamp, Rottnest Island, south-western Western Australia. Quaternary Science Reviews, 54, 40-57.

Grant, D., Stewart, T. J., Bau, R., Miller, K. A., Mason, S. A., Gutmann, M., McIntyre, G. J., Gagliardi, L., & Evans, W. J. (2012). Uranium and thorium hydride complexes as multielectron reductants: a combined neutron diffraction and quantum chemical study. Inorganic Chemistry, 51(6), 3613-3624.

Griffiths, M. L., Fohlmeister, J., Drysdale, R. N., Hua, Q., Johnson, K. R., Hellstrom, J. C., Gagan, M. K., & Zhao, J. (2012). Hydrological control of the dead carbon fraction in a Holocene tropical speleothem. Quaternary Geochronology, 14(0), 81-93.

Grover, S. P. P., Baldock, J. A., & Jacobsen, G. E. (2012). Accumulation and attrition of peat soils in the Australian Alps: Isotopic dating evidence. Austral Ecology, 37(4), 510-517.

Guagliardo, P. R., Vance, E. R., Zhang, Z., Davis, J., Williams, J. F., & Samarin, S. N. (2012). Positron annihilation lifetime studies of Nb-doped TiO_2, SnO_2, and ZrO_2. Journal of the American Ceramic Society, 95(5), 1727-1731.

Guan, B., Ciampi, S., Luais, E., James, M., Reece, P. J., & Gooding, J. J. (2012). Depth-resolved chemical modification of porous silicon by wavelength-tuned irradiation. Langmuir, 28(44), 15444-15449.

Gummow, R. J., Sharma, N., Peterson, V. K., & He, Y. (2012). Crystal chemistry of the Pmnb polymorph of Li_2MnSiO_4. Journal of Solid State Chemistry, 188, 32-37.

Hanaor, D. A. H., Chironi, I., Karatchevtseva, I., Triani, G., & Sorrell, C. C. (2012). Single and mixed phase TiO_2 powders prepared by excess hydrolysis of titanium alkoxide. Advances in Applied Ceramics, 111(3), 149-158.

Haque, R., Beynon, J. H., Durandet, Y., Kirstein, O., & Blacket, S. (2012). Feasibility of measuring residual stress profile in different self-pierce riveted joints. Science and Technology of Welding and Joining, 17(1), 60-68.

Haque, R.,Beynon, J. H., Kirstein, O., Wong, Y. C., & Durandet, Y.(2012). Evaluation of Residual Stress in SPR Joint by Neutron Diffraction. Advanced Material Research, 409, 575-580.

Haverkate, L. A., Zbiri, M., Johnson, M. R., Deme, B., de Groot, H. J. M., Lefeber, F., Kotlewski, A., Picken, S. J., Mulder, F.M., & Kearley, G.J. (2012). On the morphology of a discotic liquid crystalline charge transfer complex. Journal of Physical Chemistry B, 116(43), 13098-13105.

Heikkilae, U., & Smith, A. M. (2012). Influence of model resolution on the atmospheric transport of Be-10. Atmospheric Chemistry and Physics, 12(21), 10601-10612.

Hong, D., Shin, K., James, M., & Tae, G. (2012). Mimicking the receptor-aided binding of HIV-1 TAT protein transduction domains to phospholipid monolayers at the air-water interface. Soft Matter, 8(33), 8616-8623.

Hotchkis, M. A. C., Child, D. P., & Wilcken, K. (2012). Applications of accelerator mass spectrometry in nuclear verification. J. Nucl. Mater. Manage. Journal of Nuclear Materials Management, 40(4), 60-68.

Howarth, J. D., Fitzsimons, S. J., Norris, R. J., & Jacobsen, G. E. (2012). Lake sediments record cycles of sediment flux driven by large earthquakes on the Alpine fault, New Zealand. Geology, 40(12), 1091-1094.

Hsu, Y-C., Weir, M. P., Truss, R. W., Garvey, C. J., Nicholson, T. M., & Halley, P. J. (2012). A fundamental study on photo-oxidative degradation of linear low density polyethylene films at embrittlement. Polymer, 53(12), 2385-2393.

Hua, Q., Barbetti, M., Levchenko, V. A., D'Arrigo, R. D., Buckley, B. M., & Smith, A. M. (2012). Monsoonal influence on Southern Hemisphere (CO_2)-C-14. Geophysical Research Letters, 39, Art. No. L19806.

Hua, Q., McDonald, J., Redwood, D., Drysdale, R., Lee, S., Fallon, S., & Hellstrom, J. (2012). Robust chronological reconstruction for young speleothems using radiocarbon. Quaternary Geochronology, 14, 67-80.

Hudson, M. R., Queen, W. L., Mason, J. A., Fickel, D. W., Lobo, R. F., & Brown, C. M. (2012). Unconventional, highly selective CO_2 adsorption in zeolite SSZ-13. Journal of the American Chemical Society, 134(4), 1970-1973.

Hughes, A. E., Mayo, S., Yang, Y. S., Markley, T., Smith, S. V., Sellaiyan, S.,Uedono, A., Hardin, S. G., & Muster, T. H. (2012). Using X-ray tomography, PALS and Raman spectroscopy for characterization of inhibitors in epoxy coatings. Progress in Organic Coatings, 74(4), 726-733.

Hughes, C. E., & Crawford, J. (2012). A new precipitation weighted method for determining the meteoric water line for hydrological applications demonstrated using Australian and Global GNIP data. Journal of Hydrology, 464, 344-351.

Huh, M., Jung, M.-H., Park, Y. S., Kang, T.-B., Nah, C., Russell, R. A., Holden, P. J., & Yun, S. I. (2012). Fabrication of honeycomb-structured porous films from Poly(3-hydroxybutyrate) and Poly(3-hydroxybutyrate-co-3-hydroxyvalerate) via the breath figures method. Polymer Engineering and Science, 52(4), 920-926

Hutchison, W. D., Goossens, D. J., Whitfield, R. E., Studer, A. J., Nishimura, K., & Mizushima, T. (2012). Field-induced incommensurate spin structure of $TbNiAl_4$. Physical Review B, 86(1), Art. No. 014412.

Hynson, R. M. G., Jeffries, C. M., Trewhella, J., & Cocklin, S. (2012). Solution structure studies of monomeric human TIP47/perilipin-3 reveal a highly extended conformation. Proteins-Structure Function and Bioinformatics, 80(8), 2046-2055.

Ionescu, M., Winton, B., Wexler, D., Siegele, R., Deslantes, A., Stelcer, E., Atanacio, A., & Cohen, D. D. (2012). Enhanced biocompatibility of PDMS (Polydimethylsiloxane) polymer films by ion irradiation. Nuclear Instruments & Methods in Physics Research Section B-Beam Interactions with Materials and Atoms, 273, 161-163.

Jagodzinski, R., Sternal, B., Szczucinski, W., Chague-Goff, C., & Sugawara, D. (2012). Heavy minerals in the 2011 Tohoku-oki tsunami deposits-insights into sediment sources and hydrodynamics. Sedimentary Geology, 282, 57-64.

Johansen, M. P., Barnett, C. L., Beresford, N. A., Brown, J. E., Cerne, M., Howard, B. J., Kamboj, S., Keum, D. K., Smodis, B., Twining, J. R., Vandenhove, H., Batlle, J. V. I., Wood, M. D., & Yu, C. (2012). Assessing doses to terrestrial wildlife at a radioactive waste disposal site: Inter-comparison of modelling approaches. Science of the Total Environment, 427, 238-246.

Jones, A. O. F., Lemee-Cailleau, M.-H., Martins, D. M. S., McIntyre, G. J., Oswald, I. D. H., Pulham, C. R., Spanswick, C. K., Thomas, L. H., & Wilson, C. C. (2012). Temperature dependent solid-state proton migration in dimethylurea-oxalic acid complexes. Physical Chemistry Chemical Physics, 14(38), 13273-13283.

Jones, J. L., Aksel, E., Tutuncu, G., Usher, T.-M., Chen, J., Xing, X., & Studer, A. J. (2012). Domain wall and interphase boundary motion in a two-phase morphotropic phase boundary ferroelectric: Frequency dispersion and contribution to piezoelectric and dielectric properties. Physical Review B, 86(2), Art. No. 024104.

Juarez-Arellano, E. A., Avdeev, M., Yakovlev, S., Lopez-de-la-Torre, L., Bayarjargal, L., Winkler, B., Friedrich, A., & Kharton, V. V. (2012). High-pressure behavior and equations of state of the cobaltates $YBaCo_4O_7$, $YBaCo_4O_{7+delta}$, $YBaCoZn_3O_7$ and $BaCoO_{3-x}$. Journal of Solid State Chemistry, 196, 209-216.

Kam, W. W.i-Y., Meikle, S. R., Dunstan, C. R., & Banati, R. B. (2012). The 18 kDa translocator protein (peripheral benzodiazepine receptor) expression in the bone of normal, osteoprotegerin or low calcium diet treated mice. Plos One, 7(1), Art. No. e30623.

Kandemir, T., Girgsdies, F., Kasatkin, I., Kunkes, E., Liss, K-D., Peterson, V. K., Schlögl, R., & Behrens, M. (2012)., Heterogeneous Catalysis under pressure - In-situ neutron diffraction under industrial conditions. JPCS, 340(1), Art. No. 012053.

Kandemir, T., Wallacher, D., Hansen, T., Liss, K.-D., d'Alnoncourt, R. N., Schloegl, R., & Behrens, M. (2012). In situ neutron diffraction under high pressure-Providing an insight into working catalysts. Nuclear Instruments & Methods in Physics Research Section a-Accelerators Spectrometers Detectors and Associated Equipment, 673, 51-55.

Kaneko, F., Sasaki, K., Kawaguchi, T., Ute, K., & Hester, J. (2012). Neutron diffraction and IR spectroscopy study on crystalline complexation of syndiotactic polystyrene with 15-crown-5 and 18-crown-6. Chemistry Letters, 41(3), 284-286.

Kearley, G. J., Stare, J., Kutteh, R., Daemen, L. L., Hartl, M. A., & Eckert, J. (2012). Methyl dynamics flattens barrier to proton transfer in crystalline tetraacetylethane. Journal of Physical Chemistry A, 116(9), 2283-2291.

Keegan, E., Wallenius, M., Mayer, K., Varga, Z., & Rasmussen, G. (2012). Attribution of uranium ore concentrates using elemental and anionic data. Applied Geochemistry, 27(8), 1600-1609.

Keiser, D. D., Jr., Jue, J.F., Robinson, A. B., Medvedev, P., Gan, J., Miller, B. D., Wachs, D. M., Moore, G. A., Clark, C. R., Meyer, M. K., & Finlay, M. R. (2012). Effects of irradiation on the microstructure of U-7Mo dispersion fuel with Al-2Si matrix. Journal of Nuclear Materials, 425(1-3), 156-172.

Keliang, Z., Xiaoqiang, L., Xinying, Z., Dodson, J., & Ming, J.(2012). Characteristics of agricultural activities and its impact on the environment at Xintala site, Xinjiang, reconstructed from archaeological plant remains. Quaternary Sciences, 32, 219-225.

Kennaway, C. K., Taylor, J. E., Song, C. F., Potrzebowski, W., Nicholson, W., White, J. H., Swiderska, A., Obarska-Kosinska, A., Callow, P., Cooper, L. P., Roberts, G. A., Artero, J.B., Bujnicki, J. M., Trinick, J., Kneale, G. G., & Dryden, D. T. F. (2012). Structure and operation of the DNA-translocating type I DNA restriction enzymes. Genes & Development, 26(1), 92-104.

Knupfer, S. M., Paradowska, A. M., Kirstein, O., & Moore, A. J. (2012). Characterization of the residual strains in iterative laser forming. Journal of Materials Processing Technology, 212(1), 90-99.

Kolesnik, S., Dabrowski, B., Chmaissem, O., Avci, S., Hodges, J. P., Avdeev, M., & Swierczek, K. (2012). Enhancement of the Curie temperature in $NdBaCo_2O_{5.5}$ by A-site Ca substitution. Physical Review B, 86(6), Art. No. 064434.

Kong, L., Karatchevtseva, I., Blackford, M., Chironi, I., & Triani, G. (2012). Synthesis and characterization of rutile nanocrystals prepared in aqueous media at low temperature. Journal of the American Ceramic Society, 95(2), 816-822.

Latella, B. A., & Ignat, M. (2012). Interface fracture surface energy of sol-gel bonded silicon wafers by three-point bending. Journal of Materials Science-Materials in Electronics, 23(1), 8-13.

Lauw, Y., Horne, M. D., Rodopoulos, T., Lockett, V., Akgun, B., Hamilton, W. A., & Nelson, A. R. J. (2012). Structure of C(4)mpyr NTf2 room-temperature ionic liquid at charged gold interfaces. Langmuir, 28(19), 7374-7381.

Law, M., & Luzin, V. (2012). Measured residual stresses and integrity of pipeline girth welds. Science and Technology of Welding and Joining, 17(8), 694-698.

Law, M., Kirstein, O., & Luzin, V. (2012). Effect of residual stress on the integrity of a branch connection. International Journal of Pressure Vessels and Piping, 96-97, 24-29.

Le Brun, A. P., Chow, J., Bax, D. V., Nelson, A., Weiss, A. S., & James, M. (2012). Molecular orientation of tropoelastin is determined by surface hydrophobicity. Biomacromolecules, 13(2), 379-386.

Lee, E., Park, C-H., Shoemaker, D. P., Avdeev, M., & Kim, Y-I. (2012). Crystal structure analysis of tungsten bronzes beta-$SrTa_2O_6$ and beta '-$SrTa_2O_6$ by synchrotron X-ray and neutron powder diffraction. Journal of Solid State Chemistry, 191, 232-238.

Lehnert, W., Gregoire, M.-C., Reilhac, A., & Meikle, S. R. (2012). Characterisation of partial volume effect and region-based correction in small animal positron emission tomography (PET) of the rat brain. Neuroimage, 60(4), 2144-2157.

Lewis, S. E., Wüst, R. A. J., Webster, J. M., Shields, G. A., Renema, W., Lough, J. M., & Jacobsen, G. E. (2012). Development of an inshore fringing coral reef using textural, compositional and stratigraphic data from Magnetic Island, Great Barrier Reef, Australia. Marine Geology, 299–302(0), 18-32.

Li, D., Huang, Y., Sharma, N., Chen, Z., Jia, D., & Guo, Z. (2012). Enhanced electrochemical properties of $LiFePO_4$ by Mo-substitution and graphitic carbon-coating via a facile and fast microwave-assisted solid-state reaction. Physical Chemistry Chemical Physics, 14(10), 3634-3639.

Li, H., Baikie, T., Pramana, S. S., Shin, J. F., Slater, P. R., Brink, F., Hester, J., Wallwork, K., & White, T. J. (2012). Synthesis and characterisation of vanadium doped alkaline earth lanthanum germanate oxyapatite electrolyte. Journal of Materials Chemistry, 22(6), 2658-2669.

Li, Q., Liu, Y., Luzin, V., Studer, A. J., Wan, Y., Li, Z., Noren, L., Withers, R. L., & Xu, Z. (2012). In-situ neutron diffraction study of $Pb(In_{1/2}Nb_{1/2})O_3$-$Pb(Mg_{1/3}Nb_{2/3})O_3$-$PbTiO_3$ single crystals under uniaxial mechanical stress. Journal of Applied Physics, 111(8), Art. No. 084110.

Li, X., Sun, N., Dodson, J., & Zhou, X. (2012). Human activity and its impact on the landscape at the Xishanping site in the western Loess Plateau during 4800-4300 cal yr BP based on the fossil charcoal record. Journal of Archaeological Science, 39(10), 3141-3147.

Li, Y., Scales, N., Blankenship, R. E., Willows, R. D., & Chen, M. (2012). Extinction coefficient for red-shifted chlorophylls: Chlorophyll d and chlorophyll f. Biochimica Et Biophysica Acta-Bioenergetics, 1817(8), 1292-1298.

Li, Y., Yu, G., Chan, M. K., Baledent, V., Li, Yangmu, Barisic, N., Zhao, X., Hradil, K., Mole, R. A., Sidis, Y., Steffens, P., Bourges, P., & Greven, M. (2012). Two Ising-like magnetic excitations in a single-layer cuprate superconductor. Nature Physics, 8(5), 404-410.

Liao, P.-K., Fang, C.-S., Edwards, A.J., Kahlal, S., Saillard, J.-Y., & Liu, C. W. (2012). Hydrido copper clusters supported by dithiocarbamates: oxidative hydride removal and neutron diffraction analysis of Cu-7(H) {S2C(aza-15-crown-5)}(6). Inorganic Chemistry, 51(12), 6577-6591.

Ling, C. D., Miiler, W., Johnson, M. R., Richard, D., Rols, S., Madge, J., & Evans, I. R. (2012). Local structure, dynamics, and the mechanisms of oxide ionic conduction in $Bi_{26}Mo_{10}O_{69}$. Chemistry of Materials, 24(23), 4607-4614.

Liu, F., Romanova, N., Lee, E. A., Ahmed, R., Evans, M., Gilbert, E.P., Morell, M. K., Emes, M. J., & Tetlow, I. J. (2012). Glucan affinity of starch synthase IIa determines binding of starch synthase I and starch-branching enzyme IIb to starch granules. Biochemical Journal, 448, 373-387.

Liu, J., Toulouse, C., Rovillain, P., Cazayous, M., Gallais, Y., Measson, M. A., Lee, N., Cheong, S. W., & Sacuto, A. (2012). Lattice and spin excitations in multiferroic h-$YbMnO_3$. Physical Review B, 86(18), Art. No. 184410.

Liu, S., Miiller, W., Liu, Y., Avdeev, M., & Ling, C. D. (2012). Sillen-Aurivillius intergrowth phases as templates for naturally layered multiferroics. Chemistry of Materials, 24(20), 3932-3942.

Liu, Y., Noren, L., Studer, A. J., Withers, R. L., Guo, Y., Li, Y., Yang, H., & Wang, J-Z. (2012). Response of intergrown microstructure to an electric field and its consequences in the lead-free piezoelectric bismuth sodium titanate. Journal of Solid State Chemistry, 187, 309-315.

Liu, Y., Withers, R. L., Wang, J., Norén, L., Studer, A. J., & Li, Y. (2012). Local microstructure evolution of bismuth sodium titanate-based lead-free piezoelectric systems across the morphotropic phase boundary region. Journal of Advanced Dielectrics, 2(4), Art. No. 1230012.

Low, H. R., Avdeev, M., Ramesh, K., & White, T. J. (2012). Zinc hydroxyapatite catalyst for decomposition of 2-propanol. Advanced Materials, 24(30), 4175-4179.

Low, J. M., Curtain, B., Philipps, M., Liu, Z. Q., & Ionescu, M. (2012). High temperature diffraction study of in-situ crystallization of nanostructured TiO_2 photocatalysts. Journal of the Australian Ceramic Society, 48(2), 198-204.

Lu, Y., Kwan, A. H., Jeffries, C. M., Guss, J. M., & Trewhella, J. (2012). The motif of human cardiac myosin-binding protein C is required for its Ca^{2+}-dependent Interaction with Calmodulin. Journal of Biological Chemistry, 287(37), 31596-31607.

Lumpkin, G. R., Leung, S. H. F., & Ferenczy, J. (2012). Chemistry, microstructure, and alpha decay damage of natural brannerite. Chemical Geology, 291, 55-68.

Luo, H., Yamani, Z., Chen, Y., Lu, X., Wang, M., Li, S., Maier, T. A., Danilkin, S. A., Adroja, D. T., & Dai, P. (2012). Electron doping evolution of the anisotropic spin excitations in $BaFe_{2-x}Ni_xAs_2$. Physical Review B, 86(2), Art. No. 024508.

Maley, M., Burling, S., & Ring, R. (2012). Effect of oxidation-reduction potential and ferric iron concentration on leaching of uranium ores. CIM Journal,, 3(2), 62-68.

Mazumder, D., Johansen, M., Saintilan, N., Iles, J., Kobayashi, T., Knowles, L., & Wen, L. (2012). Trophic shifts Involving native and exotic fish during hydrologic recession in floodplain wetlands. Wetlands, 32(2), 267-275.

McNamara, A. L., Guatelli, S., Prokopovich, D. A., Reinhard, M. I., & Rosenfeld, A. B. (2012). A comparison of X-ray and proton beam low energy secondary electron track structures using the low energy models of Geant4. International Journal of Radiation Biology, 88(1-2), 164-170.

McNamara, A. L., Heijnis, H., Fierro, D., & Reinhard, M. I. (2012). The determination of the efficiency of a Compton suppressed HPGe detector using Monte Carlo simulations. Journal of Environmental Radioactivity, 106, 1-7.

McNiven, I. J., Crouch, J., Richards, T., Dolby, N., Jacobsen, G., & Gunditj Mirring Traditional, Owners. (2012). Dating Aboriginal stone-walled fishtraps at Lake Condah, Southeast Australia. Journal of Archaeological Science, 39(2), 268-286.

Menzies, D. J., Nelson, A., Shen, H-H., McLean, K. M., Forsythe, J. S., Gengenbach, T., Fong, C., & Muir, B. W. (2012). An X-ray and neutron reflectometry study of 'PEG-like' plasma polymer films. Journal of the Royal Society Interface, 9(70), 1008-1019.

Meredith, K., Cendón, D. I., Pigois, J.-P., Hollins, S., & Jacobsen, G. E. (2012). Using ^{14}C and ^{3}H to delineate a recharge 'window' into the Perth Basin aquifers, North Gnangara groundwater system, Western Australia. Science of The Total Environment, 414(0), 456-469.

Miiller, W., Auckett, J. E., Avdeev, M., & Ling, C. D. (2012). Coexistence of spin glass and antiferromagnetic orders in $Ba_3Fe_{2.15}W_{0.8}5O_{8.72}$. Journal of Physics-Condensed Matter, 24(20), Art. No. 206004.

Miiller, W., Avdeev, M., Zhou, Q., Kennedy, B. J., Sharma, N., Kutteh, R., Kearley, G. J., Schmid, S., Knight, K. S., Blanchard, P. E. R., & Ling, C. D. (2012). Giant magnetoelastic effect at the opening of a spin-gap in $Ba_3BiIr_2O_9$. Journal of the American Chemical Society, 134(6), 3265-3270.

Miiller, W., Kearley, G. J., & Ling, C. D. (2012). Ab initio parametrized polarizable force field for rutile-type SnO_2. Theoretical Chemistry Accounts, 131(5), Art. No. 1216.

Minakshi, M., Singh, P., Ralph, D., Appadoo, D., Blackford, M., & Ionescu, M. (2012). Structural characteristics of olivine $Li(Mg_{0.5}Ni_{0.5})PO_4$ via TEM analysis. Ionics, 18(6), 583-590.

Mitchell, M. R., Carnevale, D., Orr, R., Whittle, K. R., & Ashbrook, S. E. (2012). Exploiting the chemical shielding anisotropy to probe structure and disorder in ceramics: Y-89 MAS NMR and first-principles calculations. Journal of Physical Chemistry C, 116(6), 4273-4286.

Morris, V. K., Linser, R., Wilde, K. L., Duff, A. P., Sunde, M., & Kwan, A. H. (2012). Solid-state NMR spectroscopy of functional amyloid from a fungal hydrophobin: a well-ordered beta-sheet core amidst structural heterogeneity. Angewandte Chemie-International Edition, 51(50), 12621-12625.

Mueller, K., Foerstendorf, H., Meusel, T., Brendler, V., Lefevre, G., Comarmond, M. J., & Payne, T. E. (2012). Sorption of U(VI) at the TiO_2-water interface: An in situ vibrational spectroscopic study. Geochimica Et Cosmochimica Acta, 76, 191-205.

Muransky, O., Hamelin, C. J., Smith, M. C., Bendeich, P. J., & Edwards, L. (2012). The effect of plasticity theory on predicted residual stress fields in numerical weld analyses. Computational Materials Science, 54, 125-134.

Muransky, O., Smith, M. C., Bendeich, P. J., Holden, T. M., Luzin, V., Martins, R. V., & Edwards, L. (2012). Comprehensive numerical analysis of a three-pass bead-in-slot weld and its critical validation using neutron and synchrotron diffraction residual stress measurements. International Journal of Solids and Structures, 49(9), 1045-1062.

Murugaraj, P., Mainwaring, D. E., Al Kobaisi, M., & Siegele, R. (2012). Stable doped sp(2) C-hybrid nanostructures by reactive ion beam irradiation. Journal of Materials Chemistry, 22(35), 18403-18410.

Nambu, Y., Ohgushi, K., Suzuki, S., Du, F., Avdeev, M., Uwatoko, Y., Munakata, K., Fukazawa, H., Chi, S., Ueda, Y., & Sato, T. J. (2012). Block magnetism coupled with local distortion in the iron-based spin-ladder compound $BaFe_2Se_3$. Physical Review B, 85(6), Art. No. 064413.

Ng, M. C. C., Harper, J. B., Stampfl, A. P. J., Kearley, G. J., Rols, S., & Stride, J.A. (2012). Central-atom Size effects on the methyl torsions of group XIV tetratolyls. Chemistry-a European Journal, 18(41), 13018-13024.

Nguyen, V. H., Verdurand, M., Dedeurwaerdere, S., Wang, H., Zahra, D., Gregoire, M.-C., & Zavitsanou, K. (2012). Increased brain metabolism after acute administration of the synthetic cannabinoid HU210: A small animal PET imaging study with F-18-FDG. Brain Research Bulletin, 87(2-3), 172-179.

Nguyen, V. H., Wang, H., Verdurand, M., & Zavitsanou, K. (2012). Differential treatment regimen-related effects of HU210 on CB1 and D-2-like receptor functionality in the rat basal ganglia. Pharmacology, 89(1-2), 64-73.

Omrani, A. A., Deng, G., Radenovic, A., Kis, A., & Ronnow, H. M. (2012). Micro-fabrication process for small transport devices of layered manganite. Journal of Applied Physics, 111(7), Art. No. 07E129.

Paddea, S., Francis, J. A., Paradowska, A. M., Bouchard, P. J., & Shibli, I. A. (2012). Residual stress distributions in a P91 steel-pipe girth weld before and after post weld heat treatment. Materials Science and Engineering a-Structural Materials Properties Microstructure and Processing, 534, 663-672.

Payten, W. M., Dean, D., & Snowden, K. U. (2012). Analysis of creep ductility in a ferritic martensitic steel using a hybrid strain energy technique. Materials & Design, 33, 491-495.

Pedro, J. B., McConnell, J. R., van Ommen, T. D., Fink, D., Curran, M. A. J., Smith, A. M., Simon, K. J., Moy, A. D., & Das, S. B. (2012). Solar and climate influences on ice core Be-10 records from Antarctica and Greenland during the neutron monitor era. Earth and Planetary Science Letters, 355, 174-186.

Photongkam, P., Zhang, Y. B., Assadi, M. H. N., Li, S., Yu, D., Ionescu, M., & Pan, A. V. (2010). Enhancement of Co substitution induced by Eu Codoping in ZnO-based diluted magnetic semiconducting thin films. Journal of Applied Physics, 107(3).

Pierret, S., Evans, A., Paradowska, A. M., Kaestner, A., James, J., Etter, T., & Van Swygenhoven, H. (2012). Combining neutron diffraction and imaging for residual strain measurements in a single crystal turbine blade. Ndt & E International, 45(1), 39-45.

Pilarczyk, J. E., Horton, B. P., Witter, R. C., Vane, C. H., Chague-Goff, C., & Goff, J. (2012). Sedimentary and foraminiferal evidence of the 2011 Tohoku-oki tsunami on the Sendai coastal plain, Japan. Sedimentary Geology, 282, 78-89.

Preston, R., Jakubek, J., Prokopovich, D., & Uher, J. (2012). Proton beam characterisation of a prototype thin-tile plastic scintillator detector with SiPM readout for use in fast-neutron tracker. Journal of Instrumentation, 7, Art. No. P02007.

Princep, A. J., Mulders, A. M., Schierle, E., Weschke, E., Hester, J., Hutchison, W. D., Tanaka, Y., Terada, N., Narumi, Y., & Nakamura, T. (2012). High-order Ho multipoles in HoB_2C_2 observed with soft resonant x-ray diffraction. Journal of Physics-Condensed Matter, 24(7), Art. No. 075602.

Queen, W. L., Bloch, E. D., Brown, C. M., Hudson, M. R., Mason, J. A., Murray, L. J., Ramirez-Cuesta, A. J., Peterson, V. K., & Long, J. R. (2012). Hydrogen adsorption in the metal-organic frameworks Fe-2(dobdc) and Fe-2(O-2)(dobdc). Dalton Transactions, 41(14), 4180-4187.

Quintero-Castro, D. L., Lake, B., Islam, A. T. M. N., Wheeler, E. M., Balz, C., Mansson, M., Rule, K. C., Gvasaliya, S., & Zheludev, A. (2012). Asymmetric Thermal line shape broadening in a gapped 3D antiferromagnet: evidence for strong correlations at finite temperature. Physical Review Letters, 109(12), Art. No. 127206.

Ramirez-Herrera, M.-T., Lagos, M., Hutchinson, I., Kostoglodov, V., Luisa Machain, M., Caballero, M., Goguitchaichvili, A., Aguilar, B., Chague-Goff, C., Goff, J., Ruiz-Fernandez, A-C., Ortiz, M., Nava, H., Bautista, F., Lopez, G. I., & Quintana, P. (2012). Extreme wave deposits on the Pacific coast of Mexico: Tsunamis or storms? - A multi-proxy approach. Geomorphology, 139, 360-371.

Ranson, M., Berghofer, P., Vine, K. L., Greguric, I., Shepherd, R., & Katsifis, A. (2012). Different radiolabelling methods alter the pharmacokinetic and biodistribution properties of Plasminogen Activator Inhibitor Type 2 (PAI-2) forms. Nuclear Medicine and Biology, 39(6), 833-839.

Ravel, B., Hester, J. R., Sole, V. A., & Newville, M. (2012). Towards data format standardization for X-ray absorption spectroscopy. Journal of Synchrotron Radiation, 19, 869-874.

Rayavarapu, P. R., Sharma, N., Peterson, V. K., & Adams, S. (2012). Variation in structure and Li^+-ion migration in argyrodite-type Li_6PS_5X (X = Cl, Br, I) solid electrolytes. Journal of Solid State Electrochemistry, 16(5), 1807-1813.

Reehuis, M., Ulrich, C., Maljuk, A., Niedermayer, Ch, Ouladdiaf, B., Hoser, A., Hofmann, T., & Keimer, B. (2012). Neutron diffraction study of spin and charge ordering in $SrFeO_{3-delta}$. Physical Review B, 85(18), Art. No. 184109.

Regina, A., Blazek, J., Gilbert, E. P., Flanagan, B. M., Gidley, M. J., Cavanagh, C., Ral, J-P., Larroque, O., Bird, A. R., Li, Z., & Morell, M. K. (2012). Differential effects of genetically distinct mechanisms of elevating amylose on barley starch characteristics. Carbohydrate Polymers, 89(3), 979-991.

Rekas, A., Ahn, K. J., Kim, J., & Carver, J. A. (2012). The chaperone activity of a-synuclein: Utilizing deletion mutants to map its interaction with target proteins. Proteins-Structure Function and Bioinformatics, 80(5), 1316-1325.

Reynolds, E., Blanchard, P. E. R., Zhou, Q., Kennedy, B. J., Zhang, Z., & Jang, L-Y. (2012). Structural and spectroscopic studies of $La_2Ce_2O_7$: Disordered fluorite versus pyrochlore structure. Physical Review B, 85(13), Art. No. 132101.

Richmond, B., Szczucinski, W., Chague-Goff, C., Goto, K., Sugawara, D., Witter, R. C., Tappin, D. R., Jaffe, B., Fujino, S., Nishimura, Y., & Goff, J. (2012). Erosion, deposition and landscape change on the Sendai coastal plain, Japan, resulting from the March 11, 2011 Tohoku-oki tsunami. Sedimentary Geology, 282, 27-39.

Robinson, J. S., Tanner, D. A., Truman, C. E., Paradowska, A. M., & Wimpory, R. C. (2012). The influence of quench sensitivity on residual stresses in the aluminium alloys 7010 and 7075. Materials Characterization, 65, 73-85.

Robinson, M., Marks, N. A., Whittle, K. R., & Lumpkin, G. R. (2012). Systematic calculation of threshold displacement energies: Case study in rutile. Physical Review B, 85(10), Art. No. 104105.

Rolph, J., Evans, A., Paradowska, A. M., Hofmann, M., Hardy, M., & Preuss, M. (2012). Stress relaxation through ageing heat treatment - a comparison between in situ and ex situ neutron diffraction techniques. Comptes Rendus Physique, 13(3), 307-315.

Rotundu, C. R., Tian, W., Rule, K. C., Forrest, T. R., Zhao, J., Zarestky, J. L., & Birgeneau, R. J. (2012). Neutron scattering study of underdoped $Ba_{1-x}K_xFe_2As_2$ (x=0.09 and 0.17) self-flux-grown single crystals and the universality of the tricritical point. Physical Review B, 85(14), Art. No. 144506.

Rovillain, P., Liu, J., Cazayous, M., Gallais, Y., Measson, M. A., Sakata, H., & Sacuto, A. (2012). Electromagnon and phonon excitations in multiferroic $TbMnO_3$. Physical Review B, 86(1), Art. No. 014437.

Saerbeck, T., Klose, F., Le Brun, A. P., Fuezi, J., Brule, A., Nelson, A., Holt, S. A., & James, M. (2012). Invited Article: Polarization "Down Under": The polarized time-of-flight neutron reflectometer PLATYPUS. Review of Scientific Instruments, 83(8), Art. No. 081301.

Saerbeck, T., Loh, N., Lott, D., Toperverg, B. P., Mulders, A. M., Ali, M., Hickey, B. J., Stampfl, A. P. J., Klose, F., & Stamps, R. L. (2012). Specular and off-specular polarized neutron reflectometry of canted magnetic domains in loose spin coupled CuMn/Co multilayers. Physical Review B, 85(1), Art. No. 014411.

Sakaguchi, T., Kobayashi, Y., Yajima, T., Ohkura, M., Tassel, C., Takeiri, F., Mitsuoka, S., Ohkubo, H., Yamamoto, T., Kim, J. E., Tsuji, N., Fujihara, A., Matsushita, Y., Hester, J., Avdeev, M., Ohoyama, K., & Kageyama, H. (2012). Oxyhydrides of (Ca,Sr,Ba)TiO_3 Perovskite Solid Solutions. Inorganic Chemistry, 51(21), 11371-11376.

Salako, G. O., Hopke, P. K., Cohen, D. D., Begum, B. A., Biswas, S. K., Pandit, G. G., Chung, Y.S., Abd Rahman, S., Hamzah, M. S., Davy, P., Markwitz, A., Shagjjamba, D., Lodoysamba, S., Wimolwattanapun, W., & Bunprapob, S. (2012). Exploring the variation between EC and BC in a variety of locations. Aerosol and Air Quality Research, 12(1), 1-7.

Sale, M., & Avdeev, M. (2012). 3DBVSMAPPER: a program for automatically generating bond-valence sum landscapes. Journal of Applied Crystallography, 45, 1054-1056.

Salim, N. V., Hanley, T. L., Waddington, L., Hartley, P. G., & Guo, Q. (2012). A simple and effective approach to vesicles and large compound vesicles via complexation of amphiphilic block copolymer with polyelectrolyte in water. Macromolecular Rapid Communications, 33(5), 401-406.

Sang, Y., Yu, D., Avdeev, M., Qin, H., Wang, J., Liu, H., & Lv, Y. (2012). Yttrium aluminum garnet Nanoparticles with low antisite Defects studied with neutron and X-ray diffraction. Journal of Solid State Chemistry, 192, 366-370.

Satapathy, D. K., Uribe-Laverde, M. A., Marozau, I., Malik, V. K., Das, S., Wagner, Th, Marcelot, C., Stahn, J., Brueck, S., Ruehm, A. , Macke, S., Tietze, T., Goering, E., Frano, A., Kim, J. H., Wu, M., Benckiser, E., Keimer, B., Devishvili, A., Toperverg, B. P., Merz, M., Nagel, P., Schuppler, S., & Bernhard, C. (2012). Magnetic proximity effect in $YBa_2Cu_3O_7$/$La_{2/3}Ca_{1/3}MnO_3$ and $YBa_2Cu_3O_7$/$LaMnO_{3+delta}$ superlattices. Physical Review Letters, 108(19), Art. No. 197201.

Schiemer, J., Withers, R. L., Carpenter, M. A., Liu, Y., Wang, J. L., Noren, L., Li, Q., & Hutchison, W. (2012). Temperature-dependent electrical, elastic and magnetic properties of sol-gel synthesized $Bi_{0.9}Ln_{0.1}FeO_3$ (Ln = Nd, Sm). Journal of Physics-Condensed Matter, 24(12), Art. No. 125901.

Schmid, S., & Fung, V. (2012). Incommensurate modulated structures in the Ta_2O_5-Al_2O_3 system. Australian Journal of Chemistry, 65(7), 851-859.

Sharma, N., & Peterson, V. K. (2012). In situ neutron powder diffraction studies of lithium-ion batteries. Journal of Solid State Electrochemistry, 16(5), 1849-1856.

Sharma, N., Guo, X., Du, G., Guo, Z., Wang, J., Wang, Z., & Peterson, V. K. (2012). Direct evidence of concurrent solid-solution and two-phase reactions and the nonequilibrium structural evolution of $LiFePO_4$. Journal of the American Chemical Society, 134(18), 7867-7873.

Shrestha, A. K., Blazek, J., Flanagan, B. M., Dhital, S., Larroque, O., Morell, M. K., Gilbert, E. P., & Gidley, M. J. (2012). Molecular, mesoscopic and microscopic structure evolution during amylase digestion of maize starch granules. Carbohydrate Polymers, 90(1), 23-33.

Shueh, C., Chen, P-S., Cortie, D. L., Klose, F., Chen, W-C., Wu, T-H., van Lierop, J., & Lin, K-W. (2012). Correlating uncompensated antiferromagnetic moments and exchange coupling interactions in interface ion-beam bombarded $Co_{90}Fe_{10}$/CoFe-oxide bilayers. Japanese Journal of Applied Physics, 51(11), Art. No. 11PG02.

Shueh, C., Cortie, D. L., Klose, F., van Lierop, J., & Lin, K. W. (2012). Modulating the magneto-crystalline anisotropy and the exchange bias field in CoFe/(Co,Fe)O bilayers using ion-beam bombardment and single crystalline substrates. IEEE Transactions on Magnetics, 48(11), 2892-2895.

Simons, H., Glaum, J., Daniels, J. E., Studer, A. J., Liess, A., Roedel, J., & Hoffman, M. (2012). Domain fragmentation during cyclic fatigue in 94%($Bi_{1/2}Na_{1/2}$)TiO_3-6%$BaTiO_3$. Journal of Applied Physics, 112(4).

Smith, A. R. G., Lee, K. H., Nelson, A., James, M., Burn, P. L., & Gentle, I. R. (2012). Diffusion - the hidden menace in organic optoelectronic devices. Advanced Materials, 24(6), 822-826.

Smith, H.G., Sheridan, G. J., Nyman, P., Child, D. P., Lane, P. N. J., Hotchkis, M. A. C., & Jacobsen, G. E. (2012). Quantifying sources of fine sediment supplied to post-fire debris flows using fallout radionuclide tracers. Geomorphology, 139, 403-415.

Smith, M. C., Bouchard, P. J., Turski, M., Edwards, L., & Dennis, R. J. (2012). Accurate prediction of residual stress in stainless steel welds. Computational Materials Science, 54, 312-328.

Soeprobowati, T. R., Hadisusanto, S., Gell, P., & Zawadski, A. (2012). The Diatom Stratigraphy of Rawapening Lake, implying Eutrophication History. American journal of environmental sciences, 8(3), 334.

Spencer, K., Luzin, V., Matthews, N., & Zhang, M. X. (2012). Residual stresses in cold spray Al coatings: The effect of alloying and of process parameters. Surface & Coatings Technology, 206(19-20), 4249-4255.

Stadler, A. M., Garvey, C. J., Bocahut, A., Sacquin-Mora, S., Digel, I., Schneider, G. J., Natali, F., Artmann, G. M., & Zaccai, G. (2012). Thermal fluctuations of haemoglobin from different species: adaptation to temperature via conformational dynamics. Journal of the Royal Society Interface, 9(76), 2845-2855.

Stapleton, A., Vaughan, B., Xue, B., Sesa, E., Burke, K., Zhou, X., Bryant, G., Werzer, O., Nelson, A., Kilcoyne, A. L. D., Thomsen, L., Wanless, E., Belcher, W., & Dastoor, P. (2012). A multilayered approach to polyfluorene water-based organic photovoltaics. Solar Energy Materials and Solar Cells, 102, 114-124.

Stock, C., Broholm, C., Zhao, Y., Demmel, F., Kang, H. J., Rule, K. C., & Petrovic, C. (2012). Magnetic field splitting of the spin resonance in $CeCoIn_5$. Physical Review Letters, 109(16), Art. No. 167207.

Styles, M. J., Rowles, M. R., Madsen, I. C., McGregor, K., Urban, A. J., Snook, G. A., Scarlett, N. V. Y., & Riley, D. P. (2012). A furnace and environmental cell for the in situ investigation of molten salt electrolysis using high-energy X-ray diffraction. Journal of Synchrotron Radiation, 19, 39-47.

Sullivan, E., Avdeev, M., & Vogt, T. (2012). Structural distortions in $Sr_{3-x}A_xMO_4F$ (A=Ca, Ba; M=Al, Ga, In) anti-Perovskites and corresponding changes in photoluminescence. Journal of Solid State Chemistry, 194, 297-306.

Susilo, R. A., Pérez, S., M., Cobas, R., Cadogan, J. M., & Avdeev, M. (2012). Magnetic order and spin-reorientation in HoGa. JPCS, 340(1), Art. No. 012071.

Sweetman, L. J., Nghiem, L., Chironi, I., Triani, G., Panhuis, M. I. H., & Ralph, S. F. (2012). Synthesis, properties and water permeability of SWNT buckypapers. Journal of Materials Chemistry, 22(27), 13800-13810.

Szabo, . M., Howell, . R., Pellegrini, P., Greguric, I., & Katsifis, A. (2012). Development and validation of competition binding assays for affinity to the extracellular matrix receptors, alpha(v)beta(3) and alpha(IIb)beta(3) integrin. Analytical Biochemistry, 423(1), 70-77.

Szczucinski, W., Kokocinski, M., Rzeszewski, M., Chague-Goff, C., Cachao, M., Goto, K., & Sugawara, D. (2012). Sediment sources and sedimentation processes of 2011 Tohoku-oki tsunami deposits on the Sendai Plain, Japan - Insights from diatoms, nannoliths and grain size distribution. Sedimentary Geology, 282, 40-56.

Tan, T-Y., Kennedy, B. J., Zhou, Q., Ling, C. D., Miiller, W., Howard, C. J., Carpenter, M. A., & Knight, K. S. (2012). Impact of Jahn-Teller active Mn^{3+} on strain effects and phase transitions in $Sr_{0.65}Pr_{0.35}MnO_3$. Physical Review B, 85(10), Art. No. 104107.

Taylor, J. E., Chow, J. Y. H., Jeffries, C. M., Kwan, A. H., Duff, A. P., Hamilton, W. A., & Trewhella, J. (2012). Calmodulin binds a highly extended HIV-1 MA protein that refolds upon its release. Biophysical Journal, 103(3), 541-549.

Thomas, L. H., Cheung, E., Jones, A. O. F., Kallay, A. A., Lemee-Cailleau, M-H., McIntyre, G. J., & Wilson, C. C. (2012). 4-Phenoxyphenol: A porous molecular material. Crystal Growth & Design, 12(4), 1746-1751.

Thomsen, L., Tadich, A., Riley, D. P., Cowie, B. C. C., & Gladys, M. J. (2012). Investigating the enantioselectivity of alanine on a chiral Cu{421}(R) surface. Journal of Physical Chemistry C, 116(17), 9472-9480.

Tong, X., Jiang, C. Y., Lauter, V., Ambaye, H., Brown, D., Crow, L., Gentile, T. R., Goyette, R., Lee, W. T., Parizzi, A., & Robertson, J. L. (2012). In situ polarized He-3 system for the Magnetism Reflectometer at the Spallation Neutron Source. Review of Scientific Instruments, 83(7) 75101.

Toth, S., Lake, B., Hradil, K., Guidi, T., Rule, K. C., Stone, M. B., & Islam, A. T. M. N. (2012). Magnetic soft modes in the distorted triangular antiferromagnet alpha-$CaCr_2O_4$. Physical Review Letters, 109(12), Art. No. 127203.

Tremsin, A. S., McPhate, J. B., Steuwer, A., Kockelmann, W., Paradowska, A. M., Kelleher, J. F., Vallerga, J. V., Siegmund, O. H. W., & Feller, W. B. (2012). High-resolution strain mapping through time-of-flight neutron transmission diffraction with a microchannel plate neutron counting detector. Strain, 48(4), 296-305.

Tsai, P-H., Assadi, M. H. N., Zhang, T., Ulrich, C., Tan, T. T., Donelson, R., & Li, S. (2012). Immobilization of Na Ions for substantial power factor enhancement: site-specific defect engineering in $Na_{0.8}CoO_2$. Journal of Physical Chemistry C, 116(6), 4324-4329.

Turner, D. R., Edwards, A. J., & Piltz, R. O. (2012). Nitrile groups as hydrogen-bond acceptors in a donor-rich hydrogen-bonding network. Crystengcomm, 14(20), 6447-6451.

Turski, M., Paradowska, A. M., Zhang, S-Y., Mortensen, D., Fjaer, H., Grandfield, J., Davis, B., & DeLorme, R. (2012). Validation of predicted residual stresses within direct chill cast magnesium alloy slab. Metallurgical and Materials Transactions a-Physical Metallurgy and Materials Science, 43A(5), 1547-1557.

Usov, P. M., Fabian, C. P., & D'Alessandro, D. M. (2012). Rapid determination of the optical and redox properties of a metal-organic framework via in situ solid state spectroelectrochemistry. Chemical Communications, 48(33), 3945-3947.

Vance, E. R., Davis, J., Olufson, K., Chironi, I., Karatchevtseva, I., & Farnan, I. (2012). Candidate waste forms for immobilisation of waste chloride salt from pyroprocessing of spent nuclear fuel. Journal of Nuclear Materials, 420(1-3), 396-404.

Vance, E. R., Hanna, J. V., & Hadley, J. H., Jr. (2012). Cation vacancies in perovskites doped with La and Gd. Advances in Applied Ceramics, 111(1-2), 94-98.

Vance, E. R., Zhang, Y., McLeod, T., & Jovanovic, M. (2012). Preparation of Pu-doped fluorapatite. Journal of Nuclear Materials, 426(1-3), 223-225.

Veder, J-P., Patel, K., Sohail, M., Jiang, S. P., James, M., & De Marco, R. (2012). An electrochemical impedance spectroscopy/neutron reflectometry study of water uptake in the poly(3,4-thylenedioxythiophene):poly(styrene sulfonate)/polymethyl methacrylate-molydecyl methacrylate copolymer solid-contact ion-selective electrode. Electroanalysis, 24(1), 140-145.

Verschuer, J. D., Towson, J., Eberl, S., Katsifis, A., Henderson, D., Lam, P., Wen, L., Loc'h, C., Mattner, F., Thomson, S., Mohamed, A. & Fulham, M. J. (2012). Radiation dosimetry of the translocator protein ligands F-18 PBR111 and F-18 PBR102. Nuclear Medicine and Biology, 39(5), 742-753.

Vorontsov, V. A., Voskoboinikov, R. E., & Rae, C. M. F. (2012). Shearing of gamma ' precipitates in Ni-base superalloys: a phase field study incorporating the effective gamma-surface. Philosophical Magazine, 92(5), 608-634.

Vunckx, K., Atre, A., Baete, K., Reilhac, A., Deroose, C. M., Van Laere, K., & Nuyts, J. (2012). Evaluation of three MRI-based anatomical priors for quantitative PET brain imaging. IEEE Transactions on Medical Imaging, 31(3), 599-612.

Wada, T., Sakuma, T., Sakai, R., Uehara, H., Xianglian, Takahashi, H., Kamishima, O., Igawa, N., & Danilkin, S. A. (2012). Inter-atomic force constants of Ag_2O from diffuse neutron scattering measurement. Solid State Ionics, 225, 18-21.

Waerenborgh, J. C., Tsipis, E. V., Pereira, L. C. J., Avdeev, M., Naumovich, E. N., & Kharton, V. V. (2012). Magnetization, Mossbauer and isothermal dilatometric behavior of oxidized $YBa(Co,Fe)_4O_{7+delta}$. Dalton Transactions, 41(2), 667-678.

Wakeham, D., Niga, P., Ridings, C., Andersson, G., Nelson, A., Warr, G. G., Baldelli, S., Rutland, M. W., & Atkin, R. (2012). Surface structure of a "non-amphiphilic" protic ionic liquid. Physical Chemistry Chemical Physics, 14(15), 5106-5114.

Walsh, R. B., Howard, S. C., Nelson, A., Skinner, W. M., Liu, G. J., & Craig, V. S. J. (2012). Model Surfaces Produced by Atomic Layer Deposition. Chemistry Letters, 41(10), 1247-1249.

Walsh, R. B., Nelson, A., Skinner, W. M., Parsons, D., & Craig, V.S. J. (2012). Direct measurement of van der Waals and diffuse double-layer forces between titanium dioxide surfaces produced by atomic layer deposition. Journal of Physical Chemistry C, 116(14), 7838-7847.

Wang, C. K., Wacklin, H. P., & Craik, D. J. (2012). Cyclotides insert into lipid bilayers to form membrane pores and destabilize the membrane through hydrophobic and phosphoethanolamine-specific Interactions. Journal of Biological Chemistry, 287(52), 43884-43898.

Wang, J. L., Campbell, S. J., Hofmann, M., Hoelzel, M., Zeng, R., Dou, S. X., & Kennedy, S. J. (2012). Structural properties and magnetic phase transition in $HoNi_2Mn$ (Fe-57). Journal of Applied Physics, 111(7) 07E334.

Wang, J. L., Campbell, S. J., Kennedy, S. J., Dou, S. X., & Wu, G. H. (2012). $DyNi_2Mn$ - magnetisation and Mössbauer spectroscopy. Hyperfine Interacteractions. 208(1-3), 43-48.

Wang, J. L., Studer, A. J., Kennedy, S. J., Zeng, R., Dou, S. X., & Campbell, S. J. (2012). Magnetovolume effect in $Ho_2Fe_{17-x}Mn_x$ compounds. Journal of Applied Physics, 111(7), Art. No. 07A911.

Wang, S., Blazek, J., Gilbert, E. P., & Copeland, L. (2012). New insights on the mechanism of acid degradation of pea starch. Carbohydrate Polymers, 87(3), 1941-1949.

Wang, X., Blackford, M., Prince, K. E., & Caruso, R. A. (2012). Preparation of boron-doped porous titania networks containing gold nanoparticles with enhanced visible-light photocatalytic activity. Acs Applied Materials & Interfaces, 4(1), 476-482.

Wang, X., Dornom, T., Blackford, M., & Caruso, R.A. (2012). Solvothermal synthesis and photocatalytic application of porous Au/TiO_2 nanocomposites. Journal of Materials Chemistry, 22(23), 11701-11710.

Wang, Z., Garbe, U., Li, H., Studer, A. J., Harrison, R. P., Callaghan, M. D., Wang, Y., & Liao, X. (2012). Hydrogen-induced microstructure, texture and mechanical property evolutions in a high-pressure torsion processed zirconium alloy. Scripta Materialia, 67(9), 752-755.

Wang, Z. Y., Li, H. J., Garbe, U., Callaghan, M.D., Wang, Y. B., & Liao, X. Z. (2012). Microstructural evolution during gaseous hydrogen charging of Zircaloy-4 processed by high-pressure torsion: A comparative study. Material Letters, 68, 310-313.

Webster, N. A. S., Loan, M. J., Madsen, I. C., Knott, R. B., Brodie, G. M., & Kimpton, J. A. (2012). An in situ synchrotron X-ray diffraction investigation of lepidocrocite and ferrihydrite-seeded $Al(OH)_3$ crystallisation from supersaturated sodium aluminate liquor. Journal of Crystal Growth, 340(1), 112-117.

Webster, N. A. S., Pownceby, M. I., Madsen, I. C., & Kimpton, J. A. (2012). Silico-ferrite of calcium and aluminum (SFCA) iron ore sinter bonding phases: new insights into their formation during heating and cooling, metallurgical and materials transactions b-process metallurgy and materials processing science. 43(6), 1344-1357.

Weisler, M. I., Yamano, H., & Hua, Q. (2012). A Multidisciplinary approach for dating human colonization of Pacific Atolls. Journal of Island & Coastal Archaeology, 7(1), 102-125.

Wensrich, C. M., Kisi, E. H., Zhang, J. F., & Kirstein, O. (2012). Measurement and analysis of the stress distribution during die compaction using neutron diffraction. Granular Matter, 14(6), 671-680.

Werry, E. L., Liu, G. J., Lovelace, M. D., Nagarajah, R., & Bennett, M. R. (2012). Glutamate potentiates lipopolysaccharide-stimulated interleukin-10 release from neonatal rat spinal cord astrocytes. Neuroscience, 207, 12-24.

White, D. A., Hafsteinsdottir, E. G., Gore, D. B., Thorogood, G., & Stark, S. C. (2012). Formation and stability of Pb-, Zn- & $Cu-PO_4$ phases at low temperatures: Implications for heavy metal fixation in polar environments. Environmental Pollution, 161, 143-153.

Whitfield, R. E., Goossens, D. J., Studer, A. J., & Forrester, J. S. (2012). Measuring single-crystal diffuse neutron scattering on the Wombat high-intensity powder diffractometer. Metallurgical and Materials Transactions a-Physical Metallurgy and Materials Science, 43A(5), 1423-1428.

Whittle, K.R., Hyatt, N. C., Smith, K. L., Margiolaki, I., Berry, F.J., Knight, K. S., & Lumpkin, G. R. (2012). Combined neutron and X-ray diffraction determination of disorder in doped zirconolite-2M. American Mineralogist, 97(2-3), 291-298.

Wildes, A. R., Rule, K. C., Bewley, R. I., Enderle, M., & Hicks, T. J. (2012). The magnon dynamics and spin exchange parameters of $FePS_3$. Journal of Physics-Condensed Matter, 24(41), Art. No. 416004.

Willenberg, B., Schaepers, M., Rule, K. C., Suellow, S., Reehuis, M., Ryll, H., Klemke, B., Kiefer, K., Schottenhamel, W., Buechner, B., Ouladdiaf, B., Uhlarz, M., Beyer, R., Wosnitza, J., & Wolter, A. U. B. (2012). Magnetic frustration in a quantum spin chain: the case of linarite $PbCuSO_4(OH)_2$. Physical Review Letters, 108(11), Art. No. 117202.

Wimberley, C., Fischer, K., Pilcher, B. J., & Gregoire, M. C. (2012). Validation of the partial saturation approach for in vivo quantification of striatal dopamine D2 receptors with C-11 raclopride. Journal of Cerebral Blood Flow and Metabolism, 32, S35-S36.

Winkler, S. R., Steier, P., & Carilli, J. (2012). Bomb fall-out U-236 as a global oceanic tracer using an annually resolved coral core. Earth and Planetary Science Letters, 359, 124-130.

Witt, T., Doutch, J., Gilbert, E. P., & Gilbert, R. G. (2012). Relations between Molecular, Crystalline, and Lamellar Structures of Amylopectin. Biomacromolecules, 13(12), 4273-4282.

Wolter, A. U. B., Lipps, F., Schaepers, M., Drechsler, S. L., Nishimoto, S., Vogel, R., Kataev, V., Buechner, B., Rosner, H., Schmitt, M., Uhlarz, M., Skourski, Y., Wosnitza, J., Suellow, S., & Rule, K. C. (2012). Magnetic properties and exchange integrals of the frustrated chain cuprate linarite $PbCuSO_4(OH)_2$. Physical Review B, 85(1) 014407.

Woodroffe, C. D., McGregor, H. V., Lambeck, K., Smithers, S. G., & Fink, D. (2012). Mid-Pacific microatolls record sea-level stability over the past 5000 yr. Geology, 40(10), 951-954.

Wu, W., Lee, S. Y., Paradowska, A. M., Gao, Y. F., & Liaw, P. K. (2012). Twinning-detwinning behavior during fatigue-crack propagation in a wrought magnesium alloy AZ31B. Materials Science and Engineering A-Structural Materials Properties Microstructure and Processes, 556, 278-286.

Xia, F., Brugger, J., Qian, G., Ngothai, Y., O'Neill, B., Zhao, J., Pullen, S., Olsen, S., & Pring, A. (2012). Single-pass flow-through reaction cell for high-temperature and high-pressure in situ neutron diffraction studies of hydrothermal crystallization processes. Journal of Applied Crystallography, 45, 166-173.

Yahia, H. B., Shikano, M., Koike, S., Tatsumi, K., Kobayashi, H., Kawaji, H., Avdeev, M., Miiller, W., Ling, C. D., Liu, J., &Whangbo, M.-H. (2012). Synthesis and characterization of the crystal structure and magnetic properties of the new fluorophosphate $LiNaCo[PO_4]F$. Inorganic Chemistry, 51(16), 8729-8738.

Yahia, H.B., Shikano, M., Sakaebe, H., Koike, S., Tabuchi, M., Kobayashi, H., Kawaji, H., Avdeev, M., Miiller, W., & Ling, C. D. (2012). Synthesis and characterization of the crystal structure, the magnetic and the electrochemical properties of the new fluorophosphate $LiNaFe[PO_4]F$. Dalton Transactions, 41(38), 11692-11699.

Yajima, T., Nakano, K., Takeiri, F., Ono, T., Hosokoshi, Y., Matsushita, Y., Hester, J., Kobayashi, Y., & Kageyama, H. (2012). Superconductivity in $BaTi_2Sb_2O$ with a d(1) square lattice. Journal of the Physical Society of Japan, 81(10), Art. No. 103706.

Yang, P-W., Lin, T-L., Liu, I. T., Hu, Y., & James, M. (2012). In situ neutron reflectivity studies of the adsorption of DNA by charged diblock copolymer monolayers at the air-water interface. Soft Matter, 8(27), 7161-7168.

Yang, X., Yuan, L., Peterson, V. K., Minett, A. I., Yin, Y., & Harris, A. T. (2012). Facile preparation of free-standing carbon nanotube arrays produced using two-step floating-ferrocene chemical vapor deposition. ACS Applied Materials & Interfaces, 4(3), 1417-1422.

Yao, S., Sang, Y., Yu, D., Avdeev, M., Liu, H., Wang, J., & Zhang, N. (2012). Low temperature neutron diffraction on congruent and near stoichiometric $LiNbO_3$. Modern Physics Letters B, 26(22), Art. No. 1250142.

Yibmantasiri, P., Leahy, D. C., Busby, B. P., Angermayr, S. A., Sorgo, A. G., Boeger, K., Heathcott, R., Barber, J. M., Moraes, G., Matthews, J. H., Northcote, P. T., Atkinson, P. H., & Bellows, D. S. (2012). Molecular basis for fungicidal action of neothyonidioside, a triterpene glycoside from the sea cucumber, Australostichopus mollis. Molecular Biosystems, 8(3), 902-912.

Zhang, J. Z., Bryce, N. S., Siegele, R., Carter, E. A., Paterson, D., de Jonge, M. D., Howard, D. L., Ryan, C. G., & Hambley, T. W. (2012). The use of spectroscopic imaging and mapping techniques in the characterisation and study of DLD-1 cell spheroid tumour models. Integrative Biology, 4(9), 1072-1080.

Zhang, Y., Vance, E. R., & McLeod, T. (2012). Diffuse reflectance spectroscopy of Np and Pu in zirconia and pyrochlore-structured $Y_2Ti_2O_7$. Journal of Nuclear Materials, 420(1-3), 278-281.

Zhang, Z., Kennedy, B. J., Howard, C. J., Carpenter, M. A., Miiller, W., Knight, K. S., Matsuda, M., & Miyake, M. (2012). Crystal structures, strain analysis, and physical properties of $Sr_{0.7}Ce_{0.3}MnO_3$. Physical Review B, 85(17).

Zhao, K., Li, X., Dodson, J., Atahan, P., Zhou, X., & Bertuch, F. (2012). Climatic variations over the last 4000 cal yr BP in the western margin of the Tarim Basin, Xinjiang, reconstructed from pollen data. Palaeogeography, Palaeoclimatology, Palaeoecology, 321–322(0), 16-23.

Zhao, M., Yang, X., Church, T. L., & Harris, A. T. (2012). Novel $CaO\text{-}SiO_2$ Sorbent and Bifunctional $Ni/Co\text{-}CaO/SiO_2$ Complex for selective H-2 synthesis from cellulose. Environmental Science & Technology, 46(5), 2976-2983.

Zhou, Q., Blanchard, P., Kennedy, B.J., Reynolds, E., Zhang, Z., Miiller, W., Aitken, J. B., Avdeev, M., Jang, L-Y., & Kimpton, J. A. (2012). Synthesis, structural and magnetic studies of the double perovskites Ba_2CeMO_6 (M = Ta, Nb). Chemistry of Materials, 24(15), 2978-2986.

Zhou, X., Li, X., Dodson, J., Zhao, K., Atahan, N., Nan, S., & Qing, Y. (2012). Land degradation during the Bronze Age in Hexi Corridor (Gansu, China). Quaternary International, 254, 42-48.

Zhu, H., Wei, T., Couper, M. J., & Dahle, A. K. (2012). Effect of Fe-rich particles on the formation of die streaks on anodized aluminum extrusions. JOM, 64(2), 337-345.

Zhu, P., Wu, Y., Reddy, M. V., Nair, A. S., Peng, S., Sharma, N., Peterson, V. K., Chowdari, B. V. R., & Ramakrishna, S. (2012). TiO_2 nanoparticles synthesized by the molten salt method as a dual functional material for dye-sensitized solar cells. RSC Advances, 2(12), 5123-5126.

Edited Book Chapters and Others

Book Chapters

Gilbert, E. P., Mata, J.P., & Hamiltonin, W. A. (2012). Time-Resolved Small Angle Neutron Scattering: Application to Non-equilibrium Kinetic Studies. In V. Garcia Sakai, C. Alba-Simionesco, S.-H. Chen (Eds.), Dynamics of Soft Matter (chapter 11, pp. 289-318). New York: Springer.

Gilbert, E. P., Lopez-Rubio, A., & Gidley, M. (2012). Characterisation Techniques in Food Materials Science. In B. Bhandari and Y. Roos (Eds.), Food Materials Science and Engineering (chapter 3, pp. 52-93). Wiley-Blackwell.

Hughes, C.E., Stone, D.J.M., Gibson, J.J., Sadek, M.S., Cendón, D.I., Hankin, S.I., Hollins, S.E., & Morrison, T.N. (2012). Stable Water Isotope Investigation of the Barwon-Darling River System in Australia. In Monitoring Isotopes in Rivers: Creation of the Global Network of Isotopes in Rivers (GNIR), IAEA-TECDOC-1673, (pp. 97-110).

Jeffries, C. M., Farrugia, W., & Ramsland, P.A. (2012). Crystallography and Small-Angle Scattering of Carbohydrate–Protein Complexes and Glycoproteins. In E. Yuriev and PA. Ramsland (Eds.), Structural Glycobiology (Chapman & Hall/CRC Press). (pp. 3-27).

Koetzle, T. F., & McIntyre, G.J. (2012). Single-crystal neutron diffraction. In E.N. Kaufmann (Eds.), Characterization of Materials, 2nd edition. (pp. 1307-1315). John Wiley and Sons.

Jeffries, C.M., & Trewhella, J. (2012). Small-Angle Scattering. In M.E.Wall (Eds.), Quantitative Biology: From Molecular to Cellular Systems (Chapman & Hall/CRC Press). (pp. 111-149).

Lumpkin, G.R., & Geisler-Wierwille, T. (2012). Minerals and Natural Analogues. In Rudy J.M. Lonings (Ed.), Comprehensive Nuclear Materials. Volume 5, Material Performance and Corrosion/Waste Materials. (chapter 5.22, pp. 563-600). Elsevier.

Mattner, F., Staykova, M., Callaghan, P., Berghofer, P., Ballantyne, P., Gregoire, M. C., Fordham, S., Pham, T., Rahardjo, G., Jackson, T., Mattner, F., Linares D., & Katsifis, A. (2012). Assessment of Neuroinflammation in Transferred EAE Via a Translocator Protein Ligand. In R. Weissert (Ed.), Experimental Autoimmune Encephalomyelitis - Models, Disease Biology and Experimental Therapy (pp. 47-64). Rijeka, Croatia: InTech (2012).

Ochs, M., Payne, T. E., & Brendler, V. (2012). NEA Sorption Project Phase III: Thermodynamic sorption modeling in support of radioactive waste disposal safety cases. A guideline document. M. Ochs, T.E. Payne and V. Brendler. May 2012. Pages: 153 ISBN: 9789264177819 OECD Code: 662012021P1.

Payne, T. E., & Edis, R. (2012). Chapter 3 - Mobility of Radionuclides in Tropical Soils and Groundwater. In R. T. John (Eds.), Radioactivity in the Environment. Volume 18 (pp. 93-120).

Pröhl G., Twining J.R., & Crawford J. (2012). Radiological Consequences Modelling. In J.R. Twining (Eds.), Tropical Radioecology, Radioactivity in the Environment. Volume 18, (chapter 7, pp. 281-342).

Vance, E.R. (2012). Ceramic Waster Forms. In Rudy J.M. Konings (Ed.), Comprehensive Nuclear Materials. Volume 5, Material Performance and Corrosion/Waste Materials. (chapter 5.19, pp. 485-503). Elsevier.

Technical Reports

Kang, C-H., Kim, W-H., Hu, C-G., Chambers, S., Zahorowski, W., & Crawford, J. (2012). Realtime Monitoring of Radon (Rn-222) Background Concentration and its Application as a Transportation Tracer (in Korean). Report to Research Agency for Climate Science / Korea Meteorological Administration. Report Number RACS 2011-1015.

Kang, C-H., Hu, C-G., Chambers, S., Zahorowski, W., & Crawford, J. (2012). Monitoring of Atmospheric Radon at Gosan Site, Jeju Island (in Korean). Report to Center for Atmospheric Sciences and Earthquake Research, Korea Meteorological Administration. Report Number CATER 2012-3012.

Keywood, M., Galbally, I., Crumeyrolle, S., Miljevic, B., Cheng, M., Boast, K., Fedele, R.,Gillett, R., Chambers, S., Griffiths, A., Harnwell, J., Lawson, S., Molloy, S., Powell, J., Reisen,F., Ristovski, Z., Selleck, P., Ward, J., Chuanfu, Z., Jianrong, Z., Cope, M., & Emmerson, K. (2012). Sydney Particle Study- Stage-I: Executive Summary. A report by The Centre for Australian Weather and Climate Research.

Payne, T.E. (2012). Background Report on the Little Forest Burial Ground Legacy Waste Site. External Report ANSTO/E-780.

Stuart, H. (2012). Little Forest Burial Ground – Geology, Geophysics and well installation 2009-2010. External Report ANSTO/E-781.

Editing of Special Journals

Buttner, H. G. (2012). (Ed.) Neutron News 23 (1-4). Philadelphia, USA: Taylor and Francis Group.

Theses

Larsen, J. (2012). "Aspects of the contemporary and palaeo- hydrology of the Lake Eyre Basin, central Australia" (PhD Thesis) - University of Wollongong, Australia.

Markowska, M. (2012). "Characterising drip water hydrology of the karst unsaturated zone in Harrie Wood Cave, Yarrangobilly" (Honours Thesis) - University of New South Wales, Australia.

Fernandez, D. (2012). "Membrane Interactions of Australian Antimicrobial Peptides" (PhD Thesis) – The University of Melbourne, Australia.

Styles, M. J. (2012). "In situ studies of the structure and oxidation of Magnéli phase electrodes and their application in molten salt electrolysis" (PhD Thesis) - The University of Melbourne, Australia.

Griffith, M. (2012). "Charge Generation and Recombination in Porphyrin Based Dye Sensitized Solar Cells" (PhD Thesis) - University of Wollongong, Australia.

Dimitrijev-Dwyer, M. (2012). "Properties of novel biosurfactants: linking the molecular, meso- and macro-length scales" (PhD Thesis) - University of Queensland, Australia.

Saerbeck, T. (2012) "Magnetic Coupling Phenomena in Systems with Reduced Dimensionality studied with Polarized Neutron Reflectometry" (PhD Thesis) - University of Western Australia, Australia

Published Conference Proceedings

Agamalian, M., Carpenter, J.M., & Rehm, Ch. (2012). The Advanced Multi-Wavelength Bonse-Hart Ultra-Small-Angle Neutron Scattering (USANS) Technique for the Study of Hierarchical Structures. D. McGillivray (ED), Proceeding of the 15th International Small-Angle Scattering Conference: [CD]. November 18th-23rd, 2012, Sydney, Australia.

Almond, O.C., Holt, S.A., & Valenzuela, S.M. (2012). Chloride Intracellular Ion Channel Protein 1, Cholesterol Impact Upon Membrane Insertion. Conference: 10th AINSE-ANBUG Neutron Scattering Symposium (AANSS). November 7th-9th, 2012, (pp. 68). Sydney, Australia.

Aly, Z., Davis, J., & Hanley, T. (2012). Fabrication and Characterisation of Mesoporous Polymer-Coated Polyacrylonitrile Beads and Subsequent Carbon Structures. D. McGillivray (ED), Proceeding of the 15th International Small-Angle Scattering Conference: [CD]. November 18th-23rd, 2012, Sydney, Australia.

Awin, L.A., Kennedy, B.J., & Avdeev, M. (2012). Influence of Water on the Structure of Anion Deficient Perovskites AA*(B B*)$O_{5.5}$ (A& A* = Sr^{2+} or Ba^{2+}, B* = Sr^{2+}, B= Nb^{5+} or Ta^{5+}). Conference: 10th AINSE-ANBUG Neutron Scattering Symposium (AANSS). November 7th-9th, 2012, (pp. 59). Sydney, Australia.

Baranyai, K.J., Reynolds, P.A., Gilbert, E.P., Henderson, M.J., Mata, J.P., & White, J.W. (2012). High Internal Phase Emulsion Stability - Oil Solvency Effects. D. McGillivray (ED), Proceeding of the 15th International Small-Angle Scattering Conference: [CD]. November 18th-23rd, 2012, Sydney, Australia.

Barber, F.J., Tallon, J.L., Mallett, B.P.P., & Avdeev, M. (2012). Oxygen Isotope Effect in High Temperature Superconductors - Phonons or Magnons? Conference: 10th AINSE-ANBUG Neutron Scattering Symposium (AANSS). November 7th-9th, 2012, (pp. 25). Sydney, Australia.

Bendich, A. J., Muransky, O., Hamelin, C., Luzin, V., Smith, M.C., & Edwards, L. (2012). Verification of Welding Simulations with Measurement. Workshop: Current State and Future of Neutron Stress Diffractometers. January 10th-12th, 2012, (pp. 28). Sydney, Australia.

Benedetto, A., Jeffries, C., Magazù, C., & Gilbert, E.P. (2012). The Effect of Disaccharide Bioprotectants on the Clustering and Association of Proteins in Solution. D. McGillivray (ED), Proceeding of the 15th International Small-Angle Scattering Conference: [CD]. November 18th-23rd, 2012, Sydney, Australia.

Bertinshaw, J., Brück, S., Maran, R., Valanoor, N., Danilkin, S., Klose, F., & Ulrich, C. (2012). Polarised Neutron and X-Ray Resonant Magnetic Reflectivity Studies of Multiferroic Thin Films. Conference: 10th AINSE-ANBUG Neutron Scattering Symposium (AANSS). November 7th-9th, 2012, (pp. 60). Sydney, Australia.

Bertinshaw, J., Maran, R., Valanoor, N., Klose, F., & Ulrich, C. (2012). Neutron Studies of Functional Multiferroic $BiFeO_3$ Thin Films. Conference: 36th Annual Condensed Matter and Materials Meeting. January 31st - February 3rd, 2012, (pp. 67). Wagga Wagga, NSW, Australia.

Blackley, R., Fox, L. (2012). Radiation Protection in the remediation and Environmental Management of Radioactive Sand Mine Tailings. Conference: ARPS Radiation Safety: Bridging The Gap. October 14th-17th, 2012, (pp. 64). Sydney, NSW, Australia.

Blazek, J., & Gilbert, E.P. (2012). Investigation of Digestion Kinetics in Commercial Starches using In-Situ Small-Angle Neutron Scattering. ID. McGillivray (ED), Proceeding of the 15th International Small-Angle Scattering Conference: [CD]. November 18th-23rd, 2012, Sydney, Australia.

Boldeman, J. (2012). Options for an Australian Hadron Therapy Facility. Workshop: A Hadron Therapy Strategy for Australia. April 20th, 2012, (pp.3). Sydney, Australia.

Booth, N., Olsen, S.R., Reynolds, N.M., Nguyen, T., Piltz, R.O., Glazer, R.M., & Edwards. A.J. (2012). Commissioning of a Cobra™ Crystal Cooler on a Neutron Laue Diffractometer at the Bragg Institute. Workshop: 7th International Workshop on Sample Environment at Neutron Scattering Facilities. September 16th-20th, 2012, (pp. 44). Sydney, Australia.

Booth, S., & Imperia, P. (2012). High Voltage Sample Environment Development at the Bragg Institute. Workshop: 7th International Workshop on Sample Environment at Neutron Scattering Facilities. September 16th-20th, 2012, (pp. 25). Sydney, Australia.

Bot, A., Gilbert, E., Bouwman, W., Sawalha, H., Adel, R.-d., Haramus, V., Venema, P., Linden E.v-d., & Flöter, E. (2012). Small-Angle Neutron Scattering Study on Self-Assembled Sitosterol-Oryzanol Tubules. D. McGillivray (ED), Proceeding of the 15th International Small-Angle Scattering Conference: [CD]. November 18th-23rd, 2012, Sydney, Australia.

Brück, S., Cortie, D., Brown, J., Saerbeck, T., Ulrich, C., Klose, F., & Downes, J. (2012). Polarized Neutron Reflectometry of Rare-Earth Nitride Thin Films. Conference: 36th Annual Condensed Matter and Materials Meeting. January 31st - February 3rd, 2012, (pp. 109). Wagga Wagga, NSW, Australia.

Brück, S., Paul, M., Tian, H., Müller, A., Fauth, K., Goering, E., Verbeeck, J., Van Tendeloo, G., Sing, M., & Claessen, R. (2012). Local Magnetic Structure at the Fe_3O_4/ZnO Interface. Conference: 36th Annual Condensed Matter and Materials Meeting. January 31st - February 3rd, 2012, (pp. 68). Wagga Wagga, NSW, Australia.

Button, D.T., Hotchkis, M., Greenlees, B., Magee, C., & Roberts, E. (2012). Performance of a New Compact ECR Ion Source for Stable Isotope Mass Spectrometry. In Button (Ed.), Workshop: 20th International Workshop on Electron Cyclotron Resonance Ion Sources (ECRIS-2012). September 25th-28th, 2012, (pp. 33).Sydney, Australia.

Chandra, T., Ionescu, M., & Mantovani, D. (2012). Fabrication and Characterisation of Diluted Magnetic Semiconductors Thin Films Using Ion Beams. International Conference on processing & manufacturing of advanced materials (THERMEC'2011), 1st-5th August 2011. Quebec City, Canada. In M. Ionescu et al (Ed), THERMEC 2011: Materials Science Forum, 706-709, 2869.

Clarke, G., L'Hopital, L.S., McTrustry, S., Pullen, S., Freeland, E., Rakha, K., Ovallet, R., Olsen, S., & Imperia, P. (2012). New Developments for the Use of a Rapid Sample Quencher with Solid Metallic Samples. Workshop: 7th International Workshop on Sample Environment at Neutron Scattering Facilities. September 16th-20th, 2012, (pp. 46). Sydney, Australia.

Colella, M. (2012). ANSTO's Emergency Preparedness and Response Capabilities. Conference: ARPS Radiation Safety: Bridging The Gap. October 14th-17th, 2012, (pp. 62). Sydney, NSW, Australia.

Cong, W.W., Garvey, C.J., She, F.H., & Kong, L.X. (2012). Alignment of Nanostructure Templated from Lyotropic Liquid Crystals in Membrane Preparation. Conference: 10th AINSE-ANBUG Neutron Scattering Symposium (AANSS). November 7th-9th, 2012, (pp. 30). Sydney, Australia.

Cortie, D., Brück, S., Saerbeck, T., Brown, J., Downes, J., Wang, X., & Klose, F. (2012). Spin-Polarized Neutron Reflectometry Investigation of Rare-Earth Nitride Thin Films: DyN, HoN and ErN. Conference: 10th AINSE-ANBUG Neutron Scattering Symposium (AANSS). November 7th-9th, 2012, (pp. 61). Sydney, Australia.

Cortie, D.L., Du, Y., Cheng, Z.X., Klose, F., & Wang, X.L. (2012). Suppression of the Spim Spiral in an Antiferromagnetic $BiFe_{0.5}Mn_{0.5}O_3$ Thin Film and Powder. Conference: 36th Annual Condensed Matter and Materials Meeting. January 31st - February 3rd, 2012, (pp. 44). Wagga Wagga, NSW, Australia.

Cottam, R., Luzin, V., Luic, Q., Wong, Y., & Brandt, M. (2012). Laser Materials Processing and Residual Stress Formation for Several Metallic Materials. Conference: 10th AINSE-ANBUG Neutron Scattering Symposium (AANSS). November 7th-9th, 2012, (pp. 51). Sydney, Australia.

Cousland, G.P., Mole, R., Elcombe, M., Cui, X.Y., Smith, A.E., Stampfl, C.M., & Stampfl, A.P.J. (2012). The Structure of Yttria-Stabilised Zirconia: a Combined Synchrotron Photoemission, Neutron Scattering and Ab-Inition Investigation. Conference: 36th Annual Condensed Matter and Materials Meeting. January 31st - February 3rd, 2012, (pp. 93). Wagga Wagga, NSW, Australia.

Daniels, J.E., Kimpton, J., Liss, K.D., & Welberry, T.R. (2012). The Advanced Diffraction and Scattering Beamline: A High-Energy X-Ray Beamline at the Australian Synchrotron for Materials Research. Conference: 10th AINSE-ANBUG Neutron Scattering Symposium (AANSS). November 7th-9th, 2012, (pp. 43). Sydney, Australia.

Darwish, R., Luks, E., Moraes, G., Holden, P.M., & James, M. (2012). Molecular Deuteration for Contrast Variation in Neutron Studies of Multi-Component Nanoscale System. D. McGillivray (ED), Proceeding of the 15th International Small-Angle Scattering Conference: [CD]. November 18th-23rd, 2012, Sydney, Australia.

Das, A., Duyker, S., Peterson, V., & D'Alessandro, D.M. (2012). Mechanics and Kinetics of Carbon Dioxide Adsorption in Metal Organic Frameworks. Conference: 10th AINSE-ANBUG Neutron Scattering Symposium (AANSS). November 7th-9th, 2012, (pp. 62). Sydney, Australia.

Davidson, C.J., Finlayson, T.R., Griffiths, J.R., Luzin, V., & Wang, Q.G. (2012). Neutron Diffraction of Macro and Microstressess in an Al-Si-Mg Composite and Observed Changes with Plastic Strain. Conference: 36th Annual Condensed Matter and Materials Meeting. January 31st - February 3rd, 2012, (pp. 58). Wagga Wagga, NSW, Australia.

Dawson, J.L., Hua, Q., & Smithers, S.G. (2012). Benthic foraminifera: their importance to future reef island resilience. The Proceedings of the 12th International Coral Reef Symposium, July 9th-13th, 2012. Cairns, Australia.

De Campo, K., Moghaddam, M.J., Varslot, T., Mittelbach, R., Castle, T., Garvey, C.J., Kirby, N., & Hyde, S.T. (2012). Star-Polyphile Liquid Crystals: Experiment and Theory of Bicontinuous Cubic Phases with a Demixed Hydrocarbon/Fluorocarbon Bilayer. D. McGillivray (ED), Proceeding of the 15th International Small-Angle Scattering Conference: [CD]. November 18th-23rd, 2012, Sydney, Australia.

De Campo, L., Moghaddam, M.J., Varsiot, T., Mittelbach, R., Castle T., Garvey, C., Kirby, N., & Hyde, S.T. (2012). The Bicontinuous Cubic Phase in Star-Polyphiles. Conference: 10th AINSE-ANBUG Neutron Scattering Symposium (AANSS). November 7th-9th, 2012, (pp. 27). Sydney, Australia.

Deng, G., Danilkin, S., Zhang, H., Li, X., & Luo, H. (2012). Lattice Dynamics of A-Site Relaxor Ferroelectric ($Na_{1/2}Bi_{1/2}$) TiO_3 Near Phase Transition. Conference: 10th AINSE-ANBUG Neutron Scattering Symposium (AANSS). November 7th-9th, 2012, (pp. 63). Sydney, Australia.

Deng, G., Vorderwisch, P., Wu, C-M., McIntyre, G., & Li, W-H. (2012). Simulation of Multiple Operation Modes for the Cold Neutron Triple Axis Spectrometer SIKA at Bragg Institute. Conference: 36th Annual Condensed Matter and Materials Meeting. January 31st - February 3rd, 2012, (pp. 102). Wagga Wagga, NSW, Australia.

Dimitrovski, L., & Donlevy, T. (2012). The Return of Australia's Intermediate Level Waste from France. Conference: ARPS Radiation Safety: Bridging The Gap. October 14th-17th, 2012, (pp. 51). Sydney, NSW, Australia.

Doutch, J., & Gilbert, E.P. (2012). Larger Scale Structures in Starch Granules Characterised Via Small-Angle Neutron and X-Ray Scattering. Conference: 10th AINSE-ANBUG Neutron Scattering Symposium (AANSS). November 7th-9th, 2012, (pp. 64). Sydney, Australia.

Doutch, J., & Gilbert, E.P. (2012). Larger Scale Structures in Starch Granules Characterised Via Small-Angle Neutron and X-Ray Scattering. ID. McGillivray (ED), Proceeding of the 15th International Small-Angle Scattering Conference: [CD]. November 18th-23rd, 2012, Sydney, Australia.

Doutch, J., Bason., M., Franceschini, F., James, K., Clowes, D., & Gilbert, E.P. (2012). Structural Transitions During Starch Pasting Using Simultaneous Rapid Visco Analysis and Small-Angle Neutron Scattering. D. McGillivray (ED), Proceeding of the 15th International Small-Angle Scattering Conference: [CD]. November 18th-23rd, 2012, Sydney, Australia.

Duff, A.P., Sawicki, A., Sokolova, A.V., Lake, V., Wood, K., Kriegel, A.M., Wilson, N., Trewhella, J., & Willows, R.D. (2012). The Structure of the 750 kDa Protein Complex, Magnesium Chelatase, by SAXS and SANS. D. McGillivray (ED), Proceeding of the 15th International Small-Angle Scattering Conference: [CD]. November 18th-23rd, 2012, Sydney, Australia.

Duff, A.P., Sokolova, A.V., Phang, J.M., Harrop, S., & Curmi, P.M.G. (2012). The Solution Structure of Full Length Human Ezrin by SAXS and Protein Crystallography. D. McGillivray (ED), Proceeding of the 15th International Small-Angle Scattering Conference: [CD]. November 18th-23rd, 2012, Sydney, Australia.

Duyker, S.G., Peterson, V.K., Ogilvie, S.H., Turner, D.R., Hill, M.R., D'Alessandro, D.M., & Kepert, C.J. (2012). Neutron Diffraction and In Situ Gas-Loading Investigations of Functional MOFs for Energy-Relevant Gas Separations. Conference: 10th AINSE-ANBUG Neutron Scattering Symposium (AANSS). November 7th-9th, 2012, (pp. 36). Sydney, Australia.

Edwards, A.J. (2012). Accurate Chemical Characterization - Fascinating Discoveries and Proofs from KOALA, the Single Crystal Laue Neutron Diffractometer at OPAL. Conference: 10th AINSE-ANBUG Neutron Scattering Symposium (AANSS). November 7th-9th, 2012, (pp. 31). Sydney, Australia.

Elliot, E.P., Doutch, J., Bason, M., Franceschini, F., Clowes, D., & James, K. (2012). Simultaneous SANS and Rapid Visco-Analysis - Probing Changes in Nanostructure during Starch Cooking. Workshop: 7th International Workshop on Sample Environment at Neutron Scattering Facilities. September 16th-20th, 2012, (pp. 36). Sydney, Australia.

Fong, W.-K., Hanley, T.L., Thierry, B., Kirby, N., & Boyd, B.J. (2012). Light Responsive Liquid Crystalline Nanostructures as On-Demand Drug Delivery Systems. D. McGillivray (ED), Proceeding of the 15th International Small-Angle Scattering Conference: [CD]. November 18th-23rd, 2012, Sydney, Australia.

Foster, L.J.R., Russell, R.A., & Holden, P.J. (2012). Polyhydroxylaknoates and their Biopegylated Hybrids: Characterisation Using Biodeuteration and SANS. D. McGillivray (ED), Proceeding of the 15th International Small-Angle Scattering Conference: [CD]. November 18th-23rd, 2012, Sydney, Australia.

Garbe, U. (2012). The new neutron imaging station DINGO at OPAL. Workshop: Current State and Future of Neutron Stress Diffractometers. January 10th-12th, 2012, (pp. 25). Sydney, Australia.

Garvey, C.J., & Ersez, T. (2012). Shear Rate Dependant Ordering in Pluronic F127. ID. McGillivray (ED), Proceeding of the 15th International Small-Angle Scattering Conference: [CD]. November 18th-23rd, 2012, Sydney, Australia.

Garvey, C.J., Booth, N., Franceschini, F., & Mannicke, D. (2012). RheoSANS: Simultaneous SANS and Rheology measurements on the Quokka SANS Instrument. Conference: 10th AINSE-ANBUG Neutron Scattering Symposium (AANSS). November 7th-9th, 2012, (pp. 42). Sydney, Australia.

Garvey, C.J., Kent, B., Turner, M., Mudie, S., & Schroeder-Turk, G. (2012). Structural Uniformity and Texture of the Gyroid Phase in Butterfly Wing Scales. D. McGillivray (ED), Proceeding of the 15th International Small-Angle Scattering Conference: [CD]. November 18th-23rd, 2012, Sydney, Australia.

Garvey, C.J., Tabor, R., & Dagastine, R.R. (2012). Structure and Interactions Between Micelles in Solution by Modelling of SANS Data. D. McGillivray (ED), Proceeding of the 15th International Small-Angle Scattering Conference: [CD]. November 18th-23rd, 2012, Sydney, Australia.

Garvey, C.J., Wood, K., & Gilbert, E.P. (2012). Recent Results from QUOKKA - the SANS Instrument at OPAL. D. McGillivray (ED), Proceeding of the 15th International Small-Angle Scattering Conference: [CD]. November 18th-23rd, 2012, Sydney, Australia.

Gatta, G.D., & McIntyre, G.J. (2012). Crystal Chemistry of Boron-Containing Minerals by Single-Crystal Neutron Diffraction. Conference: 10th AINSE-ANBUG Neutron Scattering Symposium (AANSS). November 7th-9th, 2012, (pp. 35). Sydney, Australia.

Gentle, I.R., Cavaye, H., Smith, A.R.G., Lee, K.H., Shaw, P.E., James, M., Darwish, T.A., Burn, P.L., & Meredith, P. (2012). Interfacial Structure and Diffusion in Multilayer Optoelectronic Devices. In White (Ed.). Symposium: Structure and Dynamics of Condensed Matter by Scattering Methods. November 25th-28th, 2012, (pp. 13). Sydney, Australia.

Gilbert, E.P., Blazek, J., Doutch, J., & Lopez-Rubio, A. (2012). The Role of Small-Angle X-Ray and Neutron Scattering Techniques in Understanding Starch Structure. In White (Ed.). Symposium: Structure and Dynamics of Condensed Matter by Scattering Methods. November 25th-28th, 2012, (pp. 43). Sydney, Australia.

Goder, J.N.D., Rafi, N.A.M., Bryant, G., Hunt, T., Kent, B., & Garvey, C.L. (2012). Study of the effect of Penetratin on the Gyroid to Diamond Phase Transition in Myverol. Conference: 36th Annual Condensed Matter and Materials Meeting. January 31st - February 3rd, 2012, (pp. 62). Wagga Wagga, NSW, Australia.

Graham, P.J., Bartkowiak, M., Mulders, A.M., Yethiraj, M., Pomjakushina, E., & Ulrich, C. (2012). Raman Scattering on Multiferroic $TbMnO_3$. Conference: 36th Annual Condensed Matter and Materials Meeting. January 31st - February 3rd, 2012, (pp. 73). Wagga Wagga, NSW, Australia.

Gregg, D.J., Zhang, Y.J., Zhang, Z.M., Karatchevtseva, I., Blackford, M.G., Triani, G., Lumpkin, G.R., & Vance, E.R. (2012). Preparation and Characterization of Uranium-doped Gadolinium Zirconates. Conference: 36th Annual Condensed Matter and Materials Meeting. January 31st - February 3rd, 2012, (wp 38). Wagga Wagga, NSW, Australia.

Griffiths, A.D., Williams, A.G., Chambers, S.D., Parkes, S.D., & McCabe, M.F. (2012). Combining Lidar and Radon-222 to Measure Mixing Height. Poster presentation at the AMS 20th Symposium on Boundary Layers and Turbulence. July 9th-13th, 2012. Boston MA (USA).

Gyürky, G., Farkas, J., Halász, Z., Fülöp, Z., Somorjai, E., Szücs, T., Mohr, P., & Wallner, A. (2012). Experimental study of α-induced reactions on ^{64}Zn for the astrophysical γ-process. Journal of Physics: Conference Series, 337, 012009.

Hall, G.S., Edwards, A.J., Batten, S.R., & Turner, D.R. (2012). Investigation of Hydrogen Bonding Networks Using Neutron Diffraction. Conference: 10th AINSE-ANBUG Neutron Scattering Symposium (AANSS). November 7th-9th, 2012, (pp. 34). Sydney, Australia.

Hameed, N., Salim, N.V., Hanley, T.L., & Guo, Q. (2012). A Small Angle X-Ray Scattering Study of Carbon Nanotube Dispersed in Ionic Liquids. D. McGillivray (ED), Proceeding of the 15th International Small-Angle Scattering Conference: [CD]. November 18th-23rd, 2012, Sydney, Australia.

Haque, R., Durandet, Y., & Paradowska, A. (2012). Effect of Sheet Material Properties on Residual Stress Profile in Self-Pierce Riveted Joint. Conference: 10th AINSE-ANBUG Neutron Scattering Symposium (AANSS). November 7th-9th, 2012, (pp. 67). Sydney, Australia.

Henning, M., Roosen-Runge, F., Zhang, F., Zorn, S., Skoda, W.A., Jacobs, R.M.J., Sztucki, M., Schober, H., Seydel, T., & Schreiber, F. (2012). Dynamics of Globular Proteins in Crowded Electrolyte Solutions. Conference: 36th Annual Condensed Matter and Materials Meeting. January 31st - February 3rd, 2012, (pp. 40). Wagga Wagga, NSW, Australia.

Hester, J.R. (2012). The Datamodel: Key to Developing a SAS Data Transfer Framework. D. McGillivray (ED), Proceeding of the 15th International Small-Angle Scattering Conference: [CD]. November 18th-23rd, 2012, Sydney, Australia.

Holden, P.J., Darwish, T.A., Duff, A.P., Gillon, M., Lake, V., Luks, E., Moraes, G., Rekas, A., Russell, R.A., Wilde, K.L., Yepuri, R., & James, M. (2012). Molecular Deuteration at the National Deuteration Facility (NDF). Conference: 10th AINSE-ANBUG Neutron Scattering Symposium (AANSS). November 7th-9th, 2012, (pp. 18). Sydney, Australia.

Holden, P.J., Darwish, T.A., Duff, A.P., Lake, V., Luks, E., Moraes, G., Rekas, A., Russell, R.A., Wilde, K.L., & James, M. (2012). Molecular Deuteration at the Australian National Deuteration Facility. D. McGillivray (ED), Proceeding of the 15th International Small-Angle Scattering Conference: [CD]. November 18th-23rd, 2012, Sydney, Australia.

Holt, S.A., Almond, O.C., & Valenzuela, S. (2012). Chloride Intracellular Ion Channel Protein 1, Cholesterol Impact Upon Membrane Insertion. In White (Ed.). Symposium: Structure and Dynamics of Condensed Matter by Scattering Methods. November 25th-28th, 2012, (pp. 45). Sydney, Australia.

Holt, S.A., Mayfield, T., & Le Brun, A.P. (2012). Mimicking the Outer Membrane of Gram Negative Bacteria. In White (Ed.). Symposium: Structure and Dynamics of Condensed Matter by Scattering Methods. November 25th-28th, 2012, (pp. 51). Sydney, Australia.

Hong, F., Cheng, Z., Wang, J., Studer, A., Wang, X., & Dou, S., (2012). Neutron Diffraction Study on the Frustrated Multiferroic $TbMn_{1-x}Fe_xO_3$. Conference: 10th AINSE-ANBUG Neutron Scattering Symposium (AANSS). November 7th-9th, 2012, (pp. 69). Sydney, Australia.

Hudspeth, J.M., Goossens, D.J., Gutmann, M.J., Studer, A.J., & Welberry, T.R. (2012). Investigating Short-Range Order in Triglycine Sulphate Using X-Ray and Neutron Diffuse Scattering. Conference: 36th Annual Condensed Matter and Materials Meeting. January 31st - February 3rd, 2012, (pp. 29). Wagga Wagga, NSW, Australia.

Hughes, A.V., Holt, S.A., & Lakey, J.H. (2012). Thiolipid Self Assembled Monolayers on Gold as Supports for Floating Lipid Bilayers. Conference: 10th AINSE-ANBUG Neutron Scattering Symposium (AANSS). November 7th-9th, 2012, (pp. 40). Sydney, Australia.

Hughes, C.E. (2012). Modelling Evaporative Losses from the Darling River During Drought Using δ^2H and $\delta^{18}O$. Conference: Hydrology & Water Resources Symposium. November 19th-22nd, 2012, (pp. 48). Dockside, Cockle Bay Sydney, NSW, Australia.

Hughes, C.E. (2012).Precipitation Stable Isotopes δ^2H and $\delta^{18}O$ in the Sydney Basin. Conference: Hydrology & Water Resources Symposium. November 19th-22nd, 2012, (pp. 120). Dockside, Cockle Bay Sydney, NSW, Australia.

Hughes, C.E., Crawford, J., Parkes, S., & Hollins, S. (2012). Precipitation stable isotopes δ^2H and $\delta^{18}O$ in the Sydney Basin. The Proceedings of the 34th Hydrology & Water Resources Symposium, 19-22 November 2012, Sydney, Australia. Engineers Australia, 1586-1593.

Hughes, C.E., Hollins, S.E., Crawford, J., Meredith, K.T., & Cendón, D.I. (2012). Modelling evaporative losses from the Darling River during drought using δ^2H and $\delta^{18}O$. The Proceedings of the 34th Hydrology & Water Resources Symposium. November 19th-22nd, 2012. Sydney, Australia. Engineers Australia, 423-428.

Hunt, T., Bryant, G., Darwish, T., Lenné, T., Kent, B., & Garvey, C.J. (2012). Localilty of Cryoprotective Sugars in Membranes. Conference: 10th AINSE-ANBUG Neutron Scattering Symposium (AANSS). November 7th-9th, 2012, (pp. 19). Sydney, Australia.

Hunt, T., Bryant, G., Kent, B., & Garvey, C.J. (2012). Structure and Stability of Lipid Rafts. D. McGillivray (ED), Proceeding of the 15th International Small-Angle Scattering Conference: [CD]. November 18th-23rd, 2012, Sydney, Australia.

Imperia, P. (2012). Low Temperatures and High Magnetic Fields at the Bragg Institute. Conference: 10th AINSE-ANBUG Neutron Scattering Symposium (AANSS). November 7th-9th, 2012, (pp. 56). Sydney, Australia.

Imperia, P. (2012). Sample Environments Updates at the Bragg Institute. Conference: 36th Annual Condensed Matter and Materials Meeting. January 31st - February 3rd, 2012, (pp. 100). Wagga Wagga, NSW, Australia.

James, J.A., Burca, G., Kockelemann, W., Zhang, S.Y., Paradowska, A.M., & Pierret, S. (2012). Combined Imaging and Diffraction Techniques. Workshop: Current State and Future of Neutron Stress Diffractometers. January 10th-12th, 2012, (pp. 24). Sydney, Australia.

James, M., Ciampi, S., & Gooding, J.J. (2012). "Click" Chemistry for the Functionalisation of Silicon for Chemical and Biological Sensing. In White (Ed.). Symposium: Structure and Dynamics of Condensed Matter by Scattering Methods. November 25th-28th, 2012, (pp. 46). Sydney, Australia.

James, M., Nelson, A., Holt, S., Hsu, T., Saerbech, T., Corties, D., Klose, F., & Le Brun, A. (2012). 2009 - 2012: The Age of Platypus Neutron Reflectometry at OPAL. Conference: 10th AINSE-ANBUG Neutron Scattering Symposium (AANSS). November 7th-9th, 2012, (pp. 70). Sydney, Australia.

James, M., Nelson, A., Holt, S.A., Hsu, T., Saerbeck, T., Klose, F., & Le Brun, A.P. (2012). 2009-2012: The Age of Platypus Neutron Reflectometry at Australia's Opal Reactor. In White (Ed.). Symposium: Structure and Dynamics of Condensed Matter by Scattering Methods. November 25th-28th, 2012, (pp. 24). Sydney, Australia.

Jeffries, C.M. (2012). Insight, Discovery and New Directions: Small-Angle Scattering and Cardiac Myosin Binding Protein C. D. McGillivray (ED), Proceeding of the 15th International Small-Angle Scattering Conference: [CD]. November 18th-23rd, 2012, Sydney, Australia.

Jeffries, C.M., Hynson, R.M., Rey, T., Knott, R.B., Cowieson, N.P., & Lee, L.K. (2012). It's Different! Probing Bacterial Flagellar Torque Protein Conformation(s) in Solution with SAXS. D. McGillivray (ED), Proceeding of the 15th International Small-Angle Scattering Conference: [CD]. November 18th-23rd, 2012, Sydney, Australia.

Jemian, P.R., Jackson, A.J., King, S.M., Butler, P.R., Nelson, A.R.J., Ghosh, R.E., Richter, T., Doucet, M., & Rennie, A.R. (2012). The canSAS Format for Storage and Interchange of Reduced Multi-Dimensional Small-Angle Scattering Data. D. McGillivray (ED), Proceeding of the 15th International Small-Angle Scattering Conference: [CD]. November 18th-23rd, 2012, Sydney, Australia.

Kam, W., Banati, R., McNamara, A., & Davis, J. (2012). 100 The Response of Messenger RNA to Ionizing Radiation - Mitochondrial Genes are More Susceptible. Paper presented at the RADION Radiotherapy and Oncology: Supplement 1.

Kearley, G.J. (2012). Developments in "Vibrational Spectroscopy with Neutrons" Since JWW First Used It. In White (Ed.). Symposium: Structure and Dynamics of Condensed Matter by Scattering Methods. November 25th-28th, 2012, (pp. 25). Sydney, Australia.

Kent, B., Bryant, G., Hunt, T., & Garvey, C.J. (2012). Studying Lipid Membrane - Solute Interaction with Specular and Off-Specular Neutron Scattering. Conference: 10th AINSE-ANBUG Neutron Scattering Symposium (AANSS). November 7th-9th, 2012, (pp. 39). Sydney, Australia.

Khan, M., Mashiri, F.R., Paradowska, A., Uy, B., & Tao, Z. (2012). Residual Stresses in High Strength Steel Tubes for Large Scale Infrastructure. Conference: 10th AINSE-ANBUG Neutron Scattering Symposium (AANSS). November 7th-9th, 2012, (pp. 75). Sydney, Australia.

Khodabakshi, B., Mutton, P., Paradowska, A., & Ibrahim, R. (2012). Measurement of Residual Stresses in Aluminothermic Rail Welds Using Neutron Diffraction Technique. Conference: 10th AINSE-ANBUG Neutron Scattering Symposium (AANSS). November 7th-9th, 2012, (pp. 53). Sydney, Australia.

Kisi, E.H., Wensrich, C.M., Kirstein, O., Luzin, V., & Zhang, J.F. (2012). Stress Distribution in Particulate Materials: 1 - Die Compaction. Conference: 10th AINSE-ANBUG Neutron Scattering Symposium (AANSS). November 7th-9th, 2012, (pp. 50). Sydney, Australia.

Knobloch, J.J., Nelson, A.J., & McGillivray, D.J. (2012). Characterising the Structure of Oxidised Model Membranes in Solution. In White (Ed.). Symposium: Structure and Dynamics of Condensed Matter by Scattering Methods. November 25th-28th, 2012, (pp. 41). Sydney, Australia.

Knobloch, J.J., Nelson, A.J., Hofmann, A., Lake, V., Duff, A.P., & McGillivray, D.J. (2012). Cellular Membrane Interactions of Plant Annexin GH1 Following Oxidatives Stress. D. McGillivray (ED), Proceeding of the 15th International Small-Angle Scattering Conference: [CD]. November 18th-23rd, 2012, Sydney, Australia.

Knobloch, J.K., Nelson, A.J., & McGillivray, D.J. (2012). Determining the Effect of Oxidative Damage on the Degradation of Cellular Membranes by Phospholipase A2. Conference: 10th AINSE-ANBUG Neutron Scattering Symposium (AANSS). November 7th-9th, 2012, (pp. 38). Sydney, Australia.

Lakey, J.H., Johnson, C.L., Clifton, L.A., Le Brun, A.P., Hughes, A., & Holt, S.A., (2012). Targeting the Bacterial Outer Membrane with Neutrons. In White (Ed.). Symposium: Structure and Dynamics of Condensed Matter by Scattering Methods. November 25th-28th, 2012, (pp. 27). Sydney, Australia.

Lamb, K., De Marco, R., Jiang, S.P., & Peterson, V. (2012). Investigating HPA Functionalized Mesoporous Silica Materials for Use as High Temperature Proton Exchange Membranes. Conference: 10th AINSE-ANBUG Neutron Scattering Symposium (AANSS). November 7th-9th, 2012, (pp. 72). Sydney, Australia.

Law, M. (2012). Measuring Residual Stress in Active Materials. Workshop: Current State and Future of Neutron Stress Diffractometers. January 10th-12th, 2012, (pp. 35). Sydney, Australia.

Le Brun, A.P., Clifton, L.A., Lakey, J.H., & Holt, S.A. (2012). Mimicking Membrane Fluidity: The Structure of Mixed Porin / Lipopolysaccharide Monolayers at the Air-Water Interface. Conference: 10th AINSE-ANBUG Neutron Scattering Symposium (AANSS). November 7th-9th, 2012, (pp. 37). Sydney, Australia.

Le Brun, A.P., Fernandez, D.I., Whitwell, T.C., Bansal, P., James, M., & Separovic, F. (2012). The Location of Antimicrobial Peptides from Australian Frogs in Model Biological Membranes Determined by Neutron Reflectometry. In White (Ed.). Symposium: Structure and Dynamics of Condensed Matter by Scattering Methods. November 25th-28th, 2012, (pp. 28). Sydney, Australia.

Lee, J.J., Ionescu, M., Xing, G.Z., & Li, S. (2012). Depth Distribution Profile of the Implanted Cobalt (Co) and Europium (Eu) ions in ZnO:Co and ZnO:Eu Thin Film. Conference: 10th AINSE-ANBUG Neutron Scattering Symposium (AANSS). November 7th-9th, 2012, (pp. 73). Sydney, Australia.

Lee, W.T., Klose, F., D'Adam, T., Jullien, D., Courtois, P., & Andersen, K. (2012). Up-Coming Polarised Neutron Capabilities on ANSTO Instruments Using Polarised ^{3}He Neutron Spin Filters. Conference: 10th AINSE-ANBUG Neutron Scattering Symposium (AANSS). November 7th-9th, 2012, (pp. 55). Sydney, Australia.

Lee, W.T., Klose, F., Jullien, D., & Andersen, K. (2012). Polarised ^{3}He based Neutron Polarisers and Analysers for Magnetism Research on ANSTO Instruments. Conference: 36th Annual Condensed Matter and Materials Meeting. January 31st - February 3rd, 2012, (pp. 101). Wagga Wagga, NSW, Australia.

Li, F., Narayanan, N., Mulders, A.M., Hutchison, W.D., Ulrich, C., & McIntyre, G. (2012). The Effect of Oxygen Isotope Substitution on Magnetism in Multiferroic $CaMn_7O_{12}$. Conference: 10th AINSE-ANBUG Neutron Scattering Symposium (AANSS). November 7th-9th, 2012, (pp. 74). Sydney, Australia.

Li, Q., Liu, Y., Danilkin, S., Studer, A.J., Deng, G., Li, Z., Withers, R., & Xu, Z. (2012). Elastic and Inelastic Neutron Scattering Studies on Lead-Based Relaxor Ferroelectric Single Crystals. Conference: 10th AINSE-ANBUG Neutron Scattering Symposium (AANSS). November 7th-9th, 2012, (pp. 49). Sydney, Australia.

Lin, T-L., Yang, P-W., Liu, I-T., Cheng, K-H., Hu, Y., Jeng, U-S., & Gilbert, E. (2012). Small-Angle Neutron and X-ray Scattering Studies on the Adsorption of DNA by Cationic Diblockcopolymer/ Lipid Complexes and Diblockcopolymer Micelles. D. McGillivray (ED), Proceeding of the 15th International Small-Angle Scattering Conference: [CD]. November 18th-23rd, 2012, Sydney, Australia.

Liss, K-D. (2012). X-Rays of the Future: Thinking Energy Recovery Linac. Conference: 36th Annual Condensed Matter and Materials Meeting. January 31st - February 3rd, 2012, (pp. 105). Wagga Wagga, NSW, Australia.

Liss, K-D., Yan, K., Thoennessen, L., Kabraa, S., Carr, D.G., Reid, M., Dehghan-Manshadi, A., Harrison, R.P., & Dippenaar, R.J. (2012). Metals Behaviour at Very High Temperature. Conference: 10th AINSE-ANBUG Neutron Scattering Symposium (AANSS). November 7th-9th, 2012, (pp. 52). Sydney, Australia.

Lyndon, E. (2012). Future Engineering Residual Stress Measurements. Workshop: Current State and Future of Neutron Stress Diffractometers. January 10th-12th, 2012, (pp. 12). Sydney, Australia.

Mannicke, D., Xiong, N., Lam, T., Lesha, M., & Hauser, N. (2012). Time-Rebinning of Instrument Data for SANS. D. McGillivray (ED), Proceeding of the 15th International Small-Angle Scattering Conference: [CD]. November 18th-23rd, 2012, Sydney, Australia.

Mata, J.P., Moon, E.M., Griffith, C.S., & Soldenhoff, K.H. (2012). Application of Small Angle Scattering in Mineral Processing Science. In White (Ed.). Symposium: Structure and Dynamics of Condensed Matter by Scattering Methods. November 25th-28th, 2012, (pp. 39). Sydney, Australia.

Mata, J.P., Udabage, P., & Gilbert, E.P. (2012). Structure of Casin Micelles in Milk Protein Concentrate Powders Via Small Angle X-Ray Scattering. D. McGillivray (ED), Proceeding of the 15th International Small-Angle Scattering Conference: [CD]. November 18th-23rd, 2012, Sydney, Australia.

McCarthy, L. (2012). Emergence of Competency Based Training in Radiation Safety and Developing Training Courses Incorporating these Units. Oh! What a Task! Conference: ARPS Radiation Safety: Bridging The Gap. October 14th-17th, 2012, (pp. 44). Sydney, NSW, Australia.

McCarthy, L. (2012). Trials & Tribulations of Communicating Ionising Radiation to the Public - 30 Years of Reflection. Conference: ARPS Radiation Safety: Bridging The Gap. October 14th-17th, 2012, (pp. 42). Sydney, NSW, Australia.

McIntyre, G.J. (2012). Protein Crystallography: What can Nuclear Polarisation do for us?. In White (Ed.). Symposium: Structure and Dynamics of Condensed Matter by Scattering Methods. November 25th-28th, 2012, (pp. 22). Sydney, Australia.

McIntyre, G.J., Kohlmann, H., & Willis, B.T.M. (2012). Phonons Observed by Neutron Laue Diffraction. Conference: 36th Annual Condensed Matter and Materials Meeting. January 31st - February 3rd, 2012, (pp. 104). Wagga Wagga, NSW, Australia.

McIntyre, G.J., Outladdiaf, B., Zeyen, C.M.E., Benoit, A., Thomas, F., & Pujol, S. (2012). Four-Circle Diffractometry at mK Temperatures. Workshop: 7th International Workshop on Sample Environment at Neutron Scattering Facilities. September 16th-20th, 2012, (pp. 30). Sydney, Australia.

Minakshi, M., Meyrick, D., Sharma, N., & Appadoo, D. (2012). Olivine $Li(Co_{0.5}Ni_{0.5})PO_4$ Cathode for Battery Applications. Conference: 10th AINSE-ANBUG Neutron Scattering Symposium (AANSS). November 7th-9th, 2012, (pp. 48). Sydney, Australia.

Mole, R.A., & Yu, D. (2012). Pelican: An Inelastic Neutron Scattering Spectrometer with Polarization Analysis. Conference: 36th Annual Condensed Matter and Materials Meeting. January 31st - February 3rd, 2012, (pp. 103). Wagga Wagga, NSW, Australia.

Mole, R.A., & Yu, D. (2012). Pelican: An Inelastic Neutron Scattering Spectrometer with Polarization Analysis. In White (Ed.). Symposium: Structure and Dynamics of Condensed Matter by Scattering Methods. November 25th-28th, 2012, (pp. 52). Sydney, Australia.

Mole, R.A., Montero, L.F., Nadeem, M., Peterson, V.K., Piltz, R., & Stride, J.A. (2012). Neutron Scattering Studies of Magnetic Coordination Polymers. Conference: 36th Annual Condensed Matter and Materials Meeting. January 31st - February 3rd, 2012, (pp. 71). Wagga Wagga, NSW, Australia.

Moon, E.M., Mata, J.P., & Griffith, C.S. (2012). Deducing the Nanostructure of Zirconium Colloids Formed in Sulphate Based Mineral Processing Liquors. D. McGillivray (ED), Proceeding of the 15th International Small-Angle Scattering Conference: [CD]. November 18th-23rd, 2012, Sydney, Australia.

Mulders, A.M., Bartkowiak, M., Hester, J.R., Pomjakushina, E., & Conder, K. (2012). Ferroelectric Charge Order Stabilized by Antiferromagnetism in Multiferroic $LuFe_2O_4$. Conference: 36th Annual Condensed Matter and Materials Meeting. January 31st - February 3rd, 2012, (pp. 115). Wagga Wagga, NSW, Australia.

Narayanan, N., Li, F., Hutchison, W., Mulders, A.M., Reynolds, N., Rovillain, P., Ulrich, C., Hester, J., & McIntyre, G. (2012). Neutron Powder Diffraction Experiments on Multiferroic $DyMnO_3$. Conference: 10th AINSE-ANBUG Neutron Scattering Symposium (AANSS). November 7th-9th, 2012, (pp. 78). Sydney, Australia.

Nelson, A., Lesha, M., Gerth, S., & Magerl, A. (2012). List Mode Acquisition for Examining Kinetic Processes in Thin Film Systems. Conference: 10th AINSE-ANBUG Neutron Scattering Symposium (AANSS). November 7th-9th, 2012, (pp. 41). Sydney, Australia.

Nelson, A., Wakeham, D., Warr, G.G., & Atkin, R. (2012). Probing Protic Ionic Liquid Surfaces Using X-Ray Reflectivity. In White (Ed.). Symposium: Structure and Dynamics of Condensed Matter by Scattering Methods. November 25th-28th, 2012, (pp. 44). Sydney, Australia.

Norwood, S., Shaw, D., Swarbrick, J., Duff, A., Wood, K., & Collins, B. (2012). Assembly and Solution Structure of the Retromer Complex. D. McGillivray (ED), Proceeding of the 15th International Small-Angle Scattering Conference: [CD]. November 18th-23rd, 2012, Sydney, Australia.

Ogilvie, S.H., Duyker, S.G., Peterson, V.K., & Kepert, C.J. (2012). Coordination Frameworks: Host-Guest Chemistry and Structural Dynamics. Conference: 10th AINSE-ANBUG Neutron Scattering Symposium (AANSS). November 7th-9th, 2012, (pp. 79). Sydney, Australia.

Olsen, S., Pangelis, S., Pullen, S., Palmer, J., Ogrin, A., Stampfl, A., New, M., & Imperia. P. (2012). Maximising Flexibility in Neutron Beam Instrument Upgrades and Designs to Allow for the Widest Possible Range of Sample Environments. Workshop: 7th International Workshop on Sample Environment at Neutron Scattering Facilities. September 16th-20th, 2012, (pp. 42). Sydney, Australia.

Pangelis, S., Olsen, S.R., Scherschligt, J., Leão, J.B., Pullen, S.A., Dender, D., Hester, J., & Imperia, P. (2012). Safety Interlock and Vent System to Alleviate Potentially Dangerous Ice Blockage of Top-Loading Cryostat Sample Sticks. Workshop: 7th International Workshop on Sample Environment at Neutron Scattering Facilities. September 16th-20th, 2012, (pp. 29). Sydney, Australia.

Paradowska, A. (2012). How Neutrons Support Modern Materials Engineering and Helps Unravel Some Historical Engineering Puzzles. Conference: 36th Annual Condensed Matter and Materials Meeting. January 31st - February 3rd, 2012, (pp. 45). Wagga Wagga, NSW, Australia.

Pelliccia, D., Orlov, D., Nikulin, A.Y., Hester, J., Estrin, Y., & Kirby, N. (2012). Characterization of Nanoscale Precipitates in Alloys by Small Angle X-Ray Scattering and Diffraction Imaging. D. McGillivray (ED), Proceeding of the 15th International Small-Angle Scattering Conference: [CD]. November 18th-23rd, 2012, Sydney, Australia.

Pham, C.L.L., Kirby, N., Wood, K., Knott, R.B., Cappai, R., Curtain, C.C., & Rekas, A. (2012). Structure of Dopamine-Induced α-Synuclein Oligomers: A Small Angle Scattering Study. D. McGillivray (ED), Proceeding of the 15th International Small-Angle Scattering Conference: [CD]. November 18th-23rd, 2012, Sydney, Australia.

Princep, A.J., Mulders, A.M., Schierle, E., Weschke, E., Hester, J., Hutchison, W.D., Tanaka, Y., Terada, N., Narumi, Y., Staub, U., Scagnoli, V., Nakamura, T., Kikkawa, A., Lovesey, S.W., & Balcar, E. (2012). Resonant X-Ray Diffraction and the Observation of Strange Quantities. Conference: 36th Annual Condensed Matter and Materials Meeting. January 31st - February 3rd, 2012, (pp. 76). Wagga Wagga, NSW, Australia.

Pullen, S. (2012). Project Management Methods in the Field of Sample Environment Development. Workshop: 7th International Workshop on Sample Environment at Neutron Scattering Facilities. September 16th-20th, 2012, (pp. 20). Sydney, Australia.

Qasim, I., Kennedy, B., & Avdeev, M. (2012). Crystallographic Studies on Ru and Ir-Based $SrB_{1-x}M_xO_3$- Type Perovskites. Conference: 10th AINSE-ANBUG Neutron Scattering Symposium (AANSS). November 7th-9th, 2012, (pp. 82). Sydney, Australia.

Rath, E.R., Duff, A., Doherty, G., Knott, R.B., & Church, W.B. (2012). Structural Investigation of the Anti-Cancer Complex, Bamlet, by Small-Angle X-Ray Scattering. D. McGillivray (ED), Proceeding of the 15th International Small-Angle Scattering Conference: [CD]. November 18th-23rd, 2012, Sydney, Australia.

Rehm, C., Brûlė, A., Freund, A., & Kennedy, S. (2012). Kookaburra: The New USANS Instrument at ANSTO. In White (Ed.). Symposium: Structure and Dynamics of Condensed Matter by Scattering Methods. November 25th-28th, 2012, (pp. 54). Sydney, Australia.

Rehm, C., Brûlé, A., Freund, A., & Kennedy, S. (2012). The KOOKABURRA USANS Instrument at ANSTO. D. McGillivray (ED), Proceeding of the 15th International Small-Angle Scattering Conference: [CD]. November 18th-23rd, 2012, Sydney, Australia.

Rehm, C., Brûlé, A., Freund, A., & Kennedy, S. (2012). Ultra-Small-Angle Neutron Scattering in the Southern Hemisphere. D. McGillivray (ED), Proceeding of the 15th International Small-Angle Scattering Conference: [CD]. November 18th-23rd, 2012, Sydney, Australia.

Rehm, C., Brûlé, A., Freund, A., & Kennedy, S. (2012). Ultra-Small-Angle Neutron Scattering: Large-Scale Structure Determination from a Bird's Eye View. Conference: 10th AINSE-ANBUG Neutron Scattering Symposium (AANSS). November 7th-9th, 2012, (pp. 44). Sydney, Australia.

Rennie, A.R., Hellsing, M.S., Wood, K., Gilbert, E.P., Porcar, L., Schweins, R., Dewhurst, C.D., Lindner, P., Heenan, R.K., Rogers, S.E., Butler, P.D., Krzywon, J., Ghosh, R.E., & Jackson, A.J. (2012). What is Learnt About SANS Instruments and Data Reduction from Round Robin Measurements? - A Polymer Latex 'Standard'. D. McGillivray (ED), Proceeding of the 15th International Small-Angle Scattering Conference: [CD]. November 18th-23rd, 2012, Sydney, Australia.

Reynolds, N., Rovillain, P., Narayanan, N., Fujioka, F., Tokura, Y., Danilkin, S., Mulders, A.M., McIntyre, G., & Ulrich, C. (2012). Comparison of the Magnetic and Crystal Field Excitations in Orthorhombically Distorted Vanadates and Multiferroic Manganites. Conference: 10th AINSE-ANBUG Neutron Scattering Symposium (AANSS). November 7th-9th, 2012, (pp. 84). Sydney, Australia.

Reynolds, N.M., Graham, P., Mulders, A.M., McIntyre, G., Danilkin, S., Fujioka, J., Tokura, Y., Keimer, B., Reehuis, M., & Ulrich, C. (2012). Inelastic Neutron Scattering in Multiferroic Materials. Conference: 36th Annual Condensed Matter and Materials Meeting. January 31st - February 3rd, 2012, (pp. 114). Wagga Wagga, NSW, Australia.

Rovillain, P., de Sousa, R., Gallais, Y., Sacuto, A., Measson, M-A., Colson, D., Forget, A., Bibes, M., Barthelemy, A., & Cazayous, M. (2012). Electric Control of Spin Wave Modes at Room Temperature in BiFeO3. Conference: 36th Annual Condensed Matter and Materials Meeting. January 31st - February 3rd, 2012, (pp. 72). Wagga Wagga, NSW, Australia.

Rovillain, P., Graham, P., Reynolds, N., Narayannan, N., Gallais, Y., Sacuto, A., Measson, M.A., Sakata, H., McIntyre, G., Mulders, A.M., Ulrich, C., & Cazayous, M. (2012). Electromagnons in Multiferroics Probed by Raman Light Scattering Comparison to Neutron Scattering Investigations. Conference: 10th AINSE-ANBUG Neutron Scattering Symposium (AANSS). November 7th-9th, 2012, (pp. 22). Sydney, Australia.

Russell, R.A., Darwish, T.A., Moraes, G., Gillon, M., Foster, L.J.R., & Holden, P.J. (2012). Biodeuterated Microbial Chitosan for Characterisation by Neutron Scattering and Development of New Biocompatible Materials. Conference: 10th AINSE-ANBUG Neutron Scattering Symposium (AANSS). November 7th-9th, 2012, (pp. 20). Sydney, Australia.

Ruzicka, J., Abu Baker, F., Muramdhani, I., Rhem, C., Knott, R., Ingham, B., & Golovko, V.B. (2012). In Situ SAXS Analysis of Titanium Dioxide Growth. D. McGillivray (ED), Proceeding of the 15th International Small-Angle Scattering Conference: [CD]. November 18th-23rd, 2012, Sydney, Australia.

Salim, N.V., Hanley, T.L., Hameed, N., & Guo, Q. (2012). Investigation of Block Copolymer/Homopolymer Blends and Complexes Using Small Angle X-Ray Scattering (SAXS) Technique. D. McGillivray (ED), Proceeding of the 15th International Small-Angle Scattering Conference: [CD]. November 18th-23rd, 2012, Sydney, Australia.

Sang, Y., Yu, D., Avdeev, M., Piltz, R., Sharma, N., & Wang, J. (2012). X-Ray and Neutron Diffraction Studies of Flux and Hydrothermally Grown Nonlinear Optical Material $KBe_2BO_3F_2$. Conference: 10th AINSE-ANBUG Neutron Scattering Symposium (AANSS). November 7th-9th, 2012, (pp. 92). Sydney, Australia.

Schulz, J. (2012). Overview of the OPAL Neutron Beam Facility. Conference: ARPS Radiation Safety: Bridging The Gap. October 14th-17th, 2012, (pp. 52). Sydney, NSW, Australia.

Sharma, N., Yu, D., Zhu, Y., Wu, Y., & Peterson, V.K. (2012). Lithium Position and Occupancy Fluctuations in a Cathode During Charge/Discharge Cycling of a Lithium-Ion Battery. Conference: 10th AINSE-ANBUG Neutron Scattering Symposium (AANSS). November 7th-9th, 2012, (pp. 85). Sydney, Australia.

Shaw, P.E., Cavaye, H., Chen, S.S.Y., James, M., Gentle, I.R., & Burn, P.L. (2012). Probing the Absorption and Release of Nitroaromatic Vapours from Fluorescent Dendrimer Films for the Detection of Explosives. Conference: 10th AINSE-ANBUG Neutron Scattering Symposium (AANSS). November 7th-9th, 2012, (pp. 29). Sydney, Australia.

Shen, C., Paradowska, A.M., Larkin, N., Li, H., Pan, Z., & Law, M. (2012). Neutron Diffraction Residual Stress Measurements of Weldments for Shipbuilding Application. Conference: 10th AINSE-ANBUG Neutron Scattering Symposium (AANSS). November 7th-9th, 2012, (pp. 54). Sydney, Australia.

Shoko, E., Peterson, V.K., & Kearley, G.J. (2012). Alkali Metal Dynamics in the β-Pyrochlories AOs_2O_6 (A = K, Rb, Cs) and Their Prospects as Thermoelectric Materials. Conference: 10th AINSE-ANBUG Neutron Scattering Symposium (AANSS). November 7th-9th, 2012, (pp. 26). Sydney, Australia.

Sokolova, A. (2012). BILBY: New Time-of-Flight Small Angle Scattering Instrument at ANSTO. D. McGillivray (ED), Proceeding of the 15th International Small-Angle Scattering Conference: [CD]. November 18th-23rd, 2012, Sydney, Australia.

Spratt, H., Rintoul, L., Avdeev, M., & Martens, W. (2012). Location of Hydrogen Atoms in Hydronium and Ammoniojarosite. Conference: 10th AINSE-ANBUG Neutron Scattering Symposium (AANSS). November 7th-9th, 2012, (pp. 86). Sydney, Australia.

Studer, A.J. (2012). Wombat: Beyond Powder Diffraction. Conference: 10th AINSE-ANBUG Neutron Scattering Symposium (AANSS). November 7th-9th, 2012, (pp. 57). Sydney, Australia.

Suzuki, H., & Vladimir, L. (2012). Slit System vs. Radial Collimators: Experimental Study on Kowari. Workshop: Current State and Future of Neutron Stress Diffractometers. January 10th-12th, 2012, (pp. 21). Sydney, Australia.

Tangso, K.J., Fong, W-K., Darwish, T., Hanley, T.L., Kirby, N., & Boyd, B.J. (2012). Investigation of Spiropyran Derivatives as Light Responsive Liquid Crystalline Components. D. McGillivray (ED), Proceeding of the 15th International Small-Angle Scattering Conference: [CD]. November 18th-23rd, 2012, Sydney, Australia.

Thoennessen, L., Liss, K.D., Dippenaar, R., & Dehghan-Manshadi, A. (2012). Phase Development in the near-β Titanium Alloy Ti-1Al-8V-5Fe. Conference: 10th AINSE-ANBUG Neutron Scattering Symposium (AANSS). November 7th-9th, 2012, (pp. 87). Sydney, Australia.

Thoennessen, L., Liss, K.D., Dippenaar, R., & Dehghan-Manshadi, A. (2012). Thermomechanical Processing of Titanium Alloys. Conference: 36th Annual Condensed Matter and Materials Meeting. January 31st - February 3rd, 2012, (pp. 60). Wagga Wagga, NSW, Australia.

Tilley, A.J., Dong, Y-D., Chong, J.Y.T., Hanley, T., Kirby, N., Drummond, C.J., & Boyd, B.J. (2012). Transfer of Lipid between Triglyceride Dispersions and Lyotropic Liquid Crystal Nanostructured Particles Using Time-Resolved SAXS. D. McGillivray (ED), Proceeding of the 15th International Small-Angle Scattering Conference: [CD]. November 18th-23rd, 2012, Sydney, Australia.

Tilley, A.J., Hanley, T., Darwish, R., Gilbert, E., Drummond, C.J., & Boyd, B.J. (2012). Characterisation of the Structure of the Stabilizer on Surface of Lyotropic Liquid Crystal Nanostructured Particles. D. McGillivray (ED), Proceeding of the 15th International Small-Angle Scattering Conference: [CD]. November 18th-23rd, 2012, Sydney, Australia.

Tsutakawa, S., & Tainer, J. (2012). Combining Computational Modelling with Small Angle X-Ray Scattering in Structural Analysis of Ubiquitinated PCNA. D. McGillivray (ED), Proceeding of the 15th International Small-Angle Scattering Conference: [CD]. November 18th-23rd, 2012, Sydney, Australia.

Ulrich, C. (2012). Orbital Physics in Titanates and Vanadates. Conference: 36th Annual Condensed Matter and Materials Meeting. January 31st - February 3rd, 2012, (pp. 51). Wagga Wagga, NSW, Australia.

Ulrich, C., Reehuis, M., Khaliullin, G., Ivanov, A., Schmalzl, K., Niedermayer, Ch., Hradil, K., Maljuk, A., & Keimer, B. (2012). Spin Wave Dispersion in Helically Spin Ordered $SrFeO_{3-\delta}$ and $CaFeO_3$. Conference: 10th AINSE-ANBUG Neutron Scattering Symposium (AANSS). November 7th-9th, 2012, (pp. 88). Sydney, Australia.

Vance, E.R. (2012). Positron Annihilation Lifetime Spectroscopy within CAMS. Conference: 36th Annual Condensed Matter and Materials Meeting. January 31st - February 3rd, 2012, (pp. 38). Wagga Wagga, NSW, Australia.

Vanston, C.R., Edwards, A.J., Kearley, G.J., Darwish, T.A., de Souza, N.R., & Gardiner, M.G. (2012). Examination of Solid State Hydride Dynamics of a $[\{\mu\text{-bis(NHC)}\}_2Pd_2H]+$ Complex Through Neutron Scattering Techniques. Conference: 10th AINSE-ANBUG Neutron Scattering Symposium (AANSS). November 7th-9th, 2012, (pp. 89). Sydney, Australia.

Veliscek-Carolan, J., & Hanley, T. (2012). Investigation of the Factors Controlling Formation of Mesoporous Titania Using SAXS. D. McGillivray (ED), Proceeding of the 15th International Small-Angle Scattering Conference: [CD]. November 18th-23rd, 2012, Sydney, Australia.

Venter, A., & Luzin, V. (2012). Study of Interactive Stresses in WC-Co Surface Coated Systems. Workshop: Current State and Future of Neutron Stress Diffractometers. January 10th-12th, 2012, (pp. 31). Sydney, Australia.

Vittorio, D., & Summerfield, M. (2012). Period Safety Review of the OPAL Research Reactor. Conference: ARPS Radiation Safety: Bridging The Gap. October 14th-17th, 2012, (pp. 45). Sydney, NSW, Australia.

Vladimir, L. (2012). Advances in synchrotron radiation techniques for stress measurements. Workshop: Current State and Future of Neutron Stress Diffractometers. January 10th-12th, 2012, (pp. 11). Sydney, Australia.

Vladimir, L., & Kirstein. O. (2012). Current State of Kowari and Ideas on Further Instrument Development: is Double Detector System Pracitcal on the Constant Wavelength Diffractometer? Workshop: Current State and Future of Neutron Stress Diffractometers. January 10th-12th, 2012, (pp. 16). Sydney, Australia.

Wang, J.L., Campbell, S.J., Kennedy, S.J., Shamba, P., Zeng, R., & Dou, S.X. (2012). Magnetic Phase Transition and Thermal Expansion in $LaFe_{13-x-y}Co_ySi_z$. Conference: 36th Annual Condensed Matter and Materials Meeting. January 31st - February 3rd, 2012, (pp. 110). Wagga Wagga, NSW, Australia.

Wang, Y., Sharma, N., Su, D., Bishop, D., Ahn, H., & Wang, G.X. (2012). High Capacity Spherical $Li[Li_{0.24}Mn_{0.55}Co_{0.14}Ni_{0.07}]O_2$ Cathode Material for Lithium Ion Batteries. Conference: 10th AINSE-ANBUG Neutron Scattering Symposium (AANSS). November 7th-9th, 2012, (pp. 90). Sydney, Australia.

Weir, M.P., & Garvey, C.J. (2012). Analysing Small-Angle-Scattering Data Using the Linear Correlation Function. D. McGillivray (ED), Proceeding of the 15th International Small-Angle Scattering Conference: [CD]. November 18th-23rd, 2012, Sydney, Australia.

Whitfield, R.E., & Goossens, D.J. (2012). Pair Distribution Function and Single Crystal Neutron Diffuse Scattering of $PbZn_{1/3}Nb_{2/3}O$. Conference: 10th AINSE-ANBUG Neutron Scattering Symposium (AANSS). November 7th-9th, 2012, (pp. 45). Sydney, Australia.

Williams, A.G., Chambers, S., Griffiths, A., & Zahorowski, W. (2012). Bulk Richardson Number, surface decoupling and the mixing of scalars in the nocturnal stable boundary layer over land. Oral presentation at the AMS 20th Symposium on Boundary Layers and Turbulence. July 9th-13th, 2012. Boston MA (USA).

Wilson, C., Luzin, V., & Piazzolo, S. (2012). Neutron Diffraction for Geological Applications: Current and Future Experiments on Kowari. Workshop: Current State and Future of Neutron Stress Diffractometers. January 10th-12th, 2012, (pp. 32). Sydney, Australia.

Wood, K. (2012). Exploring Protein Dynamical Heterogeneity of Proteins Using Neutron Scattering and Isotope Labelling. Conference: 10th AINSE-ANBUG Neutron Scattering Symposium (AANSS). November 7th-9th, 2012, (pp. 21). Sydney, Australia.

Wood, K., Oesterhelt, D., Weik, M., Mulder, F.A.A., & Zaccai, G. (2012). Exploring Protein Dynamical Heterogeneity of Proteins Using Neutron Scattering and Isotope Labelling. In White (Ed.). Symposium: Structure and Dynamics of Condensed Matter by Scattering Methods. November 25th-28th, 2012, (pp. 33). Sydney, Australia.

Wu, C-M., Imamovic, E., Peng, J-C., Vorderwisch, P., Deng, G., & Li, W-H. (2012). The Current Status of SIKA - the Taiwan Contract Dougle-Focusing, Multi-Analyzer Cold Neutron Triple-Axis Spectrometer at OPAL. In White (Ed.). Symposium: Structure and Dynamics of Condensed Matter by Scattering Methods. November 25th-28th, 2012, (pp. 57). Sydney, Australia.

Yordanov, I., Knott, R., & Hanley, T. (2012). Preparation of Nano-Crystals of Zeolite-A, Using Copper-Edta as a Co-Template. D. McGillivray (ED), Proceeding of the 15th International Small-Angle Scattering Conference: [CD]. November 18th-23rd, 2012, Sydney, Australia.

Yu, D.H., & Mole, R. (2012). A Time of Flight Polarization Analysis Spectrometer - Pelican. Conference: 10th AINSE-ANBUG Neutron Scattering Symposium (AANSS). November 7th-9th, 2012, (pp. 58). Sydney, Australia.

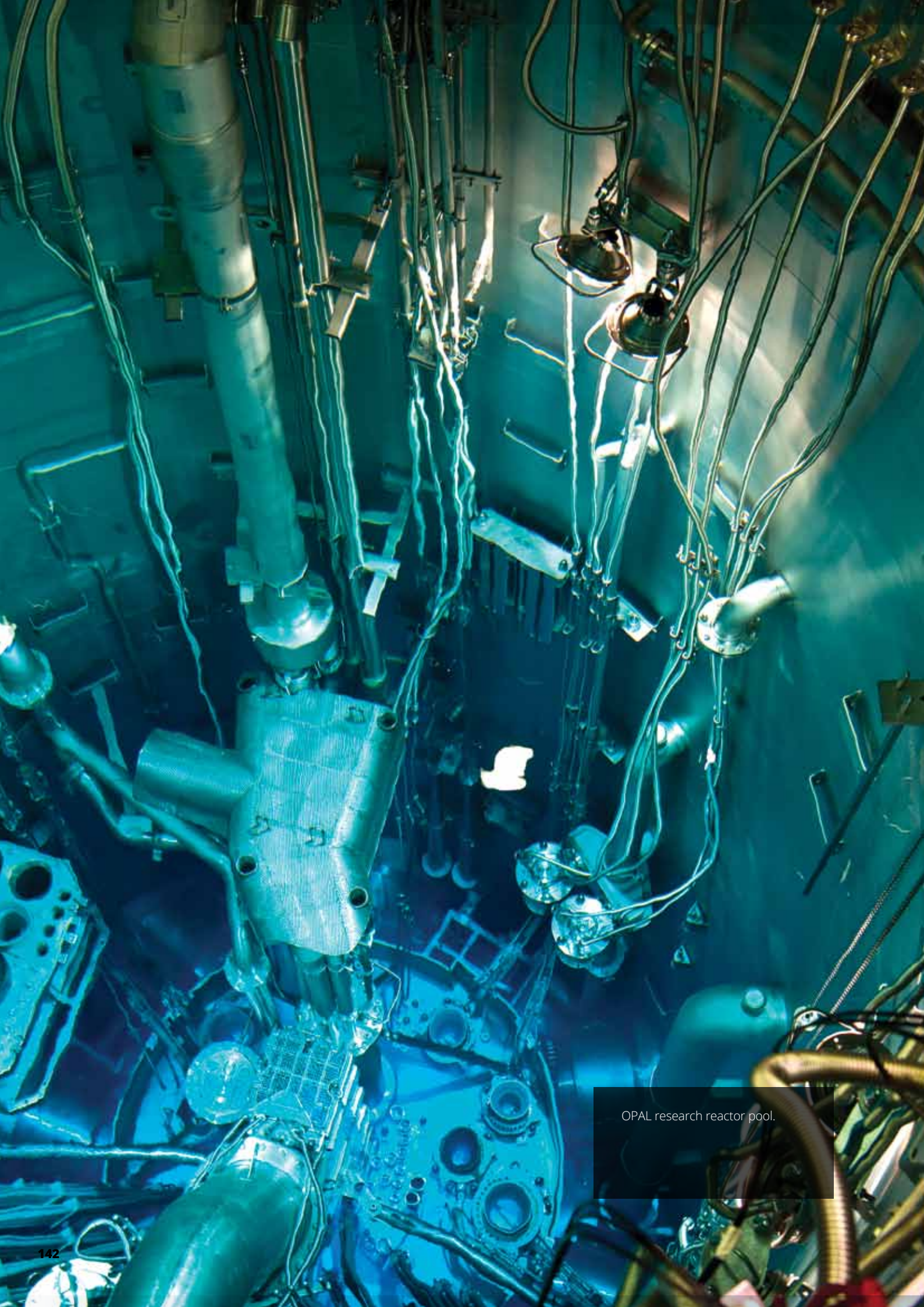

OPAL research reactor pool.

www.ansto.gov.au